

## Single-molecule conductance measurements

### Correlations between chemical design and electronic properties

Olavarria Contreras, Ignacio

#### DOI

[10.4233/uuid:da689def-97eb-4199-88a9-0637d820e47b](https://doi.org/10.4233/uuid:da689def-97eb-4199-88a9-0637d820e47b)

#### Publication date

2018

#### Document Version

Final published version

#### Citation (APA)

Olavarria Contreras, I. (2018). *Single-molecule conductance measurements: Correlations between chemical design and electronic properties*. [Dissertation (TU Delft), Delft University of Technology]. <https://doi.org/10.4233/uuid:da689def-97eb-4199-88a9-0637d820e47b>

#### Important note

To cite this publication, please use the final published version (if applicable).  
Please check the document version above.

#### Copyright

Other than for strictly personal use, it is not permitted to download, forward or distribute the text or part of it, without the consent of the author(s) and/or copyright holder(s), unless the work is under an open content license such as Creative Commons.

#### Takedown policy

Please contact us and provide details if you believe this document breaches copyrights.  
We will remove access to the work immediately and investigate your claim.

# **SINGLE-MOLECULE CONDUCTANCE MEASUREMENTS:**

CORRELATIONS BETWEEN CHEMICAL DESIGN AND  
ELECTRONIC PROPERTIES



# **SINGLE–MOLECULE CONDUCTANCE MEASUREMENTS:**

**CORRELATIONS BETWEEN CHEMICAL DESIGN AND  
ELECTRONIC PROPERTIES**

## **Proefschrift**

ter verkrijging van de graad van doctor  
aan de Technische Universiteit Delft,  
op gezag van de Rector Magnificus Prof. dr. ir. T. H. J. J. van der Hagen,  
voorzitter van het College voor Promoties,  
in het openbaar te verdedigen op maandag 2 juli 2018 om 10:00 uur

door

**Ignacio José OLAVARRIA CONTRERAS**

Master in Sciences with mention in Physics,  
Universidad de Chile, Santiago, Chile,  
geboren te Santiago, Chile.



Dit proefschrift is goedgekeurd door de

promotor: Prof. dr. H.S.J. van der Zant

promotor: Prof. dr. D. Dulić

Samenstelling promotiecommissie:

Rector Magnificus

Prof. dr. ir. H.S.J. van der Zant

Prof. dr. D. Dulić

voorzitter

Technische Universiteit Delft

Universidad de Chile

*Onafhankelijke leden:*

Dr. J. Thijssen

Prof. Dr. P. G. Steeneken

Dr. N. Aliaga Alcalde

Prof. dr. J.M. van Ruitenbeek

Dr. I. Diez Perez

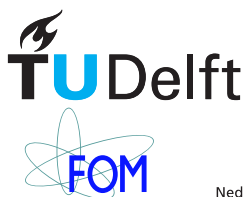
Technische Universiteit Delft

Technische Universiteit Delft

Institut de Ciència de Materials de Barcelona

Universiteit Leiden

University of Barcelona



Delft  
University of  
Technology



Nederlandse Organisatie voor Wetenschappelijk Onderzoek

*Keywords:* single-molecule electronics, conductance measurements, mechanically controlled break junction, quantum transport, curcuminoids, salen, carbon-gold bond.

*Printed by:* IPSKAMP PRINTING

*Front & Back:* In the same way exploration brought spices to our knowledge, exploration on spices-inspired compounds bring new insights on how molecules work.

Copyright © 2018 by I.J. Olavarria

Casimir PhD-Series 2018-23

ISBN 978-90-8593-352-6

An electronic version of this dissertation is available at

<http://repository.tudelft.nl/>.

# CONTENTS

<b>1</b>	<b>Introduction</b>	<b>1</b>
1.1	Introduction to single-molecule electronics.	2
1.2	Theoretical context	3
1.3	State of the art: advantages and drawbacks of measuring methods	7
1.3.1	Electromigrated break junctions	7
1.3.2	Scanning tunneling microscope	8
1.3.3	Mechanically controlled break junctions (MCBJ).	8
1.4	Implementation of the MCBJ technique	9
1.4.1	samples	9
1.4.2	Measurement set-up.	10
1.4.3	Electronics and operation	10
1.5	From Conductance traces to histograms	11
1.5.1	Conductance measurement	12
1.6	This thesis	13
	References	13
<b>2</b>	<b>Measurement protocols and data analysis</b>	<b>17</b>
2.1	Filtering, selection and criteria for molecular fingerprints	18
2.2	Junction-formation yield	24
2.3	The importance of cleaning procedures.	27
2.4	Distance modulation	31
	References	33
<b>3</b>	<b>Direct carbon Gold contacted molecules</b>	<b>35</b>
3.1	Conductance measurements	37
3.2	Functionalized molecules: Radicals	42
3.2.1	Conductance measurements.	45
3.2.2	Theoretical calculation.	48
3.2.3	Conclusions	50
	References	50
<b>4</b>	<b>Curcuminoids: Single-molecule conductance of thiophene anchored compounds</b>	<b>57</b>
4.1	Introduction to Curcuminoids	58
4.2	Discussion on chemical characterization	59
4.3	Conductance measurements	62
4.4	Transport calculations	64
4.5	Discussion and conclusions.	67
	References	67

<b>5</b>	<b>Single-molecule measurement on curcuminoid compounds: B and Cu substitution</b>	<b>71</b>
5.1	Description of the molecules . . . . .	72
5.2	Conductance measurements . . . . .	74
5.3	Boron substituted curcuminoid . . . . .	78
5.4	Discussion . . . . .	80
5.5	Conclusions. . . . .	80
	References . . . . .	81
5.A	Appendices . . . . .	84
5.A.1	Additional histograms and filtering procedures . . . . .	84
5.A.2	Fitting method . . . . .	85
5.A.3	Fit parameters MeS-BF <sub>2</sub> -CCM and time traces . . . . .	86
5.A.4	Additional measurements on the molecules with thiocarbamate anchoring (S-CCM and S-CCM-BF <sub>2</sub> ) . . . . .	88
5.A.5	Additional measurements on the copper derivative . . . . .	89
5.A.6	Measurement on Cu-curcuminoids with a double backbone. . . . .	90
5.A.7	Curcuminoid-like molecules: dibenzoylmethane derivatives . . . . .	92
<b>6</b>	<b>The role of side groups as anchoring sites in curcuminoids</b>	<b>103</b>
6.1	Molecules with different pathways for charge transport. . . . .	104
6.2	Conductance measurements . . . . .	106
6.2.1	Distance modulation. . . . .	108
6.3	Discussion . . . . .	111
	References . . . . .	111
6.A	Appendices . . . . .	114
6.A.1	measurements on additional samples . . . . .	114
6.A.2	Frequency detection . . . . .	114
<b>7</b>	<b>Salen and salophen compounds</b>	<b>119</b>
7.1	Salen and salophenes . . . . .	120
7.2	Electronic measurements. . . . .	122
	References . . . . .	129
<b>8</b>	<b>The conductance of miscellaneous molecular systems</b>	<b>133</b>
8.1	Other interesting systems . . . . .	134
8.2	Redox centers: TTF-Indenofluorenes . . . . .	134
8.3	polyoxometalates (POM) . . . . .	138
8.4	Outlook . . . . .	142
	References . . . . .	143
	<b>Summary</b>	<b>147</b>
	<b>Samenvatting</b>	<b>151</b>
	<b>Acknowledgements</b>	<b>155</b>
	<b>Curriculum Vitae</b>	<b>159</b>
	<b>List of Publications</b>	<b>161</b>

# 1

## INTRODUCTION

*There are two words that will open you many doors  
pull and push.*

les luthiers

*Y he aquí que una buena mañana, después de una noche de preciosos sueños y delicadas  
pesadillas, el poeta se levanta y grita a la madre Natura: Non serviam.*

Vicente Huidobro

*This chapter introduces the field of single-molecule electronics, discussing the motivations, the evolution and the theoretical background of the field. The main experimental methods to address single molecules are generally described, namely, electromigrated break junctions (EM), STM-break junctions (STM-BJ) and the mechanically controlled break junction technique (MCBJ). Since the latter one the technique of choice for the experiments in this dissertation, it is explained in more detail.*

## 1.1. INTRODUCTION TO SINGLE-MOLECULE ELECTRONICS

Many of the processes that shape our lives rely on electrons flowing one way or the other through organic molecules. Examples are ubiquitous in biological systems including, photosynthesis, enzymatic catalysis, energy conversion, etc. Nature seems to have mastered the design of molecular machinery that manage charge across different conducting channels and barriers. Since the origin of electronics and circuitry the tools that we have used to move electrons around have evolved from rudimentary metals to complicated semiconductor architectures. Nevertheless we have not reached the level of complexity seen in nature. Scientists have put forward the idea that a single-molecule could perform tasks as an electronic component[1] dreaming with the use of molecules as the building block of a circuits. The realization of such a dream would not come easy but the lesson learned opened a whole new subject in science called molecular electronics[2, 3].

Molecules have the advantage that chemists can make a huge number of atomically identical molecules design to perform the same function. This was one of the main motivations to envision them as active components in electronic circuitry [4, 5]; in principle, they could overcome the inherent variability of top-down fabrication when the device dimensions reach the atomic size, as predicted by Moore's law [6]. In the beginning, many techniques were developed to measure current through organic molecules relying on self assembled mono-layers (SAM) to measure ensembles of molecules [7]. As technology advanced, single-molecule measurements became possible [2, 8, 9]. Despite the success of this quest scientists quickly realize that reproducibility of the results was a challenge, as even the same molecule could show very different current-voltage (IV) characteristics depending on the exact atomic configuration of the molecule in the gap [10]. Because the current-voltage characteristic nor the conductance traces were the same from sample to sample, statistical analysis and large amounts of data gathering were needed to get reproducible results[11, 12]. Nevertheless different functionalities were founded in single-molecules: resistors [12], diodes [13–17] and switches[18, 19] are good examples.

As experiments succeeded in measuring the electronic properties of single molecules the experimental results revealed that theoretical models did not capture the complexity of the electrode-molecule-electrode system. The theoretical models advanced from simple tight binding ones [1] to complex quantum chemistry calculations [11, 20]. The problem of electrical current flowing through single molecules turned from a technological challenge to a problem of fundamentals physics. As the technical challenges were solved (or partially solved), theoreticians had to work hard to match their prediction with the experimental results.

One of the achievements of the field of single-molecule electronics was the ability to design molecules with specific functionalities and demonstrate, that indeed, the molecule showed it when measured[13, 17–19, 21], good examples of that are the diode reported in reference [17] based in two conjugated parts weakly coupled that differed in their electron withdrawing character or the molecular switch on reference [18], where, upon UV-light exposure the molecule changed its conjugation pattern and therefore its conductance. Nevertheless measurements rely on repetition to find the overall trend and the variability. This meant that despite the good capability on the molecular synthesis, experiments lacked the control over the molecular configuration when attached to electrodes. This has not changed much in the last decades; there is still not a reliable way to

determine and, even less, to control the exact configuration of molecules contacted to two electrodes.

The aim of this dissertation is not to give a definitive answer to such issues, but contribute to the building up of knowledge of how simple molecules conduct electrical current when contacted between two metallic electrodes. We focus on the comparison of different chemical designs and correlate the differences and similarities with the molecular structure.

## 1.2. THEORETICAL CONTEXT

Molecules are collections of electrons wobbling around a quasi-fixed frame of nuclei. The standard way to model them is in terms of the Schrödinger equation  $\hat{H}\Phi = E\Phi$  where  $E$  the energy of the system and  $\hat{H}$  is the electrons hamiltonian and  $\Phi$  the many-body wave functions describing the electrons in the molecule. To approximate the solution of this problem the most used approach is to express it in terms of single electron wave functions or molecular orbitals (MO). The ground states of the system is the one in which the states are filled with two electron each (one for each spin state) from the lowest energy upwards due to the Pauli exclusion principle. In this way the higher occupied molecular orbital (HOMO) represent the single-electron state with the highest possible energy when all the states below are filled. The next available state is known as the lowest unoccupied molecular orbital (LUMO). Importantly, the energy difference between the HOMO and the LUMO (HOMO-LUMO gap) coincides with the energy difference between the ground states and the first excited state so, from here on, we will make no distinction between them. In most of organic molecules the HOMO-LUMO gap is in the range of a few eV. Since the energy related to thermal fluctuations are in the range of tenths of meV at room temperature we can safely assume that there are no thermally excited process occurring in an isolated molecule.

Solving the Schrödinger equation typically relies on quantum chemistry calculation using the density functional formalism (DFT) derived by Kohn and Sham [22, 23]. This formalism allows for powerful predictions about the molecular levels and HOMO-LUMO gaps, but shows strong discrepancy with experiments when, for example, metallic electrodes are included. This is usually because the calculations do not take properly into account electron-electron interactions. Another theoretical tool to approximate the electronic behaviour of molecules is called the Hartree-Fock approximation which is a mean field theory. It works with the many-body wave function ( $\Phi$ ) explicitly and, therefore, is computationally expensive [24]. The most successful attempts to predict molecular conductance values use a combination of the two methods[25], but an in depth description of them goes beyond the scope of this thesis.

The picture of discrete energy states is modified when one introduces electrodes to the simple MO model. In general terms, the energy distribution is broadened by the interaction between the molecule and the continuous states of electrodes. The strength of this interaction is determined by a parameter  $\Gamma_{L(R)}$  for the left ( $L$ ) and right ( $R$ ) electrode respectively that encodes the overlapping of the MOs with the states in the electrodes. Depending on the relation between the total coupling ( $\Gamma = \Gamma_L + \Gamma_R$ ) and the other relevant energy scales, one can identify three different regimes: weak, intermediate and strong coupling. In the weak coupling case,  $\Gamma$  term is smaller than the charging energy

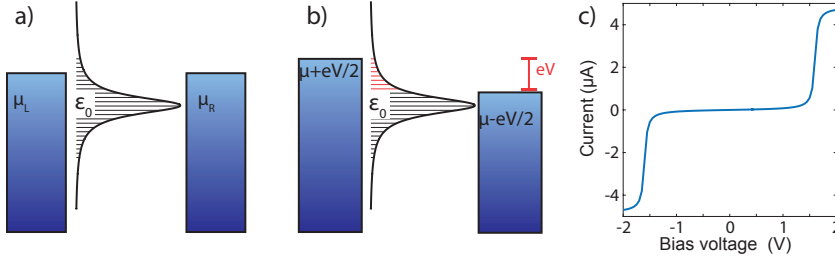


Figure 1.1: Schematic of the chemical potential of a molecule with a single level (HOMO) in between two electrodes. a) System in equilibrium with  $V = 0$  V and b) with an applied bias voltage ( $V$ ). The red dashed region corresponds to electrons that contribute to transport. c) Current-voltage ( $IV$ ) characteristic of a single level model with  $\epsilon_0 = 0.8$  eV and  $\Gamma_L = \Gamma_R = 10$  meV.

$E_C$  of the molecules  $\Gamma \ll E_C = \frac{e^2}{2C}$  where  $C$  is the capacitance of the molecular junction. This situation translates into electrons that sequentially tunnel from the source electrode to the molecule, stay in the molecule long enough to lose information about their original quantum state and then tunnel to the drain electrode. In this regime, the charge on the molecule is well defined and it is an integer multiple of the electron charge  $e$ . In contrast, when the system is in the strong coupling regime,  $\Gamma$  is larger than the charging energy ( $E_C \ll \Gamma$ ); in this case the states of the molecule strongly hybridize with the states of the electrodes. This produces a partial charge transfer between the electrodes and the molecule. Thus, the charge on the molecule is not necessarily an integer multiple of  $e$  and the electrons flow through the molecule without losing information about their original quantum states. The intermediate regime is the one in which all the energy contributions have approximately the same weight. The system is then difficult to describe and the usual way to approach this problem is to combine the theoretical approximations in the other two regimes.

If we take the toy model of a single level coupled to electrodes with a coupling energy  $\Gamma$ , there is a simple analytical expression for the energy distributions that has a Lorentzian peak shape:

$$D(E) = \frac{1}{\pi} \frac{\Gamma}{(E - \epsilon_0)^2 + (\Gamma/2)^2}, \quad (1.1)$$

where the term  $(E - \epsilon_0)$  corresponds to the level alignment between the Fermi energy of the electrodes and the ‘molecular’ level at  $\epsilon_0$ . The electrodes, on the other hand, can be described as two thermal reservoirs at temperature  $T$  and with a chemical potential  $\mu_{L(R)}$ . In equilibrium, both chemical potentials have the same value (see Fig. 1.1 a), but when a bias voltage ( $V$ ) is applied between the two electrodes the chemical potential shift such that  $\mu_L - \mu_R = eV$  (see Fig. 1.1 b). In this situation, the molecule is the channel that connects both reservoirs; it is thus held in a non-equilibrium situation. The Landauer-Buttiker formula gives the expression for the current through the molecule when electrons flow phase-coherently from one electrode to the other:

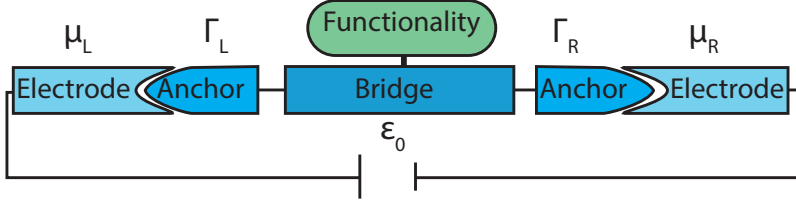


Figure 1.2: Diagram of a molecular junction, the electrodes are modelled as semi-infinite reservoirs with chemical potential  $\mu_{L(R)}$  and temperature  $T$ . The anchors are the part of the molecule with affinity to metals that provides the mechanical stability of the metal-molecule-metal system. The bridge corresponds to the body of the molecule and attached to it functionalities can be added. The energy  $\epsilon_0$  is the level alignment corresponding to the distance between the Fermi energy of the electrodes and the nearest molecular orbital.

$$I(V) = \frac{G_0}{e} \int_{-\infty}^{\infty} T(E) (f(E, \mu_L) - f(E, \mu_R)) dE, \quad (1.2)$$

where  $T(E)$  is the transmission function through the ‘molecule’ and  $f(E, \mu)$  the Fermi Energy distribution:

$$f(E, \mu) = \frac{1}{1 + \exp\left(\frac{E - \mu}{k_B T}\right)}. \quad (1.3)$$

In the case of the single level description,  $T(E) = 2\pi D(E) \frac{\Gamma_L + \Gamma_R}{\Gamma}$ . Replacing this in equation 1.2 and solving the integral at zero temperature one gets the expression for the current flowing through a single level system as a function of the bias voltage applied across it:

$$I(V) = \frac{G_0}{e} \frac{4\Gamma_L\Gamma_R}{\Gamma} \left\{ \arctan\left(\frac{\epsilon_0 + \frac{eV}{2}}{\Gamma}\right) - \arctan\left(\frac{\epsilon_0 - \frac{eV}{2}}{\Gamma}\right) \right\}. \quad (1.4)$$

Here we have assumed that the voltage drop is symmetrical across the contacts. The parameter  $G_0 = \frac{2e^2}{h}$  ( $= 77.48 \mu S$ ) is the conductance quantum ( $h$  is the Plank constant). Figure 1.1 c) displays a theoretical current-voltage ( $IV$ ) characteristic of a single-level model with  $\epsilon_0 = 0.8$  eV and  $\Gamma_L = \Gamma_R = 10$  meV. This result can be used to gain some intuition about the role of the level alignment and the coupling term on the expected current through a molecule. The parameter  $\epsilon_0$  determines at which voltage a non-linear  $IV$  dependence can be expected. Typical values for the level alignment of molecules with gold electrodes are around 1 eV while the coupling parameter  $\Gamma$  varies in the range of one to ten meV. The higher the  $\Gamma$ s’ the more hybridized is (are) the molecular level(s), so that, states far away from the Fermi energy of the electrodes can still have a significant contribution to the current.

A schematic picture of a molecular junction is displayed in Fig. 1.2. The electrodes set the level of the left and right chemical potentials ( $\mu_L$  and  $\mu_R$ ). In an analogous way the



coupling terms, are related to a part of the molecule called anchoring group. In the real, world these anchoring groups are chemical moieties designed to strongly interact with the metallic electrodes. They provide mechanical stability by the formation of chemical bonds and also tune the interaction of the molecular levels with the states the electrodes. Thus,  $\Gamma$  depends strongly on them. Usual anchoring groups are thiol, methyl-thiol, thio-phenes, pyridines, amines, among others.

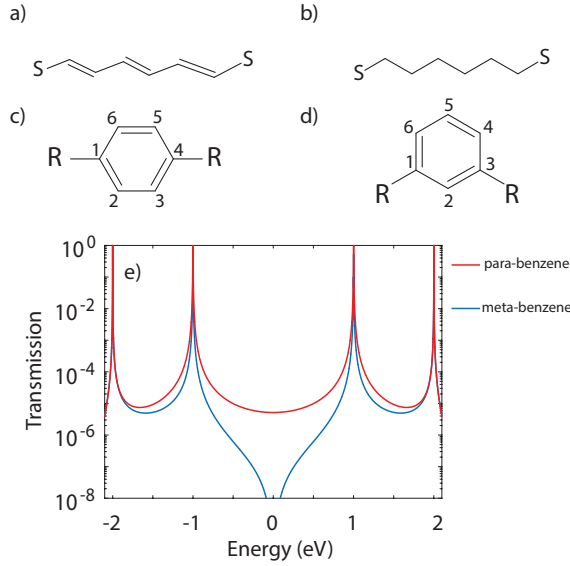


Figure 1.3: Drawing of a) a polyvinyl chains, b) a polyethylene chain, c) a para-configured benzene ring and d) a meta-configured benzene ring. Hydrogen atoms have been omitted for simplicity. Panel e) displays the transmission function from sulfur to sulfur atom for the para- and meta-configured benzene ring computed using the tight binding model of reference [26]. The site self-energy is zero, inter-site coupling is 1.2 eV and the electrodes to molecule coupling ( $\Gamma_{L(R)}$ ) is 10 meV.

In the context of transport, when short molecules ( $<5$  nm) strongly interact with the electrodes the time that they expend in the molecule is proportional to the inverse of the coupling ( $\tau_{el} \propto \frac{\hbar}{\Gamma}$ ). When this time is smaller than the time between electron-electron interaction ( $\tau_{e-e} \propto \frac{\hbar}{U}$ ), the electrons are in the ballistic tunneling regime. Under these conditions, the scattering region is smaller than the free path of the electrons. Since the size of the molecules studied in this dissertation is below the coherence length of electrons in gold at room-temperature (approximately 10 nm[27]), the electrons flowing through them do not change their phase. This regime is known as ballistic and phase-coherent transport. It is characterized by  $L < L_{\text{mfp}}, L_{\Phi}, 1$  where  $L$  is the size of the scattering region,  $L_{\text{mfp}}$  the mean free path and  $L_{\Phi}$  the phase coherence length. In this regime, one can expect to observe quantum phenomena even at room temperature, for example, interference.

Coming back again to the picture of molecular orbitals, an important characteristic of the electron states, that allow for charge transport, is the de-localization of electrons

over most the molecule. In organic chemistry, the  $\pi$ -system is the family of orbitals that extend for most of the molecule; they are the states that align perpendicular to the axes of the molecular chain. When these states connect the points in which the molecule is attached they are the main conduction channel through molecular systems. For example, the structure of the molecule in Fig. 1.3 a) has a larger conductance than the one in panel b) because of the de-localization that the  $\pi$ -system provides.

Since at the molecular scale one needs to consider quantum effects the merely distinction of conjugated versus non-conjugated is not enough to explain the most basic relations between conductance and structure. A clear example of this is the phenomenon of quantum interference in a benzene rings. Remarkably, even the most simple tight-binding model predicts a significant difference in conductance if a benzene ring is connected in a diametrical manner like the one depicted in Fig. 1.3 c), compared to the same ring connected like the one in Fig. 1.3 d). This difference is explained by the interference between the pathways of the charge carriers. The two interfering paths are the frontier orbitals, the HOMO and LUMO. Since a electron can go through each channel at the same time and depending on the phase acquired in each one of them, the transmitted wave functions can add up or cancel the contribution of the channels. In Fig. 1.3 e), the transmission function of both configurations is displayed as a function of the energy; notoriously, the values of the meta-configured ring are lower, showing a pronounce dip or 'anti-resonance'. This feature is considered to be the fingerprint of destructive quantum interference [28, 29]. The para-configured benzene ring in contrast shows no dip between the resonances because quantum interference works constructively in this case.

### 1.3. STATE OF THE ART: ADVANTAGES AND DRAWBACKS OF MEASURING METHODS

From the time in which the first single-molecule circuit was proposed [1], thirty years passed before the first single-molecule was actually trapped between electrodes [2]. The main achievement that allowed for such experiments was the formation of a nano-gap between two metallic leads. Here we will discuss the main strategies that allow for the formation of such gap. Table 1.1 summarizes the advantages and drawbacks of the different methods to electronically address single-molecules.

#### 1.3.1. ELECTROMIGRATED BREAK JUNCTIONS

Electromigration is a technique to make nano-gaps starting from a continuous metallic wire (usually gold) with a lithographically patterned constriction. This part of the wire is then opened by applying a high current that drives atoms from the constriction away thereby creating a gap [30, 31]. The achievable control in this technique depends on the feedback control over the junction resistance. Specifically, it is important to quickly turn on and off the applied bias voltages as the resistance of the junction changes. In that way, one can prevent the abrupt opening of the junction due to overheating. The current state of the art allows for the reliable formation of gaps ranging from one to a few nanometers. The advantages of this technique are a good stability of the electrodes and a fixed inter electrode distance that allows for the use of an on-chip electrical gate. Having fixed electrodes after the gap formation allows for using this technique at cryogenic

Technique	Gate	Statistic	Moving electrodes	Stability	Imaging
Electromigration	✓	limited	✗	high	✗
STM-BJ	limited	✓	✓	poor	✓
MCBJ	limited	✓	✓	high	✗

Table 1.1: Comparison table among the main techniques to electronically address single-molecules: electromigration, scanning tunnelling microscope break-junctions (STM-BJ) and the mechanically controlled break junction (MCBJ) technique.

temperatures giving access to high resolution measurements necessary for spectroscopy of the ground state of the electrode-molecule-electrode system and its low energy excitations. Moreover, electromigration has been extended to other materials than gold, including graphene (electroburning) [32]. Since a single device is able to measure only one molecular configuration, it is typically not used to acquire statistics over a large number of them. The second limitation comes from the limited control over the gap size; with the current state of the art it is possible to open small gaps but there is no means to tune it on the nanometer scale afterwards.

### 1.3.2. SCANNING TUNNELING MICROSCOPE

The scanning tunneling microscope, has been used from the very beginning of the single-molecule electronics field. There are at least two different ways to use it: the scanning mode and the break junction (BJ) mode. The first consists on depositing the molecules on a surface, usually forming a SAM and, in this the case, the tip of the microscope does not chemically interact with the molecule(s). The corresponding system can be described as metal-molecule-vacuum-metal [2]; we will not discuss this method in further detail. For the break junction (STM-BJ) approach a modified microscope is needed in such a way that it can measure currents flowing when the tip 'touches' the metallic surface ( $G > 1G_0$ ) and, at the same time, currents flowing through molecular junctions ( $G \ll 1G_0$ ) [33, 34]. This enables pushing the STM tip onto the substrate and then pulling it out while measuring the current; this better defines the metal-molecule-tip geometry but makes harder to obtain good quality of images. STM-BJ has the advantages of: allowing non-symmetrical environment, for example, temperature gradients [35] or different tip and surface materials [36]; the introduction of solvents or other environments is relatively easy and it possible to gather statistically significant amount of data. The drawbacks of this technique are related to the drifting of the tip positioning that makes difficult to measure single-molecules over the time scale of seconds. It is also hard to include a third electrode near the junction, but the use of liquid-gating allows for gating in the presence of solvents; this only works near room temperature.

### 1.3.3. MECHANICALLY CONTROLLED BREAK JUNCTIONS (MCBJ)

All the experiments carried out in this dissertation were performed using the MCBJ technique. This technique allows for electronically contact single-molecules and gathering statistically meaningful data sets with an outstanding mechanical stability even at room temperature [37]. The elegance of this technique lies in the simple and effective way to make nano-gaps and, at the same time, to fine-tune their size. The mechanism works as

follows: on a flexible substrate a thin gold wire is deposited. The sample is clamped to the end points of a three point bending mechanism as schematically shown in Fig. 1.5 a). The third contact point (pushing rod) lies in the middle of the sample and its movement drives the bending as it causes a compressive stress in the lower part of the substrate and, simultaneously, an extensive stress in the upper part similarly to the bending of a double-metal strip bar under a thermal expansion. This movement stretches the gold wire and eventually breaks it at its narrower point forming two electrodes. Importantly, the horizontal stretching of the gold wire has a tiny proportionality relation with the vertical displacement of the pushing rod (approximately  $1 \times 10^{-5}$  for our devices). This provides the exceptional control over the distance between the two electrodes (10 pm) that can be fused back again and re-opened thousands times.

Thanks to this mechanism the MCBJ technique has a remarkable mechanical stability and a very low sensibility to external vibrations in contrast to the STM-BJ case [38]. On the other hand, the sample fabrication of lithographically patterned MCBJ's samples is more laborious and time consuming and the technique does not allow for imaging of the molecules. Although electrical gating is possible, the coupling to the energy levels of the molecules is low [17].

## 1.4. IMPLEMENTATION OF THE MCBJ TECHNIQUE

Detailed explanations of the experimental design of our MCBJ implementation (TU Delft) can be found in references [39, 40]. Importantly, in this implementation the rod is driven by a stepper motor or a piezoelectric actuator at choice. This action cause the gold wires to stretch and, subsequently, break leaving two atomically sharp electrodes. In the reminder of this section we will describe the samples, the experimental set-up and electronics in more detail.

### 1.4.1. SAMPLES

Fig. 1.4 b) shows a scanning tunneling microscopy (SEM) micrography of a MCBJ device artificially colored; each of the four yellow wires is a MCBJ device. The breaking point lies in the narrower part of the wire which is suspended one  $\mu\text{m}$  above the polyimide substrate (see Fig. 1.4 c). The process to make the devices starts with a polished phosphorus bronze wafer; a 6  $\mu\text{m}$  layer of polyimide is then spin-coated on the wafer; subsequently, using electron-beam lithography the pattern of the device is written and a 80 nm thick layer of gold is evaporated on top forming the wires. Finally a layer of polymer resist is spin-coated as a protective layer. Each 5 cm  $\times$  5 cm wafer is used to make ten individual samples. They are cut off from the wafer using laser cutting and then stored until they are used for single-molecule experiments. The last fabrication step is carried out no longer than a week before the measuring procedure. This step consists of a reactive ion etching process that etches away part of the polyimide suspending, in this way, the narrower part of the gold wire. This step forms the bridge that will be broken to perform the experiments. The dimension of the samples are chosen such that the ratio between the pushing rod displacement and the electrode displacement is around  $5 \times 10^{-5}$ .

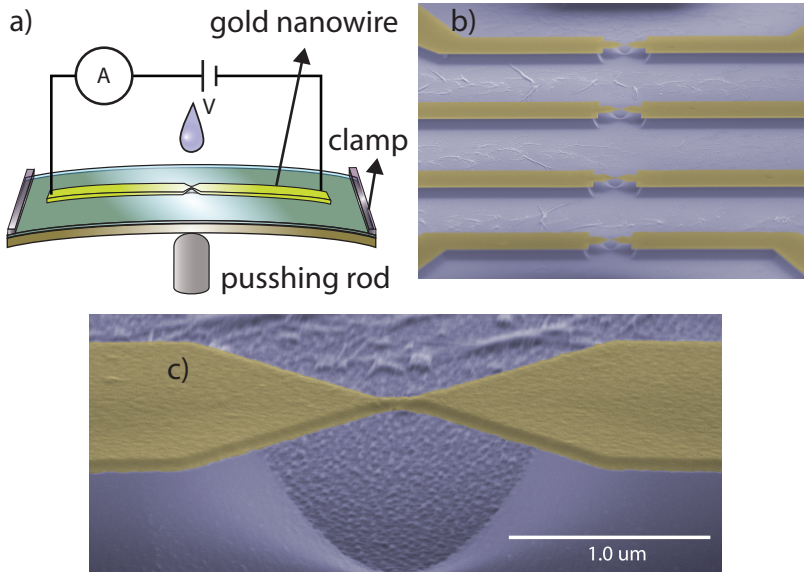


Figure 1.4: a) Schematic of the MCBJ sample, the black lines represent the electrical connections through which the bias voltage is applied and the current measured. b) Artificially colored SEM micrography of an actual device which shows the four junctions of a single chip. c) Zoom in on a single junction.

### 1.4.2. MEASUREMENT SET-UP

The used experimental set-up of the MCBJ technique has been described previously in the work of Christian Martin *et al.*[41]. In a nutshell, the set-up is based on a dip-stick design carrying the three-points bending mechanism at the bottom. There are two actuators that drive the bending of the samples: a servo motor and a piezoelectric element. For coarse movement and mechanical control at low temperatures a brushless servo motor (Faulhaber) is used as it provides a wide range of displacement. The motor is connected to a gear box with attenuation 246:1 and after that, the movement is transferred to the vertical direction by a differential screw with a pitch of 150  $\mu\text{m}$  per turn. The shortest step possible is approximately 0.1  $\mu\text{m}$  corresponding to about 5  $\mu\text{m}$  of horizontal displacement. The maximal speed is 5  $\mu\text{m/s}$  in the vertical direction (corresponding to 0.25  $\text{nm/s}$  of electrode separation speed). The fine and fast movement is driven by a piezoelectric-stack connected to the pushing rod through a lever mechanism. It can drive the electrodes at a maximum speed of around 40  $\text{nm/s}$  with a step of 0.15  $\mu\text{m}$ . The bending mechanism is placed at the bottom of a dip-stick that can be pumped down to a base pressure of approximately  $1 \times 10^{-6}$  mbar. It can be cooled down to 4 K, but at such temperature the piezo-actuator can not be used.

### 1.4.3. ELECTRONICS AND OPERATION

The electronic equipment used in the measurements was develop by Raymond Schouten (TU Delft). It is hosted in a shielded rack (IVVI rack) powered by two batteries and it is

controlled via an optically coupled interface. Different modules like voltage sources, current sources, current amplifiers, current-voltage converters can be placed in the IVVI rack allowing for customizing the measurements. The electronic isolation makes this system ideal for low-noise measurement of low current signals. For the MCBJ measurement a logarithmic amplifier is used that has a dynamic range of ten orders of magnitude. This is a requirement for measuring conductances from the metallic regime of a gold nano-wire ( $100\text{'s } \Omega$ ) down to conductances of poorly conducting molecules ( $\approx 1\text{ G}\Omega$ ).

In measurements of single-molecule conductance timing is a crucial aspect. For this reason, the direct control of the electronic measurements is performed using a Adwin gold system. It holds two analog-digital converters (ADC) and two analog-digital converter (DAC), each of them with a resolution of 16 bits for a range of  $\pm 10\text{ V}$ . The processing frequency of the Adwin is 40 MHz allowing an acquisition rate up to 100 KHz. The DAC's are used to control the bias voltage and the voltage of the piezo-actuator, respectively. It is its operational frequency what determines the limits of data acquisition rate. The ADC's are use to read out the current from the logarithmic amplifier and the information is stored in an internal memory (32 MB) until the data is retrieved from the computer controller.

The control of the experiments is performed through two layers of software: the user interface consists of a home made python script with which the parameters of each measurement are set and the results retrieved from the Adwin gold; the second layer corresponds to a home made Ad-basic script that runs on the Adwin gold system taking care of the real-time control of the applied voltages across the junction and piezo-stack as well as the reading and storing of the data before it is moved to the computer.

## 1.5. FROM CONDUCTANCE TRACES TO HISTOGRAMS

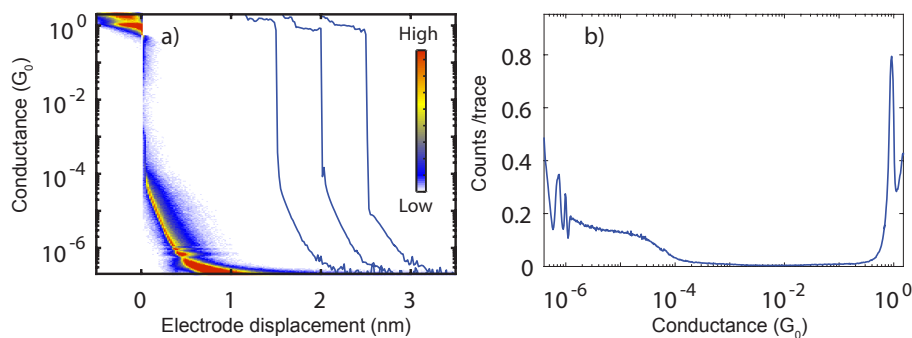


Figure 1.5: a) Blue lines correspond to a set of representative traces from a bare gold sample (offset in the x-direction for clarity) the colored data on the left represents a two-dimensional conductance vs. electrode displacement histogram of a MCBJ constructed from 10000 consecutive traces measured in a sample without any molecule. b) One-dimensional (1D) conductance histogram of the same measurement obtained by integration along the x-axes of the histogram in a). The peak at  $1\text{ G}_0$  at the right hand side correspond to a single gold atom contact.

### 1.5.1. CONDUCTANCE MEASUREMENT

In a typical measurement of molecular conductance, a clean sample is loaded in the three-point breaking mechanism and the sample is electrically connected to the set-up electronics. A bias voltage is applied between the two ends of the gold wire. Subsequently, the pushing rod is pressed against the sample and bends it. The conductance of the wire ( $G=I/V$ ) is monitored as it is stretched until the wire breaks (motor controlled) at the constriction creating two sharp electrodes. When this happens the electrodes are pushed back together in such a way that the breaking and making of the metallic contact can be achieved using only the range of the piezoelectric element.

A conductance trace consists of recording the conductance value ( $G$ ) as a function of the electrode displacement. When the wire is stretched the conductance decreases as the cross section of the wire thins down. When the wire is only a few atoms thick (1-5 atoms), the conductance decreases in a stepwise manner showing values close to integer multiples of the conductance value ( $G_0=77.48\ \mu\text{S}$ ). When the constriction is held only by 1 gold atom the conductance is equal to  $1\ G_0$ , corresponding to a single perfectly transmitting quantum channel.

As the electrodes are pulled further apart there is a sharp drop of the conductance value due to the loss of metallic contact; it is known that the electrodes snap back like cutting a rubber band under tension. On average, the electrode retraction is about 0.5 nm. After that point the current is caused by electrons tunneling from the source to the drain electrodes through the nano-gap. This tunneling is characterized by an exponential decay of the conductance as a function of the electrode displacement as seen in the blue drawn lines of Fig. 1.5 a). No two conductance traces are the same and to obtain the general trend the traces are aligned at the sharp drop and these point is defined as zero displacement. Subsequently, all are compiled in a two-dimensional (2D) conductance vs. electrode displacement histogram. An example of such a histogram constructed from 10000 traces is displayed in Fig. 1.5. The color scale represents the frequency with which each value of conductance was observed at every point of displacement.

To gain a more specific insight of the conductance distribution a one-dimensional (1D) conductance histograms is constructed by integrating the counts on the displacement axes. Figure 1.5 b) shows the conductance histogram corresponding to the same experiment as the one shown in panel a) of the same figure. An important feature is the sharp peak at  $1\ G_0$  which is an indication of the formation of atomically sharp electrodes. For lower conductance values the distribution is near zero between  $1$  to a few times  $10^{-4}\ G_0$ . Then from  $10^{-4}\ G_0$  downwards there is an onset of the tunneling current that smoothly increases as the conductance decreases. The data in Fig. 1.5 corresponds to measurements in which no molecule was deposited in the device and constitutes the base line of all the measurement discussed in this dissertation.

Summarizing, a standard conductance measurement consists of a few thousands traces that are displayed in the form of 2D- and 1D- histograms; the presence of a sharp  $1\ G_0$  peak indicates the formation of atomically sharp electrodes. Deviations from the histograms in Fig.1.5 may indicate the presence of molecules or other objects bridging the gap.



## 1.6. THIS THESIS

Following this introduction, Chapter 2 describes the experimental and analysis methods used in the following chapters. Subsequently, several molecular families are studied: Chapter 3 introduces a new strategy for anchoring molecules to metallic electrodes, in particular a method to make direct C-Au bonds in the context of single-molecule electronics. Chapters 4, 5 and 6 discuss the single-molecule electrical properties of curcumin inspired molecules divided in series of compounds that shares specific characteristics. The first group of molecules is used to explore the influence of the sulfur atom position in the thiophene anchoring group. The second group deals with the modifications to the molecular backbone and, in particular, it is shown that boron difluorine groups give rise to a bi-stable system. The last group of curcuminoids compounds exhibit modifications to the backbone with moieties with affinity to metals; a system with three anchoring sites is thus formed. Chapter 7 deals with metal-organic complexes called salen and salophenes, there the relation between the charge carrier pathway and the metallic functionalization of the free ligands is studied. Finally, various examples are discussed in the context of the outlook of this dissertation and the future of single-molecule electronics field is described following the view of the author.

## REFERENCES

- [1] A. Aviram and M. A. Ratner, *Molecular rectifiers*, [Chemical Physics Letters](#) **29** (1974).
- [2] C. Joachim, J. K. Gimzewski, R. R. Schlittler, and C. Chavy, *Electronic transparence of a single  $C_{60}$  molecule*, [Phys. Rev. Lett.](#) **74**, 2102 (1995).
- [3] C. Dekker, S. Tans, M. Devoret, H. Dai, R. E. Smalley, A. Thess, and L. Georliga, *Individual single-wall carbon nanotubes as quantum wires*, *Nature* **386** (6624), 474 (1997).
- [4] E. Lörtscher, *Wiring molecules into circuits*, *Nature Nanotechnology* **8**, 381 (2013).
- [5] M. Ratner, *A brief history of molecular electronics*, *Nature Nanotechnology* **8**, 378 (2013).
- [6] I. Present, *Cramming more components onto integrated circuits*, *Readings in computer architecture* **56** (2000).
- [7] C. P. Collier, E. W. Wong, M. Belohradský, F. M. Raymo, J. F. Stoddart, P. J. Kuekes, R. S. Williams, and J. R. Heath, *Electronically configurable molecular-based logic gates*, [Science](#) **285**, 391 (1999).
- [8] M. A. Reed, C. Zhou, C. J. Muller, T. P. Burgin, and J. M. Tour, *Conductance of a molecular junction*, [Science](#) **278**, 252 (1997).
- [9] C. Muller, J. van Ruitenbeek, and L. de Jongh, *Experimental observation of the transition from weak link to tunnel junction*, [Physica C: Superconductivity](#) **191**, 485 (1992).



- [10] T. A. Su, M. Neupane, M. L. Steigerwald, L. Venkataraman, and C. Nuckolls, *Chemical principles of single-molecule electronics*, *Nature Reviews Materials* **1**, 16002 (2016).
- [11] A. Nitzan and M. A. Ratner, *Electron Transport in Molecular Wire Junctions*, *Science* **300**, 1384 (2003), 0208239 .
- [12] X. D. Cui, A. Primak, X. Zarate, J. Tomfohr, O. F. Sankey, A. L. Moore, T. A. Moore, D. Gust, G. Harris, and S. M. Lindsay, *Reproducible measurement of single-molecule conductivity*, *Science* **294**, 571 (2001).
- [13] M. Elbing, R. Ochs, M. Koentopp, M. Fischer, C. von Hänisch, F. Weigend, F. Evers, H. B. Weber, and M. Mayor, *A single-molecule diode*, *Proceedings of the National Academy of Sciences* **102**, 8815 (2005).
- [14] I. Díez-Pérez, J. Hihath, Y. Lee, L. Yu, L. Adamska, M. A. Kozhushner, I. I. Oleynik, and N. Tao, *Rectification and stability of a single molecular diode with controlled orientation*, *Nature Chemistry* **1**, 635 (2009).
- [15] E. Lörtscher, B. Gotsmann, Y. Lee, L. Yu, C. Rettner, and H. Riel, *Transport properties of a single-molecule diode*, *ACS Nano* **6**, 4931 (2012).
- [16] A. Batra, P. Darancet, Q. Chen, J. S. Meisner, J. R. Widawsky, J. B. Neaton, C. Nuckolls, and L. Venkataraman, *Tuning rectification in single-molecular diodes*, *Nano Letters* **13**, 6233 (2013).
- [17] M. L. Perrin, E. Galan, R. Eelkema, J. M. Thijssen, F. Grozema, and H. S. J. van der Zant, *A gate-tunable single-molecule diode*, *Nanoscale* **8**, 8919 (2016).
- [18] D. Dulić, S. J. van der Molen, T. Kudernac, H. T. Jonkman, J. J. D. de Jong, T. N. Bowden, J. van Esch, B. L. Feringa, and B. J. van Wees, *One-way optoelectronic switching of photochromic molecules on gold*, *Phys. Rev. Lett.* **91**, 207402 (2003).
- [19] N. Darwish, I. Díez-Pérez, P. DaSilva, N. Tao, J. J. Gooding, and M. N. Paddon-Row, *Observation of electrochemically controlled quantum interference in a single anthraquinone-based norbornylogous bridge molecule*, *Angewandte Chemie International Edition* **51**, 3203 (2012).
- [20] J. C. Cuevas, J. Heurich, F. Pauly, W. Wenzel, and G. Schön, *Theoretical description of the electrical conduction in atomic and molecular junctions*, *Nanotechnology* **14**, R29 (2003).
- [21] L. Sun, Y. A. Diaz-Fernandez, T. A. Gschneidtner, F. Westerlund, S. Lara-Avila, and K. Moth-Poulsen, *Single-molecule electronics: from chemical design to functional devices*, *Chem. Soc. Rev.* **43**, 7378 (2014).
- [22] P. Hohenberg and W. Kohn, *Inhomogeneous electron gas*, *Phys. Rev.* **136**, B864 (1964).

- [23] W. Kohn and L. J. Sham, *Self-consistent equations including exchange and correlation effects*, *Phys. Rev.* **140**, A1133 (1965).
- [24] T. Tsuneda, *Density functional theory in quantum chemistry* (Springer, 2016).
- [25] S. Y. Quek, L. Venkataraman, H. J. Choi, S. G. Louie, M. S. Hybertsen, and J. B. Neaton, *Aminegold linked single-molecule circuits: experiment and theory*, *Nano Letters* **7**, 3477 (2007).
- [26] C. J. Lambert, *Basic concepts of quantum interference and electron transport in single-molecule electronics*, *Chem. Soc. Rev.* **44**, 875 (2015).
- [27] S. Elke and C. J. Carlos, *Molecular electronics: an introduction to theory and experiment*, Vol. 15 (World Scientific, 2017).
- [28] D. Z. Manrique, C. Huang, M. Baghernejad, X. Zhao, O. a. Al-owaedi, H. Sadeghi, V. Kaliginedi, W. Hong, M. Gulcur, T. Wandlowski, M. R. Bryce, and C. J. Lambert, *A quantum circuit rule for interference effects in single-molecule electrical junctions*, *Nature Communications* **6**, 1 (2015).
- [29] T. Markussen, R. Stadler, and K. S. Thygesen, *The relation between structure and quantum interference in single molecule junctions*, *Nano Letters* **10**, 4260 (2010).
- [30] H. Park, A. K. Lim, A. P. Alivisatos, J. Park, and P. L. McEuen, *Fabrication of metallic electrodes with nanometer separation by electromigration*, *Applied Physics Letters* **75**, 301 (1999).
- [31] P. S. Ho and T. Kwok, *Electromigration in metals*, *Reports on Progress in Physics* **52**, 301 (1989).
- [32] F. Prins, A. Barreiro, J. W. Ruitenbergh, J. S. Seldenthuis, N. Aliaga-Alcalde, L. M. K. Vandersypen, and H. S. J. van der Zant, *Room-temperature gating of molecular junctions using few-layer graphene nanogap electrodes*, *Nano Letters* **11**, 4607 (2011).
- [33] B. Xu and N. J. Tao, *Measurement of single-molecule resistance by repeated formation of molecular junctions*, *Science* **301**, 1221 (2003).
- [34] S. Y. Quek, L. Venkataraman, H. J. Choi, S. G. Louie, M. S. Hybertsen, and J. B. Neaton, *Amine - Gold linked single-molecule circuits: Experiment and theory*, *Nano Letters* **7**, 3477 (2007).
- [35] J. R. Widawsky, P. Darancet, J. B. Neaton, and L. Venkataraman, *Simultaneous determination of conductance and thermopower of single molecule junctions*, *Nano Letters* **12**, 354 (2012).
- [36] A. V. Rudnev, V. Kaliginedi, A. Droghetti, H. Ozawa, A. Kuzume, M.-a. Haga, P. Broekmann, and I. Rungger, *Stable anchoring chemistry for room temperature charge transport through graphite-molecule contacts*, *Science Advances* **3** (2017), 10.1126/sciadv.1602297.

- [37] C. Untiedt, M. J. Caturla, M. R. Calvo, J. J. Palacios, R. C. Segers, and J. M. van Ruitenbeek, *Formation of a metallic contact: Jump to contact revisited*, [Phys. Rev. Lett. \*\*98\*\*, 206801 \(2007\)](#).
- [38] M. S. Hybertsen, L. Venkataraman, J. E. Klare, A. C. Whalley, M. L. Steigerwald, and C. Nuckolls, *Amine-linked single-molecule circuits: systematic trends across molecular families*, [Journal of Physics: Condensed Matter \*\*20\*\*, 374115 \(2008\)](#).
- [39] C. A. Martin, D. Ding, H. S. J. van der Zant, and J. M. van Ruitenbeek, *Lithographic mechanical break junctions for single-molecule measurements in vacuum: possibilities and limitations*, [New Journal of Physics \*\*10\*\*, 065008 \(2008\)](#).
- [40] C. A. Martin, *Charge transport through single molecules in two-and three-terminal mechanical break junctions* (2011) PhD. Thesis.
- [41] C. a. Martin, R. H. M. Smit, R. V. Egmond, H. S. J. Van Der Zant, and J. M. Van Ruitenbeek, *A versatile low-temperature setup for the electrical characterization of single-molecule junctions*, [Review of Scientific Instruments \*\*82\*\*, 053907 \(2011\)](#).

# 2

## MEASUREMENT PROTOCOLS AND DATA ANALYSIS

*POESÍA POESÍA todo poesía  
hacemos poesía  
hasta cuando vamos a la sala de baño*

Nicanor Parra

*The elegance of the mechanically controlled break junction (MCBJ) technique is often overshadowed by the limited control over variables such as the exact atomic configuration or the alignment between the frontier orbitals and the Fermi energy of the electrodes. The usual strategy to overcome these difficulties is to gather large amounts of data to obtain statistically significant information from the random arrangement of molecular junctions. In this chapter we will describe different methods to extract valuable information from single-molecule conductance measurements. We will discuss methods to identify molecular features and describe a method to determine the yield of junction formation in fast breaking experiments using a filtering procedure. Subsequently, we will examine the impact of the yield of junction formation on the obtained values of conductance. Finally, we will comment on how contamination plays a role on experiments and how it can be minimized.*

## 2.1. FILTERING, SELECTION AND CRITERIA FOR MOLECULAR FIN-GERPRINTS

2

In an ideal single-molecule conductance measurement one can distinguish the cases in which molecules are trapped between the electrodes from the ones in which no molecule bridges both electrodes. Due to the large amount of information collected in such experiments, it is necessary to establish criteria to split the data in meaningful subsets. In other words, a filter is needed to allow the identification of traces in which a molecule is trapped between the electrodes. The yield of junction formation is then defined by the ratio of molecular traces and the total amount of traces.

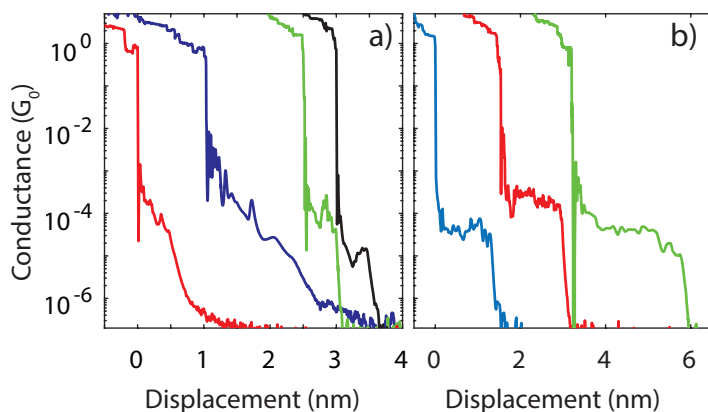


Figure 2.1: a) Examples of single breaking traces, from left to right: a trace of a pristine gold sample, one in which a pyridine terminated curcuminoid was deposited, one where MeS-OPE3 is measured and one in which a Alkynyl terminated phenyl ring is measured (OPA1). The traces are offset for clarity. All these traces represent a problem for selection methods because they are longer than the average empty trace, but do not show a clear plateau structure. b) Three clear molecular traces are displayed from left to right for a MeS-OPE3, a methyl sulfide terminated curcuminoid with a BF<sub>2</sub> central group and a trace from the measurement of an alkynyl terminated oligo-phenylene (OPA3).

In literature, several criteria have been used to select the set of data that is taken into account for further analysis [1, 2]. In the early days of the field, this task was performed manually. On top of the inconvenience of doing so with large amount of data, the usage of supervised methods increases the chances of creating artificial artifacts or features on the data. This can originate by either confirmation bias or undetermined thresholds. Other methods rely on the length of the traces, which allow a clear definition of the yield of junction formation when the molecular traces show long plateaus but fail to capture short features in the traces.

By inspecting individual traces of a ‘bare gold experiment’ one could give a qualitative description of an empty trace as follows: the trace begins in the metallic regime, and the conductance decreases smoothly upon stretching until it reaches a value of a few  $G_0$  (3 to 5  $G_0$ ). From there it evolves in a stepwise manner until a value close to 1  $G_0$  has been established. Upon further stretching, the conductances sharply drops to around

$1 \times 10^{-4} G_0$  (usually called 'onset of the current') followed by a smooth exponential decay of the conductance at a rate of around 4 dec/nm.

One inconvenience of this description is that it does not hold for all the traces in a 'bare gold experiment', either because non-ideal elastic breaking of the gold wire or due to the presence of contamination. The latter point will be addressed in a subsequent section. In Fig. 2.1a) several examples of single traces are displayed: in red a trace taken from a 'bare gold measurement', the blue is from a measurement of a pyridine terminated curcuminoid, green is coming from a measurement on a (MeS-OPE3), and in black from a measurement of an alkynyl terminated phenyl ring. Although these traces come from different measurements they share a particular feature, which is that they differ from the standard 'empty trace' but they do not show a clear plateau-like behavior. This illustrates the challenge in establishing criteria to differentiate molecular traces from the ones which are empty. In contrast, in Fig. 2.1b) clear plateaus are displayed. The traces correspond to MeS-terminated OPE3, a BF<sub>2</sub> substituted curcuminoid and an alkynyl terminated 4-phenylene (OPA4). These kind of traces can be unambiguously attributed to molecular junctions, and any filtering method should, therefore, label them as molecular traces.

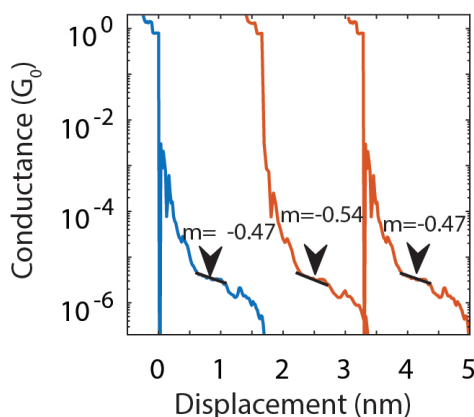


Figure 2.2: Examples of a single trace from a measurement of a OPA 1 molecule. In blue the full trace and in red the same trace compressed to a resolution of 80 bins per decade in conductance and 24 (center) and 54 (right) bins per nm in displacement. The traces has been offset for clarity. The black lines represent the linear fit of  $\log_{10}(G)$  which has the higher slope (lower decay rate) in each case in a window of 0.5 nm. The slopes are indicated on top of each line.

In this section we elaborate a different kind of method to split the information from single-molecule conductance experiments. We start with the observation that conductance traces of empty junctions decay sharply with the inter-electrode displacement. When a molecule or other object bridges the electrodes this dependence is weakened; the conductance drops off more slowly as a function of inter-electrode displacement. A good way to establish the likelihood of a trace originated from a molecular junction is, thus, to look at the way it decays as a function of inter-electrode distance.

With this in mind, we choose to look in each conductance trace for a window of displacement ( $\Delta x$ ) in which the decay of the conductance is small. Here, ‘small’ needs a more rigorous definition. For that we define the decay inside the window  $\Delta x$  as the slope ( $m$ ) of the linear fit of  $\log_{10}(G/G_0)$ . In this way  $m$  represents the rate at which the trace is changing as a function of electrode displacement inside the chosen window, in decades per nanometer (dec/nm). In this context,  $m = 0$  means a plateau-like behavior in which the conductance stays relatively constant; if for a particular window  $m = -1$  means that the trace is decaying on average one order of magnitude per nanometer and, contrarily,  $m = 1$  would mean that the conductance has an upturn with an average increase of one order of magnitude per nanometer. It is worth mentioning that this methodology does not take into account the shape, fluctuations or oscillations of the trace but the average slope of the trace in a certain window.

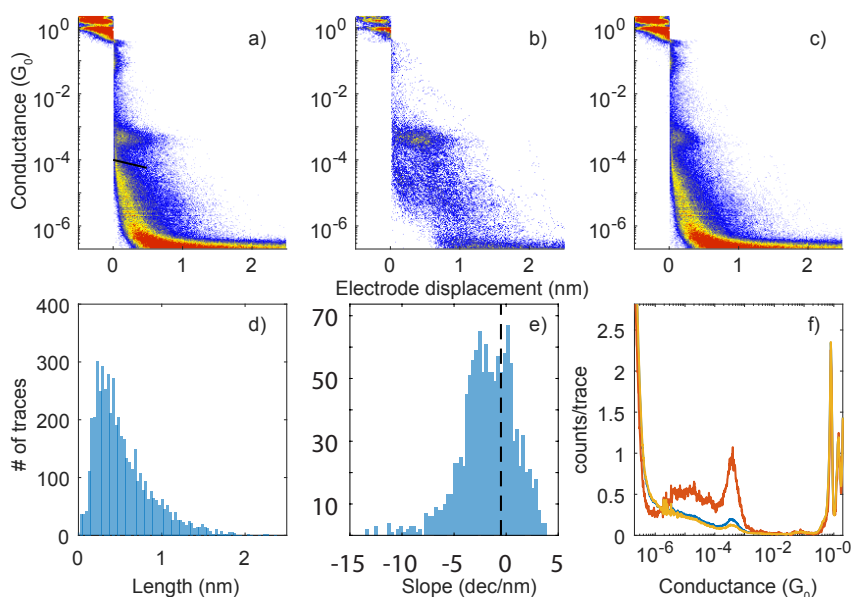


Figure 2.3: a) 2D-Histogram of a sample with a thiophene terminated curcuminoid built up from 5000 consecutive breaking traces. As a reference the short black solid line is 0.5 nm long and has a slope of -0.5 dec/nm. b) 2D-histogram of the selected traces using ( $\Delta x=0.5$  and  $m_{\text{thrs}}=-0.5$  dec/nm). c) 2-D-histograms of the unselected traces. d) The length histogram of the traces of the same measurement. e) Histogram of the maximum slope of the measurement using a displacement window ( $\Delta x=0.5$  nm). The vertical dashed line indicates a slope of -0.5 used as the threshold for selection ( $m_{\text{thrs}}$ ). f) 1D-histograms of the selected traces (red), unselected traces (orange) and total traces (blue).

Before describing the selection method in more detail it is worth enumerating some important features observed in a typical experiment. When a trace transits from the metallic regime to the tunneling one following the breaking point ( $1 G_0$ ), it is often seen a dramatic drop in conductance, below the onset of the current ( $\approx 1 \times 10^{-4} G_0$ ) and, sometimes, below the detection limit. This can be seen in the red and green traces in

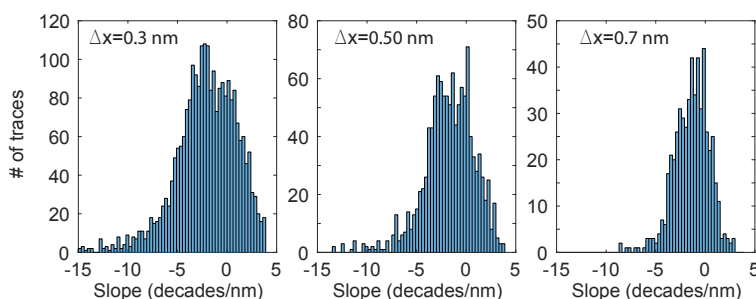


Figure 2.4: Distribution of the maximum slope found in the traces of the measurement displayed in Fig. 2.3 for a window width ( $\Delta x$ ) of a) 0.3, b) 0.5, c) 0.7 nm.

Fig. 2.1a) and the green trace in the panel b) of the same figure. This is an artifact due to an overshoot of the current amplifier caused by the fast snapping of the electrodes out of contact. Subsequently, the measurement recovers to what we could call a normal behavior without artifacts caused by rapid changes in current. Another important characteristic is that when a molecule bridges the gap between the electrodes the conductance is not always stable; it often fluctuates and jumps between different values. Ultimately, a single trace is composed of thousands of points (between 5000 to 12000) and a typical measurement consist of around 2000 to 20000 of such traces. These characteristics constitute the framework in which the filtering method has to be applied.

To account for the high sensitivity of linear fits to extreme points, the fitting procedure is performed on a compressed version of each trace, in which large fluctuations are smeared. This also allows for the speeding up the procedure and to make the analysis *in-situ* while an experiment is running. In Fig. 2.2 a trace is displayed using different compression settings: in the blue curve all points are represented; in red, the trace was compressed to the resolution of a 2D-histogram with 80 bins per decade in the conductance axis, 24 (left) and 54 (right) bins per nanometer in the displacement axis. It is clear that the roughest compression (24 bins/nm) removes the artificial drop in conductance at zero displacement while the fine compression preserves this characteristic. In the same figure the black lines correspond to the linear fit of  $\log_{10}(G)$  in a window of 0.5 nm which has the highest slope (lowest decay rate) in the trace. Notably, regardless of the compression the algorithm has selected the same part of the trace. The maximum slope obtained in the case of the roughest compression (middle line) is somewhat lower than the one obtained with the other compression settings. Since we want to preserve as much as possible the characteristics of the original trace we decided to impose an extra requirement to the window of each trace that holds the lower decay rate: in the region defined by the window  $\Delta x$  no point can drop below the conductance detection limit, which nominally is  $1 \times 10^{-6} G_0$ . From here we can now define the 'trace slope' as the maximum of such slopes from all the possible windows  $\Delta x$  nm long along the positive side of the displacement axis.

If we now apply the same method to every trace of a measurement of 5000 traces of, for example, a thiophene terminated curcuminoid we can obtain the information



displayed in Fig. 2.3. Panel a) displays the usual 2D-conductance vs. displacement histogram including all the data. The solid black line is a guide to the eye that is 0.5 nm wide and has a decay rate of -0.5 dec/nm. Panel b) shows the 2D-conductance vs. displacement histogram of the traces which have a 'trace slope' larger than -0.5 dec/nm in, at least, a window of 0.5 nm in displacement. It is interesting that by constructing an histogram from only traces selected this way it is possible to highlight features that characterize molecular junctions. In Fig. 2.3f), the red line corresponds to the 1D-histogram of these traces. It shows a pronounced peak in the region in which the complete data set (blue line) shows a smaller peak. In Fig. 2.3c) the 2D-histogram of the traces that were not selected is displayed as well; it evidences that the unselected traces still hold features of molecular junctions, which is also visible as the small peak on the green conductance histogram in panel f). These molecular-like features could be associated with plateau-like regions that are shorter than 0.5 nm.

One can visualize what this method does if for each trace the maximum slope in every window  $\Delta x = 0.5$  nm wide is computed and plotted in the form of a distribution; see for example in Fig. 2.3e). This plot shows two accumulation centers, one around  $m = -3$  and the other around  $m = 0.3$ . The vertical dashed line located at  $m_{\text{thr}} = -0.5$  dec/nm represents the threshold above which the algorithm labels a trace as molecular. In contrast, the length distribution of all traces shown in Fig. 2.3 d) only presents one peak at 0.5 nm with an asymmetric tale towards larger lengths. In this particular case the use of a filter based on the slope of the traces allows for the distinction of sorts of traces while the distinction by length does not provide it.

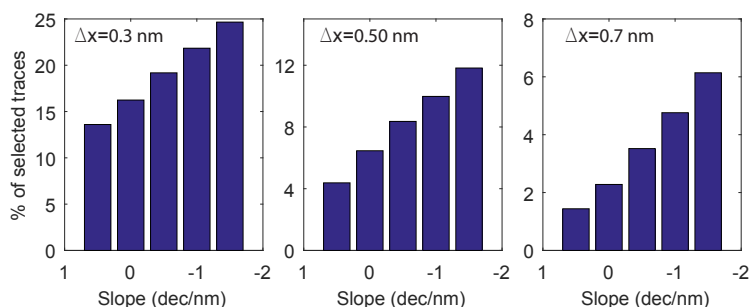


Figure 2.5: Charts displaying the percentage of selected traces from the measurement displayed in Fig. 2.3 for different threshold ( $m_{\text{thr}}$  from -1.5 to 0.5 dec/nm). The window of displacement considered in each chart are displayed in the upper left corner of each panel.

This example nicely illustrates the capability of our method to extract a meaningful subset of the traces and highlights the conductance distribution and the electrode displacement dependence of the molecular conductance. Nevertheless, the green 1D-histogram in Fig. 2.3d) shows a smaller but still noticeable peak in the same region as the one containing the selected traces. This means that there is a sizable amount of traces that are mistakenly taken out, the false negatives. It is important, to define a standard window size ( $\Delta x$ ) such that we can reliably capture molecular features in the conductance measurements and, at the same time, minimize the false negative counts.

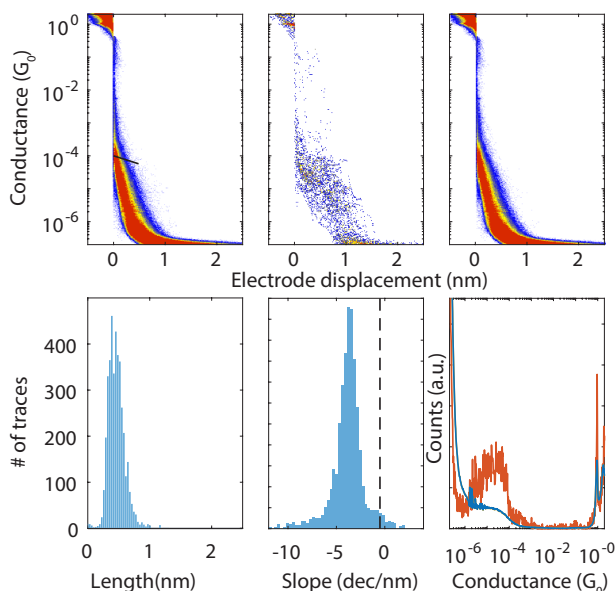


Figure 2.6: a) 2D-Histogram of a clean bare gold sample including 10000 traces. b) 2D-histogram of the selected traces using ( $\Delta x = 0.5$  and  $m_{thr} = -0.5$  dec/nm). c) displays the 2-D-histograms of the unselected traces. d) length histogram of the traces in the same measurement. e) Histogram of the maximum slope of the measurement using the indicated window and slope the vertical dashed line indicates a slope of -0.5 (dec/nm) used as the threshold for selection. d) 1D-histograms of the selected traces (red), unselected traces (orange, indistinguishable from the blue) and total traces (blue).

To illustrate how this works we construct the slope histograms of the data in Fig. 2.3 for different values of  $\Delta x$  and check what are the parameters that allow separation between molecular and empty traces in the best way. Fig. 2.4 displays three histograms of the ‘trace slope’ considering  $\Delta x$  values of 0.3, 0.5 and 0.7 nm respectively. The middle panel repeats the information on Fig. 2.3 e). By Comparing these plots one can see that the smaller the window size the higher the amount of traces is considered. This means that more and more traces have the minimum amount of points above the detection limit as we decrease the window size. Regarding the selectivity, on the other hand, the plots with  $\Delta x = 0.3$  nm and 0.5 nm show a structure that can be interpreted as two peaks, while for 0.7 nm there is only one recognizable group.

The aim of this analysis is to set a threshold slope ( $m_{thr}$ ) above which a trace would be considered molecular. We tried several values for this threshold. The result can be seen in the bar plots shown in Fig. 2.5 in which the x-axis represents  $m_{thr}$  and the y-axis the percentage of traces selected. The x-axis is inverted in such a way that steeper traces are plotted on the right hand side. As expected, the lower the required slope the more traces are identified as molecular, but the figure does not provide further information

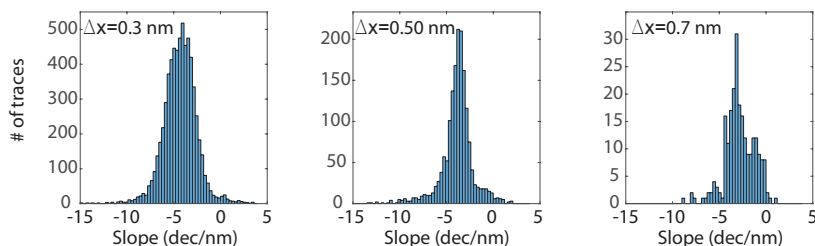


Figure 2.7: Distribution of the maximum fitted slope computed by a linear fit of  $\log(G)$  of the measurement displayed in Fig. 2.6 in a window ( $\Delta x$ ) indicated in each panel.

about which is the better choice for  $\Delta x$  and  $m_{\text{thrs}}$ .

The problem in the other extreme case is the issue of false positive cases, meaning the amount of traces in which the target molecule was not trapped but the filter still labels it as a molecular trace. To gain more insight on this point we performed the same analysis on a clean sample in which no molecule has been deposited. Fig. 2.6 displays 10000 traces of a ‘bare gold measurement’ in the same fashion as in Fig. 2.3. Both, length and slope histograms only show a single peak. In this case the tail of the slope distribution to the right of  $-0.5$  dec/nm (black dashed line) contains only 0.6% of the total amount of traces. The slope histogram for different  $\Delta x$  windows is displayed in Fig. 2.7. In the case of  $\Delta x = 0.7$  nm, an almost negligible amount of traces are labeled as molecular; this would mean a very low rate of false positives. In the case of  $\Delta x = 0.3$  nm most of the traces show a slope around  $-4$  dec/nm with a broad distribution. We find that a good compromise between the false positive and false negative can be achieved with  $\Delta x = 0.5$  nm and  $m_{\text{thrs}} = 0.5$  dec/nm; a threshold that produces below 1% of false positive counts in the case of a clean junction. This choice is rather arbitrary but gives an unsupervised manner to split data in meaningful subsets. We point out that the accuracy of this method may vary depending on the molecular system to which it is applied and modification to the parameters we discuss may need to be tuned to obtain optimal results. From here on, unless otherwise mentioned, we will define the yield of junction formation as the ratio between the traces selected with this method (with  $\Delta x = 0.5$  nm and  $m_{\text{thrs}} = -0.5$  dec/nm) and the total amount of traces.

## 2.2. JUNCTION-FORMATION YIELD

One may think that by increasing or decreasing the concentration of the solution deposited on a device, the chances of trapping a molecule when breaking the electrodes would increase or decrease. However, this relation has proven not to be so simple. Experiments have shown that using different concentrations and methods to determine the single-molecule conductance are nearly independent of the concentration. This has been rationalized by the fact that the experiments are sensible only to a very restricted volume around the breaking point rather than to the average concentration of the used solution. In addition, the atomic sharpness of the electrodes makes the scenario of a

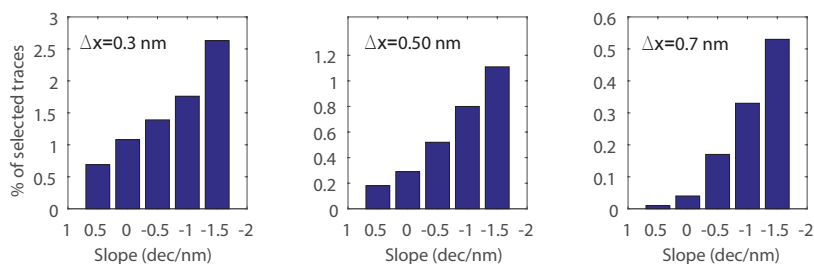


Figure 2.8: Selected traces as a function of the threshold slope as explained in the main text for three different window width ( $\Delta x$ ) as indicated in the insets. The measurements contain 10000 consecutive conductance traces of a 'bare gold measurement'. The total number of included traces varies because the ones that extend for less than the window width are excluded from the counting.

single-molecule bridging the gap the more likely, instead of an ensemble of molecules between them.

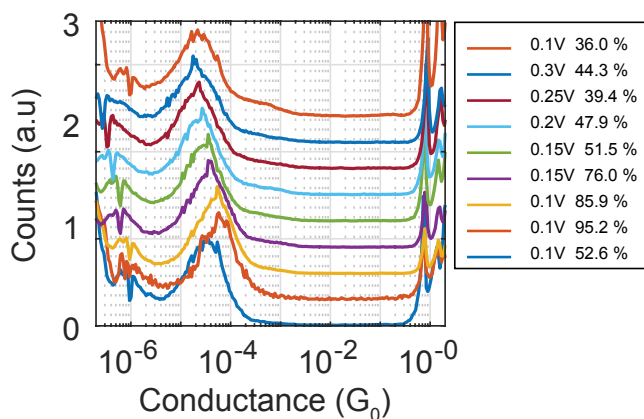


Figure 2.9: Series of 1D-histograms of the full data sets acquired on a single junction in which a di-methyl-sulfide OPE-3 was deposited. The histograms collect information from thousands of traces each. The legend next to the figure displays the bias voltage used in each case and the yield of junction formation, defined as the percentage of selected traces using the filter described in the previous section with  $m_{\text{ths}} = -0.5$  dec/nm and  $\Delta x = 0.5$  nm. The curves are normalized to the molecular peak and offset for clarity. Notably there is a clear shift of the peak which does not follow a clear trend.

There has been no systematic study on the influence of the yield of the conductance values obtained from the measurements. Thanks to the mechanical stability of the MCBJ devices we have been able to run experiments on a single junction for nearly hundred thousand times. Interestingly, we have seen variations that are not exclusively at-

tributable to degradation of the target molecules. Figure 2.9 shows a series of normalized 1D-histograms which are offset for clarity; the data was recorded from a single junction in which a solution of methylsulfide terminated OPE 3 molecules in dichloromethane was drop-casted. Each histogram is constructed from at least 1000 consecutive traces up to 2000. The legend displays the bias voltage and the yield of junction formation as determined using the algorithm described in the previous section. The measurements are sorted from the bottom to the top in a temporal order and the bottom (first) curve and the last one share more characteristic features than the bottom one and the second one. The distribution of the conductance of the selected traces has been fitted to log-normal distributions. The peak conductance values and the full width half maximum (FWHM) are plotted in Figure 2.10 as a function of bias voltage and yield. An uprise of the conductance is seen as a function of yield while there is no clear dependence on the bias. It seems that the more likely trapping a molecule, the higher the obtained conductance. It is worth mentioning that the width of the peaks stays almost the same for all bias voltages and yields.

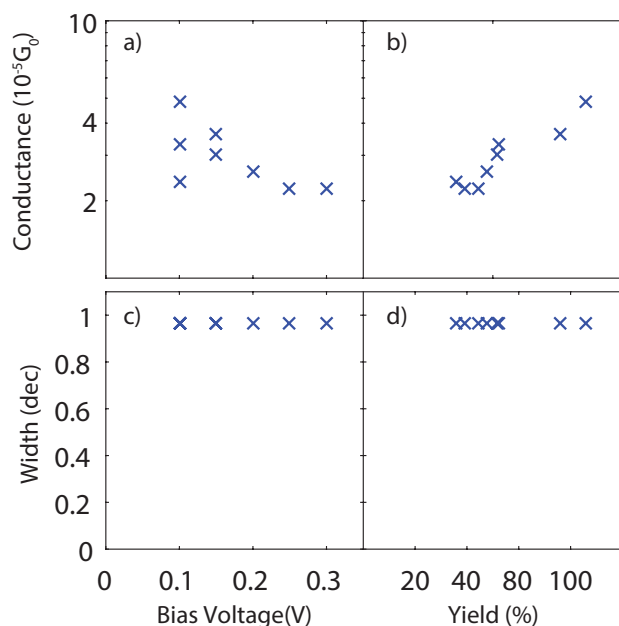


Figure 2.10: Conductance values obtained by fitting a log-normal curve to the selected traces from the measurements displayed in Figure 2.9 as a function of a) bias voltage and b) yield of junction formation. The full width half maximum of such fits is displayed as a function of: c) bias voltage and d) yield.

A reasonable explanation for this behavior is that the more probable it is to trap a molecule, the higher the chance to trap more than one. So if the yield of junction formation approaches 100%, it is less likely that the junction holds just a single-molecule. Therefore, one should be careful in claiming single-molecule conductance values es-

pecially when the yield of junction formation is high. For the sake of determining the conductance of single-molecules it is important to aim for a yield of junction formation low enough to ensure that the most likely configuration is a single-molecule bridging the electrodes. As a rule of thumb, we estimate a safe upper limit around 60 to 70%. The lower limit has to do with the capability of distinguishing the measurement on a bare gold sample from the one in which molecules have been deposited. This has to do with how clean are the samples and the set-up. We will discuss this aspect in the next section.

## 2.3. THE IMPORTANCE OF CLEANING PROCEDURES

One of the main requirements for single-molecule conductance measurements is that the obtained data that is used to extract information about the measured molecule, does not contain features from other sources [3–5]. For this reason before performing single-molecule conductance measurements, normally a ‘control experiment’ or ‘bare gold experiment’ is executed to check that there is no contamination [4, 6]. However, often there are indications of small amounts of contamination. When the expected signal of the target molecule is sufficiently distinctive from that of the spurious additional features, either with respect to yield, length or conductance value, the molecule is drop-casted and the experiment is carried out. On the contrary, it is interrupted and a new sample is mounted or additional cleaning procedures have to be considered.

An aspect that is often overlooked is the fact that the number of breaking traces on the bare gold sample are fewer than those taken on the target molecules. Under certain circumstances this can lead to an underestimation of the contamination present in the system. In this section we show that clean samples can show features similar to molecular plateaus when one does not take care of the appropriate cleaning procedures. We also propose a protocol which reduces the level of contamination in our samples to values of less than one percent in the number of breaking traces. This value is sufficiently low to ensure a proper analysis of the molecular features in the data.

We have measured a clean MCBJ sample for 20000 consecutive conductance traces without depositing molecules on it; the duration of the experiment was 21 hours. In Fig. 2.11 a set of 2D-conductance vs. displacement histograms is displayed, each one represents the information of 2500 consecutive traces of the described experiment and are numbered in chronological order. The presence of contamination is seen as traces that extend to around one nanometer. It is important to mention that the histogram in panel number 1 of Fig. 2.11 shows a small amount of contamination as it is reflected in the 3% of selected traces using our filter method (see Fig. 2.14). If a particular molecule would be measured in this device, OPE 3 for example, then just by looking at this first histogram one could decide to deposit the target molecule and continue the experiment. If, however, the control measurement would look more like the one depicted in the second panel in Fig. 2.11 then one would start doubting about the quality of the sample. Thus, as more and more breaking traces are taken on the bare gold junction, the number of traces that are considered to lead to spurious counts, increases, at least in this case.

If the filtering method described in the previous section is used in the aforementioned experiment, 1508 traces are labelled as ‘molecular’, corresponding to 7.5% of the total. Figure 2.15 a) shows the 2D-histogram of those traces. Interestingly, the shape resembles a plateau-like structure usually seen when measuring molecular wires; the con-

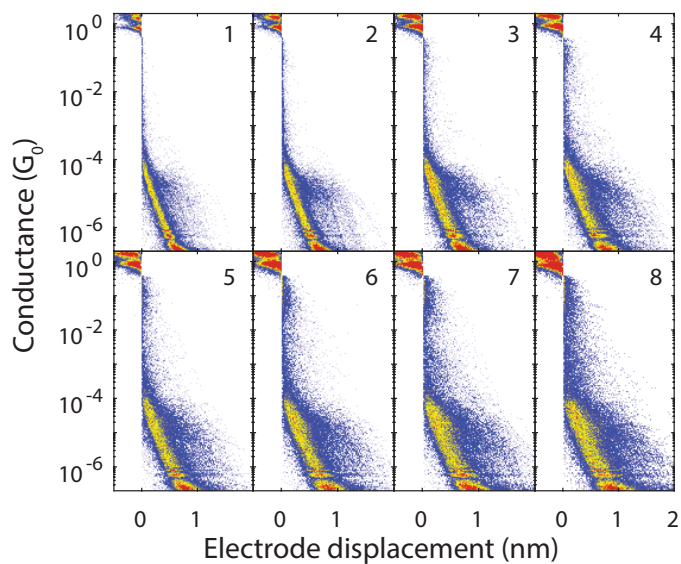


Figure 2.11: Series of 2D-histograms of a bare gold sample prior to ozone cleaning. Each histogram is constructed from 2500 consecutive traces from a total of 20000. Time increases from the upper left corner to the bottom right one. Contamination is seen as the presence of traces that extend to displacements of about 1 nm.

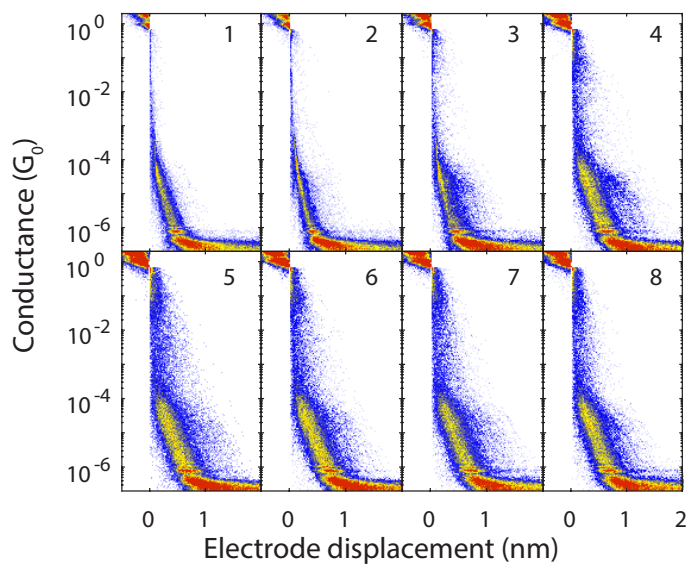


Figure 2.12: Series of 2D-histograms of a bare gold sample after ozone cleaning. Each histogram is constructed from 2500 consecutive traces from a total of 20000. Time increases from the upper left corner to the bottom right one. Contamination is seen as the presence of traces that extend to displacements of about 1 nm.

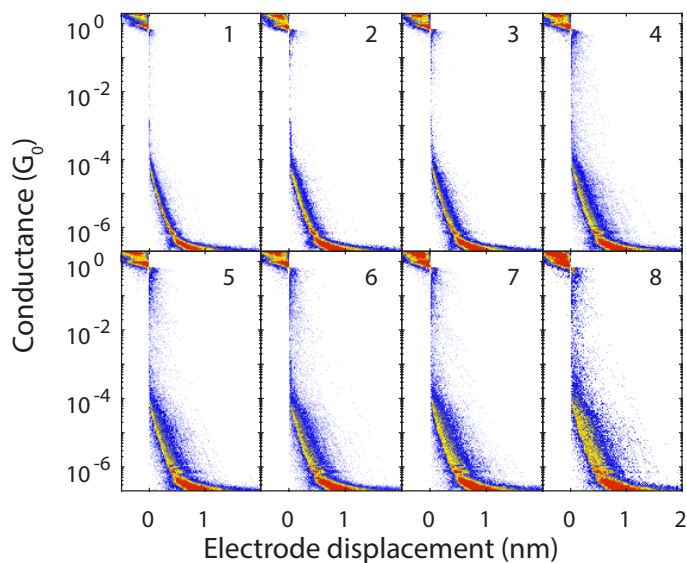


Figure 2.13: Series of 2D-histograms of a clean sample after two steps of ozone cleaning and cap cleaning procedure as described in the main text. Each histogram is constructed from 2500 traces except for the last one which contains the remaining traces from a total of 19148. Time increases from the upper left corner to the bottom right one. The presence of long traces is less prominent than in the measurements before the cleaning protocols.

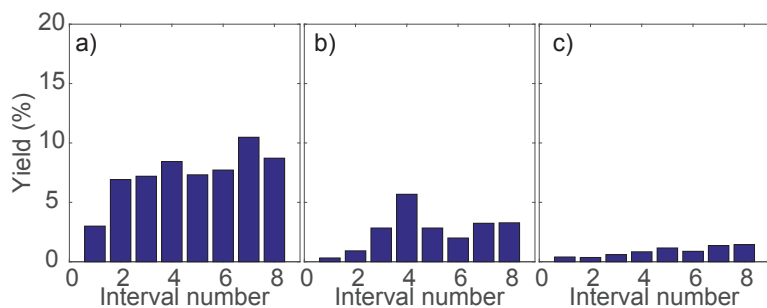


Figure 2.14: Yield computed as the fraction of the number of traces that is selected by the filter described in section 2.1. The values on the x-axis correspond to the numbers indicated in Figures 2.11, 2.12 and 2.13 in a), b) and c), respectively.

ductance distribution of the selected traces (red line in Fig. 2.15 d) shows a peak around  $2 \times 10^{-5} G_0$ .

We cleaned the same sample using an UV-ozone cleaning system for one minute. Subsequently, we performed the same experiment recording again 20000 consecutive



breaking traces. Fig. 2.12 displays a set of 2D-histograms in the same fashion as Fig. 2.11. The presence of contamination is almost negligible in the first two panels (below 1% of filtered traces) but in the third and fourth panels a small amount of contamination in the form of plateaus becomes visible. This is seen in Fig. 2.14b) in which the  $x$ -axis represents the numbers used as label in Fig. 2.12 and the  $y$ -axis the percentage of filtered traces in the respective 2500 traces subset. When comparing Fig. 2.14 a) and b) a clear decrease in the number of selected traces is observed which we attribute to a lower contamination level. The cleaning procedure using ozone is, therefore, useful to diminish the contamination; this observation suggests that the contamination has an organic nature. It is also worth mentioning that the 2D-conductance vs. displacement histogram of the selected traces (Fig. 2.15 b) shows a similar plateau structure and the conductance distribution (blue line in Figure 2.15d) peaks at the same value as in the experiment before the ozone cleaning.

Until this point, the observable trend has been that a clean sample can start showing signals of contamination after a few thousands traces. This suggests that contamination can be coming from the sample environment inside the set-up as well. We hypothesize that some of the molecules measured previously in the same set-up have been redeposited on the inner side of the chamber and the cap protecting the sample. From there they could desorb again and in turn be redeposited on a new sample while another experiment is running.

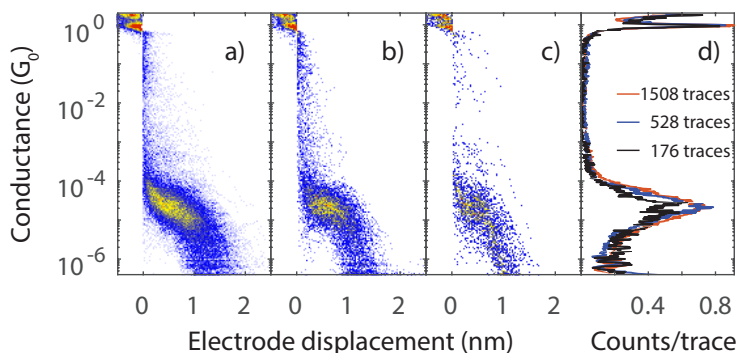


Figure 2.15: 2D-histograms of the traces selected by the filter in the case of: a) 20000 traces of bare gold before adopting a cleaning procedure, b) 20000 traces after first ozone cleaning procedure and c) 19148 traces after a second step of ozone cleaning and a cleaning procedure of the cap. d) Corresponding 1D-histograms from a) in red, b) in blue and c) in red. Although the presence of contamination decreases with the cleaning steps in all cases a peak around  $2 \times 10^{-5} G_0$  is visible.

The part of the set-up that provides the larger area in the vicinity of the sample is the bronze cap that seals the dip-stick. We decided to establish a cleaning protocol for both, i.e., for contaminated samples and the set-up: the sample is ozone cleaned for 5 min. and separately, the cap undergoes an extensive cleaning process. Firstly, the cap is wiped clean with acetone to remove residues of vacuum grease or dirt on the inside

of the cup. Subsequently, it is flushed with dichlorometane, which is the most common solvent used for our single-molecule conductance measurement. Then, the cap is put in an ultrasonic bath at 40 °C with soap and de-ionized water, flushed with de-ionized water, put back in ultra-sonic bath in hot acetone for 30 minutes (40 °C) and, finally, put in an ultrasonic bath of hot isopropanol (IPA) for 30 min. The removable parts of the set-up were wiped and sonicated in acetone and IPA in the same way as the cap, while the non removable parts of the dip-stick were wiped with ethanol and dried with a nitrogen flow.

Afterwards, using the same sample used for the experiment of Fig. 2.11, we performed again the same experiment recording 19148 consecutive conductance traces. In the same way as in the prior cases, data is displayed in Fig. 2.13 in subsets of 2500 traces except for the last one that is constructed with the remaining traces to complete the set. It can be seen that the presence of contamination is lower in this case. The diagram in Fig. 2.14 c) shows a yield of selected traces using our filtering method below 1%. When all 176 selected traces are collected in a single histogram (Fig. 2.15 c) and the black line in panel d) the structure resembles the same single peak structure around  $2 \times 10^{-5} G_0$ .

The important lesson that can be learned from this experiment is that contaminations can be originated from the close environment of the sample. If one does not take care of this sources and still perform an experiment, then one could mistakenly probe contamination (molecules measured in previous runs) with the target molecules. Nevertheless, even when the equipment and samples are recently cleaned, the filter still select a few traces on a 'bare gold experiment'. This can be interpreted as having a molecular origin. These traces can have two sources: a small amount of contamination around the junction that remains present even after cleaning or a 'false positive' selection by the used method to filter the data. Either way we conclude that measurements in which the yield of junction formation is small (a low percentage) it would be difficult to unmistakably relate observed features to those of target molecules. To be on the safe side we suggest a minimum of 10 % yield to ensure a high enough contrast from the control experiments.

## 2.4. DISTANCE MODULATION

Given the mechanical stability and control of the inter-electrode distances of the MCBJ technique it is a promising platform for mechanical actuation of single-molecules. At low temperatures MCBJ has been used to tune the strength of the image charge effect in single-molecule junctions [7]. Modulation of the tip-surface distance has been used in STM-break junctions to study conductance of molecular switches [8–12]. In one of them, for example, the changes in dihedral angles among the bonds at the molecule-electrode interface drive the switching mechanism. MCBJ devices are very insensitive to drift in the electrode positions even at room temperature, Thanks to their mechanical attenuation. Using this advantage we implemented a similar measurement technique to the one used in STM break junctions. The conductance is measured as a function of the electrode displacement, but with the difference that the inter-electrode distance is modulated in a non-uniform manner as described below.

A distance modulation measurement consists on recording the conductance ( $G = I/V$ ) as a function of time while the electrodes are moving, similarly to the fast breaking

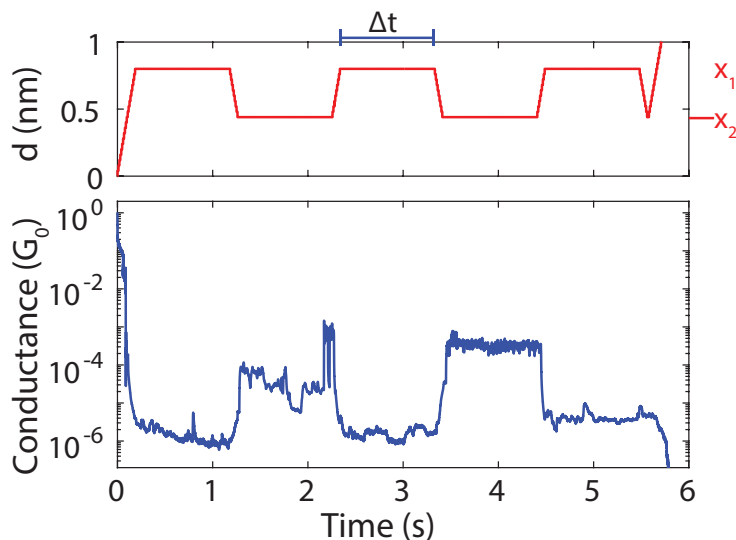


Figure 2.16: The lower panel displays a single modulated trace of a measurement on a MeS-CCM-pyr molecule at a bias voltage of 0.1V and an electrode speed of 4 nm/s. The modulation parameters are  $x_1 = 0.8$  nm,  $x_2 = 0.4$  nm and  $\Delta t = 1$  s. The upper panel shows the electrode displacement as a function of time in the same measurement.

experiment. The difference lays in the electrodes movement, which is non-monotonous as a function of time. In Fig. 2.16 the blue line depicts the conductance as a function of time while the red one in the upper panel describes the inter-electrode distance during the same period. The control parameters introduced in this measurement are the time span that the electrodes are kept steady ( $\Delta t$ ) and the two distances at which the electrodes are stationary ( $x_1$  and  $x_2$ ). These distances are measured from the point where the metallic regime is lost (i.e., when the conductance drops below  $1 G_0$ ). Keeping the electrodes fixed for a certain amount of time allows for studying the stability of the molecular junctions. The parameter  $\Delta t$  can be tuned from a few milliseconds to tenths of minutes. The modulation of the inter-electrode distance is used mainly for two purposes: identifying the event of junction formation and gathering information about the mechanical stability of the different molecular configurations including its dependence on the inter-electrode distance. The first one relates to the capacity distinguish between short molecular traces from empty traces, in those cases the fast breaking experiment does not provide a sensible way to split these cases. But a small modulation in the electrodes distance for a sufficiently long time allows for observation of the conductance dependence on the electrode displacement; a strong exponential dependence on the modulated distance indicates a single barrier process that is most likely related to an empty junction; a weak dependence, on the other hand, indicates that the junctions holds at least one molecule between the electrodes. The second use of the modulation is to attempt controlling the configuration a molecule inside the junctions, for example when it shows

more than 2 possible anchoring moieties (in chapter 6 we will explore this possibility).

## REFERENCES

- [1] V. Kaliginedi, a. V. Rudnev, P. Moreno-Garcia, M. Baghernejad, C. C. Huang, W. J. Hong, and T. Wandlowski, *Promising anchoring groups for single-molecule conductance measurements*, [Physical Chemistry Chemical Physics](#) **16**, 23529 (2014).
- [2] W. Hong, H. Li, S. X. Liu, Y. Fu, J. Li, V. Kaliginedi, S. Decurtins, and T. Wandlowski, *Trimethylsilyl-terminated oligo(phenylene ethynylene)s: An approach to single-molecule junctions with covalent Au-C  $\sigma$ -bonds*, [Journal of the American Chemical Society](#) **134**, 19425 (2012).
- [3] Z. Huang, F. Chen, P. A. Bennett, and N. Tao, *Single molecule junctions formed via Au-thiol contact: Stability and breakdown mechanism*, [Journal of the American Chemical Society](#) **129**, 13225 (2007).
- [4] R. Frisenda, M. L. Perrin, H. Valkenier, J. C. Hummelen, and H. S. J. Van der Zant, *Statistical analysis of single-molecule breaking traces*, [Physica Status Solidi \(B\) Basic Research](#) **250**, 2431 (2013).
- [5] K. Hansen, S. K. Nielsen, M. Brandbyge, E. Lægsgaard, I. Stensgaard, and F. Besenbacher, *Current-voltage curves of gold quantum point contacts revisited*, [Applied Physics Letters](#) **77**, 708 (2000).
- [6] C. R. Arroyo, R. Frisenda, K. Moth-Poulsen, J. S. Seldenthuis, T. Bjørnholm, and H. S. van der Zant, *Quantum interference effects at room temperature in opv-based single-molecule junctions*, [Nanoscale Research Letters](#) **8**, 234 (2013).
- [7] M. L. Perrin, C. J. Verzijl, C. A. Martin, A. J. Shaikh, R. Eelkema, J. H. Van Esch, J. M. Van Ruitenbeek, J. M. Thijssen, H. S. Van Der Zant, and D. Dulić, *Large tunable image-charge effects in single-molecule junctions*, [Nature Nanotechnology](#) **8**, 282 (2013).
- [8] S. Y. Quek, M. Kamenetska, M. L. Steigerwald, H. J. Choi, S. G. Louie, M. S. Hybertsen, J. Neaton, and L. Venkataraman, *Mechanically controlled binary conductance switching of a single-molecule junction*, [Nature Nanotechnology](#) **4**, 230 (2009).
- [9] C. Bruot, J. Hihath, and N. Tao, *Mechanically controlled molecular orbital alignment in single molecule junctions*, [Nature Nanotechnology](#) **7**, 35 (2011).
- [10] M. Nakamura, S. Yoshida, T. Katayama, A. Taninaka, Y. Mera, S. Okada, O. Takeuchi, and H. Shigekawa, *Mechanically activated switching of Si-based single-molecule junction as imaged with three-dimensional dynamic probe*, [Nature Communications](#) **6**, 8465 (2015).
- [11] T. A. Su, H. Li, V. Zhang, M. Neupane, A. Batra, R. S. Klausen, B. Kumar, M. L. Steigerwald, L. Venkataraman, and C. Nuckolls, *Single-molecule conductance in atomically precise germanium wires*, [Journal of the American Chemical Society](#) **137**, 12400 (2015).

- [12] T. A. Su, H. Li, M. L. Steigerwald, L. Venkataraman, and C. Nuckolls, *Stereoelectronic switching in single-molecule junctions*, [Nature Chemistry](#) **7**, 215 (2015).

# 3

## DIRECT CARBON GOLD CONTACTED MOLECULES

*El adjetivo, cuando no da vida, mata  
The adjective, when it doesn't give life, kills it.*

Vicente Huidobro

*We report on an approach to realize carbon–gold (C–Au) bonded molecular junctions without the need for an additive to deprotect the alkynyl carbon as endstanding anchor group. Using the mechanically controlled break junction (MCBJ) technique, we determine the most probable conductance value of a family of alkynyl terminated oligophenylenes (OPA(*n*)) connected to gold electrodes through such an alkynyl moiety in ambient conditions. The molecules bind to the gold leads through an *sp*-hybridized carbon atom at each side. Comparing our results with other families of molecules that present organometallic C–Au bonds, we conclude that the conductance of molecules contacted via an *sp*-hybridized carbon atom is lower than the ones using *sp*<sup>3</sup> hybridization due to strong differences in the coupling of the conducting orbitals with the gold leads. Following the same strategy we demonstrate the realization of a single-molecule junction containing a purely organic radical. Experiments at low temperature suggest the presence of Kondo correlation implying that the magnetic properties of the molecule are still present after attachment to the electrodes.*

---

Parts of this chapter have been published in Journal of American Chemical Society **138**, 8465 (2016) [1] and in the same journal **140**, 1691 (2018) [2].

One of the common challenges that are encountered while designing molecules suitable for molecular electronic experiments, is the choice of the strategy to bind the molecules to the metallic electrodes. There is a vast library of possibilities of the so called anchoring groups, such moieties are chemical groups with certain affinity to metals, specially to gold. They are responsible for the mechanical stability of the metal-molecule-metal system and the efficiency of the electron injection and collection at the molecule-metal interface. Several different groups have been studied, for example, thiols[3], methylsulfide, amine[4–6] and pyridine[7] among others and careful comparison have been performed.

Recent developments of the break-junction measuring techniques [8–11] have allowed researchers to investigate charge transport through individual molecules. Strategies for contacting molecules to metallic electrodes usually rely on the use of anchoring groups such as thiols,[3], cyano[12], pyridines[7] or amines[4–6] and systematic comparisons have been carried out [13–16]. Recently, new methods have been developed to contact molecules based on a direct carbon-gold bond [17–23]. These methods employ protection groups at the extremities of the molecule that by applying different external stimuli, are removed in the solvent leaving the endstanding carbon atoms free to coordinate directly to the gold atoms of the electrodes. It has been shown that direct carbon-gold bond can give rise to a high molecular conductance.[19].

Molecules composed by a series of phenyl rings, such as oligophenylenes (OP), oligophenylethylenes (OPE) or oligophenylvinyls (OPV) are interesting systems because they possess de-localized orbitals allowing for efficient charge transport. Several research groups have reported on transport through single-molecule junctions with a direct C-Au bond using these conjugated molecular backbones [18–21]. W. Chen *et al.*[19] have studied a family of highly conductive OP(n=1-4) molecules which form a covalent C-Au bond by cleaving  $\text{SnMe}_3$  protecting groups, exposing a methylene ( $\text{sp}^3$ -hybridized carbon). The same research group also reported on the conductance of a para-phenyl (OP1) molecule connected by a  $\text{sp}^2$ -hybridized carbon to the gold using the same  $\text{SnMe}_3$  leaving groups[18]. Hong *et al.* [20] performed measurements on a trimethylsilyl oligophenylethylene (TMS-OPEN, n=1,2,3) family of molecules. Using tetrabutylammonium fluoride (TBAF) as a de-protecting agent the TMS end group was cleaved from the oligophenylethylene backbone leaving a sp-hybridized carbon free to form a Au-C  $\sigma$ -bond. Despite the advantages of the C-Au bonding there are also drawbacks to the reported approaches including the rapid formation of dimers, the need of a de-protecting agent and/or rather toxic precursors as leaving groups.

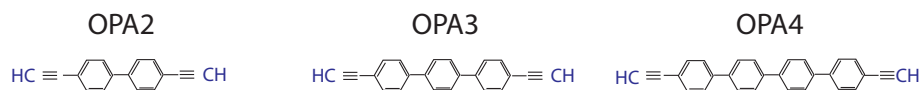


Figure 3.1: Drawings of the measured OPA series.

Here, we report on the measurement of the low-bias conductance on a family of oligophenylene ethylene OPA(n) molecules, displayed in Figure 3.1a, in which the alkynyl end-group ( $\text{R}-\text{C} \equiv \text{C}-\text{H}$ ) acts as anchoring group. These molecules directly form a C-Au bond to the leads by the *in-situ* de-protonation of the acidic C-H proton ( $\text{pK}_a \sim 26$ ) of the alkynyl groups[24–26]. This approach avoids the need of de-protecting agents

or toxic leaving groups. Moreover, the molecules do not have bulky protective groups. Measurements are performed using the mechanically controlled break junction (MCBJ) technique in ambient conditions and show the formation of molecular junctions even after several hours after deposition; the conductance values are of the same order of magnitude as similar molecules with  $sp$ - or  $sp^2$ -hybridized Au-C bonds while being an order of magnitude lower than those using  $sp^3$  Au-C hybridization[18].

### 3.1. CONDUCTANCE MEASUREMENTS

The conductance measurements are carried out in ambient conditions. A drop of a  $28\text{ }\mu\text{M}$  solution of target molecules in dichloromethane is drop casted on an MCBJ device and after the solvent dries up, 2000 conductance vs. electrode displacement traces are measured. In Figure 3.2 the 2D-histograms of OPA( $n$ ,  $n=2-4$ ) are displayed: a) OPA2, b) OPA3, c) OPA4. In each plot we can distinguish two main features. Namely, a region of exponential decay of the conductance between 0 and 0.5 nm, covering the range from  $1 \times 10^{-4} G_0$  to the noise level (depicted with black lines in the figure); we attribute these breaking traces to empty junctions. The second characteristic is a region where the conductances decay slowly upon stretching. Examples of individual traces in this regime are displayed in the insets of Figure 3.2. OPA3 (Figure 3.2b) presents this region between displacements ranging from 0 to 1 nm with a conductance around  $10^{-3} G_0$ . For OPA4 (Figure 3.2c) the same behavior is observed between 0 and 1.5 nm with a conductance around  $10^{-4} G_0$ . OPA2 requires a closer look, because it shows two such regions; the first one, around  $10^{-3} G_0$ , is characterized by displacements shorter than 0.6 nm and a second high-count region is present near  $10^{-5} G_0$  for traces between 0.5 and 2.5 nm. An interesting feature is that most of the traces show slanted plateaus rather than flat ones, which are usually seen in molecular wires.

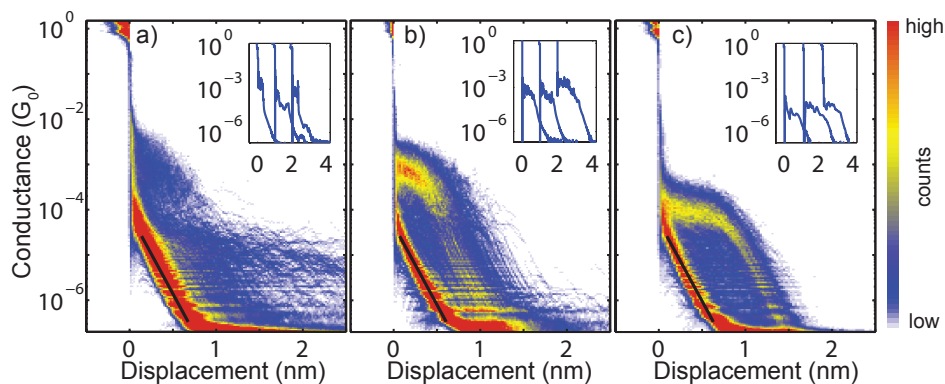


Figure 3.2: Two-dimensional conductance vs. electrode displacement histograms constructed from 2000 consecutive breaking traces measured at room-temperature in air with a 0.1 V bias voltage applied and a ramp rate of 10 nm/s. Junctions exposed to a  $28\text{ }\mu\text{M}$  molecule solution in dichloromethane for (a) OPA2, (b) OPA3, and (c) OPA4. Insets show examples of individual conductance traces with plateau-like features assigned to the presence of a molecule; traces are offset in the displacement direction.

We have also performed the same experiment on a phenyl ethylene (OPA1) molecule



but we did not observe clear molecular signatures; the molecular structure and histograms are shown in Figure 3.3. In reference [20] a similar single phenyl ring with an unprotected alkynyl anchoring group was measured: junction formation was not observed there either. On the other hand the same backbone with a TMS protecting group showed molecular features.

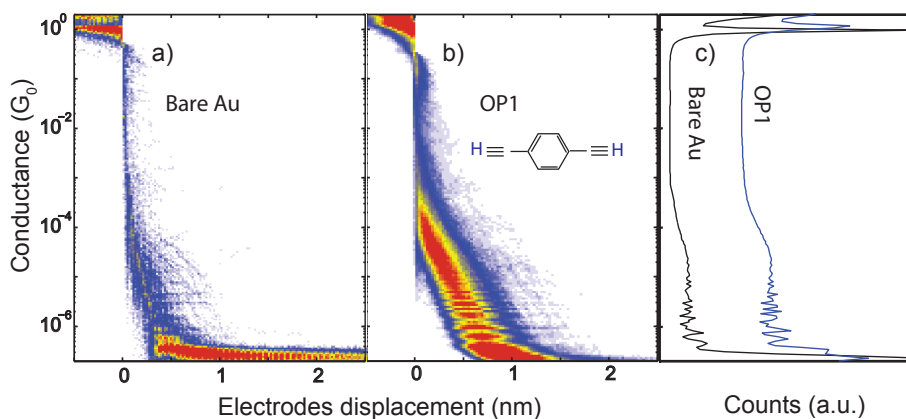


Figure 3.3: Conductance vs. electrode displacement two-dimensional histograms of a) a bare gold sample (1000 traces) and b) OPA1 molecule (2000 traces) in which no clear plateaus or regions of highly probable conductance can be identified. c) Normalized one-dimensional conductance histogram of gold (in black) and OPA1 (blue); the curves are offset for clarity. For OPA1 no features are visible in the one-dimensional histogram, indicating a very low probability of junction formation.

To determine the conductance value of the OPA(n) molecules we used the conductance histograms without any data selection (Figure 3.4a). By fitting a log-normal distribution to the conductance regions in which molecular features are observed (dotted lines in Figure 3.4a), we extract the most probable molecular conductance value for the three molecules. To ensure reproducibility at least two samples of were measured. The values of the obtained conductance are summarized in Table 5.1 and the average values are plotted with blue diamonds as a function of molecular length in Figure 3.4b. For OPA2, two values of conductance are listed; one at high conductance and one at low conductance, corresponding to the two features appearing in the two-dimensional histogram. We attribute the highest one to the molecular conductance of the molecule itself, whereas the lower value with plateau lengths exceeding the length of the molecule can be associated to the presence of dimers of the molecule[20, 21] or to  $\pi$ - $\pi$  stacking of two molecules each attached to one electrode[27]. For this molecule, we have analyzed the time evolution of the conductance vs. displacement curves in time to investigate whether the dimer formation occurs more frequently as times progresses. We have not found a clear indication for such a trend (see Figure 3.5): after four hours of measurements high and low-conductance traces are still present.

A striking characteristic of Figure 3.4b is the non-exponential decay of the conductance with molecular length (open blue diamonds) for the OPA(n=2,3,4) series. The

Molecule	Conductance ( $G_0$ )			
OPA2	$6.6 \cdot 10^{-4}$	$1.0 \cdot 10^{-5}$	$4.1 \cdot 10^{-4}$	$7.8 \cdot 10^{-6}$
OPA3	$4.6 \cdot 10^{-4}$		$4.4 \cdot 10^{-4}$	
OPA4	$5.7 \cdot 10^{-5}$		$3.9 \cdot 10^{-5}$	

Table 3.1: Most probable molecular conductance for the series of OPA(n) molecules extracted from the one-dimensional conductance histograms. The first column contains the values obtained with a concentration of  $28 \mu\text{M}$  and the values in the second column were obtained with a saturated concentration of molecules, meaning  $4.95 \text{ mM}$  for OPA2,  $0.36 \text{ mM}$  for OPA3 and  $28 \mu\text{M}$  for OPA4. The values plotted in Figure 3.4 are the average of the two measurements of each molecule. For OPA2, two values are listed, one at high conductance and one at low conductance (see text for a discussion on these values).

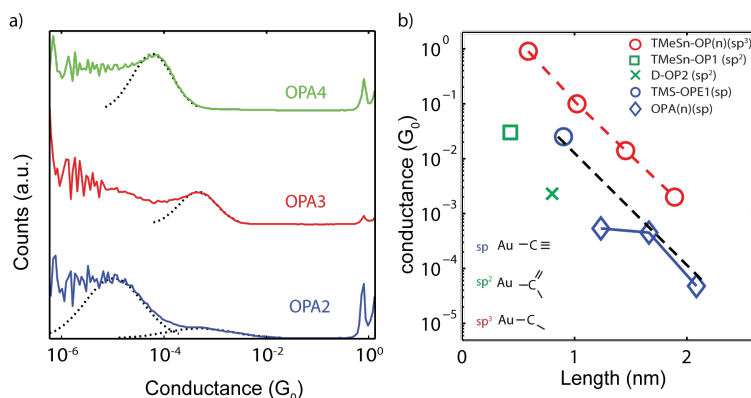


Figure 3.4: a) One-dimensional conductance histograms using a logarithmically binning (solid line) for OPA2 (blue), OPA3 (red) and OPA4 (green). Dotted lines represent log-normal fittings around the regions of high counts in the histograms and are used to extract the most probable conductance value. b) Conductance as a function of molecular length for OPA(n) (blue) compared to other molecules in the literature that form direct C-Au bonds. Different families present different hybridization of the last carbon. Red open circles represent molecules with direct  $sp^3$  C-Au bonding from reference [19]; the green square is a single benzene ring connected to gold through a  $sp^2$ -hybridized carbon; [18] the open blue circle corresponds to OPE1 connected to gold via a  $sp$ -hybridized carbon from the series in reference [citenumTMSOPE]; the green x is a diazonium terminated OP2 which is electrochemically deprotected and connected through an  $sp^2$ -hybridized carbon that was studied in [citenumHines2013]. The black dashed line connects the OPA(n= 3,4) and OPE1 in reference [19]. Note, that the structure of OPE1 corresponds to the same structure as OPA1 in this study when contacted to the gold electrodes.

fact that the conductance of OPA2 has approximately the same value as OPA3 is an unexpected result, especially because measurements on the same molecular backbone (oligophenylene) have shown an exponential decay for different anchoring groups and measurement techniques [19, 28–30], with  $\beta \approx 0.45 \text{ \AA}^{-1}$ . An interesting observation is that the de-protonated OPA1 has the same structure as the de-protected TMS-OPE1 in reference [20] when contacted to the electrodes. If we take into account this conductance value an exponential decay among TMS-OPE1, OPA3 and OPA4 (black dashed line in Figure 3.4b) is found.

To put our results in a broader context we compare our data with other molecules

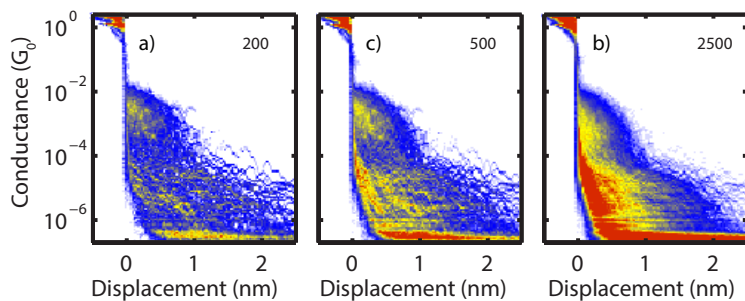


Figure 3.5: Conductance versus electrode displacement two-dimensional histograms of OPA2 considering the first a) 200, b) 500 and c) 2500 traces. The measurement were carried out during 4 hours; the same regions of high counts can be observed in all of them.

that also form a direct Au-C bonds to the leads. The conductance vs. length dependence of these molecular families is displayed in Figure 3.4b as well. We observe that the conductance of molecular chains which are connected via  $sp^3$ -hybridized carbon atoms is higher than the corresponding chain connected by  $sp$ -hybridized carbon atoms. For the single benzene ring case this observation was already discussed in reference [19] when comparing  $sp^3$ - and  $sp^2$  hybridization.

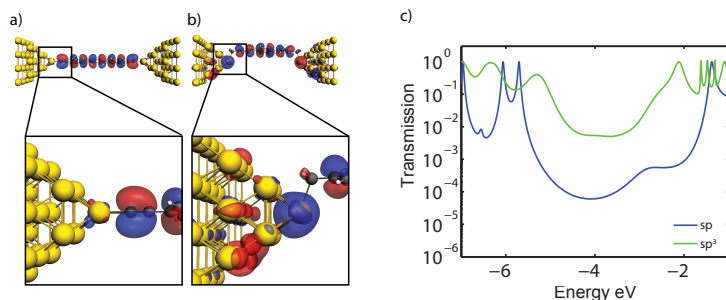


Figure 3.6: Diagram of the HOMO of a OP3 attached to gold atoms through a)  $sp$ - and b)  $sp^3$ -hybridized carbon. Zoom ins (lower panels) show the same orbitals near the Au-C interface. c) Transmissions calculated using DFT+NEGF for the OP3 molecule with  $sp$ - (blue line) and  $sp^3$ -hybridized (green line) linking to the gold.

Theoretical calculations were performed using density functional theory (DFT) methods to compute the geometries and electronic structure of OP  $n$  ( $n=2,3,4$ ) chains contacted to gold electrodes through  $sp$ - and  $sp^3$  hybridized carbon atoms, which correspond to OPA  $n$  and SnMe-OP $n$  inside the junction, respectively. The calculation were combined with the non-equilibrium Green's function (NEGF) formalism to obtain the transmission functions; self-energies were corrected using the DFT + $\Sigma$  method [4]. A detailed explanation of the methods used can be found in reference [1].

Figure [3.6] a) and b) displays the HOMO orbital of an OP3 molecule contacted via

a  $sp$  and  $sp^3$  hybridized carbon atom respectively, the lower panels are a closeup of the molecule electrode contacting region. It is clear that in both cases the orbitals are de-localized through the whole molecule but regardless of the similarities there are distinguishable characteristic that characterize each of them. The Amplitude of the wave function around the linking gold is much smaller in the case of  $sp$ -hybridization. A less evident difference lies in the symmetry of the of the atomic orbital of the gold atom that is involved in the wave function. In the case of  $sp$  hybridization, the main contribution of the gold to the wave function comes from the  $5d$  orbital, while in the case of the  $sp^3$ -hybridized carbon, the main contribution comes from the  $6s$  orbital of the gold.

When we look into the transmission functions of, for example, OP3 contacted to the electrode in the two scenarios previously described we distinguish several differences. First the value of the transmission function is higher in the case of the  $sp^3$  in most of the off resonant range. Secondly the shape of the resonance peaks is sharper in the case of  $sp$ -hybridization, this indicates a lower coupling between the electrodes and the molecule in accordance with the observation about the wave function's amplitude. The calculations further support our findings that the conductance of molecules with the same number of benzene rings differs greatly depending on the hybridization of the end standing carbon atoms:  $sp^3$ -hybridization gives a higher conductance, mainly because the favorable coupling between the gold electrodes and the molecule.

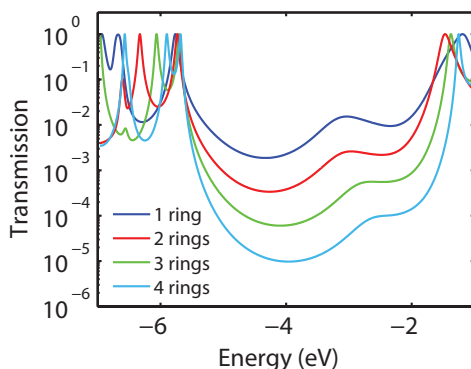


Figure 3.7: Transmission computed using NEGF-DFT for the four OP( $n$ ) series reported in this study. The distances between consecutive transmission are the same (in log scale) for level alignments between  $-5$  and  $-2$  eV.

Ultimately we analyze the dependence of the transmission on the length of the molecular backbone. In figure [3.7] the transmission function of the series OPA  $n$  ( $n=1-4$ ) contacted to gold pyramidal electrodes is shown. We observe an exponential dependence of the transmission on the molecular length. The odd behavior of the OPA2 conductance values, therefore, may be associated with degrees of freedom not captured in the calculations. For example, a non-exponential decay of conductance has also been observed for oligo-thiophene molecules[31, 32], and in that case it was attributed to the ability of a 4-thiophene to rotate toward a more conjugated configuration compare to

the 3-tiophene that cannot rotate. Another explanation may originate from the binding configuration itself. In the literature it has been proposed that alkynyl groups in contact with gold may form a rather “undetermined” binding configuration displaying a more  $sp^2$  like character; [24, 33–35] the smaller the molecule, the more likely this is expected to occur. [36] This suggestion is in line with the results displayed in Figure 3.4 which show that a line parallel to the black and red drawn lines through the  $sp^2$ -hybridized OP1 and diazonium terminated OP2 data points (open square and the green x respectively). Interestingly, it is close to the OPA2 conductance value from our study.

In conclusion, we have demonstrated that it is possible to contact single molecules through a covalent  $\sigma$ -C-Au bond formation directly from deprotonating alkynyl anchoring groups. This method removes the need for cleavage of bulky protecting groups and the use of deprotection by an external agent. In our approach, the molecules connect to the gold leads through an  $sp$ -hybridized carbon atom in such a way that it mainly couples to the 5d orbital of the gold. The involvement of the 5d orbital leads to a lower electronic coupling than for  $sp^3$ -hybridized carbon, which involves the 6s orbital of gold.

### 3.2. FUNCTIONALIZED MOLECULES: RADICALS

As discussed before the formation of covalent highly directional  $\sigma$ -bonded C-Au junctions can provide high conductance at the single-molecule level. Different anchoring groups such as trimethyl tin ( $\text{SnMe}_3$ )-terminated polymethylene chains [18] and silyl-protected acetylenes [7] have been employed for this aim. In the case of the silyl groups there is a need of *in-situ* applying desilylation chemistry to form the Au-C bond. On the contrary, the terminal acetylene ( $\text{R-C}\equiv\text{C-H}$ ) group spontaneously forms stable C-Au bonds. As shown in the previous sections this strategy has already been used to prepare self-assembled monolayers (SAMs) on Au (flat [6] and on Au nanoparticles [37]) and on Ag [38, 39]. Charge transport measurements through some of these SAMs have been performed in large-area molecular junctions (such as  $\text{Ga}_2\text{O}_3/\text{E}_{\text{GaIn}}$  as top electrode), in an STM break-junction, [40] and with electrochemical scanning tunneling spectroscopy [41]. However, up to now, single-molecule measurements through bridges incorporating a functional moiety linked through a  $\text{-C}\equiv\text{C-Au}$  bond at room-temperature (RT) are scarce.

In this section, we employ the highly persistent perchlorotriphenylmethyl (PTM) radicals as a functional moiety. The charge transport mechanism in the tunneling regime was previously studied in PTM SAMs covalently grafted to Au through a thiol group showing that the single-unoccupied molecular orbital (SUMO) played a crucial role in the transport enhancing the junction conductivity [42–44]. Electrochemical gating was also used to achieve a highly effective redox-mediated current enhancement [45]. Being all-organic, PTM radicals present an intrinsic magnetic moment, low spin-orbit coupling and small hyperfine interactions. These attractive redox and magnetic properties, absent in transition metal-based magnetic compounds, have recently attracted attention in molecular (spin)electronics [46–48] where long spin coherence times are required to preserve the information encoded in the electronic spin. The individual spin of different radical species has been detected in low-temperature electron transport measurements by means of Kondo correlations in molecular junctions [49]. The PTM radical has proved to be robust in the junction thanks to the encapsulation of the radical

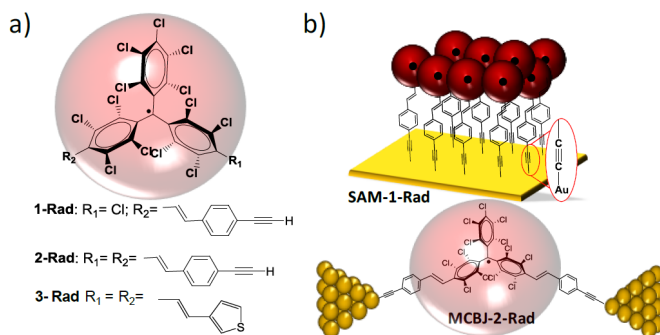


Figure 3.8: a) Chemical structure of the PTM radicals employed in this study. b) Scheme of the SAM based on 1-Rad (top) and of the MCBJ with 2-Rad bridging the two electrodes (bottom).

spin in a chlorinated-phenyl shell. Moreover, it has been shown that the magnetic state of PTM-based polyradicals can be mechanically modified [50] and electrically gated to form the basis of a quantum SWAP gate [50]. Similar OPE-based radicals have shown large magneto-resistance effects that could be used to tune charge transport in metal-molecule junctions [51]. Moreover, although it remains still to be proved, organic radicals could act as spin filters [52]. Aside from the magnetic properties, the redox properties of similar organic radicals have been used to enhance charge transport in molecular junctions [53]. All these intriguing properties depend up to some extent on the reproducibility and strength of the bond radical to the electrodes, a key-step still to improve.

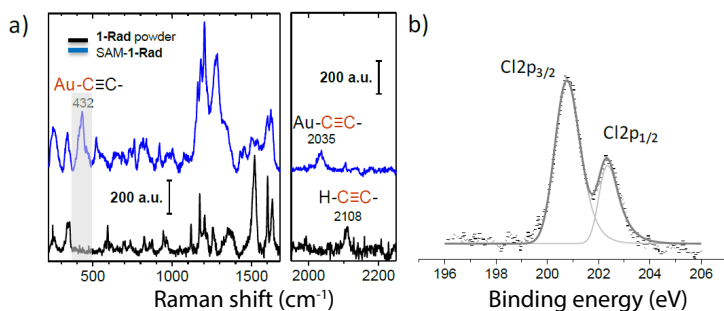


Figure 3.9: Characterization of SAM-1-Rad. a) Raman spectrum of 1-Rad in powder (black) and SAM-1-Rad (blue). b) High resolution Cl2p XPS spectrum.

In this section, we report on characterization of two novel PTM radical derivatives bearing one (1-Rad) and two (2-Rad) acetylene terminated groups (Fig. 3.8). Thanks to the stability of the alkynyl group, compared to the -SH one, there is no need of protecting and deprotecting it during the deprotonation and oxidation reactions required to generate the radical species. Additionally, these linkers once formed are stable without showing signs of oxidation in time, as it is the case of most of the thiolated compounds [54–56].

SAMs based on 1-Rad (Fig. 3.8 b) were successfully prepared. Surface characterization techniques (XPS, Raman) show the formation of a very stable metal-molecule covalent bond where the unpaired spin is preserved after bonding. Molecular junctions based on 2-Rad (Fig. 3.8 b) were prepared and compared with the equivalent bisthiophene-terminated derivative (PTM-bt3-Rad, Fig. 3.8 a) that shares the same functional core but is functionalized with thiophene anchoring groups[49]. Room-temperature electron transport measurements and the statistical analysis show that 2-Rad form a very stable bond with a better defined anchoring geometry when compared to the S-Au bond in the PTM-bt3-Rad, while still having similar current levels. Low temperature current-voltage (IV) measurement help to on 2-Rad show zero-bias peaks consistent with Kondo correlations. These findings are supported by density functional theory (DFT) and quantum transport calculations that predict a C-Au bond three times stronger than the S-Au and with a lower anchoring geometry variability.

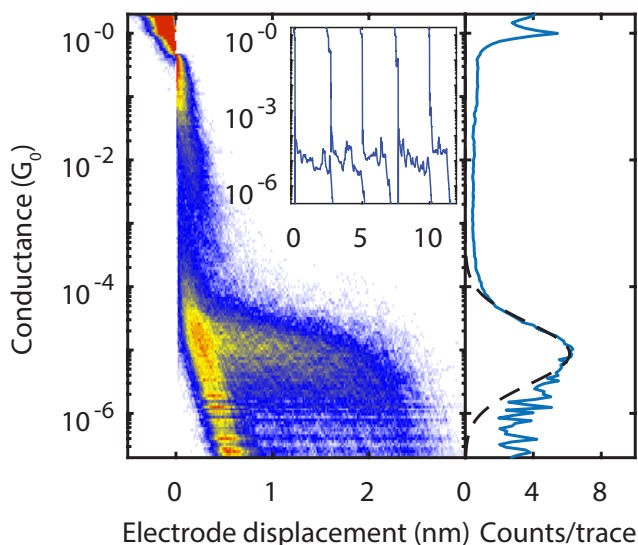


Figure 3.10: a) Two-dimensional conductance vs electrode displacement histogram of the 2-Rad molecule constructed from 2500 consecutive traces at room temperature, 0.2 V of bias voltage and an electrode speed of 6 nm/s. The inset shows five selected individual traces. b) One-dimensional conductance histogram for 2-Rad constructed by integrating over the displacement in a). The black dashed line corresponds to a log-normal fitting of the conductance distribution without data selection.

First, self-assembled monolayers (SAMs) of 1-Rad were prepared on Au(111) to investigate the formation of the C-Au bond. The SAM formation conditions were optimized to maximize the surface coverage. SAMs were prepared under inert conditions to avoid the possible oxidation of the alkyne group in presence of O<sub>2</sub> and Au, as previously reported [57]. At this point, it is worth mentioning the reactivity of the terminal acetylenes with the gold substrate. Maity *et al.* [24] studied the functionalization of gold clusters with



a series of terminal alkynes derivatives by means of a various spectroscopic methods. They demonstrated the binding motif and the loss of the terminal H through the heterolytic deprotonation of the alkyne as the key mechanism for the binding of the alkynyl group to gold [58]. Furthermore, Raman spectroscopy has been used by several authors to identify the covalent C-Au formation [20, 59, 60]. Taking all this into account, SAM-1-Rad was characterized by Raman spectroscopy (Fig. 3.9 a). The spectrum of the 1-Rad in powder was also acquired for comparison. The weak band corresponding to the C-C triple bond stretching is observed both in powder ( $2108\text{ cm}^{-1}$ ) and red-shifted on surface ( $2035\text{ cm}^{-1}$ ) confirming the integrity of the alkyne group after the monolayer formation. The displacement of the above-mentioned band is in agreement with previous studies describing the reactivity of terminal alkynes on gold [24]. Remarkable is the appearance of a new sharp band at  $432\text{ cm}^{-1}$  in the SAM spectrum. According to literature, [20, 59, 60] this band can be assigned to the characteristic C-Au stretching mode, and constitutes a strong proof of the covalent character of the binding between the PTM 1-Rad and the gold surface. These observations point to an up-right configuration of 1-Rad maintaining the directional triple bond and losing a hydrogen atom. In addition, X-ray photoelectron spectra (XPS) confirmed the presence of chlorine (Fig. 3.9 b). The Cl2p spectrum showed the typical doublet corresponding to Cl<sub>2p1/2</sub> and Cl<sub>2p3/2</sub> at 202.4 eV and 200.8 eV, respectively.

### 3.2.1. CONDUCTANCE MEASUREMENTS

We have performed room-temperature charge transport measurements through individual 2-Rad molecules using the MCBJ technique described in Refs [1, 23]. Briefly, a 2  $\mu\text{L}$  drop of a 50  $\mu\text{M}$  solution of the molecule in dichloromethane was drop casted on a clean MCBJ sample. Subsequently, the setup was pumped down until the pressure reached  $5 \times 10^{-6}$  mbar to avoid degradation of the target molecule due to the presence of oxygen. Only then the fast breaking experiment was performed by measuring the conductance ( $G=I/V$ ) while the electrodes are moved apart and reconnected thousand of times.

Figure 3.10 a) shows a two-dimensional conductance vs electrode displacement histogram for 2-Rad molecules. The histogram is made using 2500 consecutive traces recorded at an electrode speed of 6 nm/s and an applied bias voltage of 0.2 V. Two characteristic features are present: first, the conductance drops exponentially from  $10^{-4} G_0$  to the noise level for electrode displacements between 0 and 0.7 nm with a characteristic length of 0.5 nm corresponding to the left peak in the length histogram in Fig. 3.11. These traces are attributed to empty junctions with no molecules bridging the electrodes. The second feature is a single flat plateau with a characteristic length of 2.3 nm after (right peak in fig. 3.11) which the conductance drops abruptly. Individual examples of these traces can be observed in the inset of Fig. 3.10 a). The plateau is indicative of the formation of a molecular junction that breaks when the gap between the electrodes is too wide for the 2-Rad molecule to bind to both electrodes. Interestingly, the plateau length plus the snap-back correction (0.5 nm) approximately matches the length of the relaxed 2-Rad molecule bonded to Au (2.7 nm).

The conductance value of the plateau in Fig. 3.10 a) is determined from the one-dimensional conductance histogram shown in Fig. 3.10 b). The dotted line is a log-normal distribution fit around the conductance regions displaying molecular features.



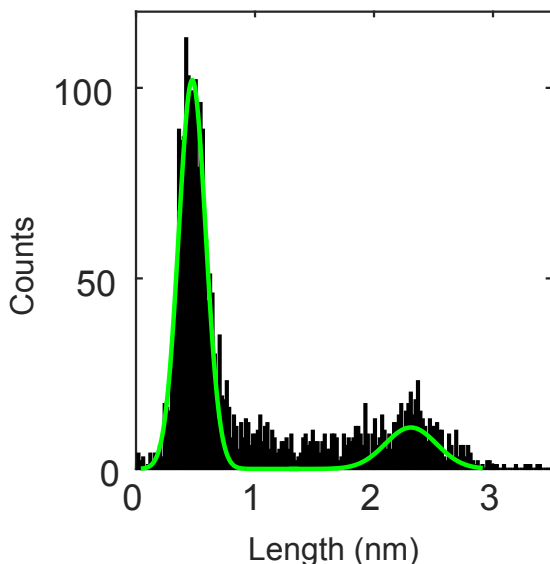


Figure 3.11: Length histogram of the traces compiled in Fig. 3.10. The green solid line correspond to a Gaussian peaks characterized by a position and full width half maximum of 0.47 and 0.28 nm in the case of the left peak and 2.3 and 0.36 nm for the right peak.

The most probable conductance value for the 2-Rad molecule is  $8.8 \times 10^{-6} G_0$ . To gain a deeper insight, we have compared these results with the conductance characteristics of a similar PTM moiety functionalized with thiophene anchoring groups measured with STM-BJ technique (measurement performed by Alexander Rudnev's group at University of Bern). In the latter case, the conductance values appear more spread between two conductance features at  $G_{\text{high}} = 1 \times 10^{-4} G_0$  and  $G_{\text{low}} = 4 \times 10^{-6} G_0$ . Moreover, the size of the plateau (plus snap-back) extends only up to 0.95 nm, whereas the length of the fully stretched molecules is 1.7 nm. These results point to a stronger mechanical bond in the case of 2-Rad. In addition, 2-Rad provides a better-defined molecule-electrode anchoring geometry when compared with the thiophene anchoring group. Note, that the strength in the mechanical bond is not straightforwardly translated into a higher conductance.

To evaluate the presence of the magnetic moiety we performed IV measurements using a low-temperature set-up. It is expected that a magnetic molecule generates a localized Kondo cloud at the Fermi energy, creating a state through which charge can pass [49]. That would give rise to a zero-bias peak in the  $dI/dV$  curve.

Using a dipstick set-up we cool down a sample on which a fresh solution of 2-Rad was dropcasted as described before, down to liquid helium temperatures. To improve the thermal contact helium exchange gas was used so that the actual temperature of the sample was around 6 K. The experiment consisted of measuring the IV characteristic

<sup>1</sup>These measurements have been performed in Berns University by the group of Prof. Alexander Rudnev.

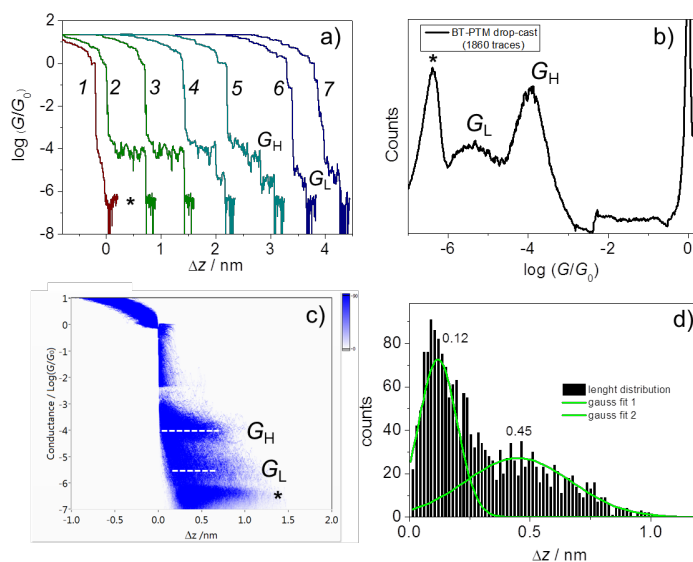


Figure 3.12: a) Individual conductance traces without and with molecular plateaus for PTM-bt3-Rad, obtained by STM-BJ with  $V = 0.1$  V and a stretching rate of  $87 \text{ nm s}^{-1}$ . b) 1D and c) 2D conductance histograms for PTM-bt3-Rad. The asterisk indicates the noise level of the set-up. The small spike at  $\log(G/G_0) \approx -2.2$  in panel b) is an artefact related to the switching of the amplifier stage. d) Characteristic length distribution between  $10^{-4.6} G_0$  and  $10^{-0.3} G_0$ . The measurements were performed at room-temperature in argon atmosphere after drop casting  $20 \mu\text{L}$  of  $0.08 \text{ mM}$  PTM-bis-thiophene in dichloromethane and drying in a gentle argon stream.<sup>1</sup>

of the junction while breaking. Figure 3.13a) show an example of a breaking trace that shows molecular features. The spacing between each point is approximately 0.01 nm. In the same figure three IV b), c) and d) are displayed. The three of them share a characteristic feature: a zero-bias peak in the  $dI/dV$ , depicted in panels e), f) and g). The sharp dip at zero-bias is an electronic artifact caused by the logarithmic amplifier that was used.

An interesting characteristic that repeats in the cases of the presence of a zero-bias peak is that the conductance values measured at the points that shows such feature is several order of magnitude higher than the conductance value measured at room-temperature. The amount of traces that shows zero-bias peak is around 10 % of the traces that showed molecular features. This provides an indication that the magnetic nature of 2-Rad is intact there after been contacted by gold electrodes. We point out that the the Kondo interpretation of the peak is not the only one but it draws a consistent picture between the molecular structure and the electronic measurement on the single molecules and therefore provides an indication that the spin degree of freedom remains active after connecting the molecule to the electrodes.

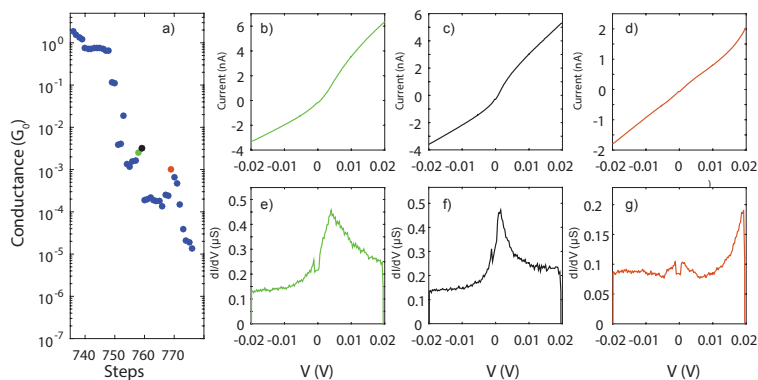


Figure 3.13: a) Individual conductance trace of 2-Rad, obtained using a low temperature (6 K) MCBJ technique. For each point a IV curve was measured. b), c) and d) IV curves measured during the breaking on the points highlighted with the same colors in a). e), f) and g) are the corresponding  $dI/dV$  curves. The sharp dip at zero-bias is an electronic artifact caused by the logarithmic amplifier that was used.

### 3.2.2. THEORETICAL CALCULATION

The strength of the mechanical bond between the molecule and Au is quantified by means of the maximum rupture force  $F$  and of the bond dissociation energy  $D$  [61]. These cannot be directly obtained from our experiments, but they can be estimated by calculating the potential energy surface (PES) for the stretched bond with DFT, and then fitting the PES with a Morse potential. We find  $F = 3.05$  nN and  $D = 3.5$  eV for the Au-C bond in the bridge configuration. Furthermore, such an Au-C bond has to be elongated by about 0.5 Å under an applied force as large as 3.85 nN for the Au-C bond-breaking activation energy to equal room temperature. This means that in RT-MCBJs experiments the Au-C bond will not break until it is stretched up to 0.3 Å. Overall the results support the obser-

variations about the mechanical junction stability in Figure 3.14. In contrast, a thiophene linker establishes no covalent bond with a flat Au surface, so it is physisorbed. A covalent bond can only be established between the thiophene S atom and an Au adatom on a corrugated surface. In this case, for the adatom-S bond,  $F$  and  $D$  are just 0.45 nN and 0.3 eV, respectively, and the bond-breaking activation energy equals  $K_b T$  (where  $K_b$  is the Boltzmann constant) when the bond is stretched by less than 0.1 Å. For comparison, we also point out that for the S-Au bond of standard thiol linkers used in previous experiments [62],  $F$  and  $D$  are about three times smaller than for the Au-C bond, i.e.  $F=1.45$  nN and  $D=1.26$  eV.

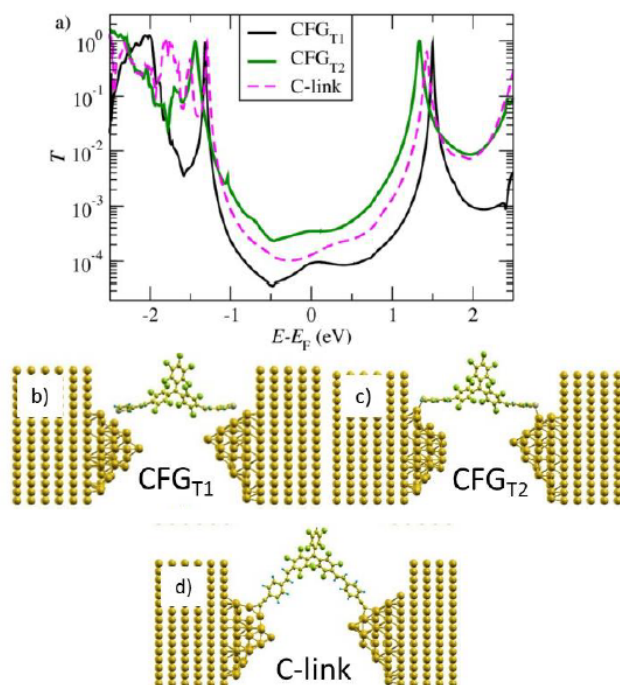


Figure 3.14: a) Transmission as a function of energy for different atomic configurations (CFGs): b) CFG T1 and c) CFG T2 are two typical structures expected to be found in high temperature break-junction measurements with PTM-bisthiophene and Au; d) with 2-Rad directly bonded via C-Au link.

We also performed charge transport calculation based on DFT and non-equilibrium Green function (NEGEF) for 2-Rad and PTM-bt3-Rad. The results are displayed in Fig. 3.14. PTM-bt3-Rad can contact either a rather flat part of the electrode or a protruding adatom, and we model these two situations by considering different atomic configurations (CFGs), for instance configuration CFG T1 and CFG T2 in Fig. 3.14 b) and c). In the first case, as outlined above, the bond to the Au is non-covalent, and the molecule can therefore slide on the Au tip as the junction is elongated. The conductance is quite low due to the weak electronic coupling between Au and the molecule. For more corrugated Au tips, the covalent bond between the thiophene S atom and the protruding Au adatom

results in an increased electronic coupling and therefore in a higher conductance. This is in agreement with the experimental results, where for PTM-bt3-Rad a quite wide range of conductances between a higher and a lower value is found.

For 2-Rad, whenever the relative displacement of the electrodes is in the plateau region of Figure 3.10, the linkers establish a strong covalent bond with the electrodes, where the C atom is on the bridge site between two Au atoms (Fig. 3.14 d). The fact that the molecule binds to the electrodes with such a locally well-defined C–Au bond, independently of the overall junction geometry, drastically reduces the variability in conductance values. The calculated transmission curve lies in an intermediate range between the ones for CFG T2 and CFG T1. The low bias conductance corresponds to the transmission at the Fermi energy, for which we obtain a value around  $T \approx 10^{-4}$ . This is on the upper end of the experimentally measured conductance peak (Fig. 3.10).

### 3.2.3. CONCLUSIONS

In conclusion, the functionalization of a PTM organic radical with alkynyl end groups has led to the formation of a robust covalent binding between these electroactive and paramagnetic molecules and Au. Throughout a detailed comparison with a similar thiophene functionalized derivative we show that the Au–C bond provides a more robust and better-defined anchoring geometry but a lower conductance value as supported by DFT calculations. Our results contribute to the efforts to incorporate active elements in molecular devices, for examples the spin degree of freedom and enhance the performance of single-molecule devices in particular.

## REFERENCES

- [1] I. J. Olavarria-Contreras, M. L. Perrin, Z. Chen, S. Klyatskaya, M. Ruben, and H. S. J. van der Zant, [*C–Au covalently bonded molecular junctions using nonprotected alkynyl anchoring groups*, *Journal of the American Chemical Society* **138**, 8465 (2016).
- [2] F. Bejarano, I. J. Olavarria-Contreras, A. Droghetti, I. Rungger, A. Rudnev, D. Gutiérrez, M. Mas-Torrent, J. Veciana, H. S. J. van der Zant, C. Rovira, E. Burzuri, and N. Crivillers, *Robust organic radical molecular junctions using acetylene terminated groups for c–au bond formation*, *Journal of the American Chemical Society* **140**, 1691 (2018).
- [3] Z. Huang, F. Chen, P. A. Bennett, and N. Tao, *Single molecule junctions formed via Au–thiol contact: Stability and breakdown mechanism*, *Journal of the American Chemical Society* **129**, 13225 (2007).
- [4] S. Y. Quek, L. Venkataraman, H. J. Choi, S. G. Louie, M. S. Hybertsen, and J. B. Neaton, *Amine - Gold linked single-molecule circuits: Experiment and theory*, *Nano Letters* **7**, 3477 (2007).
- [5] Z. Li and D. S. Kosov, *Nature of well-defined conductance of amine-anchored molecular junctions: Density functional calculations*, *Physical Review B* **76**, 035415 (2007), 0702507.

- [6] M. S. Hybertsen, L. Venkataraman, J. E. Klare, A. C. Whalley, M. L. Steigerwald, and C. Nuckolls, *Amine-linked single-molecule circuits: systematic trends across molecular families*, *Journal of Physics: Condensed Matter* **20**, 374115 (2008).
- [7] M. Kamenetska, S. Y. Quek, A. C. Whalley, M. L. Steigerwald, H. J. Choi, S. G. Louie, C. Nuckolls, M. S. Hybertsen, J. B. Neaton, and L. Venkataraman, *Conductance and geometry of pyridine-linked single-molecule junctions*, *Journal of the American Chemical Society* **132**, 6817 (2010).
- [8] K. Moth-Poulsen and T. Bjørnholm, *Molecular electronics with single molecules in solid-state devices*. *Nature Nanotechnology* **4**, 551 (2009).
- [9] A. Nitzan and M. A. Ratner, *Electron Transport in Molecular Wire Junctions*, *Science* **300**, 1384 (2003), 0208239 .
- [10] S. V. Aradhya and L. Venkataraman, *Single-molecule junctions beyond electronic transport*. *Nature Nanotechnology* **8**, 399 (2013).
- [11] F. Schwarz and E. Lörtscher, *Break-junctions for investigating transport at the molecular scale*, *Journal of Physics: Condensed Matter* **26**, 474201 (2014).
- [12] M. Kiguchi, S. Miura, K. Hara, M. Sawamura, and K. Murakoshi, *Conductance of a single molecule anchored by an isocyanide substituent to gold electrodes*, *Applied Physics Letters* **89**, 213104 (2006), 0610388 .
- [13] F. Chen, X. Li, J. Hihath, Z. Huang, and N. Tao, *Effect of anchoring groups on single-molecule conductance: Comparative study of thiol-, amine-, and carboxylic-acid-terminated molecules*, *Journal of the American Chemical Society* **128**, 15874 (2006).
- [14] I. S. Kristensen, D. J. Mowbray, K. S. Thygesen, and K. W. Jacobsen, *Comparative study of anchoring groups for molecular electronics: structure and conductance of Au-S-Au and Au-NH(2)-Au junctions*. *Journal of physics. Condensed matter* **20**, 374101 (2008).
- [15] L. A. Zotti, T. Kirchner, J. C. Cuevas, F. Pauly, T. Huhn, E. Scheer, and A. Erbe, *Revealing the role of anchoring groups in the electrical conduction through single-molecule junctions*, *Small* **6**, 1529 (2010).
- [16] R. Frisenda, S. Tarkuç, E. Galán, M. L. Perrin, R. Eelkema, F. C. Grozema, and H. S. J. van der Zant, *Electrical properties and mechanical stability of anchoring groups for single-molecule electronics*, *Beilstein Journal of Nanotechnology* **6**, 1558 (2015).
- [17] D. Millar, L. Venkataraman, and L. H. Doerrer, *Efficacy of Au -Au contacts for scanning tunneling microscopy molecular conductance measurements*, *The Journal of Physical Chemistry C* **111**, 17635 (2007).
- [18] Z.-L. Cheng, R. Skouta, H. Vazquez, J. R. Widawsky, S. Schneebeli, W. Chen, M. S. Hybertsen, R. Breslow, and L. Venkataraman, *In situ formation of highly conducting covalent Au-C contacts for single-molecule junctions*. *Nature Nanotechnology* **6**, 353 (2011).

- [19] W. Chen, J. R. Widawsky, H. Vazquez, S. T. Schneebeli, M. S. Hybertsen, R. Breslow, and L. Venkataraman, *Highly Conducting  $\pi$ -Conjugated Molecular Junctions Covalently Bonded to Gold Electrodes*, *Journal of the American Chemical Society* **133**, 17160 (2011).
- [20] W. Hong, H. Li, S. X. Liu, Y. Fu, J. Li, V. Kaliginedi, S. Decurtins, and T. Wandlowski, *Trimethylsilyl-terminated oligo(phenylene ethynylene)s: An approach to single-molecule junctions with covalent Au-C  $\sigma$ -bonds*, *Journal of the American Chemical Society* **134**, 19425 (2012).
- [21] J. R. Widawsky, W. Chen, H. Vazquez, T. Kim, R. Breslow, M. S. Hybertsen, and L. Venkataraman, *Length-dependent thermopower of highly conducting Au-C bonded single molecule junctions*, *Nano Letters* **13**, 2889 (2013).
- [22] T. Hines, I. Díez-Pérez, H. Nakamura, T. Shimazaki, Y. Asai, and N. Tao, *Controlling formation of single-molecule junctions by electrochemical reduction of diazonium terminal groups*, *Journal of the American Chemical Society* **135**, 3319 (2013).
- [23] A. M. Ricci, E. J. Calvo, S. Martin, and R. J. Nichols, *Electrochemical scanning tunneling spectroscopy of redox-active molecules bound by Au-C bonds*, *Journal of the American Chemical Society* **132**, 2494 (2010).
- [24] P. Maity, S. Takano, S. Yamazoe, T. Wakabayashi, and T. Tsukuda, *Binding motif of terminal alkynes on gold clusters*, *Journal of the American Chemical Society* **135**, 9450 (2013).
- [25] Y.-Q. Zhang, J. Björk, P. Weber, R. Hellwig, K. Diller, A. C. Papageorgiou, S. C. Oh, S. Fischer, F. Allegretti, S. Klyatskaya, M. Ruben, J. V. Barth, and F. Klappenberger, *Unusual deprotonated alkynyl hydrogen bonding in metal-supported hydrocarbon assembly*, *The Journal of Physical Chemistry C* **119**, 9669 (2015).
- [26] N. Kepčija, Y. Q. Zhang, M. Kleinschrodt, J. Björk, S. Klyatskaya, F. Klappenberger, M. Ruben, and J. V. Barth, *Steering on-surface self-assembly of high-quality hydrocarbon networks with terminal alkynes*, *Journal of Physical Chemistry C* **117**, 3987 (2013).
- [27] S. Martín, I. Grace, M. R. Bryce, C. Wang, R. Jitchati, A. S. Batsanov, S. J. Higgins, C. J. Lambert, and R. J. Nichols, *Identifying diversity in nanoscale electrical break junctions*, *Journal of the American Chemical Society* **132**, 9157 (2010).
- [28] D. J. Wold, R. Haag, M. A. Rampi, and C. D. Frisbie, *Distance dependence of electron tunneling through self-assembled monolayers measured by conducting probe atomic force microscopy: Unsaturated versus saturated molecular junctions*, *Journal of Physical Chemistry B* **106**, 2813 (2002).
- [29] C. J. Querebillo, A. Terfort, D. L. Allara, and M. Zharnikov, *Static conductance of nitrile-substituted oligophenylene and oligo(phenylene ethynylene) self-assembled monolayers studied by the mercury-drop method*, *Journal of Physical Chemistry C* **117**, 25556 (2013).

- [30] D. M. Adams, L. Brus, C. E. D. Chidsey, S. Creager, C. Creutz, C. R. Kagan, P. V. Kamat, M. Lieberman, S. Lindsay, R. a. Marcus, R. M. Metzger, M. E. Michel-Beyerle, J. R. Miller, M. D. Newton, D. R. Rolison, O. Sankey, K. S. Schanze, J. Yardley, and X. Zhu, *Charge Transfer on the Nanoscale: Current Status*, *The Journal of Physical Chemistry B* **107**, 6668 (2003).
- [31] B. Capozzi, E. J. Dell, T. C. Berkelbach, D. R. Reichman, L. Venkataraman, and L. M. Campos, *Length-dependent conductance of oligothiophenes*, *Journal of the American Chemical Society* **136**, 10486 (2014).
- [32] B. Q. Xu, X. L. Li, X. Y. Xiao, H. Sakaguchi, and N. J. Tao, *Electromechanical and conductance switching properties of single oligothiophene molecules*, *Nano Letters* **5**, 1491 (2005).
- [33] M. J. Ford, R. C. Hoft, and A. McDonagh, *Theoretical study of ethynylbenzene adsorption on au(111) and implications for a new class of self-assembled monolayer*, *The Journal of Physical Chemistry B* **109**, 20387 (2005).
- [34] H. Y. Gao, J. H. Franke, H. Wagner, D. Zhong, P.-A. Held, A. Studer, and H. Fuchs, *Effect of metal surfaces in on-surface glaser coupling*, *The Journal of Physical Chemistry C* **117**, 18595 (2013).
- [35] A. M. McDonagh, H. M. Zareie, M. J. Ford, C. S. Barton, M. Ginic-Markovic, and J. G. Matison, *Ethynylbenzene monolayers on gold: a metal-molecule binding motif derived from a hydrocarbon*, *Journal of the American Chemical Society* **129**, 3533 (2007).
- [36] C. M. Bowers, D. Rappoport, M. Baghbanzadeh, F. C. Simeone, K.-C. Liao, S. N. Semenov, T. Zaba, P. Cyganik, A. Aspuru-Guzik, and G. M. Whitesides, *Tunneling across SAMs containing oligophenyl groups*, *The Journal of Physical Chemistry C* **120**, 11331 (2016).
- [37] Q. Lu, K. Liu, H. Zhang, Z. Du, X. Wang, and F. Wang, *From tunneling to hopping: A comprehensive investigation of charge transport mechanism in molecular junctions based on oligo(p-phenylene ethynylene)s*, *ACS Nano* **3**, 3861 (2009).
- [38] R. C. Hoft, M. J. Ford, A. M. McDonagh, and M. B. Cortie, *Adsorption of amine compounds on the Au(111) surface: a density functional study*, *The Journal of Physical Chemistry C* **111**, 13886 (2007).
- [39] C. M. Crudden, J. H. Horton, I. I. Ebraliidze, O. V. Zenkina, A. B. McLean, B. Drevniok, Z. She, H.-B. Kraatz, N. J. Mosey, T. Seki, *et al.*, *Ultra stable self-assembled monolayers of n-heterocyclic carbenes on gold*, *Nature Chemistry* **6**, 409 (2014).
- [40] C.-H. Ko, M.-J. Huang, M.-D. Fu, and C.-h. Chen, *Superior contact for single-molecule conductance: Electronic coupling of thiolate and isothiocyanate on pt, pd, and au*, *Journal of the American Chemical Society* **132**, 756 (2010).



- [41] Y. Xing, T.-H. Park, R. Venkatramani, S. Keinan, D. N. Beratan, M. J. Therien, and E. Borguet, *Optimizing single-molecule conductivity of conjugated organic oligomers with carbodithioate linkers*, [\*Journal of the American Chemical Society\* \*\*132\*\*, 7946 \(2010\)](#).
- [42] M. Souto, L. Yuan, D. C. Morales, L. Jiang, I. Ratera, C. A. Nijhuis, and J. Veciana, *Tuning the rectification ratio by changing the electronic nature (open-shell and closed-shell) in donor-acceptor self-assembled monolayers*, [\*Journal of the American Chemical Society\* \*\*139\*\*, 4262 \(2017\)](#).
- [43] N. Crivillers, C. Munuera, M. Mas-Torrent, C. Simão, S. T. Bromley, C. Ocal, C. Rovira, and J. Veciana, *Dramatic influence of the electronic structure on the conductivity through open- and closed-shell molecules*, [\*Advanced Materials\* \*\*21\*\*, 1177 \(2009\)](#).
- [44] L. Yuan, C. Franco, N. Crivillers, M. Mas-Torrent, L. Cao, C. S. Sangeeth, C. Rovira, J. Veciana, and C. A. Nijhuis, *Chemical control over the energy-level alignment in a two-terminal junction*, *Nature Communications* **7** (2016).
- [45] N. Crivillers, C. Munuera, M. Mas-Torrent, C. Simão, S. T. Bromley, C. Ocal, C. Rovira, and J. Veciana, *Dramatic influence of the electronic structure on the conductivity through open- and closed-shell molecules*, [\*Advanced Materials\* \*\*21\*\*, 1177 \(2009\)](#).
- [46] I. Ratera and J. Veciana, *Playing with organic radicals as building blocks for functional molecular materials*, [\*Chem. Soc. Rev.\* \*\*41\*\*, 303 \(2012\)](#).
- [47] M. MAS-TORRENT, N. CRIVILLERS, V. MUGNAINI, I. RATERA, C. ROVIRA, and J. VECIANA, *Organic radicals on surfaces: towards molecular spintronics*, *Journal of material chemistry* **19**, 1691 (2009).
- [48] M. Mas-Torrent, N. Crivillers, C. Rovira, and J. Veciana, *Attaching persistent organic free radicals to surfaces: How and why*, [\*Chemical Reviews\* \*\*112\*\*, 2506 \(2012\)](#).
- [49] R. Frisenda, R. Gaudenzi, C. Franco, M. Mas-Torrent, C. Rovira, J. Veciana, I. Alcon, S. T. Bromley, E. Burzurí, and H. S. J. van der Zant, *Kondo effect in a neutral and stable all organic radical single molecule break junction*, [\*Nano Letters\* \*\*15\*\*, 3109 \(2015\)](#).
- [50] R. Gaudenzi, E. Burzurí, D. Reta, I. d. P. R. Moreira, S. T. Bromley, C. Rovira, J. Veciana, and H. S. J. van der Zant, *Exchange coupling inversion in a high-spin organic triradical molecule*, [\*Nano Letters\* \*\*16\*\*, 2066 \(2016\)](#).
- [51] R. Hayakawa, M. A. Karimi, J. Wolf, T. Huhn, M. S. Zöllner, C. Herrmann, and E. Scheer, *Large magnetoresistance in single-radical molecular junctions*, [\*Nano Letters\* \*\*16\*\*, 4960 \(2016\)](#).
- [52] C. Herrmann, G. C. Solomon, and M. A. Ratner, *Organic radicals as spin filters*, [\*Journal of the American Chemical Society\* \*\*132\*\*, 3682 \(2010\)](#).

- [53] J. Liu, X. Zhao, Q. Al-Galiby, X. Huang, J. Zheng, R. Li, C. Huang, Y. Yang, J. Shi, D. Z. Manrique, C. J. Lambert, M. R. Bryce, and W. Hong, *Radical-enhanced charge transport in single-molecule phenothiazine electrical junctions*, *Angewandte Chemie International Edition* **56**, 13061 (2017).
- [54] L. Srisombat, A. C. Jamison, and T. R. Lee, *Stability: A key issue for self-assembled monolayers on gold as thin-film coatings and nanoparticle protectants*, *Colloids and Surfaces A: Physicochemical and Engineering Aspects* **390**, 1 (2011).
- [55] M. J. Tarlov and J. G. Newman, *Static secondary ion mass spectrometry of self-assembled alkanethiol monolayers on gold*, *Langmuir* **8**, 1398 (1992).
- [56] J. R. Scott, L. S. Baker, W. R. Everett, C. L. Wilkins, and I. Fritsch, *Laser desorption fourier transform mass spectrometry exchange studies of air-oxidized alkanethiol self-assembled monolayers on gold*, *Analytical Chemistry* **69**, 2636 (1997).
- [57] T. Zaba, A. Noworolska, C. M. Bowers, B. Breiten, G. M. Whitesides, and P. Cyganik, *Formation of highly ordered self-assembled monolayers of alkynes on au(111) substrate*, *Journal of the American Chemical Society* **136**, 11918 (2014).
- [58] X. Kang, N. B. Zuckerman, J. P. Konopelski, and S. Chen, *Alkyne-functionalized ruthenium nanoparticles: Ruthenium–vinylidene bonds at the metal–ligand interface*, *Journal of the American Chemical Society* **134**, 1412 (2012).
- [59] H. M. Osorio, P. Cea, L. M. Ballesteros, I. Gascon, S. Marques-Gonzalez, R. J. Nichols, F. Perez-Murano, P. J. Low, and S. Martin, *Preparation of nascent molecular electronic devices from gold nanoparticles and terminal alkyne functionalised monolayer films*, *J. Mater. Chem. C* **2**, 7348 (2014).
- [60] L. Laurentius, S. R. Stoyanov, S. Gusarov, A. Kovalenko, R. Du, G. P. Lopinski, and M. T. McDermott, *Diazonium-derived aryl films on gold nanoparticles: Evidence for a carbon–gold covalent bond*, *ACS Nano* **5**, 4219 (2011).
- [61] M. Grandbois, M. Beyer, M. Rief, H. Clausen-Schaumann, and H. E. Gaub, *How strong is a covalent bond?* *Science* **283**, 1727 (1999).
- [62] C. Huang, S. Chen, K. Baruël Ørnsø, D. Reber, M. Baghernejad, Y. Fu, T. Wandlowski, S. Decurtins, W. Hong, K. S. Thygesen, and S.-X. Liu, *Controlling electrical conductance through a  $\pi$ -conjugated cruciform molecule by selective anchoring to gold electrodes*, *Angewandte Chemie International Edition* **54**, 14304 (2015).



# 4

## CURCUMINOIDS: SINGLE-MOLECULE CONDUCTANCE OF THIOPHENE ANCHORED COMPOUNDS

*The most elegant solutions are found in nature.  
You just have to know where to look.*

‘Vines of the Recluse’ card, Magic the gathering game

*We studied the electrical properties of two thiophene–curcuminoid molecules, 2-thphCCM (1) and 3-thphCCM (2), in which the only structural difference is the position of the sulfur atoms in the thiophene terminal groups. We used electrochemical techniques as well as UV/Vis absorption studies to obtain the values of the HOMO–LUMO band gap energies, showing that 2-thphCCM has lower values than 3-thphCCM. Theoretical calculations show the same trend. Self-assembled monolayers (SAMs) of these molecules were studied by using electrochemistry, showing that the interaction with gold reduces drastically the HOMO–LUMO gap in both molecules to almost the same value. Single-molecule conductance measurements show that 3-thphCCM has two different conductance values, whereas 2-thphCCM exhibits only one. Based on theoretical calculations, we conclude that the lowest conductance value, similar in both molecules, corresponds to the van der Waals interaction between the thiophene ring and the electrodes. The one order of magnitude higher conductance value for 3-thphCCM corresponds to a coordinate interaction between (dative covalent) the sulfur atoms and the gold electrodes.<sup>1</sup>*

Parts of this chapter have been published in Chem. Eur. J. 2016, 22, 12808. [1].

<sup>1</sup>This information was published in Chemistry European Journal, 2016, 22, 12808 – 12818. We thank Mickael Perrin for his help with the calculations and Monica Soler, Nuria Aliaga and their teams for the synthesis and chemical characterization of the molecules.

### 4.1. INTRODUCTION TO CURCUMINOIDS

Curcuminoids are a family of molecules which are derived from the curcuma molecule found in the Indian spice turmeric. They have been intensively used as inks, anti-inflammatory and cancer treating agents [2–5]. During the long history of the use of these compounds, synthetic chemists have gained great control over their molecular structure. This characteristic, together with the conjugated nature of the curcumin backbone, makes it an interesting candidate for molecular electronic devices.

In this work we investigate the electrochemical and single-molecule charge-transport properties of two thiophene-terminated curcuminoid (CCMoid) molecules, 2-thphCCM (1) and 3-thphCCM (2) (Fig. 4.1). In particular, we have investigated the influence of the sulfur atom positions on the electronic and charge-transport properties of both molecules. These two molecules have the same atomic composition and anchoring groups with sulfur atoms (S) as linkers, but differ in the relative position of the sulfur atom of the anchoring group. 3-thphCCM has the S atoms more available (outer position) for anchoring to gold electrodes than 2-thphCCM (Fig. 4.1).

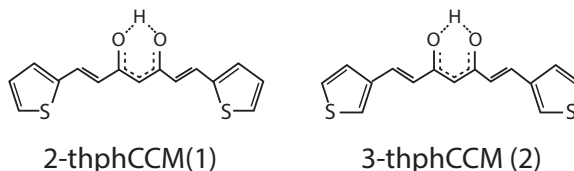


Figure 4.1: Sketch of the molecules considered in this chapter. (1) 2-thiophene curcuminoid (2Thph-CCM) compound in which the sulfur atoms in the thiophenes groups are located in position 2 with respect to the main molecular backbone. (2) 3-thiophene curcuminoid (3Thph-CCM) compound but this time the sulfur atoms are in position 3 with respect to the backbone.

To design ligands that are suitable for molecular electronics, we consider three principal aspects. First, our ligands must have proper anchoring groups to enable attachment to the electrodes; secondly, to achieve good molecular conductance, a short but highly conjugated skeleton is needed. Finally, metal complexation may introduce interesting features to molecular wires, thus a versatile structure that allows for metalization is desired. In this sense, curcuminoids were chosen because they possess a highly conjugated skeleton, have a  $\beta$ -diketone group that enables coordination, and their synthetic versatility allows the facile replacement of the aromatic groups with a wide library of commercial aldehydes with anchoring groups. These molecules represent promising building blocks for the construction of functional molecular nanocircuits as they possess structural flexibility and a well-developed synthetic chemistry methodology allowing their physical and chemical properties to be tailored. Both molecules share a  $\beta$ -diketone group placed in the center of a seven carbon conjugated chain, which allows coordination to metal ions[4–8], such as  $\text{Cu}^{\text{II}}$ ,  $\text{Zn}^{\text{II}}$ ,  $\text{Mn}^{\text{II}}$ ,  $\text{V}^{\text{IV}}$ , and  $\text{Ru}^{\text{II}}$  [5, 6], as well as lanthanides  $\text{Dy}^{\text{III}}$ ,  $\text{Tb}^{\text{III}}$ ,  $\text{Eu}^{\text{III}}$ ,  $\text{Gd}^{\text{III}}$ , and  $\text{Lu}^{\text{III}}$  [7, 8]. This  $\beta$ -diketone moiety shows a tautomeric equilibrium between a diketo and a keto-enol form, and several studies have focused their attention to elucidate which of these forms is more stable. Spec-

troscopic studies [2, 3, 9] have shown that the cis keto-enol tautomer (Fig. 4.1) is the more stable structure in solution and X-ray diffraction shows the same result in the solid state [10, 11]. Specifically, the cis keto-enol tautomer has an intramolecular hydrogen-bond (KEIHB, ketoenol intramolecular hydrogen-bond), which could affect the molecular conductance by means of an intramolecular proton transfer. On the other hand, the two terminal carbon atoms of the conjugated carbon are bound to two terminal rings, which can be chosen from a wide library of terminal substituents. The side groups can also be easily modified to improve the electrical contact with the electrodes. In this respect, the anchoring groups chosen for our molecules are thiophene units, which have affinity to gold. When a thiophene group binds a metal surface, the sulfur anchoring atom, which is in an aromatic ring, has two possible types of bonding interactions as it has two unpaired electrons. One of the unpaired electrons is de-localized in the aromatic ring, able to bind the gold surface through a p-interaction. On the other hand, the other unpaired electron can bind through a coordinated bond (dative covalent bond), in which the two electrons of the bond are donated from the sulfur atom to the surface [12]. Several examples of molecules with thiophene anchoring groups deposited between electrodes have been reported [13, 14]. Recently, an anthracene-based curcuminoid, called 9Accm, and a CuII-9Accm compound have been studied in molecular break junction devices made of a few layers of graphene (FLG) [15]. To the best of our knowledge, charge transport studies of curcuminoids using gold electrodes have not been reported before.

First, we study, in the bulk, different ways to obtain experimentally and theoretically the frontier orbitals and HOMO–LUMO band gap energies of these two curcuminoid molecules in the gas phase, in solution, and in the solid state. Generally speaking, the difference in conductance between two molecules can be estimated based on the difference in the band gap energy, although this band being near the Fermi level (5.1 eV) is also important [16]. As a first approximation, a small HOMO–LUMO gap energy is beneficial for the molecular conductance properties. However, it is known that the frontier orbital energies will change based on the hybridization of these orbital wave functions with those of the metallic leads in the electronic device [17–19]. We have performed electrochemical studies on self-assembled monolayers of these molecules to understand how the frontier orbitals and HOMO–LUMO band gap energies can change as a result of the molecule–surface interaction. Finally, we have performed single-molecule conductance measurements using the mechanically controlled break junction (MCBJ) technique to test the performance of our compounds as single-molecule wires. We support our findings by DFT calculations.

## 4.2. DISCUSSION ON CHEMICAL CHARACTERIZATION

2

The bulk characterization of the compounds was performed using electrochemical experiments and UV-visible spectroscopy in solution and solid state. The results are compared to DFT calculations for the compounds in solution and in gas phase.

The electronic absorption spectra of both molecules in the solid state were used to

<sup>2</sup>The chemical characterization was performed by the groups of Nuria Aliaga and Monica Soler in Barcelona (Spain) and Santiago (Chile). A more detail explanation can be found in reference [1].

obtain the HOMO–LUMO gap of the molecules, which are summarized in Table 4.1. Based on the absorption spectra obtained for 2-thphCCM and 3-thphCCM, the optical band gap of the frontier orbitals ( $E_g^{\text{op}}$ ) were estimated by using the cut-off (onset) of the lowest absorbed energy in their respective UV/Vis spectra. The  $E_g^{\text{op}}$  for the solid state provided values of 2.20 eV for 2-thphCCM and 2.45 eV for 3-thphCCM.

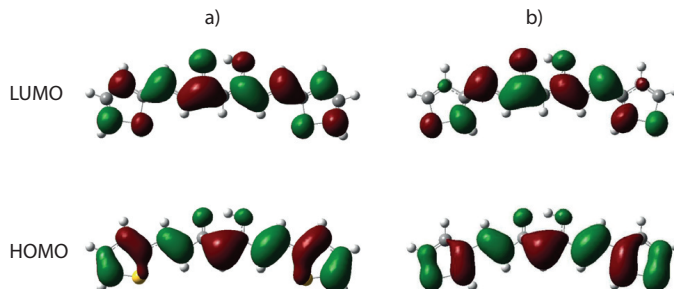


Figure 4.2: Molecular orbitals of a) 2-thphCCM (1) and b) 3-thphCCM (2).

To calculate the HOMO–LUMO gap, we have run two sets of calculations. The first is a set of density functional theory calculations (DFT) in the gas phase based on the Kohn–Sham analog of the Koopmans’ theorem (KT, valid within the Hartree–Fock framework) [20], which were demonstrated by Gritsenko and Baerends [21, 22] and expanded to other problems [23]. The second group of DFT calculations include the effect of solvent ( $\text{CH}_2\text{Cl}_2$ ) and Tomasi’s continuum polarizable method in order to compare the results with experimental measurements from the UV/Vis spectra.

In both cases, the calculations are a reasonably good estimation of the HOMO–LUMO gap and the absorption spectral characteristics. We cannot expect a perfect agreement with the experimental data, as the calculations are affected by the limits of the theoretical approach [21], the choice of the exchange–correlation functional, and the basis set.

	2thph CCM	3thph CCM
$E_g^{\text{theor}}$ gas phase	5.72	5.96
$E_g^{\text{theor}}$ solution phase	3.08	3.26
$E_g^{\text{op}}$ solid	2.20	2.45
$E_g^{\text{ec}}$ solution	2.27	2.47

Table 4.1: Comparison of the HOMO–LUMO energies of the studied molecules in gas, solution and solid phase. The methods used to obtaining these values were theoretical (theor), using DFT calculations; optical (op), using UV–Vis spectroscopy and electrochemical (ec), as the labels indicate.

Table 4.1 shows the calculated band gap energies for the molecules in the gas phase and in solution. The HOMO and LUMO calculated data, including the solvent effect, show quite good agreement with the experimental data from the UV/Vis experiments in solution. Based on the comparison of the calculated band gap energies of both molecules,

3-thphCCM has smaller energies than 2-thphCCM. The band gap energies for both molecules obtained from solid-state optical absorption or solution electrochemistry are in agreement. All the energies obtained for 2-thphCCM and 3-thphCCM show the same trend, suggesting to a first approximation that 3-thphCCM could conduct better.

Cyclic voltammetry (CV) and differential pulse voltammetry (DPV) were used to investigate the redox properties of 2-thphCCM and 3-thphCCM and to estimate values of the HOMO and LUMO energy levels of both systems. Overall, the two compounds display a similar electrochemical behavior, exhibiting a number of irreversible reductions in the -2.5 to -1.5 V region and three close irreversible oxidations in the +0.5 to +2.0 V range, with features that are similar to other thiophene species reported in the literature[24, 25]. However, a closer look at the DPV data shows that the potentials for the first oxidation and reduction processes are shifted between the two target molecules. 2-thphCCM presents the first oxidation and reduction processes at +0.87 and -1.66 V, respectively, whereas 3-thphCCM displays these processes at +0.95 and -1.80 V (both referenced vs. Fc/Fc<sup>+</sup>).

	1 <sup>st</sup> Oxid	1 <sup>st</sup> Red	E <sub>HOMO</sub>	E <sub>LUMO</sub>	E <sub>g</sub> <sup>elec</sup>
1 Sol.	+0.87	-1.66	-5.53	-3.26	2.27
2 Sol.	+0.95	-1.80	-5.58	-3.11	2.47
1 SAM	+0.78	-1.33	-5.40	-4.65	0.75
2 SAM1	+0.93	-0.30	-5.42	-4.68	0.74

Table 4.2: Electrochemical data in CH<sub>2</sub>Cl<sub>2</sub>, for 2-thphCCM and 3-thphCCM in solution and in a SAM configuration. Potentials (V) are referred to Fc/Fc<sup>+</sup>. E<sub>HOMO</sub> and E<sub>LUMO</sub> refer to the HOMO and the LUMO energy levels and E<sub>g</sub><sup>elec</sup> [eV] stands for the electrochemical energy gap.

The HOMO is estimated [26, 27] from the first oxidation potential, corresponding to the ionization potential (IP; removal of one electron from the highest occupied molecular orbital) and the LUMO is deduced from the first reduction potential, correlated with the electron affinity (EA; addition of one electron to the lowest unoccupied orbital). As a result, the corresponding HOMO and LUMO energy levels are -5.53 and -3.26 eV for 2-thphCCM, and -5.58 and -3.11 eV for 3-thphCCM. Hence, the electrochemical band gaps, E<sub>g</sub><sup>ec</sup>, are 2.27 and 2.47 eV, respectively. These energies as well as the gap values are comparable to other conjugated systems, which are of the order of donor polymers and small molecules [21, 25–28]. For both molecules, the metal Fermi level is found to lie closer to the HOMO than to the LUMO energy level.

Electrochemical studies of self-assembled monolayers (SAMs) of 2-thphCCM and 3-thphCCM on Au(111) were also carried out to evaluate the changes in the HOMO and LUMO energy levels. The results are summarized in Table 4.2.

SAM(2-thphCCM-Au(111)) presents the first oxidation and reduction processes at +0.78 and -0.33 V, respectively, and SAM(3-thphCCM-Au(111)) displays parallel redox processes at +0.93 and -0.30 V. The comparison of these potentials with the ones obtained for the molecules in solution suggests that the oxidation potentials for the SAM configurations have experienced small shifts toward positive values, whereas the reduction potentials show pronounced shifts to less negative values.



We found that the electrochemical band gaps, for 2-thphCCM and 3-thphCCM when in contact with the gold electrode, are 0.75 and 0.74 eV, respectively. This change in the band gap energies upon binding is mainly a result of the mixing of the LUMO orbitals with the orbitals of the gold electrode, as the HOMO orbitals are almost the same for both molecules. When compounds 2-thphCCM and 3-thphCCM are anchored to the gold surface, the reduction potentials (or the LUMO energies) cause the reduction of the band gap energy, resulting in smaller values than the ones obtained for the molecules in solution. Based on the electrochemical measurements of SAMs, we can conclude that the interaction with the gold electrodes reduces the LUMO energies of both molecules, ending up with a smaller and more similar band gap for both molecules, therefore as a first approximation, if everything else is the same, both molecules should show similar conductance values in a single-molecule experiment using gold electrodes.

Representations of the molecular orbitals for the HOMO and LUMO electronic states for 2-thphCCM and 3-thphCCM are presented in Fig. 4.2, which show the typical delocalization of the charge of a conjugated molecule, using p-type orbitals along the complete structure. Two observations can be made when comparing the molecular orbitals of 2-thphCCM and 3-thphCCM: (i) 2-thphCCM has a reduced capacity for charge transfer as the S atoms are less involved in the HOMO orbital; (ii) looking at the LUMO orbital, 3-thphCCM is less conjugated, as two carbon atoms of each thiophene ring are not participating in the conjugation of the complete structure, which gives a more direct path for eventual charge transport from one sulfur atom to the other in the molecule, favoring better conductance. Therefore, depending on if the charge transport is through the HOMO or the LUMO orbital, the conductance of both molecules could be different. Based on the proximity of the HOMO energies of both molecules, as obtained from electrochemistry, with the Fermi level of gold, as a first approximation, the injection could be through the HOMO.

### 4.3. CONDUCTANCE MEASUREMENTS

Single-molecule conductance measurements were performed with the controllable mechanical break junction technique (MCBJ) [29]. A 2  $\mu$ l drop of the molecular solution was drop-casted on the device before breaking the electrodes. Thousands of molecular conductance traces were collected while breaking and re-connecting the electrodes, allowing a statistical analysis. The data is visualized by the constructions of two-dimensional conductance vs. electrode displacement histograms and one-dimensional conductance histograms. Fig. 4.3 displays two-dimensional conductance versus electrode displacement histograms of MCBJ experiments (conductance in logarithmic scale). Fig. 4.3a) and c) display information about 2-thphCCM and panels b) and d) about 3-thphCCM. In these histograms, individual breaking traces have been shifted along the horizontal axis to fix the rupture of the one-atom gold contact at zero. Areas of high counts represent the most typical breaking behavior of the molecular junctions. In Fig. 4.3, panels a) and b) there are histograms constructed with the full data sets including 5000 consecutive conductance traces; the panels c) and d) display histograms built from traces that extend of over 0.7 nm above  $1 \times 10^{-5} G_0$ . In the latter case, the shortest and steepest traces have been omitted so that most it includes mainly traces in which a molecule bridges the gap.

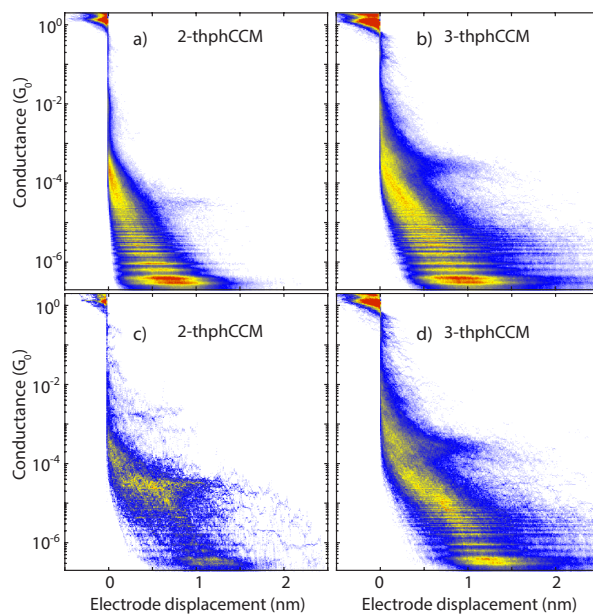


Figure 4.3: a) and b): 2D-Conductance vs. electrode displacement histograms constructed from 5000 consecutive traces of a) 3-thphCCM and b) 2-thphCCM. Panels c) and d) show 2D-Conductance vs. electrode displacement histograms constructed from 253 and 1650 traces respectively in which the distance between the last point above  $1 G_0$  and the last point above  $10^{-5} G_0$  is larger than 0.7 nm.

The two-dimensional histograms (Fig. 4.3) show that for compound 2-thphCCM, there is a region of high counts between  $10^{-4}$  and  $10^{-5} G_0$  and for compound 3-thphCCM, there are two regions of high counts, one just above  $10^{-4} G_0$  extending no further than 1.5 nm and a broad feature spreading from below  $10^{-5} G_0$  to the detection limit and reaching displacements up to 2.5 nm.

To extract the conductance values of the most probable molecular configuration, one-dimensional (1D) conductance histograms have been constructed. These 1D-histograms are presented in Fig. 4.4. The two panels show, the presence of peak at  $1 G_0$  ( $G_0 = 2e^2/h = 77$  mS), the quantum of conductance, indicating the formation of atomically sharp electrodes. The histograms for the two molecules yield a distribution of conductance values peaked around  $3.1 \times 10^{-5} G_0$  for 2-thphCCM (Fig. 4.4 a) and two conductance peaks at  $G_0$  and  $7 \times 10^{-6} G_0$  for 3-thphCCM (Fig. 4.4 a).

Comparison of both histograms yields a consistent picture in which 2-thphCCM exhibits one stable conformation with a conductance plateau that peaks at  $3.1 \times 10^{-5} G_0$ , with counts concentrated for electrode displacements between 0 and 0.7 nm, with almost no counts at larger displacements. For 3-thphCCM, the histograms reveal a maximum around  $3.2 \times 10^{-4} G_0$  and a broad maximum around  $6.9 \times 10^{-6} G_0$ , with counts spread over larger displacements, and conductance counts up to 2.5 nm of electrode displacement. Fig 4.1 shows that the observed differences have to be related to the different positions of the sulfur atoms in the terminal thiophene rings. If we compare the distance between the sulfur atoms in both molecules, 2-thphCCM has the shortest distance between them and the observed conductance counts for 3-thphCCM at higher electrode displacement is thus consistent with the molecular structure. Moreover, the lower conductance value (Fig. 4.4), which corresponds to a more stretched conformation of the molecule between the electrodes, is of the same order in both molecules, suggesting that the change in the sulfur atom position for that conformation does not affect the conductance considerably. The high conductance value seen only for 3-thphCCM, may then be related to the fact that it has the S atoms at a more favorable position for anchoring to the gold electrodes, which is better for charge injection.

#### 4.4. TRANSPORT CALCULATIONS

To compare the single-molecule conductance measurements with theoretical calculations, we have calculated the transmission through 2-thphCCM and 3-thphCCM by using the non-equilibrium Green's function method with a density functional theory (DFT) calculation of the ground-state electron density for different electrode stretching distances. We found that the exact geometry of the molecule with respect to the electrodes plays an important role in the HOMO and LUMO energy values, as well as on the transmission through the molecular junction. To investigate the evolution of the molecular conformation while stretching the junction, we performed DFT calculations for various electrode separations.

In Fig. 4.5, we present the different molecular junction configurations for 2-thphCCM and 3-thphCCM during stretching. These three configurations are marked in Fig. 4.6 a) and b) with arrows in the force versus Au–Au distance plots. The initial molecular junction configuration is presented on top, whereas the middle and lower configurations correspond to maxima in the forces/displacement curves. The colors in Fig. 4.6 a),b) are

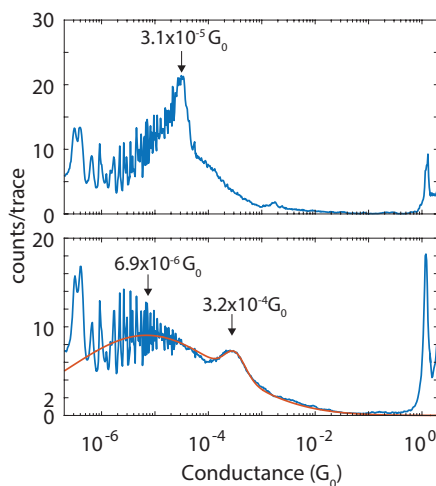


Figure 4.4: 1D-conductance histograms of a) 2-thphCCM and b) 3-thphCCM constructed from the traces collected in Fig. 4.3 c) and d) respectively. The red line in b) corresponds to the fit of two log-normal distributions. Arrows pinpoint the most probable conductance value of the different conductance states.

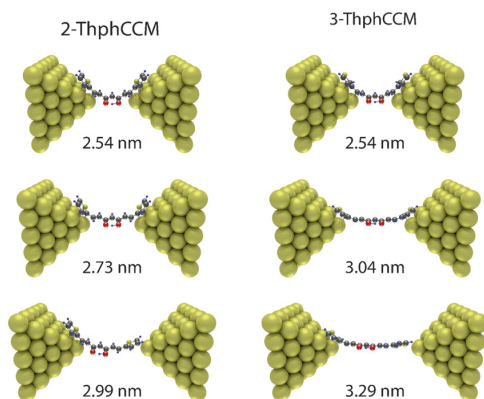


Figure 4.5: DFT calculations of the different molecular junction configurations. Top: initial molecular junction configuration; middle: the configuration at an intermediate stretch; bottom: the configuration at the point of maximum stretching for molecules 2-thphCCM and 3-thphCCM.

linked to the transmission curves shown in Fig. 4.6 c). These were calculated by using DFT+ $\Sigma$  in combination with the non-equilibrium Green's function (NEGF) formalism. Conductance values were then calculated by using the Landauer formula[30].

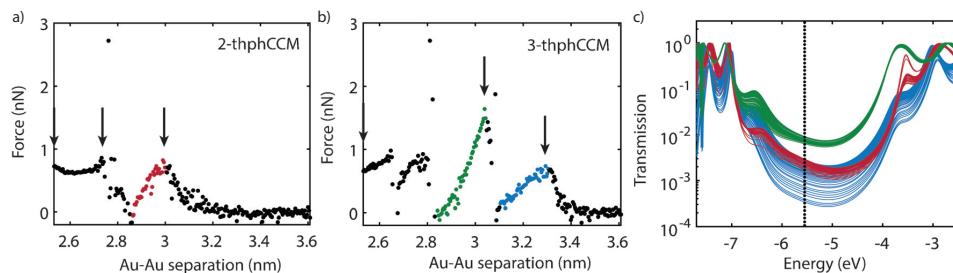


Figure 4.6: Force versus Au–Au distance curves as obtained from the DFT stretching calculations for 2-thphCCM (a) and 3-thphCCM (b). c) Transmission curves calculated by using DFT+NEGF for 2-thphCCM and 3-thphCCM. The colors of the curves are related to the junction geometry along the stretching curves shown in a) and b). The vertical dotted line indicates the estimated location of the Fermi energy.

Comparing the force–stretching curves for both molecules with the force maxima marked by the black arrows in Fig. 4.6 and the representation of the calculated molecular junction configurations shown in Fig. 4.5; the following observations can be made: first, the rupture of the molecular junction, that is, the last local maximum in the force, marked by the black arrows, occurs at 2.99 nm for molecule 1, whereas molecule 3-thphCCM can be stretched up to 3.29 nm, so essentially 3-thphCCM can be stretched more than 2-thphCCM. This may explain the shorter conductance plateaus for 2-thphCCM in the experimental conductance histograms. Second, the junction evolution for the two molecules is different. 2-thphCCM shows a second peak at 2.74 nm, with an amplitude of 0.8 nN. 3-thphCCM, on the other hand, shows multiple peaks, located at 2.62, 2.73, and 3.04 nm, with amplitudes of 0.9, 0.9, and 1.6 nN, respectively. The fact that the force is twice as high for the peak at 3.04 nm suggests a different nature for this bond compared with the others. Inspection of the different junction geometries in Fig. 4.5 suggests the following scenarios: (i) at the point of rupture of 2-thphCCM, the interaction is a weak van der Waals interaction between a distant thiophene ring and the electrode, leaving only a H atom of the ring as the last contact with the gold electrode. No coordinate S–Au bond is formed, and the molecule/electrode interaction occurs through van der Waals forces. The peak at 2.73 nm is also caused by van der Waals forces, with the entire thiophene rings interacting with the electrodes. (ii) In the case of 3-thphCCM, the situation is different. At the point of rupture (3.29 nm), the hydrogen atom is the closest to the electrode suggesting a molecule/electrode interaction occurring through van der Waals forces. This is similar to 2-thphCCM. At positions 2.64 and 2.73 nm, the thiophene rings overlap with the gold electrodes and van der Waals forces predominate again. At a distance of 3.04 nm, however, the S atoms are located close to the gold, indicating the formation of coordinate bonds. This bond formation can be related to the higher breaking force. Upon further stretching, as also seen in 2-thphCCM, the last molecule/electrode interaction is again through van der Waals forces.

This structural difference is also reflected in the transmission through the molecule while stretching, as shown in Fig. 4.6 c). For thph2, when the molecular junction is formed through van der Waals interactions with the electrodes (red), the curves cluster around a conductance value of about  $3 \times 10^{-3}$  G<sub>0</sub>. For 3-thphCCM, the conductance in the van der Waals regime (blue) is slightly lower than for molecule 1, and with a larger spread. When 3-thphCCM is connected through the S atoms (green), on the other hand, the conductance is about an order of magnitude larger. The conductance values obtained from DFT are higher than the ones found in the MCBJ experiments, and can therefore only be compared qualitatively. Nevertheless, the two different binding geometries of 3-thphCCM yield different conductance values, with an order of magnitude difference between the two. In addition, the HOMO and LUMO energies of both molecules are similar to those obtained experimentally from the electrochemical measurements on SAMs.

## 4.5. DISCUSSION AND CONCLUSIONS

The experimental data in solution and in the solid state show that the HOMO–LUMO band gap for 2-thphCCM has a lower energy value than for 3-thphCCM. Theoretical calculations show the same trend. Inspection of the HOMO and LUMO molecular orbitals show that both molecules have the typical delocalization of p-type orbitals along the complete structure of the molecule, but owing to the difference in the position of the sulfur atoms in the terminal thiophene rings, the electronic densities in the HOMO and LUMO orbitals are different. Analysis of the frontier molecular orbital electron densities suggest that if charge transport were to occur through the HOMO orbitals, 2-thphCCM could show a reduced capacity for eventual charge-transfer processes as the sulfur atom are less involved in the HOMO orbital. In the opposite case scenario, in which charge transport occurs through the LUMO energy levels of the molecules, 3-thphCCM shows a more direct path for eventual charge transport between both sulfur atoms, resulting in better conductance. Therefore, the energy band gap for 2-thphCCM is smaller than for 3-thphCCM, but the electron energies of the HOMO and the LUMO orbitals may affect differently the injected process to or from the molecule. Once the molecules are anchored on the gold electrode surfaces, the band gap energies are significantly reduced, exhibiting a lowering of the LUMO orbital energies in both cases, and the band gap of both molecules end up almost the same. Single-molecule measurements show that the conductance of 3-thphCCM is an order of magnitude higher than the conductance of 2-thphCCM. Therefore, considering that the HOMO and LUMO energies are almost the same, we attribute this difference in conductance to the ability of 3-thphCCM to form coordinate interactions with the nanogold electrodes, owing to the more available position of the sulfur atoms. We supported our findings by DFT calculations.

## REFERENCES

- [1] A. Etcheverry-Berríos, I. Olavarria, M. L. Perrin, R. Díaz-Torres, D. Jullian, I. Ponce, J. H. Zagal, J. Pavez, S. O. Vásquez, H. S. J. van der Zant, D. Dulić, N. Aliaga-Alcalde, and M. Soler, *Multiscale Approach to the Study of the Electronic Properties of Two Thiophene Curcuminoid Molecules*, *Chemistry - A European Journal* **22**, 12808 (2016).

- [2] C. F. Chignell, P. Bilskj, K. J. Reszka, A. G. Motten, R. H. Sik, and T. A. Dahl, *Spectral and photochemical properties of curcumin*, [\*Photochemistry and Photobiology\* \*\*59\*\*, 295 \(1994\)](#).
- [3] L. Nardo, A. Andreoni, M. Bondani, M. Másson, T. Haukvik, and H. H. Tønnesen, *Studies on curcumin and curcuminoids. xlv. photophysical properties of dimethoxycurcumin and bis-dehydroxycurcumin*, [\*Journal of Fluorescence\* \*\*22\*\*, 597 \(2012\)](#).
- [4] N. Aliaga-Alcalde, L. Rodríguez, M. Ferbinteanu, P. Höfer, and T. Weyhermüller, *Crystal structure, fluorescence, and nanostructuration studies of the first Zn<sub>II</sub> anthracene-based curcuminoid*, [\*Inorganic Chemistry\* \*\*51\*\*, 864 \(2012\)](#).
- [5] K. Krishnankutty and V. John, *Synthesis, characterization, and antitumour studies of metal chelates of some synthetic curcuminoids*, [\*Synthesis and Reactivity in Inorganic and Metal-Organic Chemistry\* \*\*33\*\*, 343 \(2003\)](#).
- [6] N. Aliaga-Alcalde, P. Marqués-Gallego, M. Kraaijkamp, C. Herranz-Lancho, H. den Dulk, H. Görner, O. Roubeau, S. J. Teat, T. Weyhermüller, and J. Reedijk, *Copper curcuminoids containing anthracene groups: Fluorescent molecules with cytotoxic activity*, [\*Inorganic Chemistry\* \*\*49\*\*, 9655 \(2010\)](#).
- [7] M. Menelaou, F. Ouharrou, L. Rodríguez, O. Roubeau, S. J. Teat, and N. Aliaga-Alcalde, *DyIII- and YbIII-curcuminoid compounds: Original fluorescent single-ion magnet and magnetic near-ir luminescent species*, [\*Chemistry – A European Journal\* \*\*18\*\*, 11545 \(2012\)](#).
- [8] Y. Mawani and C. Orvig, *Improved separation of the curcuminoids, syntheses of their rare earth complexes, and studies of potential antiosteoporotic activity*, [\*Journal of Inorganic Biochemistry\* \*\*132\*\*, 52 \(2014\)](#), special Issue Containing Contributions from the Third Latin American Meeting on Biological Inorganic Chemistry - LABIC 2012.
- [9] F. Payton, P. Sandusky, and W. L. Alworth, *Nmr study of the solution structure of curcumin*, [\*Journal of Natural Products\* \*\*70\*\*, 143 \(2007\)](#).
- [10] J. T. Mague, W. L. Alworth, and F. L. Payton, *Curcumin and derivatives*, [\*Acta Crystallographica Section C\* \*\*60\*\*, o608 \(2004\)](#).
- [11] H. H. Tonnensen, J. Karlsen, and A. Mostad, *Structural Studies of Curcuminoids. I. The Crystal structure of Curcumin*, *Acta Chemica Scandinavica B* **36**, 475 (1982).
- [12] J. Zhou, Y. X. Yang, P. Liu, N. Camillone, and M. G. White, *Electronic structure of the thiophene/au(111) interface probed by two-photon photoemission*, [\*The Journal of Physical Chemistry C\* \*\*114\*\*, 13670 \(2010\)](#).
- [13] I. Rattalino, V. Cauda, P. Motto, T. Limongi, G. Das, L. Razzari, F. Parenti, E. Di Fabrizio, A. Mucci, L. Schenetti, G. Piccinini, and D. Demarchi, *A nanogap-array platform for testing the optically modulated conduction of gold-octithiophene-gold junctions for molecular optoelectronics*, [\*RSC Adv.\* \*\*2\*\*, 10985 \(2012\)](#).



- [14] Y. Ie, K. Tanaka, A. Tashiro, S. K. Lee, H. R. Testai, R. Yamada, H. Tada, and Y. Aso, *Thiophene-based tripodal anchor units for hole transport in single-molecule junctions with gold electrodes*, *The Journal of Physical Chemistry Letters* **6**, 3754 (2015).
- [15] F. Prins, A. Barreiro, J. W. Ruitenber, J. S. Seldenthuis, N. Aliaga-Alcalde, L. M. K. Vandersypen, and H. S. J. van der Zant, *Room-temperature gating of molecular junctions using few-layer graphene nanogap electrodes*, *Nano Letters* **11**, 4607 (2011).
- [16] C. B. George, M. A. Ratner, and J. B. Lambert, *Strong conductance variation in conformationally constrained oligosilane tunnel junctions*, *The Journal of Physical Chemistry A* **113**, 3876 (2009).
- [17] J. Ponce, C. R. Arroyo, S. Tatay, R. Frisenda, P. Gaviña, D. Aravena, E. Ruiz, H. S. J. van der Zant, and E. Coronado, *Effect of metal complexation on the conductance of single-molecular wires measured at room temperature*, *Journal of the American Chemical Society* **136**, 8314 (2014).
- [18] V. Kaliginedi, a. V. Rudnev, P. Moreno-Garcia, M. Baghernejad, C. C. Huang, W. J. Hong, and T. Wandlowski, *Promising anchoring groups for single-molecule conductance measurements*, *Physical Chemistry Chemical Physics* **16**, 23529 (2014).
- [19] Z. Li, M. Smeu, M. A. Ratner, and E. Borguet, *Effect of anchoring groups on single molecule charge transport through porphyrins*, *The Journal of Physical Chemistry C* **117**, 14890 (2013).
- [20] T. Koopmans, *Über die zuordnung von wellenfunktionen und eigenwerten zu den einzelnen elektronen eines atoms*, *Physica* **1**, 104 (1934).
- [21] P. I. Djurovich, E. I. Mayo, S. R. Forrest, and M. E. Thompson, *Measurement of the lowest unoccupied molecular orbital energies of molecular organic semiconductors*, *Organic Electronics* **10**, 515 (2009).
- [22] D. P. Chong, O. V. Gritsenko, and E. J. Baerends, *Interpretation of the kohn–sham orbital energies as approximate vertical ionization potentials*, *The Journal of Chemical Physics* **116**, 1760 (2002).
- [23] O. V. Gritsenko and E. J. Baerends, *The analog of koopmans' theorem in spin-density functional theory*, *The Journal of Chemical Physics* **117**, 9154 (2002).
- [24] D. Liu, C. Gu, M. Xiao, M. Qiu, M. Sun, and R. Yang, *A new highly conjugated crossed benzodithiophene and its donor-acceptor copolymers for high open circuit voltages polymer solar cells*, *Polym. Chem.* **6**, 3398 (2015).
- [25] Q. Fan, Y. Liu, M. Xiao, H. Tan, Y. Wang, W. Su, D. Yu, R. Yang, and W. Zhu, *Donor-acceptor copolymers based on benzo[1,2-b:4,5-b']dithiophene and pyrene-fused phenazine for high-performance polymer solar cells*, *Organic Electronics* **15**, 3375 (2014).



- [26] J. Pommerehne, H. Vestweber, W. Guss, R. F. Mahrt, H. Bässler, M. Porsch, and J. Daub, *Efficient two layer leds on a polymer blend basis*, [Advanced Materials](#) **7**, 551 (1995).
- [27] A. P. Kulkarni, C. J. Tonzola, A. Babel, and S. A. Jenekhe, *Electron transport materials for organic light-emitting diodes*, [Chemistry of Materials](#) **16**, 4556 (2004).
- [28] C.-Y. Yu, C.-P. Chen, S.-H. Chan, G.-W. Hwang, and C. Ting, *Thiophene/phenylene/thiophene-based low-bandgap conjugated polymers for efficient near-infrared photovoltaic applications*, [Chemistry of Materials](#) **21**, 3262 (2009).
- [29] C. A. Martin, J. M. van Ruitenbeek, and H. S. J. van der Zant, *Sandwich-type gated mechanical break junctions*, [Nanotechnology](#) **21**, 265201 (2010).
- [30] M. Büttiker, Y. Imry, R. Landauer, and S. Pinhas, *Generalized many-channel conductance formula with application to small rings*, [Phys. Rev. B](#) **31**, 6207 (1985).

# 5

## SINGLE-MOLECULE MEASUREMENT ON CURCUMINOID COMPOUNDS: B AND CU SUBSTITUTION

*"You wanna know how I did it? This is how I did it, Anton:  
- I never saved anything for the swim back"*

GATTACA, Andrew Niccol, 1997

*We have studied the conductance of a family of curcuminoids, which possess different anchoring groups and have been modified with boron and copper substituents<sup>1</sup>. We find that the combination of methyl sulfide anchoring moieties and a boron difluoride group incorporated to the middle of the backbone gives rise to a switching behavior characterized by two distinctive conductance values. We corroborate the same trend with measurements on shorter curcuminoid analog compounds. We experimentally discard various possible mechanisms that give rise to conductance bistability in other molecular systems. The conclusion is that the most likely explanation lies in conformational changes related to the methyl sulfide group and the presence of the boron difluorine moiety in the center.*

---

<sup>1</sup>The molecules studied in this chapter were synthesized in the groups of Monica Soler at University of Chile (Santiago, Chile) and Nuria Aliaga at Catalan Institution for Research and Advanced Studies (Barcelona, Spain).

The realization of single-molecule circuits has opened the way to explore the electronic properties of a large variety of (in-)organic molecules. [1] Techniques such as mechanically controlled break junctions (MCBJ) [2] and the scanning tunnelling microscopy break junctions (STM-BJ) [3] are widely used to measure charge transport across molecules as short as 1 nm at ambient conditions. These single-molecule studies allow researchers to disentangle intrinsic charge transport properties from intermolecular interactions so that the relations between molecular structure and charge transport can be studied in a direct way. Conjugated organic molecules are a fruitful playground for this purpose; for example, molecular resistors [4] and diodes [5–8] have been designed and measured. On the other hand, biological molecules hold an enormous potential, but due to their complexity it is hard to establish a clear relation between the charge transport characteristics and their biological role. A way to build up knowledge in this direction is to characterize and understand the electronic properties of simple molecules that biological organisms can produce.

An important topic of interest is the inclusion of non-organic modifications to organic backbones, such as, metal ions or metalloids and their effect on the molecular conductance. Inclusion of metal ions, for example, has been studied in structures such as porphyrins, [9] in which a down-shift in the conductance value was reported up to a factor of 2.5 compared to the metal-free ligand when a metal ion was included in the structure. In a rotaxane-based molecule the inclusion of a Cu ion produced, on the other hand, no change in conductance value [10]. Metal ions can also be used to create interesting magnetic properties that can be exploited in molecular electronics like spin cross-over compounds [11] or single molecule magnets [12]. Furthermore, it is known that metal ions play an important role in the bio-functionality of certain proteins and facilitate charge transport in them. [13]

Here, we study a series of curcuminoid molecules (see Fig. 5.1) which have different anchoring groups and have a boron atom as a substituent group; a curcuminoid with a copper in is used as a reference compound. The thiocarbamate terminated molecules have a new anchoring group that to our knowledge has not been studied before in the context of single-molecule electronics. Measurements are performed with the MCBJ method in ambient conditions. In all cases, we find that stable molecular junctions can be formed and the acquisition of thousands of consecutive breaking traces allow for a statistical analysis of the data. We find that S-CCM-BF<sub>2</sub> possesses the highest conductance and that the inclusion of a boron atom in combination with MeS anchoring groups leads to a bi-stability in the conductance values.

### 5.1. DESCRIPTION OF THE MOLECULES

One of the features that has shown to be relevant in obtaining a relatively high conductance in molecular wires is the existence of a de-localized  $\pi$ -system between the two ends of the molecule. Here, we study a family of curcuminoid compounds whose structures are displayed in Figure 5.1. These molecules have been synthesized mimicking the structure of the natural compound curcumin, found in the roots of the *curcuma longa* plant. These bio-compatible molecules are short conjugated molecules with de-localized frontier orbitals. Because of the pharmaceutical use of these compounds, chemists have gained noticeable control over their structure [15–17]. In our previous

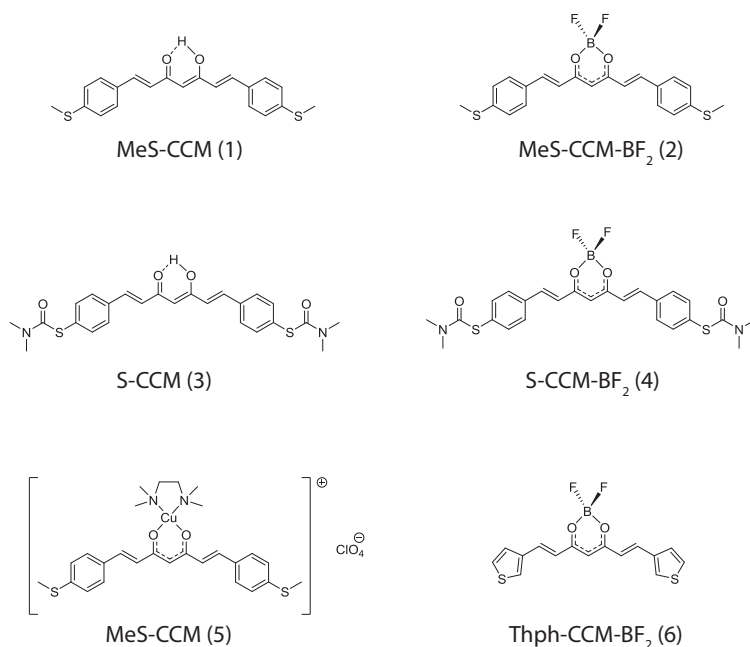


Figure 5.1: Schematic of the molecules considered in this chapter: (1) methylsulfide terminated free ligand curcuminoid, (2) methylsulfide terminated BF<sub>2</sub> substituted curcuminoid, (3) thiocarbamate terminated free ligand curcuminoid, (4) thiocarbamate terminated BF<sub>2</sub> substituted curcuminoid, (5) methylsulfide terminated Cu substituted curcuminoid and (6) thiophene terminated BF<sub>2</sub> substituted curcuminoid. The sulfur to sulfur distance of MeS-CCM and MeS-CCM-BF<sub>2</sub> is 1.86 nm obtained by X-ray diffraction, the same distance assumed for thiocarbamate terminated molecules due to the structure similarities, in the case of MeS-CCM-Cu is 1.78 nm and finally S-S distance in the Thph-CCM-BF<sub>2</sub> is assumed to be the same as the free ligand reported in [14].

work [14] we have shown that this kind of molecules can bridge two gold electrodes when connected through thiophene (Thph) endgroups.

In this chapter we explore the differences that arise in the electronic properties of curcuminoids when a metalloid (boron in this case) is introduced in the central part of the molecule (compounds 2,4,6 in Figure 5.1). The different anchoring strategies to bind these compounds to gold electrodes include methyl sulfide groups (MeS-:compounds 1,2,5 in Fig. 5.1); 3-thiophene groups (molecule 6) and a new anchoring moiety called thiocarbamate (S-:molecules 3 and 4). For comparison, a curcuminoid with a copper ion attached to the backbone (compound 5) is studied as well. The un-modified backbone (compounds 1 and 3) are used as a reference for the respective anchoring strategy.

## 5.2. CONDUCTANCE MEASUREMENTS

Single-molecule conductance measurements were performed in a mechanically controllable break junction set up. [18] The devices consist of a phosphorus bronze flexible substrate coated with a polyimide insulation layer, on top of which a lithographically defined gold wire with a constriction is patterned by e-beam lithography. The narrower part of the wire is suspended by reactive ion etching of the polyimide. The substrate is then clamped at both ends and bent by the action of a pushing rod beneath the center of the substrate until the gold wire breaks leaving two atomically sharp electrodes separated by a nanoscale gap.

The electrodes are fused and broken thousands of times at rates between 3 and 8 nm/s. During this process, the conductance ( $G = I/V$ ) is recorded using a logarithmic amplifier. Data is displayed in two-dimensional (2D) conductance vs. displacement histograms, in which the color code represents the relative frequency a particular conductance value is measured at the corresponding displacement value. Traces are aligned in such a way that zero displacement is defined as the point where the metallic contact is lost and the conductance drops sharply below the conductance quantum ( $G_0 = \frac{2e^2}{h}$ , where  $e$  is the electron charge and  $h$  Planck constant). The actual distance between the electrodes is larger than the one displayed in the 2D-histogram because the electrodes snap like a rubber band when the last atom loses contact. On average, the retraction of the electrodes after breaking is about 0.5 nm [19] and this distance should be added to the distances displayed in the 2D-histograms. One-dimensional (1D-) conductance histograms of the same data sets are obtained by integrating out the displacement axis; these 1D histograms are typically used to determine the most probable conductance value of the molecule.

Before depositing the molecule of interest, a control experiment is performed; one of the four junctions on a chip is broken and, at least, a thousand breaking traces are measured. Only if clear single gold atomic contacts are formed followed by a clean single-barrier tunnelling-like behaviour as the electrodes are separated further, a solution ( $> 50 \mu\text{M}$ ) with target molecules in dichloromethane is drop-casted onto the device ( $2 \mu\text{l}$ ) and let to dry, after which measurements are started.

Figure 5.2 displays six 2D-histograms of which each is a representative measurement of one of the molecules introduced in Fig. 5.1. Molecular-junction formation is observed as plateau-like structures for which the conductance stays almost constant as the junction breaks further and the electrode distance increases. The signal coming from empty junctions, on the other hand, is seen as a cloud of counts in the conductance that exponentially decays with the distance between the electrodes, characteristic of a single barrier tunnelling process. The relative occurrence of the two types of features is a measure for the molecular junction formation yield; for example, the absence of exponentially decaying conductance traces indicates a high chance of trapping molecules between the electrodes.

A characteristic feature that arises from comparing the six two-dimensional conductance vs. displacement histograms in Fig. 5.2 is the difference in the plateau length depending on the anchoring strategy used to contact the molecule to the gold electrodes. The order of plateau length is thiophene < methyl sulfide < thiocarbamate, indicating that the latter anchor is mechanically the more stable one among the three. An excep-

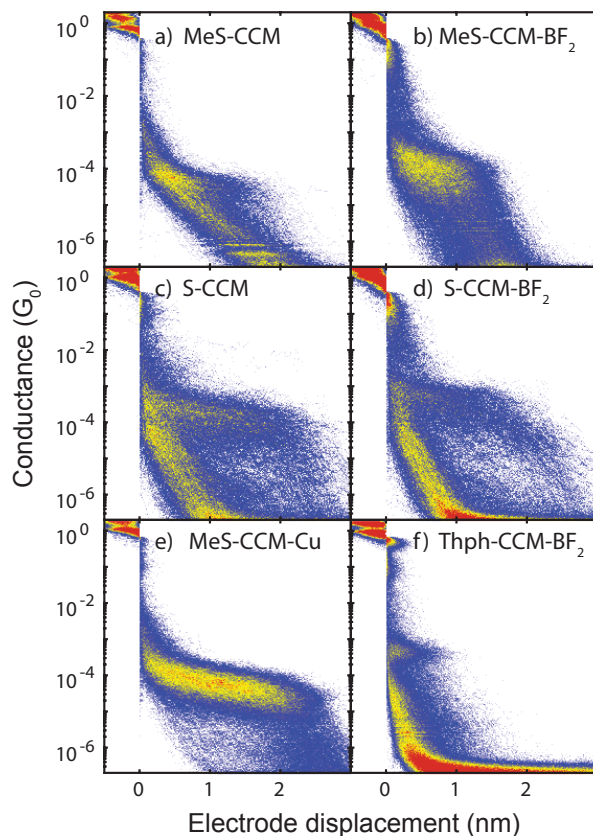


Figure 5.2: 2D-conductance vs. displacement histograms of the full data sets of a representative sample of a) MeS-CCM, b) MeS-CCM-BF<sub>2</sub>, c) S-CCM, d) S-CCM-BF<sub>2</sub>, e) MeS-CCM-Cu and f) Thph-CCM-BF<sub>2</sub>. The conductance axis is logarithmically binned with 80 bins per decade. The measurements were performed using a bias voltage of 0.1 V in ambient conditions; the electrode speed is between 3 to 8 nm/s. Each histogram contains two thousand consecutive breaking traces.

tion to this rule is seen in the case of MeS-Cu-CCM (Fig. 5.2e): the plateau-like structure has a small slope and is longer than for the other compounds that share the same anchoring group. Another particularity of the same compound is a low frequency of empty traces. Apparently, the Cu-substituted molecule exhibits a high chance to be captured in between the electrodes. It is likely that in for this molecule, the junctions contain more than one molecule. We have consistently found this high junction-formation yield for different samples and for different bias voltages, see Appendix 5.A.5. We have not analysed this behaviour in further detail but we do note that the listed single-molecule conductance value for this compound could be slightly overestimated.

To quantify the most probable conductance value of each molecule we select the

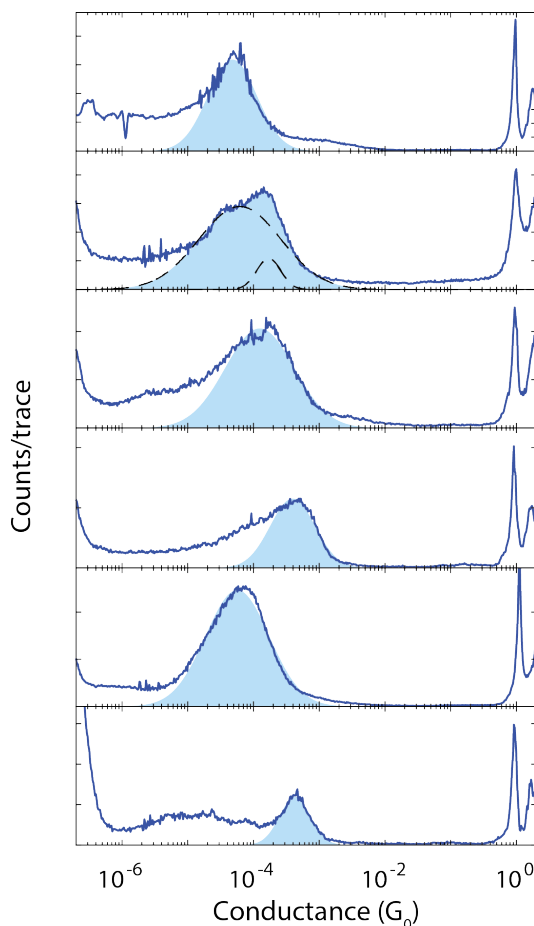


Figure 5.3: 1D-conductance histograms of selected traces corresponding to the same measurements displayed in Figure 5.2: a) MeS-CCM, b) MeS-CCM-BF<sub>2</sub>, c) S-CCM, d) S-CCM-BF<sub>2</sub>, e) MeS-CCM-Cu and f) Thph-CCM-BF<sub>2</sub>. Light blue shaded areas correspond to log-normal fits of the conductance peaks, used to determine the peak position and the full width half maximum (FWHM). For b), two log-normal distributions are used to fit the data. The individual peak shapes in this case are depicted by the black dashed lines.

traces that show molecular features using a method detailed in Appendix 5.A.1) and construct 1D-conductance histograms. A log-normal distribution is fitted to the data in a window around the peak of conductance; the fit parameters are the peak conductance values and the full width half maximum (FWHM) of the peaks. The values for these parameters are averaged among the different samples and are listed in Table 5.1. Remarkably, the data of the MeS-CCM-BF<sub>2</sub> molecule needs to be fitted with two log-normal distribution functions. A closer look at the two-dimensional histogram of this compound in Fig. 5.2 b) shows that MeS-CCM-BF<sub>2</sub> has a broad molecular feature that extends from zero displacement to the breaking point. We will analyse this double-peak structure in

Molecule	$G$ ( $G_0$ )	std ( $G_0$ )	FWHM
MeS-CCM	$3.9 \times 10^{-5}$	$4.0 \times 10^{-6}$	1.0
MeS-CCM-BF <sub>2</sub>	$1.4 \times 10^{-4}$	$2.2 \times 10^{-5}$	1.1
	$5.4 \times 10^{-5}$	$1.6 \times 10^{-5}$	0.5
S-CCM	$1.2 \times 10^{-4}$	$3.6 \times 10^{-7}$	1.2
S-CCM-BF <sub>2</sub>	$4.3 \times 10^{-4}$	$1.1 \times 10^{-4}$	0.9
MeS-CCM-Cu	$6.2 \times 10^{-5}$	$1.0 \times 10^{-5}$	1.1
Thph-CCM-BF <sub>2</sub>	$4.3 \times 10^{-4}$	-	0.6
Thph-CCM	$2.7 \times 10^{-4}$	-	0.5

Table 5.1: Most probable conductance value (first column), standard deviation (second column) and FWHM (third column) obtained from fitting the data of 1D-conductance histograms of several samples to log-normal distributions, as described in the text. The considered data sets were measured at a bias voltage of 0.1 V and the electrode speed was varied between 3 and 8 nm/s. The standard deviations are calculated using the data of two devices for MeS-CCM, six for MeS-CCM-BF<sub>2</sub>, one for S-CCM, one S-CCM-BF<sub>2</sub>, two for MeS-CCM-Cu and one for Thph-CCM-BF<sub>2</sub> and Thph-CCM respectively. The values of the free ligand with thiophene anchoring groups (bottom row) were published by us elsewhere. [14]

more detail below.

The results displayed in Table 5.1 show interesting trends. Comparing the anchoring strategies for both the free ligand and the boron substituted molecules, thiocarbamate (S-) yields conductance values similar to that of the thiophene which are around 3.9 times larger than the peak conductance value for the MeS- compounds. The FWHM, a quantity that is a measure for the variability of the molecular junctions under consideration, is the smallest for the measurements involving the thiophene anchoring group (0.5 decades) while the compounds with the other anchoring groups show a spread of around 1 decade. When a boron difluorine ion (BF<sub>2</sub>) is introduced into the curcuminoid backbone, there is a consistent increase in the conductance value by a factor of 3.6 in the case of MeS- (high conductance state) and S-, and 1.6 for Thph-. When copper is incorporated into the backbone with the MeS anchoring, the conductance value increases as well, but to lesser extent (factor of 1.8). While for MeS-CCM-BF<sub>2</sub> two peaks are needed to describe the data, the histogram of MeS-CCM-Cu contains only a single conductance peak. Until now we have compared the high-conductance peak of MeS-CCM-BF<sub>2</sub> with the rest of the molecules, but noticeable the low-conductance peak matches very well with the conductance value of the bare ligand with the same anchoring group (MeS-CCM).

We note that the 1D histograms of the two molecules with the thiocarbamate anchoring units exhibit long tails towards the low-conductance region. The histograms can also be fitted to two log-normal distributions. In the 2D histogram of S-CCM-BF<sub>2</sub> in particular, a narrow distribution is seen in the vicinity of zero displacement and as the displacement increases the cloud of molecular counts moves to lower conductance values. This behavior is distinctly different from the one observed for MeS-CCM-BF<sub>2</sub>, suggesting a different underlying mechanism. For S-CCM-BF<sub>2</sub> the high-conductance state most likely corresponds from the one in which the molecule bridges the gap between the electrodes; the lower conductance state occurs when the molecule loose contact either by going through another binding configuration with a lower coupling to the elec-



trodes or by forming a dimer ( $\pi - \pi$  stacking or covalently bonded molecule pair) with a lower conductance value, as reported before for other molecules. We have studied the double peak structure as a function of time and found that initially (first two thousand traces), the peak at low conductance values is not that prominent. In subsequent measurements, it starts appearing but there is no substantial increase in its appearance for the next 10000 traces; the bias voltage also does not have a clear influence on its formation. Additional data are presented in Appendix 5.A.3.

### 5.3. BORON SUBSTITUTED CURCUMINOID

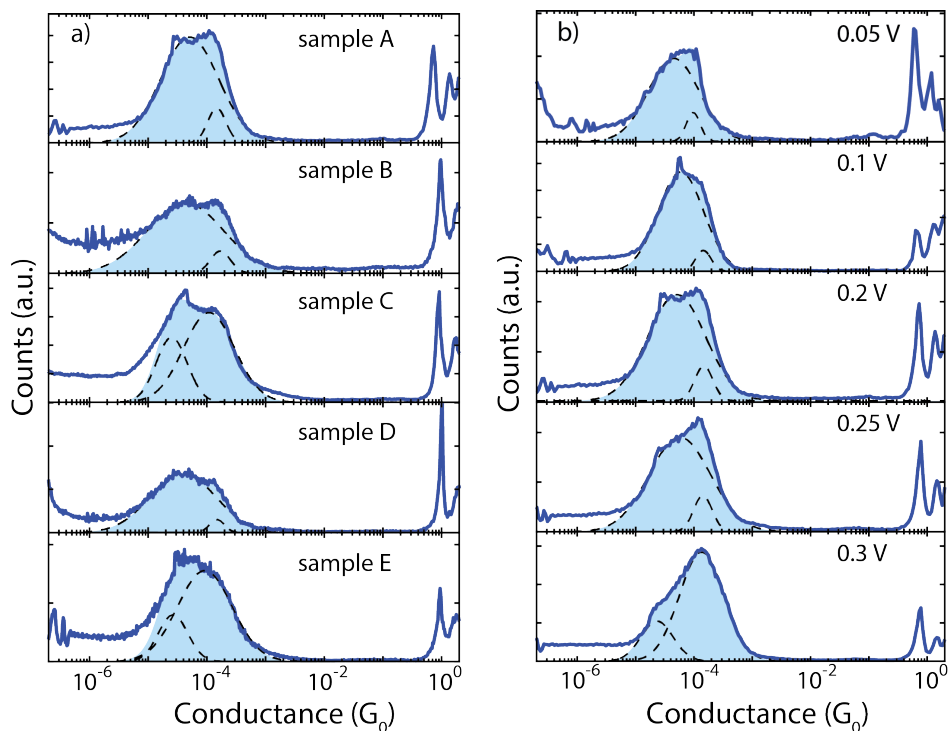


Figure 5.4: a) 1D-conductance histograms of selected traces of five different samples containing MeS-CCM-BF<sub>2</sub> measured at a bias voltage of 0.2 V. b) Series of measurements on one device with MeS-BF<sub>2</sub>-CCM for different bias voltages; the voltages are indicated in the figure. Light blue shaded areas represent fits of two log-normal distributions to the data in the region which the molecular features are seen. Black dashed lines depict the individual log-normal distributions. The values of the fit are displayed in Table 5.2.

We have investigated in further detail the double-peak structure in the conductance distribution of MeS-CCM-BF<sub>2</sub>. Several samples were measured and the applied bias voltage across the junction was varied. In Fig. 5.4 a) the conductance histograms of five different samples are displayed; these measurements were carried out using a bias voltage of 0.2 V as at this voltage the double-peak structure is clearer in most of the cases. Impor-

tantly, all samples show the double-peak structure although the relative weight of both peaks varies from sample to sample. In fitting the data we used an automatized routine in which a window along the conductance axis was defined to optimize the fitting, i.e., by making the fits less sensitive to the tails at the low conductance side. The best fits were found as a result of minimizing the error between the fit function and the data. We note, however, that by changing the window slightly, the area below the peaks and thus the FWHM can change considerably. On the other hand, the peak conductance values remain approximately the same.

Figure 5.4 b) displays an example of the evolution of the peak structure as the bias voltage varies from 50 to 300 mV. Interestingly, the appearance of the high-conductance peak becomes more prominent as the bias voltage increases. This characteristic may hint at a relation between the dipolar nature of the molecule and its conductance distribution. Although a similar behavior was observed in two other samples, the overall trend among all 6 samples was less clear.

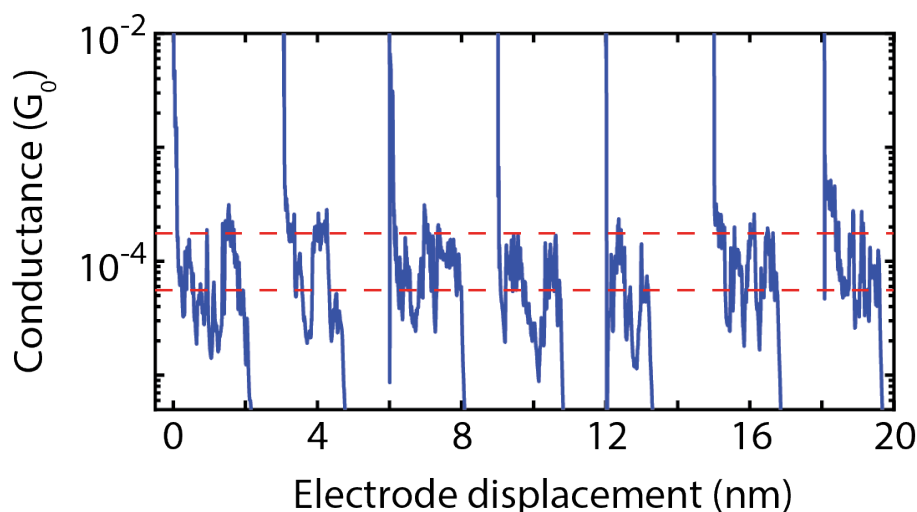


Figure 5.5: Examples of individual breaking traces of MeS-CCM-BF<sub>2</sub> in which switching events are observed. Traces are measured at a bias voltage of 0.1 V and an electrode speed of 4 nm/s. Traces switch up and down regardless of the distance. The average high- and low-conductance values of MeS-CCM-BF<sub>2</sub> from Table 5.1 are highlighted by the red and green dashed lines respectively. The traces have been offset in the *x*-direction for clarity.

Examination of individual breaking traces (see Fig. 5.5 for representative ones) reveals that within a single trace the conductance can switch back and forth between values that are consistent with the two conductance values obtained from the fitting procedure. We have studied this switching behaviour in more detail by varying the electrode speed or by taking time traces at a particular electrode separation distance. In many cases, we find a switching between two conductance states. The time traces show that the time constant for the switching can vary over various order of magnitude from a few ms to 10 s or even more. In Appendix 5.A.4 representative individual traces are shown. In

contrast, the breaking traces of molecules with the thiocarbamate show only step down switching events; the conductance then never returns to the original value (see Fig. 5.9 in Appendix 5.A.4).

## 5.4. DISCUSSION

In summary, we have shown that curcuminoid compounds attached to gold electrodes form stable electrode-molecule-electrode connections when using methyl sulfide and thiocarbamate groups. The later anchoring moiety has proven to effectively couple the molecular backbone to the electrodes, producing long molecular traces in the conductance experiments and giving rise to conductance values comparable to those of thiol connected OPE3. Nevertheless, thiocarbamate anchors also produce broad conductance peaks and the breaking behavior often goes through lower conductance state before loose contact. This may indicate the formation of another molecular conformation related to the change to a different anchoring configuration as the molecule is stretched.

On the other hand, measurements on MeS-CCM-BF<sub>2</sub> showed two conductance states that switch from one to the other in a random fashion on different time scales as seen in the individual time and breaking traces. Although the trend was not clear in all the five measured samples, the bias dependent relative peak weight favors the high conductance state, the higher the bias voltage.

It is important to stress that the ratio between the two conductance values of MeS-CCM-BF<sub>2</sub> varies from sample to sample and that it is not exactly two as expected when either one or two molecules bridge the gap [20–22]. In addition, previous reported two-states conductance features have been linked to different anchoring positions in the molecule [23, 24] or to rectification behavior [6, 7]. These scenarios can be disregarded in our measurements as the former one would yield plateaus of different lengths for each conductance state (which is not observed) and the later one needs an asymmetry in the molecular structure (which is not the case). The testing of different anchoring groups and modifications to the curcuminoid backbone point allows to conclude that the anchoring group itself does not give rise to the double peak structure seen in MeS-CCM-BF<sub>2</sub> and that it can not be purely related to anchoring configurations as in other cases [25–28].

## 5.5. CONCLUSIONS

curcuminoid compounds form stable single-molecule junctions with the three different anchoring moieties studied in this junction; the highest conductance is found for a BF<sub>2</sub> substituted and thiocarbamate ended curcuminoid. When a boron di-fluoride group is incorporated to the central part of the molecule the conductance across it increases compared to the molecule with the corresponding free ligand.

The combination of MeS- end group and boron difluoride inclusion in the curcuminoid backbone gives rise to conductance traces with a bi-stable conductance state independently of the inter electrode displacement; switching time constants vary from about a few ms to 10 s or more. The nature of the switching mechanism remains unknown, but various possible mechanisms have been discarded, namely: diode behavior, the presence of more than one molecule in the junction and conformational changes connected

to additional anchoring sites.

After completion of this chapter quantum chemistry calculations became available that provide insights to the switching mechanism and the conductance bistability.<sup>2</sup> These show that MeS-CCM-BF<sub>2</sub> can display two distinct conformers when contacted by electrodes inside a junction. These configurations only differ in the relative orientation of one of the MeS- groups with respect to the plane of the backbone (phenyl rings). This difference is enough to radically change the magnitude and direction of molecular dipole moment. Importantly, the two conformers have different conductance values and the change in dipole moment may explain the relative electric-field dependent occurrence of the two states. This mechanism has not been described previously in the context of single-molecule electronics and may provide a novel pathway to design molecular switches.

## REFERENCES

- [1] Z. Huang, F. Chen, P. A. Bennett, and N. Tao, *Single molecule junctions formed via Au-thiol contact: Stability and breakdown mechanism*, *Journal of the American Chemical Society* **129**, 13225 (2007).
- [2] R. Frisenda, S. Tarkuç, E. Galán, M. L. Perrin, R. Eelkema, F. C. Grozema, and H. S. J. van der Zant, *Electrical properties and mechanical stability of anchoring groups for single-molecule electronics*, *Beilstein Journal of Nanotechnology* **6**, 1558 (2015).
- [3] F. Chen, X. Li, J. Hihath, Z. Huang, and N. Tao, *Effect of anchoring groups on single-molecule conductance: Comparative study of thiol-, amine-, and carboxylic-acid-terminated molecules*, *Journal of the American Chemical Society* **128**, 15874 (2006).
- [4] X. D. Cui, A. Primak, X. Zarate, J. Tomfohr, O. F. Sankey, A. L. Moore, T. A. Moore, D. Gust, G. Harris, and S. M. Lindsay, *Reproducible measurement of single-molecule conductivity*, *Science* **294**, 571 (2001).
- [5] M. Elbing, R. Ochs, M. Koentopp, M. Fischer, C. von Hänisch, F. Weigend, F. Evers, H. B. Weber, and M. Mayor, *A single-molecule diode*, *Proceedings of the National Academy of Sciences* **102**, 8815 (2005).
- [6] I. Díez-Pérez, J. Hihath, Y. Lee, L. Yu, L. Adamska, M. A. Kozhushner, I. I. Oleynik, and N. Tao, *Rectification and stability of a single molecular diode with controlled orientation*, *Nature Chemistry* **1**, 635 (2009).
- [7] E. Lörtscher, B. Gotsmann, Y. Lee, L. Yu, C. Rettner, and H. Riel, *Transport properties of a single-molecule diode*, *ACS Nano* **6**, 4931 (2012).
- [8] M. L. Perrin, E. Galan, R. Eelkema, J. M. Thijssen, F. Grozema, and H. S. J. van der Zant, *A gate-tunable single-molecule diode*, *Nanoscale* **8**, 8919 (2016).

<sup>2</sup>Calculations performed by Eliseo Ruiz at the Departament de Química Inorgànica i Orgànica, Universitat de Barcelona, Barcelona, Spain

- [9] Z. F. Liu, S. Wei, H. Yoon, O. Adak, I. Ponce, Y. Jiang, W. D. Jang, L. M. Campos, L. Venkataraman, and J. B. Neaton, *Control of single-molecule junction conductance of porphyrins via a transition-metal center*, [\*Nano Letters\* \*\*14\*\*, 5365 \(2014\)](#).
- [10] J. Ponce, C. R. Arroyo, S. Tatay, R. Frisenda, P. Gaviña, D. Aravena, E. Ruiz, H. S. J. van der Zant, and E. Coronado, *Effect of metal complexation on the conductance of single-molecular wires measured at room temperature*, [\*Journal of the American Chemical Society\* \*\*136\*\*, 8314 \(2014\)](#).
- [11] C. Lefter, V. Davesne, L. Salmon, G. Molnár, P. Demont, A. Rotaru, and A. Bousseksou, *Charge transport and electrical properties of spin crossover materials: Towards nanoelectronic and spintronic devices*, [\*Magnetochemistry\* \*\*2\*\*, 18 \(2016\)](#).
- [12] E. C. Constable, G. Baum, E. Bill, R. Dyson, R. van Eldik, D. Fenske, S. Kaderli, D. Morris, A. Neubrand, M. Neuburger, D. R. Smith, K. Wieghardt, M. Zehnder, and A. D. Zuberbühler, *Control of iron(ii) spin states in 2,2':6',2''-terpyridine complexes through ligand substitution*, [\*Chemistry – A European Journal\* \*\*5\*\*, 498 \(1999\)](#).
- [13] N. Amdursky, D. Marchak, L. Sepunaru, I. Pecht, M. Sheves, and D. Cahen, *Electronic transport via proteins*, [\*Advanced Materials\* \*\*26\*\*, 7142 \(2014\)](#).
- [14] A. Etcheverry-Berríos, I. Olavarria, M. L. Perrin, R. Díaz-Torres, D. Jullian, I. Ponce, J. H. Zagal, J. Pavez, S. O. Vásquez, H. S. J. van der Zant, D. Dulić, N. Aliaga-Alcalde, and M. Soler, *Multiscale Approach to the Study of the Electronic Properties of Two Thiophene Curcuminoid Molecules*, [\*Chemistry - A European Journal\* \*\*22\*\*, 12808 \(2016\)](#).
- [15] M. Menelaou, F. Ouharrou, L. Rodríguez, O. Roubeau, S. J. Teat, and N. Aliaga-Alcalde, *DyIII- and YbIII-curcuminoid compounds: Original fluorescent single-ion magnet and magnetic near-ir luminescent species*, [\*Chemistry – A European Journal\* \*\*18\*\*, 11545 \(2012\)](#).
- [16] Y. Mawani and C. Orvig, *Improved separation of the curcuminoids, syntheses of their rare earth complexes, and studies of potential antiosteoporotic activity*, [\*Journal of Inorganic Biochemistry\* \*\*132\*\*, 52 \(2014\)](#), special Issue Containing Contributions from the Third Latin American Meeting on Biological Inorganic Chemistry - LABIC 2012.
- [17] L. Nardo, A. Andreoni, M. Bondani, M. Måsson, T. Haukvik, and H. H. Tønnesen, *Studies on curcumin and curcuminoids. xlv. photophysical properties of dimethoxy-curcumin and bis-dehydroxycurcumin*, [\*Journal of Fluorescence\* \*\*22\*\*, 597 \(2012\)](#).
- [18] C. A. Martin, J. M. van Ruitenbeek, and H. S. J. van der Zant, *Sandwich-type gated mechanical break junctions*, [\*Nanotechnology\* \*\*21\*\*, 265201 \(2010\)](#).
- [19] N. Agrait, A. L. Yeyati, and J. M. van Ruitenbeek, *Quantum properties of atomic-sized conductors*, [\*Physics Reports\* \*\*377\*\*, 81 \(2003\)](#).
- [20] B. Xu and N. J. Tao, *Measurement of single-molecule resistance by repeated formation of molecular junctions*, [\*Science\* \*\*301\*\*, 1221 \(2003\)](#).

- [21] Y. Zang, A. Pinkard, Z.-F. Liu, J. B. Neaton, M. L. Steigerwald, X. Roy, and L. Venkataraman, *Electronically transparent  $\text{Au-n}$  bonds for molecular junctions*, *Journal of the American Chemical Society* **139**, 14845 (2017).
- [22] B. Capozzi, J. Z. Low, J. Xia, Z.-F. Liu, J. B. Neaton, L. M. Campos, and L. Venkataraman, *Mapping the transmission functions of single-molecule junctions*, *Nano Letters* **16**, 3949 (2016).
- [23] T. A. Su, J. R. Widawsky, H. Li, R. S. Klausen, J. L. Leighton, M. L. Steigerwald, L. Venkataraman, and C. Nuckolls, *Silicon ring strain creates high-conductance pathways in single—molecule circuits*, *Journal of the American Chemical Society* **135**, 18331 (2013).
- [24] D. Miguel, L. Álvarez de Cienfuegos, A. Martín-Lasanta, S. P. Morcillo, L. A. Zotti, E. Leary, M. Bürkle, Y. Asai, R. Jurado, D. J. Cárdenas, G. Rubio-Bollinger, N. Agrait, J. M. Cuerva, and M. T. González, *Toward multiple conductance pathways with heterocycle-based oligo(phenyleneethynylene) derivatives*, *Journal of the American Chemical Society* **137**, 13818 (2015).
- [25] S. Y. Quek, M. Kamenetska, M. L. Steigerwald, H. J. Choi, S. G. Louie, M. S. Hybertsen, J. Neaton, and L. Venkataraman, *Mechanically controlled binary conductance switching of a single-molecule junction*, *Nature Nanotechnology* **4**, 230 (2009).
- [26] T. A. Su, H. Li, V. Zhang, M. Neupane, A. Batra, R. S. Klausen, B. Kumar, M. L. Steigerwald, L. Venkataraman, and C. Nuckolls, *Single-molecule conductance in atomically precise germanium wires*, *Journal of the American Chemical Society* **137**, 12400 (2015).
- [27] T. A. Su, H. Li, M. L. Steigerwald, L. Venkataraman, and C. Nuckolls, *Stereoelectronic switching in single-molecule junctions*, *Nature Chemistry* **7**, 215 (2015).
- [28] M. Kamenetska, S. Y. Quek, A. C. Whalley, M. L. Steigerwald, H. J. Choi, S. G. Louie, C. Nuckolls, M. S. Hybertsen, J. B. Neaton, and L. Venkataraman, *Conductance and geometry of pyridine-linked single-molecule junctions*, *Journal of the American Chemical Society* **132**, 6817 (2010).

## 5.A. APPENDICES

### 5.A.1. ADDITIONAL HISTOGRAMS AND FILTERING PROCEDURES

In this appendix we explain in more detail the filtering method employed to determine the junction-formation yield and to select the traces that make up the one-dimensional conductance histograms that were used to obtain the conductance values listed in the tables.

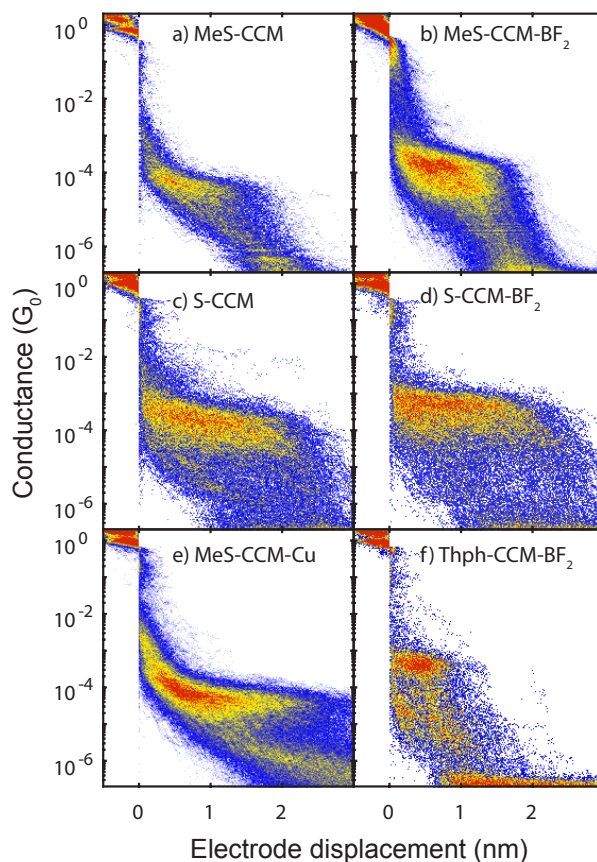


Figure 5.6: Filtered 2D-conductance vs. displacement histograms corresponding to the measurements displayed in Fig. 5.2. The window of displacement used for the selection was  $\Delta x = 0.5$  nm and the threshold slope  $m_{\text{thrs}} = 0.5$  decades per nm.

The filtering method is based on determining the decay rate of the conductance as a function of electrode displacement to distinguish between empty traces and those in which molecules bridge the electrodes. Note that the procedure is performed on the part of the traces after breaking of the metallic contact. There are two parameters that

define the filtering procedure: the displacement window ( $\Delta x$ ) and the threshold decay rate ( $m_{\text{thrs}}$ ). The procedure is as follows:

- A trace is compressed to the resolution of the 2D-conductance vs. displacement histogram (80 points per decade in conductance and 75 points per nm); this is done to avoid too much sensitivity to large conductance variations and it allows speeding up the analysis. When performing the analysis with the non-compressed data sets as a check, the results were found to be very similar.
- For every window of displacement  $\Delta x$  nanometer long, a linear fit to the data in  $\log_{10}(G)$  format is performed. The obtained slope  $m$  is defined as the decay rate of that trace in that window. The decay rate has units of decades/nm; a decay rate of  $m = -1$ , thus, means that, on average, the conductance decays by an order of magnitude per nanometer. A horizontal line corresponds to  $m = 0$  and  $m = 1$  means an average upturn of the conductance by one order of magnitude per nm for increasing displacement.
- For each trace the maximum value of  $m_{\text{max}}$  along the whole breaking trace is determined by evaluating  $m$  at each point (positive displacements only) and compared with the threshold  $m_{\text{thrs}}$ . If  $m_{\text{max}} > m_{\text{thrs}}$  the trace is labelled as a molecular trace.

In Fig. 5.6 we display the 2D-conductance vs. displacement histograms of the selected data from the same data sets as shown in Fig. 5.2. In these histograms, the contribution of the empty traces has been deleted so that the molecular features show up more clearly. As these data sets contain molecular features only, they are used in the 1D histograms to determine the value of the conductance peaks and their FWHM. We, however, generally find that values obtained from fitting the unfiltered data sets are close to the ones obtained from the filtered ones. As explained above, the filtering method also defines the yield of junction formation; for the measurements in Fig. 5.6 the yields are: 51% for MeS-CCM, 64% for MeS-CCM-BF<sub>2</sub>, 39.7 % for S-CCM, 26.7 % for S-CCM-BF<sub>2</sub>, 91% for MeS-CCM-Cu and 26% for Thph-CCM-BF<sub>2</sub>.

### 5.A.2. FITTING METHOD

For filtered and unfiltered 1D-conductance histograms we use a log-normal distribution  $N(x)$  to fit the data given by the following equation:

$$N(x) = A * \exp\left(-\left(\frac{(x - G_m)}{(0.6005615 \times FWHM)}\right)^2\right), \quad (5.1)$$

where  $x$  is expressed in  $\log_{10}$  of  $G$ ,  $A$  is the height of the peak,  $FWHM$  the full width half maximum and  $G_m$  the logarithm of the most probable conductance value. In the case of fitting two peaks, two of such curves are used with different  $G_m$ . We note that in fitting the data with two log-normal distributions, more than one combination of parameters can yield visually good fits to the data. As mentioned already in the main text, the most probable conductance varies little when changing the initial guess of the parameters or the fitting window, but the height and width of the two peaks can vary considerably; the statistical weight of the peaks can thus change significantly.



### 5.A.3. FIT PARAMETERS MeS-BF<sub>2</sub>-CCM AND TIME TRACES

In this subsection, we list the parameters of the fits shown in Fig. 5.4 of the main text. In Table 5.2, the values at 0.2 V are presented belonging to five different samples and in Table 5.3 the values for sample A at five different bias voltages are listed. When comparing the different samples, the high-conductance values vary between  $1.1$  and  $1.7 \times 10^{-4} G_0$ , while the low-conductance values vary between  $2.5$  and  $4.3 \times 10^{-5} G_0$ ; the ratio is about four in all cases. When changing the bias voltage, the high-conductance peak shifts to higher values whereas the low-conductance peak remains more or less constant. Correspondingly, the ratio between the two increases when a higher bias voltage is applied.

sample	$G_H (G_0)$	FWHM	$G_L (G_0)$	FWHM	$G_H/G_L$
A	$1.2 \times 10^{-4}$	0.5	$3.4 \times 10^{-5}$	0.8	3.5
B	$1.7 \times 10^{-4}$	0.4	$4.3 \times 10^{-5}$	1.5	3.9
C	$1.1 \times 10^{-4}$	1.0	$2.5 \times 10^{-5}$	0.6	4.4
D	$1.5 \times 10^{-4}$	0.3	$3.9 \times 10^{-5}$	1.3	3.8
E	$1.7 \times 10^{-4}$	0.4	$4.3 \times 10^{-5}$	1.5	4.0

Table 5.2: Fit parameters of the high ( $G_H$ ) and low ( $G_L$ ) conductance peaks and their respective FWHM as displayed in Fig. 5.4 a). The last column lists the ratio between the mean conductance values of the two log-normal distributions.

V (V)	$G_H (G_0)$	FWHM	$G_L (G_0)$	FWHM	$G_H/G_L$
0.05	$9.3 \times 10^{-5}$	0.4	$3.5 \times 10^{-5}$	0.8	2.7
0.1	$1.3 \times 10^{-4}$	0.3	$5.1 \times 10^{-5}$	0.7	2.5
0.2	$1.2 \times 10^{-4}$	0.5	$3.4 \times 10^{-5}$	0.8	3.5
0.25	$1.3 \times 10^{-4}$	0.5	$3.5 \times 10^{-5}$	0.8	3.7
0.3	$1.5 \times 10^{-4}$	0.7	$4.1 \times 10^{-5}$	0.9	3.6

Table 5.3: Applied bias voltage (first column), high ( $G_H$ ) and the low ( $G_L$ ) conductance values and the respective FWHM of the measurements displayed in Fig. 5.4 b) corresponding to sample A in Fig. 5.4 a). The last column lists the ratio between the mean conductance values of the two log-normal distributions.

To illustrate the intrinsic switching behavior of MeS-CCM-BF<sub>2</sub> in Fig. 5.7 we display time traces in which the conductance was monitored as a function of times: the first 3 s the electrodes were put at a prefixed distance (typically 0.15 nm) to which the snap-back distance has to be added; for the next 3 s the electrode spacing was reduced by 0.15 nm, after which the electrodes were placed at the original position. After 9 s, the electrodes were moved apart to break the molecular junctions (the red line in the upper panel of Fig. 5.7 illustrates this procedure). This procedure was used to ensure that the conductance monitored during the time trace has a molecular origin and is not due to tunnelling across a barrier. In the latter case, the conductance would drop upon an increase in electrode displacements, while, if a molecule is trapped, the conductance plateau will be hardly affected by the displacement.

The three bottom panels of Fig. 5.7 show typical time traces in which switching events are observed at different time scales. Note that there is no relation with the change of the electrode displacement as anticipated. Both, the high  $G$  and low  $G$  states, are observed to be stable on the time scale of seconds, but the switching event between the two can also occur on the millisecond time scale, e.g., the fast switching in the middle curve and in the last 2 s of the upper curve. We, thus, conclude that MeS-CCM-BF<sub>2</sub> can spontaneously jump from one state to another independently of the exact separation between the electrodes on time scales varying between a few ms to seconds. This observation shows that next to the electric field, geometrical considerations also play a role in determining which conductance state prevails. This is in line with the finding that at the lowest bias both conductance states can be found; apparently, geometrical constraints can favour one over the other. The data do show that for high electrical fields the high-conductance state is the dominant one.

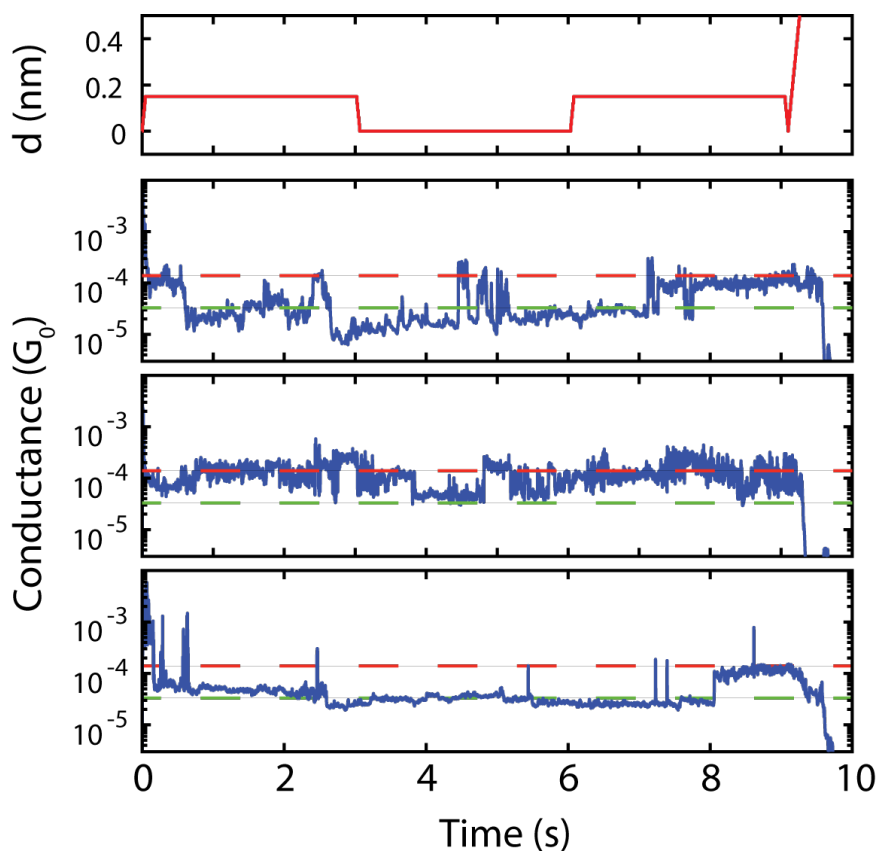


Figure 5.7: Examples of time traces of MeS-CCM-BF<sub>2</sub>. Top: electrode displacement as a function of time while the conductance is measured. Bottom three panels: examples of time traces in which switching events are observed at different time scales. The thin red and green lines represent the average conductance of the high and low conductance state of this molecule. The bias voltage across the junction is 0.2 V.

#### 5.A.4. ADDITIONAL MEASUREMENTS ON THE MOLECULES WITH THIOCARBAMATE ANCHORING (S-CCM AND S-CCM-BF<sub>2</sub>)

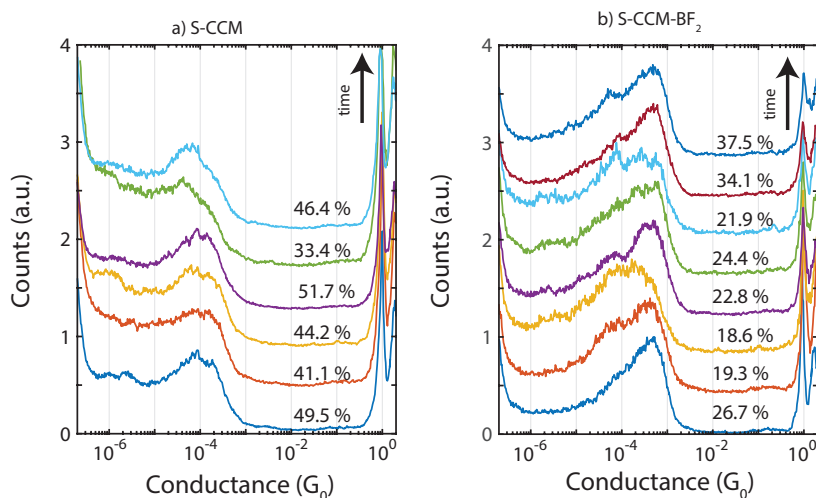


Figure 5.8: Series of normalized 1D-conductance histograms of data selected from series of 2000 consecutive traces measured at a bias voltage of 0.1 V and one after another. The percentage above each line displays the corresponding yield of junction formation. In a), the target molecule is S-CCM and in b), S-CCM-BF<sub>2</sub>. The histograms have been offset in the  $y$ -direction for clarity.

As the thiocarbamate group is not commonly used as an anchoring moiety in single-molecule electronics, we have performed additional measurements with the molecules containing this group. The advantage of this group is that it may cleave spontaneously in the presence of atomically sharp gold electrodes giving rise to a S-Au covalent bond analogous to the case of acetyl-protected thiol moiety (AcS) when a de-protecting agent is added to the solution. We have not used a de-protecting agent in the measurement reported here.

In Fig. 5.3 we show one-dimensional histograms of S-CCM (left panel) and S-CCM-BF<sub>2</sub> (right panel); in these plots the histograms are normalized meaning that the peak height of the molecular conductance feature is set to one. Each measurement is built up from selected traces obtained from data sets containing 2000 consecutive traces and this two-hour measurement is repeated 6 times for the molecule with the free ligand (S-CCM) and 8 times for the molecule with the BF<sub>2</sub> substituent. In all cases, the histograms show a very distinct peak at 1  $G_0$ , indicating the formation of clean and atomically sharp electrodes before the final breaking. The percentages listed above each curve indicate the yield of junction formation. As one can see, the yields do not systematically change as a function of time and vary between 20 and 50%. More importantly, the histograms show that after some time a low-conductance peak develops in both cases. For S-CCM, the trend continues for six data sets and, at the end, the low-conductance peak is more prominent than the high-conductance one. For S-CCM-BF<sub>2</sub>, only the first

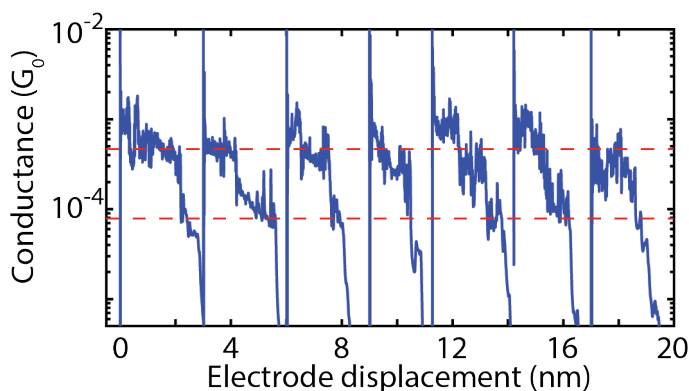


Figure 5.9: Examples of individual breaking traces of S-CCM-BF<sub>2</sub> in which the conductance switches to a low conductance value at the end of the high-conductance plateau. There are only step-down events in conductance as the inter electrode distance increase. The traces have been offset in the x-direction for clarity. Dashed lines are guides to the eye, representing the average conductance values of a double peaked structure in the conductance histograms.

measurement (i.e. the one at the bottom) show this change; for the remaining six curves there is no clear trend in this respect. Inspection of the 2D-histograms show that the low-conductance peak appears for large separation; individual traces displayed in Fig. 5.9 confirm this picture. In this figure, the dashed lines indicate the mean values of the two conductance states and, clearly, the low-conductance state is only accessed at large separation, unlike the situation for MeS-CCM-BF<sub>2</sub> as discussed in the main text.

We, thus, conclude that the cleavage of the carbamate unit between the molecules and the gold electrodes can proceed without the addition of de-protecting agents. The low-conductance counts for extended electrode spacing may indicate the presence of  $\pi - \pi$  stacking or dimerization, although as a function of time, their formation stabilizes in the case of the boron substituted compound.

#### 5.A.5. ADDITIONAL MEASUREMENTS ON THE COPPER DERIVATIVE

We studied in more detail the bias dependence and the reproducibility of the measurement of MeS-CCM-Cu. Ten different samples were measured; the results of five of them are shown here. The results in the main text are of those of sample E in the list. Fig. 5.10 shows the 1D histograms of five different samples (left panel) and for sample E, four different bias voltages. Except for sample A, the measurements show little variation of the conductance with bias voltage and a high reproducibility. A common feature of the measurements is that this molecule shows a high yield of junction formation (above 60% and generally above 70%). The fact that MeS-CCM-Cu is a charged molecule may play a role in the high yield of junction formation for this derivative.

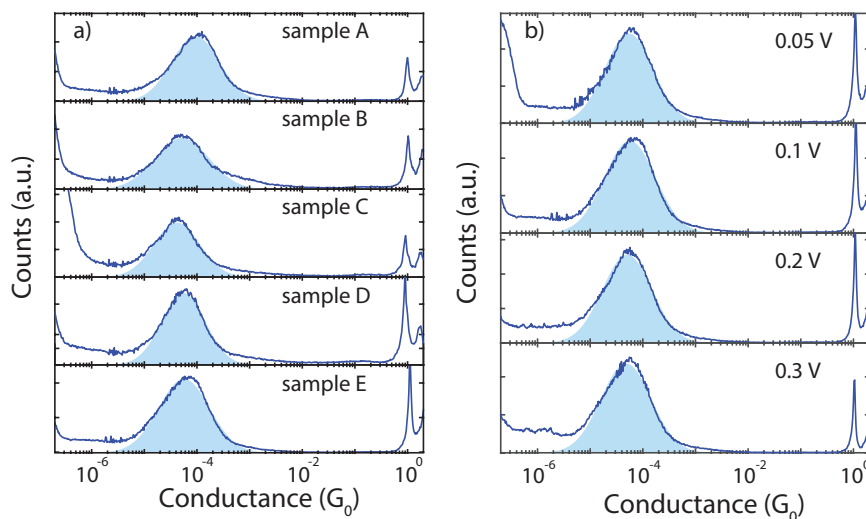


Figure 5.10: a) Series of conductance histograms of MeS-Cu-CCM corresponding to five different samples measured using a bias voltage of 0.1 V. b) Series of conductance histograms of measurements on the MeS-Cu-CCM compound (sample E) for different bias voltage; the light blue shaded areas correspond to log-normal distribution fits. The obtained parameters are shown in Table 5.4.

Sample	V (V)	G ( $G_0$ )	FWHM
A	0.1	$9.2 \times 10^{-5}$	1.1
B	0.1	$5.2 \times 10^{-5}$	1.2
C	0.1	$4.1 \times 10^{-5}$	1.0
D	0.1	$5.5 \times 10^{-5}$	1.0
E	0.05	$5.4 \times 10^{-5}$	1.1
E	0.1	$5.7 \times 10^{-5}$	1.1
E	0.2	$5.0 \times 10^{-5}$	1.1
E	0.3	$4.8 \times 10^{-5}$	1.1

Table 5.4: Mean conductance value and FWHM obtained by fitting a log-normal distribution to the measurements on MeS-Cu-CCM displayed in Fig. 5.10.

### 5.A.6. MEASUREMENT ON CU-CURCUMINOIDS WITH A DOUBLE BACKBONE

To test that the double-peak structure is not due to the *in-situ* formation of a new molecule containing two ligands, additional measurements on three samples have been performed using a compound holding two backbones attached to the same central part, mimicking this situation. We found that such a molecule with the B atom is not stable enough but with Cu incorporation such a molecule could be synthesized. The molecule is shown in Fig. 5.11 c) and here we present the conductance measurements on this molecule for one sample; the same conditions were used as for the other molecules shown in this chapter.

Fig. 5.11 a) shows a series of 1D-histogram constructed from selected traces out of

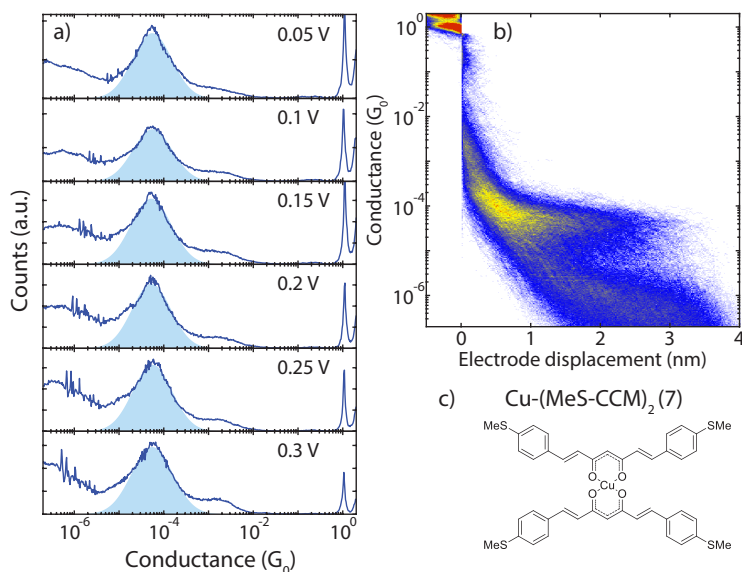


Figure 5.11: a) Series of conductance histograms of measurements on the  $2(\text{MeS-Cu})\text{-CCM}$  compound for different bias voltage; the light blue shaded areas correspond to log-normal distribution fits. The obtained parameters are shown in Table 5.5. b) 2D-conductance vs. displacement histogram of a representative sample of  $2(\text{MeS-Cu})\text{-CCM}$  constructed from 2000 consecutive traces measured at a bias voltage of 0.1 V/s and an electrode speed of 2.5 nm/s. c) Drawing of  $\text{Cu}(\text{MeS-CCM})_2$ 's structure. The estimated S to S distance in the same backbone is 1.7 nm, while this distance is 2.2 nm for two sulphur atoms in different back bones.

2000 consecutive traces at different bias voltages. A remarkable feature is the nearly independent position of the molecular conductance peak. The conductance values and FWHM of those measurements are listed in Table 5.5. These values and the ones listed for  $\text{MeS-CCM-Cu}$  (Table 5.4) appear to be very similar. This indicates that the conductance peak of  $\text{Cu}(\text{CCM-MeS})_2$  comes from a configuration in which one branch is connected to both electrodes so that the current is mainly flowing through only one of the backbones.

A closer inspection of the the 2D-conductance vs. displacement histogram displayed in Fig. 5.11 indicates the presence of molecular features at low conductance values (around  $10^{-6} G_0$ ) that extend up to 3 nm. This distance is larger than that of a single curcuminoid backbone; possibly conduction through the Cu atom with a current pathway going from one backbone to the other, contributing to this feature in the data. Nevertheless, for the largest distances, the molecular lengths are too short to support a picture and it is likely that molecule-molecule interactions play a role. We further note that we have observed similar behaviour in two other junctions; the main conductance peak in these junctions appeared at  $3.6 \times 10^{-5}$  and  $6.5 \times 10^{-5} G_0$ , respectively.

V (V)	G (G <sub>0</sub> )	FWHM
0.05	$5.5 \times 10^{-5}$	1.0
0.1	$5.6 \times 10^{-5}$	1.0
0.15	$5.2 \times 10^{-5}$	1.1
0.2	$5.3 \times 10^{-5}$	1.0
0.25	$5.6 \times 10^{-5}$	1.0
0.3	$5.5 \times 10^{-5}$	1.1

Table 5.5: Mean conductance value and FWHM obtained by fitting a log-normal distribution to the 1D-histograms of Cu(MeS-CCM)<sub>2</sub> displayed in Fig. 5.11.

### 5.A.7. CURCUMINOID-LIKE MOLECULES: DIBENZOYLMETHANE DERIVATIVES

To confirm that the combination of a SMe anchoring group and a BF<sub>2</sub> substitution in these derivatives give rise to a double peak structure in the conductance histograms, additional measurements were performed on a shorter system that resembles the structure of the curcuminoids. Fig. 5.12 displays the two dibenzoylmethane derivatives studied MeS-dbm and MeS-dbm-BF<sub>2</sub> which are the shorter analogues of MeS-CCM and MeS-CCM-BF<sub>2</sub>, respectively. The difference between the two sets of molecules is the arm length of the molecule that connects the central part with the outer phenyl rings. The distance between the sulfur atoms in the shorter molecules is about 1.3 nm, while for the longer curcuminoids it is around 1.9 nm. We have measured in detail two samples for each compound at different bias voltages and two different electrode speeds.

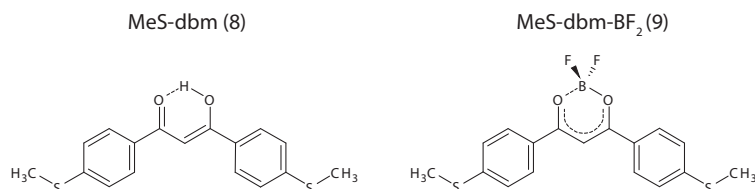


Figure 5.12: Drawings of the short versions of the curcuminoid-like derivatives with a) the free ligand mimicking the structure of MeS-CCM and b) the boron difluorine substituted compound analogous to MeS-CCM-BF<sub>2</sub>. The sulphur to sulphur distance of MeS-dbm-BF<sub>2</sub> is 1.32 nm as obtained from X-ray diffraction measurements and the one for MeS-dbm is assumed to be similar.

Four 2D-conductance vs. electrode displacement histograms of the shorter compounds are displayed in Fig. 5.13: On the left hand side MeS-dbm and on the right hand side MeS-dbm-BF<sub>2</sub>, both at two different bias and electrodes speed. Before describing and discussing the results in more detail, it is worth making some general remarks: the length of the molecular features in the top panels (fast measurements) is about 0.5 nm shorter than those of the curcuminoids analogues shown in Fig. 5.2. This difference is in good agreement with the molecular length difference between the two compounds. Furthermore, the molecular conductance features are observed at higher values in comparison with the longer curcuminoids which is expected for shorter molecules. Overall

the data shows remarkable similarities with those of the longer curcuminoids; importantly, the double-peak structure of the curcuminoid molecule with the  $\text{BF}_2$  substituent is reproduced. We will now discuss the two short molecules in more detail, starting with the bare-ligand one.

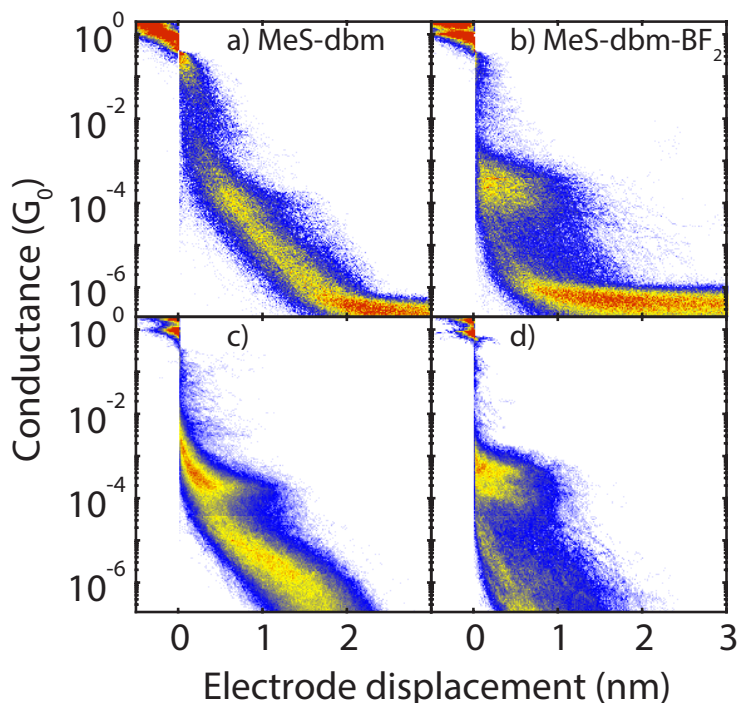


Figure 5.13: 2D conductance vs. displacement histograms of a) and c) MeS-dbm ; b) and d) MeS-dbm- $\text{BF}_2$  constructed from 2000 consecutive traces measured at 50 mV in a), 25 mV in b) and 0.25 V in c) and d). The experiments were performed in ambient conditions and with an electrode speed of 3 nm/s in a) and b); and 0.3 nm/s in c), d).

#### MEASUREMENTS ON MeS-DBM

In fig. 5.13 a) the two-dimensional of MeS-dbm shows a less steep slope for the traces in which the conductance exponentially drops to the noise level. This is also observed for the longer analogue (MeS-CCM) in Fig. 5.2 a). The shallower slope of the exponential decay in these cases may be caused by a smaller work function (inspection of the length of the  $1 G_0$  peak shows that it cannot be attributed to an error in the calibration). It should be noted that the bare-ligand molecules with the other anchoring groups do not show this extended tunnelling-like behaviour. The reason is not known but a possibility could be that the bare-ligand molecules with this anchoring group form a rather dense layer while being flat on the Au surface, thereby, altering the work function.



Importantly, these longer features in the measurements for this compound make the filtering method less effective in distinguishing molecular traces from empty ones. Therefore, all further analysis on this molecule was performed on the full data sets. In general, we found that at the electrode speeds used for the longer curcuminoids (3 nm/s), the conductance peaks in the 1 and 2D histograms were not clearly visible. We found that by reducing this speed by about a factor of 10, makes the molecular features more prominent. In addition, we found that by increasing the bias voltage, the conductance peaks become more prominent. Fig. 5.13 a) and c) show this for the 2D histograms while fig. 5.14 illustrates this for the 1D conductance histograms for the two samples studied.

The molecular features are more prominent in the slow breaking experiments and peaks are observed around  $2 \times 10^{-4} G_0$ . The background counts at low conductance values make the estimation of the most probable molecular conductance less accurate with respect to the estimates on the filtered data for the other compounds. The exception may be the high-bias measurements in Fig. 5.14 in which the conductance peaks appear to be sharper. Nevertheless, we have extracted the values of the mean conductance and the FWHM of the corresponding peaks from fitting the data to a log-normal distribution (blue shaded areas in Fig. 5.14). The values are listed in table 5.6; the values for the different bias voltages are remarkably consistent. We find that the most probable conductance for this compound is about three times larger than that of the longer curcuminoid analogue (MeS-CCM).

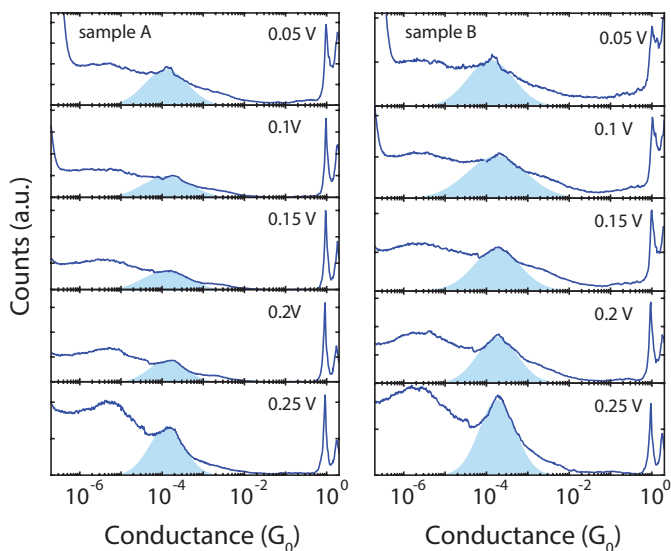


Figure 5.14: a) Series of un-filtered 1D-histograms measured at different bias voltages of MeS-dbm and at 0.3 nm/s for two different samples.

There is one more characteristic of the 1D histograms on this molecule that deserves a closer look, namely the broad peak at low conductance values that is visible mainly

sample	V (V)	G (G <sub>0</sub> )	FWHM
A	0.05	$1.2 \times 10^{-4}$	1.2
A	0.1	$1.3 \times 10^{-4}$	1.4
A	0.15	$1.2 \times 10^{-4}$	1.3
A	0.2	$1.4 \times 10^{-4}$	1.1
A	0.25	$1.3 \times 10^{-4}$	1.0
B	0.05	$1.3 \times 10^{-4}$	1.3
B	0.1	$1.8 \times 10^{-4}$	1.7
B	0.15	$1.8 \times 10^{-4}$	1.3
B	0.2	$1.8 \times 10^{-4}$	1.2
B	0.25	$1.8 \times 10^{-4}$	1.0

Table 5.6: Mean conductance values and FWHM of MeS-dbm obtained by fitting a log-normal distribution to the data in the 1D-histograms displayed in Fig. 5.14.

at high bias voltages (especially at at 0.25 V for both samples). As mention before, the long features in this measurement made the filter used in the curcuminoids ineffective. We, therefore, performed a different kind of filtering method, in which traces with a high number of counts in a particular region of interest compared to those that exhibit the average frequency of counts in that region, are selected. For example, in Fig. 5.15 we split the traces of the measurement on sample B at 0.25 V in two groups: the ones that have at least 1.3 times as much counts as the average distribution in the region between  $9.4 \times 10^{-5}$  and  $5.3 \times 10^{-4}$  G<sub>0</sub>; and the ones that do not obey this criterion. Then, 1D and 2D conductance histograms are constructed with the traces of each group. The resulting histograms are displayed in panels b) and c) of fig. 5.15 along with the 2D histogram of the full data set in a). The 2D-histograms show that the selected traces in the high-conductance region display a plateau-like behavior while in the region of low conductance the features are slanted, smoothly reaching the noise level.

In fig. 5.15 d) the three corresponding 1D-conductance histograms are displayed. The choice of the conductance region of interest matches the region where the molecular features are observed, and consequently, the strength of the conductance peak for the selected traces (red curve) is enhanced. In contrast, the 1D-conductance histogram of the unselected traces shows no features in the selected high-conductance region while the broad peak, at low conductance, is a bit more prominent.

When the same filtering is used to enhance the traces with conductance values in the region of the broad peak (Fig. 5.16), a similar picture emerges: the traces at low conductance values are slanted, but in this case the selected traces (red line in Fig. 5.16 d)) still show a small bump at the conductance value of the high conductance state. This means that the occurrence of the low-conductance state does not prevent the occurrence of the other state. The curves of the selected traces do indicate, that in addition, there is a substantial amount of traces that either follow the high-conductance peak structure or the more gradual evolution with displacement at low conductance values.

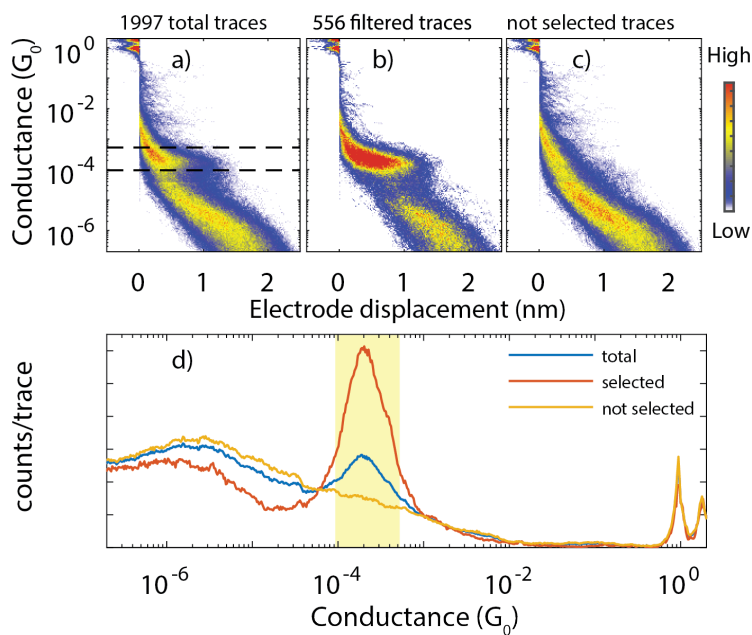


Figure 5.15: a) 2D-histogram of sample A (MeS-dbm) measured at a bias voltage of 0.25 V and an electrode speed of 0.3 nm/s. The black dashed lines mark the region of interest. b) 2D-histogram constructed from the traces in a) that have at least 1.3 times the counts of the total 1D-histogram (blue line in d) in the region depicted by the yellow shaded area (between  $9.4 \times 10^{-5}$  and  $5.3 \times 10^{-4} G_0$ ). c) 2D-histogram constructed from the traces that do not fulfill the condition considered in b). d) 1D-conductance histograms of all (blue), selected (red), and not selected (orange) traces. The yellow shaded area highlights the conductance region of interest.

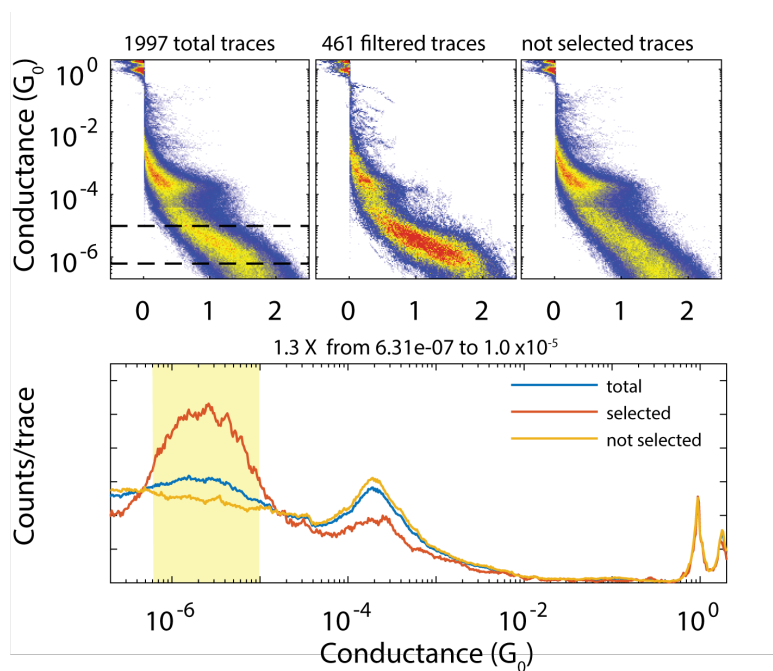


Figure 5.16: a) 2D-histogram of sample A (MeS-dbm) measured at a bias voltage of 0.25 V and an electrode speed of 0.3 nm/s. The black dashed lines mark the region of interest. b) 2D-histogram constructed from the traces that have at least 1.3 times the counts of the total 1D-histogram (blue line in d) in the region depicted by the yellow shaded area (between  $6.3 \times 10^{-7}$  and  $1.0 \times 10^{-5} G_0$ ). c) 2D-histogram constructed from the traces that do not fulfill the condition to be considered in b). d) 1D-conductance histograms of all (blue), selected (red), and not selected (orange) traces.

## MEASUREMENTS ON MeS-DBM-BF<sub>2</sub>

We have measured two samples with the MeS-dbm-BF<sub>2</sub> compound. In contrast to the free ligand, we find that the MeS-dbm-BF<sub>2</sub> compound shows clear plateaus when it bridges the gap between the electrodes. Although our filtering procedure can effectively split the data in meaningful subsets, we performed all the analysis on the un-filtered data to consistently compare it to the free ligand.

Fig. 5.17 shows the 1D-histograms of two samples at different bias voltages. A similar fitting procedure as used for the longer curcuminoid analogue was performed; the dashed lines indicate the corresponding two log-normal fits to the data. The double-peak structure is apparent in these samples especially at low bias voltages and shows a clear evolution as the bias voltage increases from 10 mV to 0.25 V. The low-conductance peaks are consistently broader and, as a consequence, the estimates of the corresponding peak conductance may be less accurate. In addition, the fitting is not unique in the sense that depending on the window chosen to fit the data, several combinations of log-normal distributions allow good fits to the data, albeit that the conductance values for those do not change much (see also discussion in Appendix 5.A.3). Nevertheless, the data show a clear change in the weight of the two conductance states: at low bias voltages both states are present and the peak heights are about the same. By increasing the bias voltage, the high-conductance peak starts to become more prominent. In both samples, this occurs at a bias of 50-100 mV and upon increasing the bias further, the high-conductance peak becomes even more prominent, especially in sample B.

Using the fitting procedure mentioned above, we have also extracted the most probable conductance values and the FWHM of the peaks from the data. The values are listed in Table 5.7 and Table 5.8 for the un-filtered and filtered data respectively. For the selected data the same criterion is used as for the longer curcuminoids discussed in the main text. Un-filtered and filtered data are presented to facilitate the comparison with the short free ligand (MeS-dbm) and the longer curcuminoid (MeS-CCM-BF<sub>2</sub>), respectively.

Interestingly, the ratio between the high conductance value of MeS-dbm-BF<sub>2</sub> and the correlative curcuminoid MeS-CCM-BF<sub>2</sub> is about 3.4 (at 0.1 V), which is close to the value found when comparing the bare ligands of the corresponding compounds. It is also interesting to investigate the ratio between the conductance values of the free ligands and the BF<sub>2</sub> substituted compound for the two classes of molecules: at a bias voltage of 0.1 V, this ratio is 3.1 for the short derivatives and 3.6 for the longer curcuminoids. The ratio between the two peak conductance in Table 5.7 fluctuates around a factor of 3.5, a value that is slightly higher than the one found for the longer curcuminoid molecule with BF<sub>2</sub> substitution (see Tables 5.2, 5.3). Finally, the time traces displayed in Fig. 5.18 again show that the switching happens while stretching the molecule and that the switches can be both down and up in conductance, very similar to what has been observed for the longer curcuminoid BF<sub>2</sub> substituted molecule. Noteworthy, the conductance values obtained from the unfiltered data are in good agreement with the ones obtained with the filtered data, but in general the filtered data produces lower FWHM values than the full data sets, thus, giving a more accurate estimation of the most probable conductance value.

In conclusion, the data on MeS-dbm-BF<sub>2</sub> show a striking resemblance with those of MeS-CCM-BF<sub>2</sub>. This consistency further strengthens the conclusion that the combina-

tion of the SMe anchoring unit and the  $\text{BF}_2$  substituent are the required ingredients for achieving the observed double-peak structure for these compounds.

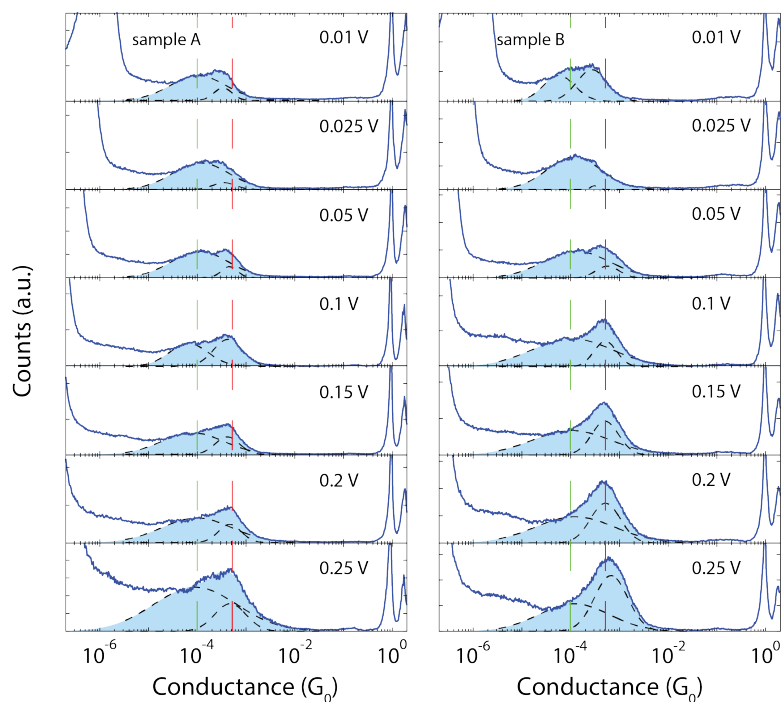


Figure 5.17: Series of un-filtered 1D-histograms measured at different bias voltages of MeS-dbm- $\text{BF}_2$  recorded at an electrode displacement speed of 3 nm/s. Vertical lines are guides to the eye, marking the average values of the conductance peaks obtained from fits at 0.25 V.

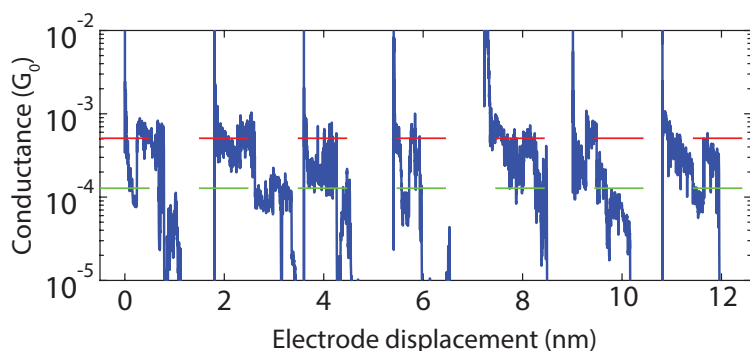


Figure 5.18: Series of single breaking traces of MeS-dbm- $\text{BF}_2$  measured at a bias voltage of 0.2 V and an electrode speed of 0.3 nm/s. Traces have been offset in the x-direction for clarity.

Sample	V (V)	$G_H$ ( $G_0$ )	FWHM	$G_L$ ( $G_0$ )	FWHM	$G_H/G_L$
A	0.01	$3.4 \times 10^{-4}$	0.4	$1.0 \times 10^{-4}$	1.3	3.2
A	0.02	$3.6 \times 10^{-4}$	0.5	$1.2 \times 10^{-4}$	1.4	3.0
A	0.05	$4.5 \times 10^{-4}$	0.4	$1.1 \times 10^{-4}$	1.4	4.0
A	0.1	$4.2 \times 10^{-4}$	0.7	$6.6 \times 10^{-5}$	0.9	6.4
A	0.15	$4.1 \times 10^{-4}$	0.6	$8.1 \times 10^{-5}$	1.5	5.1
A	0.2	$4.6 \times 10^{-4}$	0.5	$9.8 \times 10^{-5}$	1.7	4.7
A	0.25	$4.8 \times 10^{-4}$	0.8	$9.0 \times 10^{-5}$	2.0	5.3
B	0.01	$2.7 \times 10^{-4}$	0.7	$5.8 \times 10^{-5}$	0.8	4.7
B	0.02	$3.0 \times 10^{-4}$	0.2	$1.2 \times 10^{-4}$	1.3	2.6
B	0.05	$5.7 \times 10^{-4}$	0.6	$1.3 \times 10^{-4}$	1.6	4.3
B	0.1	$5.1 \times 10^{-4}$	0.5	$1.1 \times 10^{-4}$	1.9	4.8
B	0.15	$5.1 \times 10^{-4}$	0.7	$1.0 \times 10^{-4}$	1.9	4.9
B	0.2	$5.2 \times 10^{-4}$	0.7	$1.2 \times 10^{-4}$	1.9	4.2
B	0.25	$6.7 \times 10^{-4}$	0.8	$1.2 \times 10^{-4}$	1.7	5.8

Table 5.7: Fit parameters of high ( $G_H$ ) and low ( $G_L$ ) conductance peaks and their respective FWHM for MeS-dbm-BF<sub>2</sub>, as displayed in Fig. 5.17 a). The last column shows the ratio between the mean conductance values of the two log-normal distributions.

Sample	V (V)	$G_H$ ( $G_0$ )	FWHM	$G_L$ ( $G_0$ )	FWHM	$G_H/G_L$
A	0.01	$3.4 \times 10^{-4}$	0.4	$1.2 \times 10^{-4}$	1.2	2.8
A	0.02	$3.8 \times 10^{-4}$	0.5	$1.4 \times 10^{-4}$	1.2	2.7
A	0.05	$4.6 \times 10^{-4}$	0.4	$1.4 \times 10^{-4}$	1.2	3.3
A	0.1	$4.6 \times 10^{-4}$	0.5	$1.2 \times 10^{-4}$	1.4	3.7
A	0.15	$4.2 \times 10^{-4}$	0.6	$1.0 \times 10^{-4}$	1.4	4.1
A	0.2	$4.8 \times 10^{-4}$	0.5	$1.4 \times 10^{-4}$	1.5	3.5
A	0.25	$5.3 \times 10^{-4}$	0.6	$1.7 \times 10^{-4}$	1.5	3.2
B	0.01	$3.0 \times 10^{-4}$	0.4	$1.2 \times 10^{-4}$	1.1	2.4
B	0.02	$3.4 \times 10^{-4}$	0.2	$1.4 \times 10^{-4}$	1.1	2.4
B	0.05	$5.5 \times 10^{-4}$	0.6	$1.5 \times 10^{-4}$	1.4	3.7
B	0.1	$5.0 \times 10^{-4}$	0.5	$1.4 \times 10^{-4}$	1.5	3.5
B	0.15	$5.0 \times 10^{-4}$	0.6	$1.2 \times 10^{-4}$	1.7	4.1
B	0.2	$5.1 \times 10^{-4}$	0.7	$1.5 \times 10^{-4}$	1.7	3.4
B	0.25	$7.0 \times 10^{-4}$	0.8	$1.3 \times 10^{-4}$	1.5	5.4

Table 5.8: Fit parameters of high ( $G_H$ ) and low ( $G_L$ ) conductance peaks and their respective FWHM as displayed in Fig. 5.19 a) considering only the selected molecular traces. The last column shows the ratio between the mean conductance values of the two log-normal distributions.

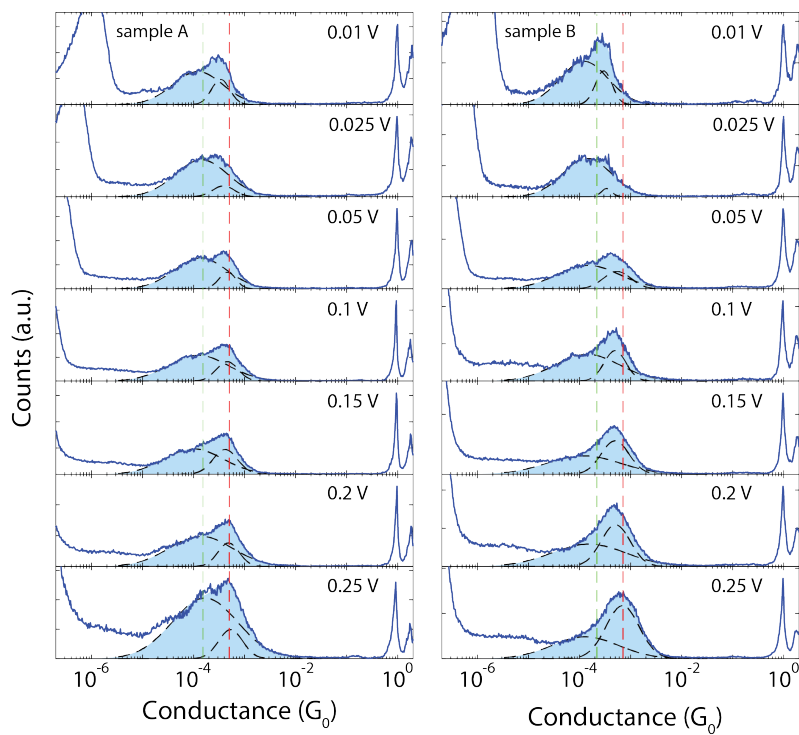


Figure 5.19: Series of filtered 1D-histograms of MeS-dbm-BF<sub>2</sub> measured at different bias voltages and at 3 nm/s. Vertical lines are guides to the eye at the average value of the conductance obtained from fits at 0.25 V.





# 6

## THE ROLE OF SIDE GROUPS AS ANCHORING SITES IN CURCUMINOIDS

*Wie weet van het spel van het kind en de vrouw  
het kind en de vrouw zijn op zoek naar vuurrood  
maar het kind noch de vrouw vindt het rood dat het wou  
en het kind en de vrouw vinden samen de dood.*

Muziek voor kijkdieren, Hans Andreus

*Using curcumin inspired molecular systems we show that the inclusion of pyrazole and isoxalozane groups in the conducting molecule leads to an alternative pathway for charge transport. Using the mechanically controlled break junction (MCBJ) technique we obtain the most probable conductance values of the two different binding configurations. These are mechanically stable on the time scale of seconds and the probability of trapping the molecule in each state can be tuned by controlling the inter-electrode distance. The high conductance states are related to the molecule attached through the nitrogenated moiety in the middle of the molecules. This high conductance arrangement can be broken and re-made unless a bulky group is attached to such group, i.e., a phenyl ring. In such case, the high conductance states can not be recovered after the breaking of the N-Au contact.*

## 6.1. MOLECULES WITH DIFFERENT PATHWAYS FOR CHARGE TRANS- PORT

One of the first challenges confronted in the field of single-molecule electronics was the method for attaching molecules to the metallic electrodes. As experience accumulated, several strategies have proven to reliably bind molecules to metallic electrodes; most of them rely on the inclusion of anchoring groups, which are moieties with an affinity to metals. Some examples include thiol [1], pyridine [2] or amine [3–5] groups. However, different strategies are better suited for some systems but give suboptimal results in others. Further exploration of this respect is, thus, needed.

A common practice in molecular electronics is to functionalize the molecules of interest with anchoring moieties at the ends of the longest axis of the molecules. Sometimes, either by design or by chance, some molecular systems present alternative anchoring moieties placed somewhere along the backbone between the main anchoring sites [6–9]. This may introduce an alternative molecular conformation of the molecule in between electrodes, providing a shorter pathway for charge carriers to cross the molecule.

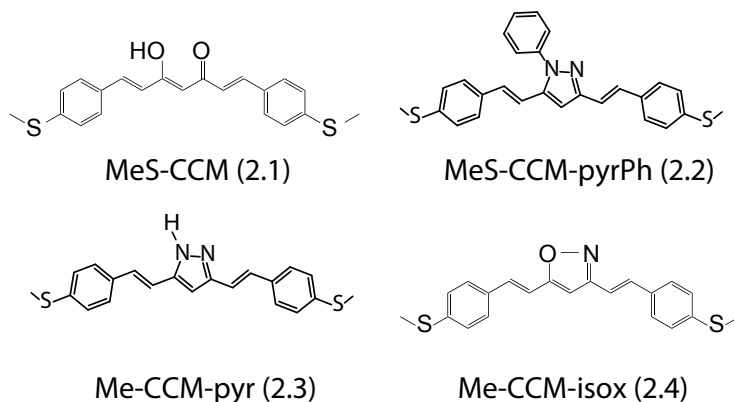


Figure 6.1: Structure of the molecules of interest in this chapter which are methyl-sulphide terminated curcuminoids: (2.1) the free ligand, (2.2) contains a pyrazole-phenyl attached to the backbone, (2.3) has a pyrazole group (un-blocked) added in the backbone and (2.4) an isoxazole group.

Curcuminoids have been introduced in chapter 4. In short, curcuminod are organic compounds with a conjugated nature that share the structure of the naturally occurring curcumin molecule found in the turmeric spice. In this chapter, we study the implications of incorporating nitrogen containing groups on the central part of the molecular structure. In Fig. 6.1, a drawing of the four molecules considered in this study is displayed. The conjugated nature of the molecular backbone is evident. When the molecule is connected to two gold electrodes, the intended pathway for electrons goes from one sulfur atom at one end, to the other sulfur atom, at the other end. The molecule MeS-CCM (2.1) does not contain an aromatic ring in the middle of the molecule; we refer to

it as the free ligand because it resembles the structure of the naturally occurring curcumin and it is used as a reference for comparison. Molecule 2.3 (MeS-CCM-pyr) holds a pyrazole group in the central part. This generates a five member aromatic ring and also introduces a group with a high affinity for metals. Molecule 2.2 (MeS-CCM-pyrPh) has the same core configuration as molecule 2.3 but, in this case the proton, in the pyrazole group is replaced by a phenyl ring. Lastly, molecule 2.4 (MeS-CCM-isox) incorporates an isoxazole group in the middle. It also exhibits an aromatic ring but has a composition that is more similar to that of the free ligand.

From the perspective of molecular electronics, the structure of these molecules allows them to form a covalent bond with gold electrodes through the MeS end groups. The process of charge exchange between the molecules and the electrodes, in this case occurs, by 'through-bond' interactions or extraction. When a molecule is physisorbed, for example, on a metallic surface charge transfer between the surface and the molecule may occur by 'through-space' injection. In general this kind of processes happen at low temperature and not in ambient conditions because thermal fluctuation can easily break the connection. In some cases, the injection (or collection) of electrons can be more effective through a 'through-space' process, because, for example, the pathway between the injection and collection points is shorter than the distance between the bonding sites at the ends of the molecule. The mechanical stability could then be provided by the chemical bond that is farther away. In the case of the molecules presented here there is the possibility that the pyrazole and the isoxazole group interact with gold atoms to form dative donor-acceptor bonds [10, 11] through the lone pair of the nitrogen atoms. This could, in principle, provide an alternative anchoring and therefore a 'through-bond' site for charge injection. In the case of MeS-CCM-pyrPh there is still the possibility of a chemical bond formation through the lone pair of the nitrogen atom that is not connected to the phenyl ring. The phenyl ring, on the other hand, could mechanically block the access to the pyrazole as a bonding site but, at the same time, an effective link for 'through-space' charge injection could appear, thanks to its pronounced  $\pi$ -cloud.

Here, we test these ideas by single-molecule conductance measurements using the mechanically controlled break junction (MCBJ) technique. By linking the results to the structure of the target molecule, we try to enhance our understanding concerning which variables in the chemical design of the molecules have impact on their electronic properties. More specifically, we can quantify the different efficiency of conduction path in molecules by measuring conductance traces in MCBJ devices.

It has been shown that if a molecule has another group that can bind to the electrodes, it is possible to observe multiple states of conductance [7, 8] related to different pathways through the molecule. Here, we demonstrate that the same phenomena can be achieved in curcuminoid complexes using pyrazole and isoxazole groups that act as alternative anchoring positions that can be successively connected and disconnected. Using the mechanical stability of the MCBJ devices, we show that single-molecules can be cycled between different anchoring configurations that differ in conductance value due to the electronics pathway that the charge carriers go through.

The chemistry between nitrogen and noble metals is very well documented. In the context of molecular electronics, nitrogen has been used to link molecules to metallic electrodes, for example, amine or pyridine groups have successfully been used to con-

nect single-molecule to gold electrodes [2, 12]. Although pyrazole groups have not been exploited as anchoring moieties, their interaction with noble metals is well established in organometallic chemistry [13].

## 6.2. CONDUCTANCE MEASUREMENTS

We performed conductance vs. electrode displacement measurements using the MCBJ technique. After a control measurement on the clean device was performed to check the absence of contamination, the molecules were drop-casted from solution ( $< 50 \mu\text{M}$  in dichloromethane for MeS-CCM and tetrahydrofuran otherwise) on an MCBJ device. Two thousand traces were recorded at electrode speed between 3 to 8 nm/s and a bias voltage of 0.1 V for each molecule. The collected data is displayed in Fig. 6.2 in the form of 2D-conductance vs. electrode displacement histograms of the 4 molecules. All 4 histograms show the formation of molecular traces in the form of plateaus in which the traces extend for more than one nanometer while the conductance remains, approximately, the same over this range. Remarkably, MeS-CCM-pyr, MeS-CCM-pyrPh and Me-CCM-isox show a second region of high counts at a higher conductance value, related to a smaller displacement of up to 1 nm.

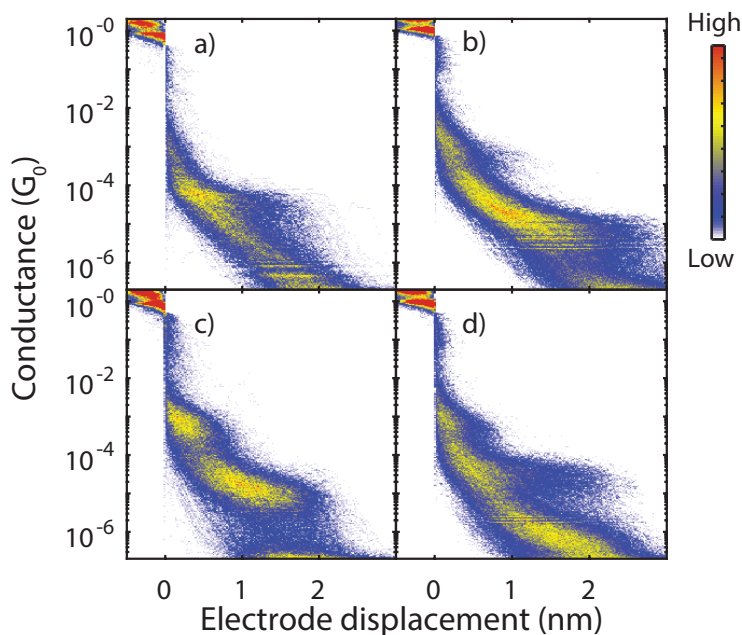


Figure 6.2: Two-dimensional conductance vs. electrode displacement histograms of the molecules displayed in Fig. 6.1 constructed from 2000 consecutive breaking traces each using 80 bins per decade and 70 bins per nm. The panels correspond to the results obtained with a) MeS-CCM, b) MeS-CCM-pyrPh, c) MeS-CCM-pyr and d) MeS-CCM-isox.

Figure 6.3 displays the corresponding 1D-conductance histograms of molecules depicted in Fig. 6.1, the considered data was filtered from the total data using a plateau selection criterion base on the slope of the traces as described in chapter 2, utilizing parameters  $\Delta x=0.5$  nm and  $m_{\text{thrs}}=0.5$  dec/nm. The green shaded areas correspond to log-normal fits of the main molecular peak and in the cases of MeS-CCM-pyr and MeS-CCM-isox a second peak was needed to fit the data (light blue shaded areas). The conductance values as well as the full with half maximum (FWHM) of these fits are listed in table 6.1 and, in the last column, the ratio between the high- and low-conductance states is displayed.

The values obtained this way reveal that the conductance of MeS-CCM and the lower peak of MeS-CCM-isox are very similar, indicating that the isoxazole group has little influence on the conductance of the sulfur to sulfur path through the entire backbone. There is a noticeable reduction of the conductance value in the cases of MeS-CCM-pyr and MeS-CCM-pyrPh with respect to MeS-CCM, being MeS-CCM-pyrPh slightly lower than MeS-CCM-pyr. Despite these differences, all the compounds but the free ligand have a similar conductance value for the high conductance peak. It is worth mentioning that the conductance histogram of MeS-CCM-isox (6.3d) also has a bump at low conductances. This could be another state or configuration related to the presence of the isoxazole group. A candidate for such behavior could be two molecules stack together by, for example, hydrogen bonding, each one attached to a different lead through one of the sulfur atoms[14], but we have not pursued this topic in detail.

Molecule	$G$ ( $G_0$ )	FWHM	$G_H/G_L$
MeS-CCM	$3.7 \times 10^{-5}$	1.1	-
MeS-CCM-pyrPh	$3.0 \times 10^{-4}$	1.7	41.1
	$7.4 \times 10^{-6}$	1.2	
MeS-CCM-pyr	$4.8 \times 10^{-4}$	1.1	36.3
	$1.4 \times 10^{-5}$	1.2	
MeS-CCM-isox	$4.7 \times 10^{-4}$	1.2	13.7
	$3.4 \times 10^{-5}$	0.8	

Table 6.1: Most probable conductance value (first column), full width half maximum (FWHM) (second column) and the conductance ratio obtained from fitting the data of 1D-histograms of each compound to log-normal distributions. The considered data sets were measured at a bias voltage of 0.1 V and the electrode speed was in the range of 3 to 8 nm/s.

The existence of high conductance states related to short displacements is an interesting feature that may be related to particular junction conformations. We made a more detailed analysis on the data of MeS-CCM-pyr (see 6.A.2) and concluded that there are at least three different classes of molecular breaking traces occurring with almost the same probability; traces that only show long plateaus at low conductance values, short plateaus with a high conductance value, and traces that start at the high conductance region and then, abruptly, transit to the low-conductance plateau behaviour. The same kind of analysis gave similar results with the compound MeS-CCM-isox with a slightly smaller proportion of traces with a transition from high- to low-conductance state. In

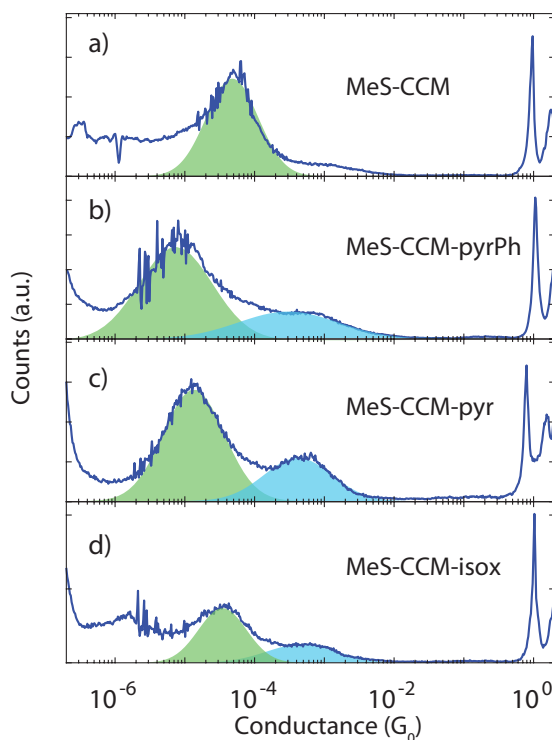


Figure 6.3: Conductance histograms of the molecules constructed from selected traces of measurements of 2000 consecutive traces measured at a bias voltage of 0.1 V and an electrode speed between 3 and 8 nm/s using MeS-CCM (a), MeS-CCM-pyrPh (b), MeS-CCM-pyr (c) and MeS-CCM-isox (d) as the target molecule. The conductance binning is 80 bins per decade. The shaded areas correspond to log normal distribution fitting of the conductance peaks, the light blue shaded areas correspond to the same kind of fitting to the high conductance states. In the cases in which two curves were fit, the procedure was run a single time with twice the fit parameters in the region of interest.

the case of MeS-CCM-pyrPh, the amount of traces showing plateaus at high conductance state were considerably less (between the 30 and the 51 % of the molecular traces).

### 6.2.1. DISTANCE MODULATION

With the aim of testing the mechanical tunability of the conductance states, we performed a conductance measurement while the inter-electrode distance was modulated in the following way: during each trace, the electrode displacement was increased from the last gold atom breaking point to a predefined displacement  $x_1$  to which the 0.5 nm snapping of the electrodes has to be added in order to obtain an estimate of the actual inter-electrode distance. Then, the electrodes were kept at that distance for a period of time ( $\Delta t$ ) after which the electrodes were pushed back together to a predetermined distance ( $x_2$ ). There the electrodes were again kept for  $\Delta t$  at this position and this process

was repeated a number of times.

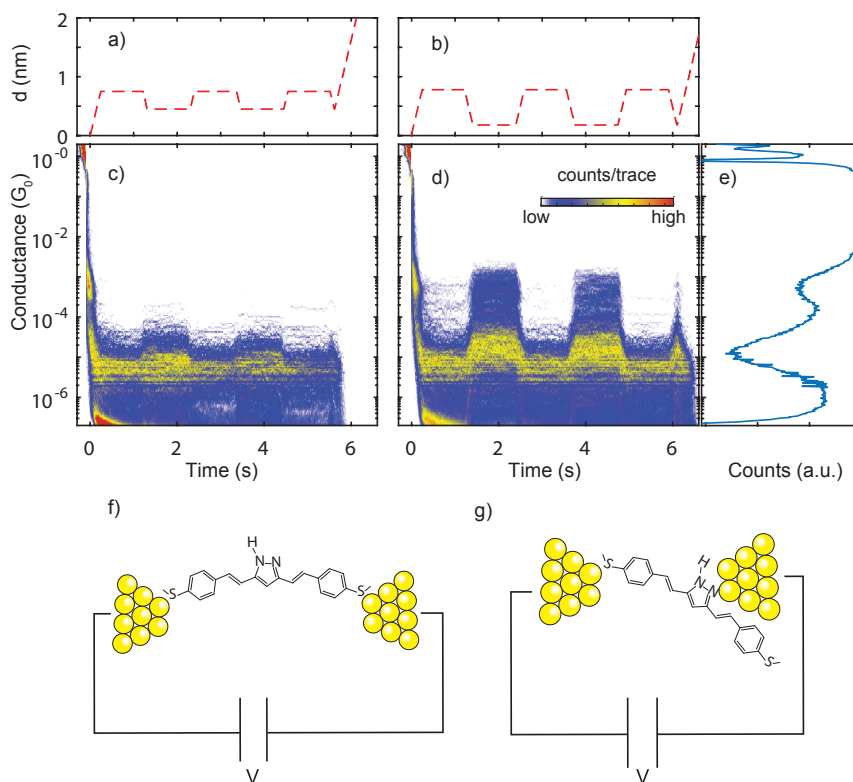


Figure 6.4: a) and b) Inter-electrode distance as a function of time for the distance modulation experiment. Zero displacement is defined as the breaking point at which the conductance drops below  $1 G_0$  which corresponds, approximately, to a distance of 0.5 nm in real space. c) and d) Conductance vs. time histograms constructed from 1200 consecutive traces in which the inter-electrodes distance was modulated as shown in a) and b), respectively. The conductance axis has been logarithmically binned with 94 bins/decade and the time axis with 100 bins/sec. The target molecule used in the measurement was MeS-CCM-pyr. In e) the one-dimensional conductance histogram obtained in the fast breaking experiment on the same junction (corresponding to 6.2c) is shown. The drawings in f) and g) schematically represent the proposed configurations of the low- and high-conductance states respectively.

Figure 6.4 c) and d) display 2D-conductance vs. time histograms of 1200 modulated traces with  $x_1 = 0.75$  nm (1.25 nm of inter-electrode distance),  $\Delta t = 1$  s and  $x_2 = 0.45$  and  $x_2 = 0.18$  nm in c) and d), respectively. The panels a) and b) of the same figure represent the corresponding electrode distance modulation of the histogram below as a function of time. The most outstanding characteristic of these measurements is the difference in the appearance of the high conductance state in each experiment. As a general trend, when the electrode displacement ( $d$ ) reaches  $x_1$ , the conductance matches either values near the noise level or the low-conductance state indicating empty traces in the former



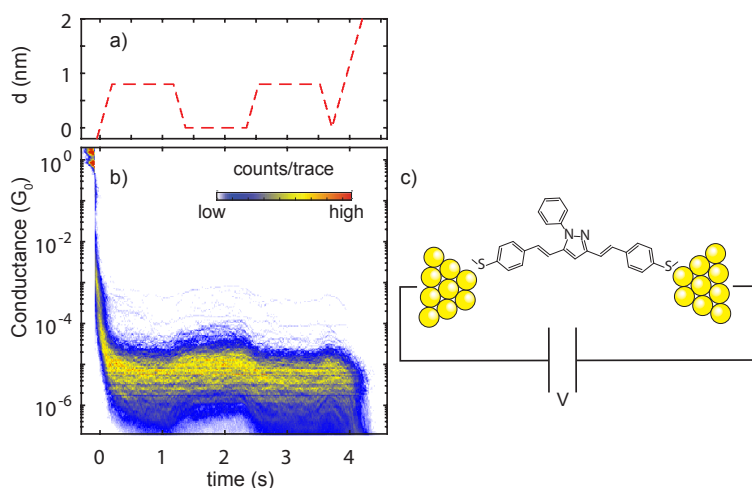


Figure 6.5: a) Inter-electrode distance as a function of time for the distance modulation experiment. Zero displacement is defined as the breaking point at which the conductance drops below  $1 G_0$  which corresponds, approximately, to a distance of 0.5 nm in real space. b) Conductance vs. time histograms constructed from 1000 consecutive traces in which the inter-electrodes distance was modulated as shown in a). The conductance axis has been logarithmically binned with 94 bins/decade and the time axis with 100 bins/sec. The target molecule used in the measurement was MeS-CCM-pyrPh. c) Shows the drawing of the expected configuration of the MeS-CCM-pyrPh inside the junction.

or the formation of single-molecule junctions in the latter case. When the electrodes are pushed back to  $x_2 = 0.45$  nm (Fig. 6.4 a) and c), the conductance values spread out (in the intervals [1.3, 2.3] s and [3.6, 4.6] s), especially towards higher values, but importantly the conductance does not reach the value of the high-conductance state. In contrast, when the electrodes are pushed together to  $x_2 = 0.18$  nm (time intervals [1.4, 2.4] s and [3.7, 4.7] s of Fig. 6.4d), there is a significant amount of counts in the high-conductance region that is reached in a sharp switching manner. It is interesting to note that consistently in both experiments, the behavior is reproducible over more than thousand traces and that the molecular junctions are stable in the range of seconds in ambient conditions.

When the same experiment is performed with MeS-CCM-pyrPh, the results are remarkably different. Regardless of how close the electrodes are pushed back together the high-conductance state is never reached. Figure 6.5 shows the conductance vs. time histogram for a measurement of 1000 consecutive modulation traces at a speed of 4 nm/s and a bias voltage of 0.1 V, with parameters  $x_1 = 0.8$  nm and  $x_2 = 0.0$  nm. Interestingly, despite the close proximity to which the electrodes are pushed back together, the conductance value did not reach the level of the high-conductance state. We point out that the only difference between MeS-CCM-pyr and MeS-CCM-pyrPh is that in the second molecule the pyrazole group is attached to a phenyl ring; it provides a physical blocking group that may prevent the re-binding of the molecule through such moiety.

## 6.3. DISCUSSION

Putting the results in a broader context, it is worth looking at similar systems that have been related with alternative pathways for charge transport: Silanes [7] are one example. These molecules containing silacycle groups along the main backbone, enabling alternative pathways for charge transport. In their paper, Su *et al.*, evaluate different compounds and conclude that the conditions for having a sulfur to silacycle pathway is associated with a high strain in the silacycle ring. Thus, this pathway can be turned off by relaxing the strain in the Si containing group (usually by chemical design). Along the same line, Delia *et al.* [6] studied oligo-phenyleneethynylene (OPE3) based compounds with a modified central ring that holds a certain affinity with metals. In this case the authors claim that nitrogen atoms can grant the compounds an alternative bonding site in the middle of the molecule, although the weak bounding made it necessary to include a second MeS anchoring group to stabilize the molecular junction in the high-conductance (short pathway) states.

For the compounds studied here there are a few remarkable features. First, all the nitrogen containing molecules showed counts at high-conductance states consistent with the idea that they provide an alternative anchoring group that provides a shorter pathway for charge transport. We find that the traces can be clasified in four groups: the ones that after the breaking of the 1  $G_0$  breaking point transit through the high-conductance state and then through low-conductance state; traces that go only through one of the conductance states; and those that do not show a clear indication of molecular junctions (see 6.A.2). The probability of having the high-conductance state in a molecular trace is approximately 2/3 (table 6.3); 1/3 for the high-conductance state alone and another 1/3 for traces with a section in the high-conductance state and a transition to the low-conductance one. This indicates that the bonding of the well-established MeS anchoring group does not seem to be more stable than the alternative pyrazole group. We see, as well, that there is no indication of traces that go back an forth between the 2 states. The case of the isoxazole group is similar to the one with pyrazole. The probability of making a connection through the nitrogen also approaches 2/3, but there the possibility of having only high-conductance states is higher than having both states in the same trace.

There is a notable difference in the percentages of traces with an indication of high-conductance state for MeS-CCM-pyrPh. A consistent high proportion of traces only show low-conductance states and between 30 and 52% of the traces show the high-conductance state, depending on how the selection is performed.

In conclusion, our results provide strong evidence that pyrozale and isoxzale groups can become an alternative anchoring site and that the inclusion of a bulky group such as a phenyl ring can prevent the availability of the pyrazole group, as an anchoring moiety.

## REFERENCES

- [1] Z. Huang, F. Chen, P. A. Bennett, and N. Tao, *Single molecule junctions formed via Au-thiol contact: Stability and breakdown mechanism*, *Journal of the American Chemical Society* **129**, 13225 (2007).
- [2] M. Kamenetska, S. Y. Quek, A. C. Whalley, M. L. Steigerwald, H. J. Choi, S. G. Louie,

- C. Nuckolls, M. S. Hybertsen, J. B. Neaton, and L. Venkataraman, *Conductance and geometry of pyridine-linked single-molecule junctions*, *Journal of the American Chemical Society* **132**, 6817 (2010).
- [3] S. Y. Quek, L. Venkataraman, H. J. Choi, S. G. Louie, M. S. Hybertsen, and J. B. Neaton, *Amine - Gold linked single-molecule circuits: Experiment and theory*, *Nano Letters* **7**, 3477 (2007).
- [4] Z. Li and D. S. Kosov, *Nature of well-defined conductance of amine-anchored molecular junctions: Density functional calculations*, *Physical Review B* **76**, 035415 (2007), 0702507.
- [5] M. S. Hybertsen, L. Venkataraman, J. E. Klare, A. C. Whalley, M. L. Steigerwald, and C. Nuckolls, *Amine-linked single-molecule circuits: systematic trends across molecular families*, *Journal of Physics: Condensed Matter* **20**, 374115 (2008).
- [6] M. Iwane, S. Fujii, T. Nishino, and M. Kiguchi, *Single tripyridyl-triazine molecular junction with multiple binding sites*, *The Journal of Physical Chemistry C* **120**, 8936 (2016).
- [7] T. A. Su, J. R. Widawsky, H. Li, R. S. Klausen, J. L. Leighton, M. L. Steigerwald, L. Venkataraman, and C. Nuckolls, *Silicon ring strain creates high-conductance pathways in single—molecule circuits*, *Journal of the American Chemical Society* **135**, 18331 (2013).
- [8] D. Miguel, L. Álvarez de Cienfuegos, A. Martín-Lasanta, S. P. Morcillo, L. A. Zotti, E. Leary, M. Bürkle, Y. Asai, R. Jurado, D. J. Cárdenas, G. Rubio-Bollinger, N. Agraït, J. M. Cuerva, and M. T. González, *Toward multiple conductance pathways with heterocycle-based oligo(phenyleneethynylene) derivatives*, *Journal of the American Chemical Society* **137**, 13818 (2015).
- [9] N. T. Kim, H. Li, L. Venkataraman, and J. L. Leighton, *High-conductance pathways in ring-strained disilanes by way of direct  $\sigma$ -Si-Si to Au coordination*, *Journal of the American Chemical Society* **138**, 11505 (2016).
- [10] G. Cardini and M. Muniz-Miranda, *Density functional study on the adsorption of pyrazole onto silver colloidal particles*, *The Journal of Physical Chemistry B* **106**, 6875 (2002).
- [11] V. Garcia-Pacios, M. Arroyo, N. Anton, D. Miguel, and F. Villafane, *Non-covalent interactions at bis(pyrazole)silver(i) or -gold(i) cations*, *Dalton Trans.*, 2135 (2009).
- [12] A. M. Ricci, E. J. Calvo, S. Martin, and R. J. Nichols, *Electrochemical scanning tunneling spectroscopy of redox-active molecules bound by Au-C bonds*, *Journal of the American Chemical Society* **132**, 2494 (2010).
- [13] V. Heras, A. Campo, M. L. Gallego, P. Ovejero, M. Cano, and M. R. Torres, *(Pyrazole) silver (I) and -gold (I) Complexes with Strong and Weak Hydrogen- Bonding Interactions as the Basis of One- or Two-Dimensional Structures*, *European Journal of Inorganic Chemistry*, 3089 (2004).

- [14] T. Nishino, N. Hayashi, and P. T. Bui, *Direct measurement of electron transfer through a hydrogen bond between single molecules*, [Journal of the American Chemical Society](#) **135**, 4592 (2013).

## 6.A. APPENDICES

### 6.A.1. MEASUREMENTS ON ADDITIONAL SAMPLES

We have measured a second junction for each molecule obtaining similar results. The conductance values obtained from two thousand consecutive traces (with the exception of MeS-CCM-isox in which case 1300 traces were collected) is displayed in table 6.2. The lack of a conductance value for the high-conductance state in the case of MeS-CCM-pyrPh is because the peak at high conductance was not clearly visible even after data selection. The second measurement on MeS-CCM-pyr gave conductance values almost a factor of 2 higher than the ones shown in the main text. A reason for this may be a higher probability of trapping more than one molecule.

Molecule	$G$ ( $G_0$ )	FWHM	$G_H/G_L$
MeS-CCM	$4.0 \times 10^{-5}$	1.1	-
MeS-CCM-pyrPh	-	-	-
	$4.0 \times 10^{-6}$	0.9	
MeS-CCM-pyr	$7.7 \times 10^{-4}$	1.0	35.0
	$2.2 \times 10^{-5}$	1.5	
MeS-CCM-isox	$4.8 \times 10^{-4}$	0.8	18.5
	$2.6 \times 10^{-5}$	0.9	

Table 6.2: Most probable conductance value (first column), FWHM (second column) and the conductance ratio obtained from fitting the data of 1D histograms of representative samples of each compound to log-normal distributions, as described in the text. The considered data sets were measured at a bias voltage of 0.1 V and the electrode speed was in the range of 3 to 8 nm/s.

### 6.A.2. FREQUENCY DETECTION

With the aim of quantifying the correlation between the appearance of the high- and low-conductance states, we perform a sequence of filtering steps based on the likelihood of each conductance state to be present on a trace. We quantify this likelihood as the ratio between the counts a conductance trace has in the region of the conductance peaks and the average of the counts in the same region over all traces. We call this ratio the prevalence ratio as the quotient between counts of a trace and the counts in the conductance histogram in a determined region of conductance values. This region is usually chosen around the conductance value of a molecular state.

In the case of MeS-CCM-pyrPh in Fig. 6.6a) we select the traces with a prevalence ratio above 1.0 in the region around the high conductance peak (between  $2.7 \times 10^{-4}$  and  $1.7 \times 10^{-3} G_0$ ). The data is then split in two subsets: selected and not-selected ones. The selected traces show an 1D-histogram (red line in Fig. 6.6 a) in which the high-conductance state is enhanced compared to the original 1D- histogram, while the unselected traces (orange line in Fig. 6.6 a) show a depletion in the same region compared to the original 1D-histogram (blue line in Fig. 6.6 a). For each subset a subsequent filtering step is applied (b) and c) in Fig 6.6). This time the prevalence is considered in the region of the low-conductance state (between  $3.8 \times 10^{-6}$  and  $5.4 \times 10^{-5} G_0$ ) and in these

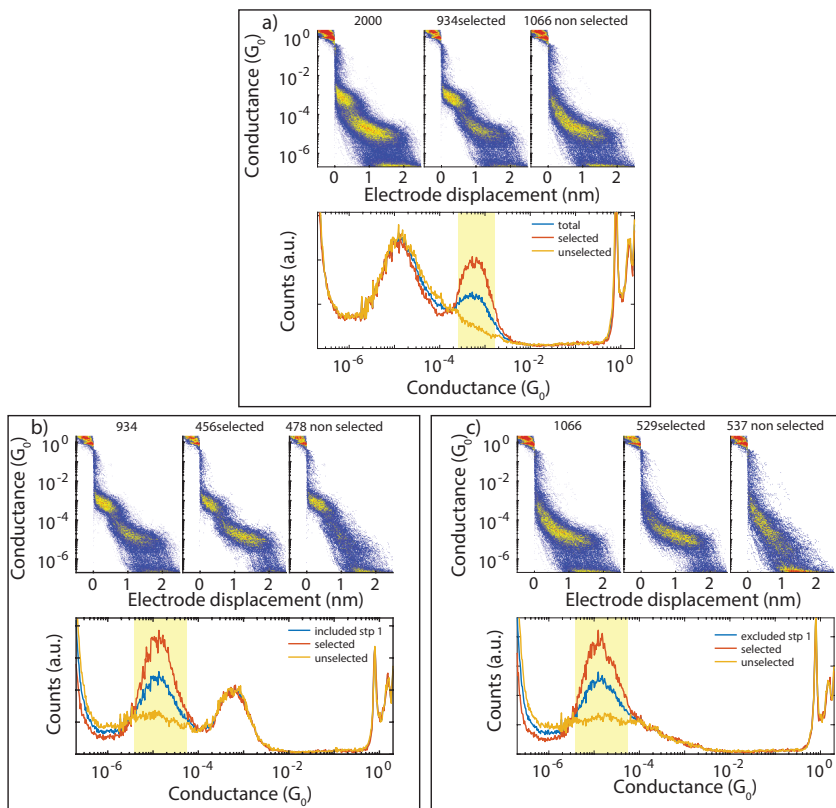


Figure 6.6: Series of filtering steps a), b) and c) in which the data set of Fig. 6.2 is divided in subsets depending on the prevalence of counts in the high- and low-conductance state. In a) the set of 2D-conductance versus displacement histograms correspond from left to right to: the original data set, the traces with a prevalence ratio greater than 1.0 and the traces with prevalence ratio lower than 1. Considering the prevalence between  $2.7 \times 10^{-4}$  and  $1.7 \times 10^{-3} G_0$  in the 1D-conductance histogram below (yellow shaded region in the lower panel). The reference is the total 1D-conductance histogram (blue line). Panels b) and c) display information in the same way as in a), but the selection is applied over the selected data b) and not-selected data c) from a). The prevalence is computed in reference to the region between  $3.8 \times 10^{-6}$  and  $5.4 \times 10^{-5} G_0$  (yellow shaded region in the conductance histograms).

cases the reference for computing the prevalence ratio is considered to be the conductance histogram of the respective subset.

In this way, the data can be split in four non-overlapping subsets related to different behaviors: traces that show both states (selected in Fig. 6.6 b); traces that show only the high-conductance state (non-selected in Fig. 6.6 b); traces that show only the low-conductance state (selected in Fig. 6.6 c) and traces that show neither (non-selected in Fig. 6.6 c). Table 6.3 shows the summary of this selection procedure, where 0 means the absence of a peak and 1 the presence of it. The third column corresponds to the filtering sequence displayed in Fig. 6.6; the fourth column is the corresponding result for the inverse order of filtering (first low conductance and then high conductance). The probability of getting either or both of the conductance states is approximately the same in both cases which show the robustness of the method. To a certain extend, the choice of the prevalence threshold is arbitrary, nevertheless, one can argue that a factor 1.0 is a good starting point because the condition for selecting a trace to have a plateau-like behavior is based on having, at least, the average number of counts in that region. We have tried factors up to 1.5 and the trend of four distinguishable subsets is preserved. However, the 2D-conductance vs. displacement histograms of the different selection steps did not add any different recognizable group and, moreover, tend to mix the ones that we have described before, so for that reason, the factor 1.0 has been chosen.

$G_H$	$G_L$	#traces $G_H \rightarrow G_L$	#traces $G_L \rightarrow G_H$
0	0	27%	26%
0	1	26%	27%
1	0	24%	23%
1	1	23%	23%

Table 6.3: Summary table of Fig. 6.6 in which the number of traces that belong to each behavior are displayed, (0 0) non molecular, (0 1) only low G, (1 0) only high G and (1 1) low and high G. The label  $G_H \rightarrow G_L$  (third column) means that the first filter was performed for selection in the high conductance region and then in the low conductance one.  $G_L \rightarrow G_H$  (fourth column) stands for the inverse order of selection.

Interestingly, the bonding with the well established MeS anchoring group does not seem more probable than the alternative pyrazole site. We see as well that there is no indication of traces that go back and forth between the 2 states. This fact is a further indication of the interpretation of the multiple anchoring sites within the molecule.

The Idea of adding a phenyl ring on the pyrazole group (MeS-CCM-pyrPh) is to impose a physical barrier that prevent the interaction of the nitrogen atoms with the gold electrodes. Although this modification did not prevent the appearance of the high-conductance peak it certainly had a blocking role. Table 6.4 summarizes the analysis on the prevalence of the high and low conductance peak. Since the fraction of counts in the region of high conductance was lower, the prevalence factor to filter in the high conductance region was chosen to be 1.5 instead of 1.0.

In the case of MeS-CCM-isox compound the trend is very similar to MeS-CCM-pyr, The features at both conductance states are clear enough, so no modification to the fac-

$G_H$	$G_L$	MeS-CCM-pyrPh		MeS-CCM-isox	
		# traces $G_H \rightarrow G_L$	# traces $G_L \rightarrow G_H$	# traces $G_H \rightarrow G_L$	# traces $G_L \rightarrow G_H$
0	0	47%	46%	42%	41%
0	1	37%	26%	20%	19%
1	0	9%	10%	25%	26%
1	1	7%	18%	13%	14%

Table 6.4: Summary table of prevalence of the two conductance states for MeS-CCM-pyrPh and MeS-CCM-isox in which the number of traces that belong to each behavior are displayed: (0 0) non molecular, (0 1) only low G, (1 0) only high G and (1 1) low and high G. The label  $G_H \rightarrow G_L$  means that the first filter was performed for selection in the high conductance region and then in the low conductance one.  $G_L \rightarrow G_H$  stands for the inverse order of selection. For MeS-CCM-pyrPh, the regions considered were:  $G_L$  between  $2.37 \times 10^{-6}$  and  $2.66 \times 10^{-5} G_0$ , and  $G_H$  between  $2.43 \times 10^{-4}$  and  $1.72 \times 10^{-3} G_0$ . For MeS-CCM-isox:  $G_L$  between  $1.29 \times 10^{-5}$  and  $1.02 \times 10^{-4} G_0$ , and  $G_H$  between  $2.82 \times 10^{-4}$  and  $1.78 \times 10^{-3} G_0$ . As explained in the text, the prevalence factor for MeS-CCM-pyrPh the region of high conductance was considered 1.5 instead of 1.0.

tors was needed to split the data in meaningful sets. The results are summarized in the same way in the previous cases in table 6.4. The amount of empty traces is larger than in the case of MeS-CCM-pyr, but the yield of only high-conductance state traces is almost equivalent to the one observed in the molecule with pyrazole mid-group. This indicates that the isoxazole group may also be working as an anchoring site and provides a shorter pathway for charge transport.





# 7

## SALEN AND SALOPHEN COMPOUNDS

*"You believe that reality is something objective, external, existing in its own right. You also believe that the nature of reality is self-evident."*

O'Brien to Winston, 1984, George Orwell

*We performed the single molecule conductance experiments on a series of salophen and salen compounds exploring different connection strategies and metal ion inclusion, including Cu, and Mg. Our results show a dramatic difference on the qualitative behavior of each molecule between metallic electrodes depending on the position on which the anchoring group is attached to the central structure. From these results we draw two related conclusions: (i) quantum interference plays a momentous role in the charge transport characteristic of the molecules, suppressing the conductance when a meta-conjugated phenyl ring is placed in the pathway and (ii) the conduction pathway goes mainly through the organic ligand. If a Cu or Zn ion is used the metal ion plays a gating role for charge carriers and provides rigidity to the molecular structure but does not constitute a separated path for electrons.*<sup>1</sup>

---

<sup>1</sup>We thanks Diana Dulic, Cristian Gutierrez and collaborators, from the University of Chile, for the chemical design and synthesis of the compounds and Nuria Aliaga, at Institut de Ciència de Materials de Barcelona, for her help in the chemical characterization and analysis.

## 7.1. SALEN AND SALOPHENES

Salen molecules are a family of chelates similar to porphyrins albeit they do not possess a closed ring structure but just half of it. They have attracted attention because of their catalytic properties and, in particular, manganese salens have shown high enantoselectivity [1, 2], meaning that they favor a particular kind of chirality over the opposite one in certain oxidation processes. Importantly, salen derivatives can be synthesized more easily than porphyrins and their structures can be manipulated to create an asymmetric environment around the active metal site in the center [2]. This makes them an interesting system to investigate the role of metalization on organic molecules. From another point of view, salen complexes hold various similarities with the catalytic activity of enzymes [3]. Studying the charge transport mechanisms through such systems could shine light on the understanding biological processes.

As stated, these compounds have shown high enantoselectivity, from the physical point of view, this may suggest a spin dependent electron transfer process [4]. Thus, they could have the potential to show spin dependent currents, but until now there have been no reports on charge transport measurement through such molecules. Many studies have focused the attention on the electrochemical properties of the salen compounds and/or on its charge transfer characteristics [5–7]. In particular, it has been shown that the locus of oxidation, i.e., the place in which the molecular charge is localized upon oxidation, can be tuned by the use of different metal complexation or by the use of ‘non-innocent’ ligands [8]. Charge transfer phenomena have also been reported and depending on which metal is placed in the center of the molecule, in particular copper and manganese, [6].

The structure of the salen compounds considered in this work is depicted in Fig. 7.1. The MeS groups at the ends of the molecules are the anchoring groups to the gold electrodes [9, 10]. These groups have been separated from the core of the molecule by a phenyl ring spacer. In this work, three aspects of the chemical design are explored: (i) the aromaticity and conjugation of the organic bridge that joins the two halves of the compound; (ii) the site with respect to the imine group (N atom) to which the phenyl spacer is connected; and (iii) the inclusion of different metal ions.

Regarding the organic bridge, we tested two different architectures: salen and salophen as specified in Fig. 7.1. In salen compounds, the bridge consists of an aliphatic chain of two carbon atoms while the salophens have a phenyl ring in ortho-substitution connecting the two halves. On one hand, the aliphatic chain is expected to split the molecule in two almost independent conjugated parts, while the phenyl ring allows for delocalization of the molecular orbitals throughout the whole molecule. On the other hand, the ortho-connection of the phenyl ring may give rise to destructive quantum interference effects for charge carriers going from one S atom. at the first end of the molecule, to the S atom, at the other end, thereby, reducing the conductance.

The connection of the spacer to the center of the molecule has to do with the site to which the phenyl spacer is attached with respect to the imine group. Two configurations were explored: meta- (m-) and para- (p-) substitution as illustrated in Fig. 7.1. This different connection may have a strong influence on the electronic properties of the molecules due to quantum interference effects [11, 12]. Meta-substitution has been related to low-conductance values because of destructive interference while para-substitu-

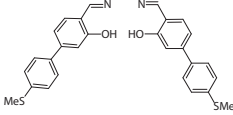
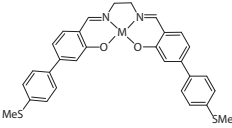
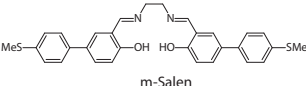
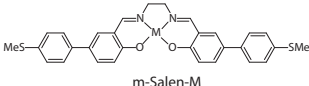
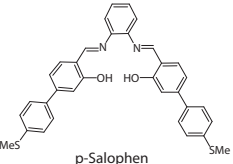
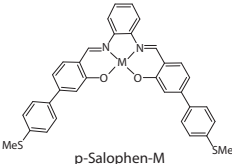
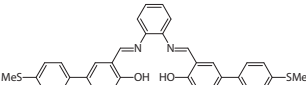
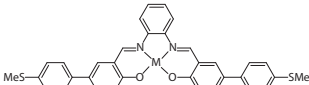
		Free ligand	Metallic complexes
Salen	para-substituted	 <p>p-Salen</p>	 <p>p-Salen-M</p>
	meta-substituted	 <p>m-Salen</p>	 <p>m-Salen-M</p>
Salophen	para-substituted	 <p>p-Salophen</p>	 <p>p-Salophen-M</p>
	meta-substituted	 <p>m-Salophen</p>	 <p>m-Salophen-M</p>

Figure 7.1: Schematic of the molecular systems addressed in this section: the first column depicts the free ligands and the the second column the metallic complexes in which M represents a metal ion (Cu and Zn were used for this study). Para-connected salen (p-Salen) and the meta-connected salen (m-Salen) are displayed in the upper half of the table while the salophenes are shown in the lower part in the corresponding configuration.

tion yields to higher conductance values [11, 13–15]. Note that in the cases in which a metal is included in the molecule, a meta-substitution with respect to the imine group leads to a para-substitution with respect to the metallic atom and vice versa. Thus, in a simplistic picture one could expect that p-salen and p-salophens promote conduction through the organic bridge while m-salen and m-salophen enhance the conduction through the metallic atom.

The role of the metallic ion in charge transport across molecules containing them is an aspect that is part of a long standing debate in the molecular electronics community [16–22]. In some cases, the metals are reported to have a gating effect on the molecular levels and, indirectly, tune the molecular conductance through the molecular backbone[16]; in other cases, the metals are part of the conducting pathway [21–23] and it has been reported that they can work as hopping centers upon charging [20]. The through-metal path in the salen and salophen compounds is connected in the opposite configuration of imine group (m-salophen-M  $\Rightarrow$  para-connected metal and vice versa). Therefore, they can be used to understand the role of metalization in charge transport in a better way, but it is a concept yet to be proven.

## 7.2. ELECTRONIC MEASUREMENTS

To begin the electrical characterization of the different metal-containing derivatives, we first establish the conductance of the free ligand chelates displayed in the left column of Fig. 7.1. Intuitively, the compounds that hold the most chances to conduct electricity are those that have a conjugated path between the two intended anchoring groups (MeS in these cases). Therefore, it is important to compare the electrical properties of the isomers p-salophen and m-salophen with each other.

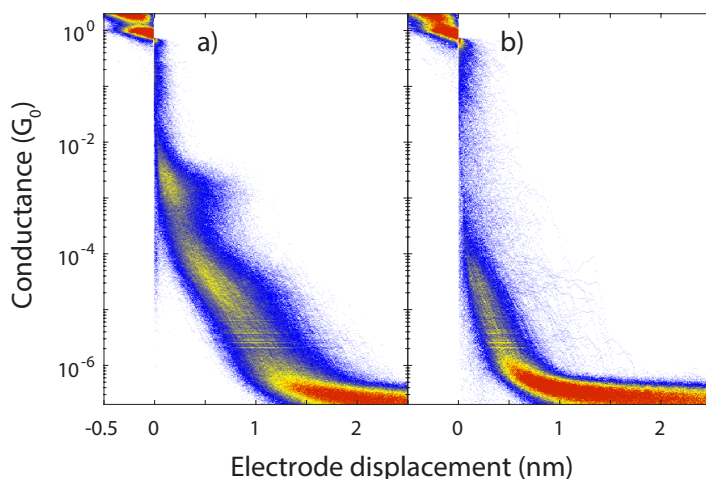


Figure 7.2: 2D-conductance vs. electrode displacement of a) p-salophen and b) m-salophen constructed from 5000 and 3000 consecutive traces respectively at a bias voltage of 0.1 V and an electrode speed of 6nm/s and using 80 bins per decade and 70 bins per nm.

The high-conductance state is related to shorter displacements, with values smaller than 1 nm. This indicates that the high-conductance state does not correspond to the molecule fully extended in between the electrodes, but to some other configuration. Possibly, one of the electrodes is connected to one of the N atoms in the central part of the molecule or interacts with the middle phenyl ring. In this case, transport through only part of the molecule would be measured. We will later see that the feature is also shared with the compounds including metal ions.

Additionally, the conductance value of the traces that extend for a larger displacement decrease as a function of electrode displacement. This may indicate that the conductance of the molecule decays as its extreme points are pulled apart.

To gain a deeper insight on the role of metal complexation we measured the same salophen framework complexed with a copper or a zinc ion. In Fig. 7.3, the 2D-conductance vs. electrode displacement of a) p-salophen-Cu, b) m-salophen-Cu, c) p-salophen-Zn and d) m-salophen-Zn are displayed. Remarkably, when the para-substitution is used, clear plateau-like structures appear in the histograms with two common features: a region of relative high counts above  $1 \times 10^{-4} G_0$  related to short displacements (smaller than 1 nm) and a region of high counts with a clear plateau structure between  $1 \times 10^{-5}$  and  $1 \times 10^{-4} G_0$  that extends for up to 2 nm in the case of p-salophen-Cu and to 2.4 nm in the case of p-salophen-Zn. The data for the meta-substituted isomers is less clear, since no clear signature of molecular plateaus is visible in either of the metal complexed. Nonetheless, m-salophen-Zn show short conductance features around  $1 \times 10^{-3} G_0$ , similar to the ones observed in p-salophen-Zn.

Fig. 7.4 displays the 1D-conductance histograms of the para-substituted (a) and the meta-substituted (b) salophens. To obtain the most probable conductance values, we filtered out the traces without molecular features using the filtering method described in chap. 2. Subsequently, a log-normal distribution was fitted to the conductance histograms of the selected traces for each peak. The corresponding conductance values and their full width at half maximum (FWHM) are listed in Table 7.1; the 1D-histograms and fitted distribution are exhibited in Fig. 7.5. Before discussing the long features that can be related to the fully extended molecule, we focus on the high-conductance state. The compounds including metal ions that show short features at high conductance values similar to p-salophen were both para-substituted salophen and m-salophen-Zn. The conductance values listed in table 7.1 evidence little variation on its values between the free ligand and the zinc compound, while the copper salophen has a conductance value almost one order of magnitude lower. We do not discard the existence of a configuration with a higher conductance value that is not statistically visible in this measurement, we will later comment on that. The fact that these states are related to a shorter displacement suggests that the current does not flow through a molecule in its full extension. Instead, it is likely that the conduction path from electrode to electrode goes through a portion of the molecule, for example, from one sulfur atom to the imine group and then directly to the drain electrode. It is not clear whether the shorter path involves another anchoring site or if the charge injection (or collection) happens in a different site than the anchoring. Neither the role of the metallic ion is clear in the presence of this mechanism.

In the case of longer features at lower conductance values, the compounds show rec-

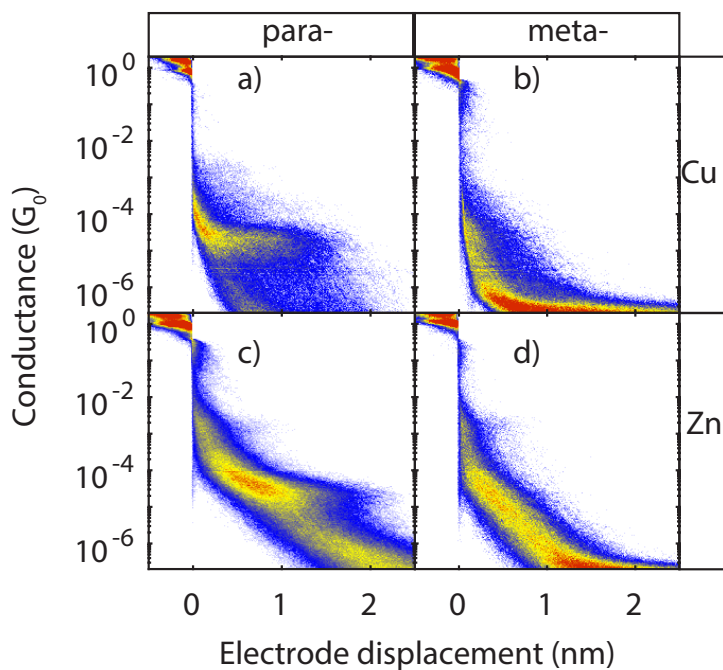


Figure 7.3: 2D-conductance vs. electrode displacement of a) p-salophen-Cu, b) m-salophen-Cu, c) p-salophen-Zn and d) m-salophen-Zn constructed from 3000 consecutive traces at a bias voltage of 0.1 V and an electrode speed between 2 to 6 nm/s. The histograms were constructed using 80 bins per decade and 70 bins per nm.

ognizable plateaus for the para- configuration. The molecular features are more clearly present when a metallic ion is incorporated in the structure; this can be seen, for instance, in the width of the low-conductance peaks in Fig. 7.5 a) as well as in full width half maximum of the fitted distributions displayed in the fifth column of Table 7.1. The spread of the p-salophen ligand has a width of 1.5 decades, while p-salophen-Zn and p-salophen-Cu only reach 1 decade of spread. Comparing the low-conductance states in the para-substituted molecules the progression of the conductance values follows the sequence  $G_{\text{p-salophen}} \approx G_{\text{p-salophen-Cu}} < G_{\text{p-salophen-Zn}}$ . Although the peak width follows the relation  $\text{FWHM}_{\text{m-salophen-Zn}} > \text{FWHM}_{\text{p-salophen}} > \text{FWHM}_{\text{p-salophen-Zn}} > \text{FWHM}_{\text{p-salophen-Cu}}$ . This fact indicates that when a metal ion is positioned in the central part of the molecules the conductance value of the system metal-molecule-metal has a narrower set of possible values.

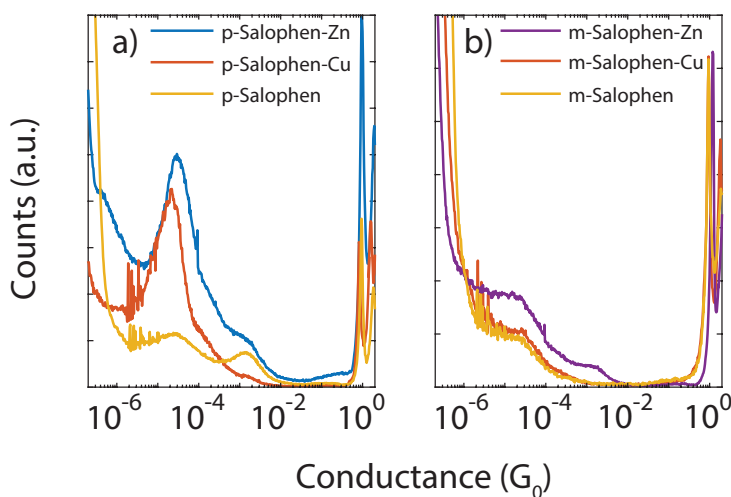


Figure 7.4: 1D-conductance histograms of a) p-salophen, p-salophen-Cu and b) p-salophen-Zn; and b) m-salophen, m-salophen-Cu and m-salophen-Zn constructed from 3000 consecutive traces at a bias voltage of 0.1 V and an electrode speed of 2 to 6 nm/s. The histograms were constructed using 80 bins per decade and 70 bins per nm.

Table 7.1 shows relevant values obtained from the measurements previously described, the last column lists the yield of junction formation defined as the fraction of traces that were selected using the filtering method described in chapter 2 (with  $m_{\text{thr}} = -0.5$  dec/nm and  $\Delta x = 0.5$  nm). The conductance histograms constructed from only molecular traces of the compounds that showed a peak structure are displayed in Fig. 7.5. The fitted log-normal distributions from which the conductance values were obtained are displayed as well. There are a few observations that are important to discuss here: the conductance value of the high-conductance peak of the p-salophen-Cu. Its value is  $1.4 \times 10^{-4} G_0$  but a quick inspection of the corresponding peak in Fig. 7.5 b) reveals that the fitted distribution follows a shoulder to the right of the low-conductance peak and does not align



Molecule	High G ( $G_0$ )	FWHM (dec)	Low G ( $G_0$ )	FWHM (dec)	Yield (%)
p-salophen	$1.3 \times 10^{-3}$	1.0	$2.1 \times 10^{-5}$	1.5	26
m-salophen	–	–	–	–	1
p-salophen-Cu	$1.4 \times 10^{-4}$	1.1	$2.0 \times 10^{-5}$	0.7	44
m-salophen-Cu	–	–	–	–	9
p-salophen-Zn	$7.1 \times 10^{-4}$	1.4	$3.0 \times 10^{-5}$	1.0	83
m-salophen-Zn	$1.4 \times 10^{-3}$	0.8	$7.6 \times 10^{-6}$	2.3	14

Table 7.1: Conductance value and full width half maximum (FWHM) of measurements of the salophen series obtained by fitting a log-normal distribution to the conductance histogram of the selected traces of measurement displayed in Fig. 7.5. The last column represents the percentage of traces that were considered after the filter procedure as a quantification of the yield of junction formation.

with the features at high conductance observed in the 2D-conductance vs. displacement histograms (Fig. 7.3). This may be caused by the low yield of the high-conductance state compared to the low-conductance one. In a lesser extend, something similar happens with p-salophen-Zn; there the peak position does not match the local maximum of the histogram, this is because the high amount of counts in the inter-peak region. In both cases the conductance value of the high-conductance state is underestimated, and consequently, if this observation correctly describes what happens with the high-conductance state, it would mean that the conductance value has a weak dependence on the metalization of the molecule.

Comparing the low-conductance peaks now, it is clear from Fig. 7.5 that the conductance distribution is narrower in the case of the copper inclusion in the para-connection. Under the same para-connection, the free ligand showed a much broader peak. This difference may be a natural consequence of the low rigidity of the free-ligand compared to the metalized compounds. Furthermore, the only meta-connected molecule that showed a substantial amount of molecular traces was the zinc complexation, giving rise to a 2 decades broad peak around  $7.6 \times 10^{-6} G_0$  (Fig. 7.5 d). This broadening may have to do with the previously mentioned quantum interference effect. Since meta-substitution is related to destructive quantum interference, the transmission function should have a dip or ‘anti-resonance’ in between the highest occupied molecular orbital (HOMO) and the lowest unoccupied molecular orbital (LUMO) [11, 24]. Thus, if the alignment of gold Fermi energy and the HOMO-LUMO gap varies slightly from one molecular configuration to another, it would have a larger effect on the measured conductance than the case of molecules with para-connection.

The experiments involving the salen structure with the non-aromatic joint between the two halves of the compounds have also been performed but turned to be less consistent. No clear and reproducible conductance measurements have been performed yet. The conductance values may be lower, close or even below the detection limit and/or very sensible to the molecular conformation inside the gap. An example of two measurements on m-salen-Cu are displayed in Fig. 7.6. There, two independent measurements show different behaviors, albeit the same molecule was deposited. Both of them

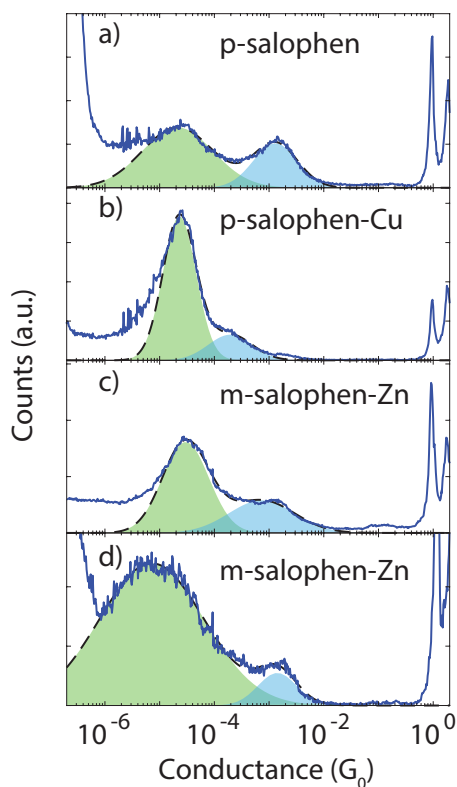


Figure 7.5: One-dimensional conductance histograms of a) p-salophen, b) p-salophen-Cu and c) p-salophen-Zn and d) m-salophen-Zn, constructed from selected traces using the filter described in chapter 2 from the measurements displayed in Fig.7.4 a) at a bias voltage of 0.1 V and an electrode speed of 2 to 6 nm/s. The shaded areas correspond to log-normal distribution fitted to the data which conductance value and width are listed in 7.1. At least two samples were measured for each compound, in the second junction the values of the low conductance peak were:  $2.0 \times 10^{-5} G_0$  for p-salophen-Cu,  $2.8 \times 10^{-5} G_0$  for p-salophen-Zn and  $2.8 \times 10^{-5} G_0$  for m-salophen-Zn.

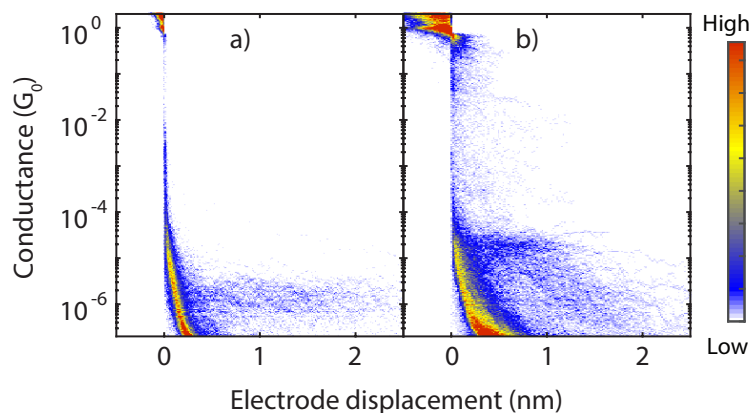


Figure 7.6: 2D-conductance vs. electrode displacement of m-Salen-Cu using 3000 consecutive traces at a bias voltage of a) 0.3 and b) 0.2 V and an electrode speed of 4 nm/s using 80 bins per decade and 70 bins per nm. The measurements were performed in two different samples.

present a low yield of plateau formation, as visible from the color contrast between the plateau traces and the empty traces background. On the left, the plateaus run parallel to the x-axis at values around  $1 \times 10^{-6} G_0$ . In contrast, in the right panel there are shorter plateaus around  $1 \times 10^{-5} G_0$  up to 1.3 nm but some traces extend for longer at values with conductance dropping to  $1 \times 10^{-6} G_0$ . So far the data is non-conclusive but certainly the salen structure shows lower conductance values than the para-substituted salophens, at least in the case of copper complexation.

In summary we have measured molecular conductance of salen and salophen complexes. The results show that the configuration, in which the salophen units are connected to the electrodes, has a dramatic influence on the electrical properties of the molecule. We can associate this influence to quantum interference effects of the para- or meta- substituted rings leading respectively to constructive or destructive interference of carriers moving along the backbone. If this interpretation is right, it implies that the main pathway for charge carriers in these molecules goes through the organic backbone and not through the metallic ion. This observation is confirmed by the fact that metal-ion inclusion only slightly changes the conductance values; it may be that the metal ions have a small gating effect on the conductance value of the molecules. In the case of zinc, the molecular conductance is enhanced while for copper it is diminished. Another important role of the metallic atoms is to grant rigidity to the molecular structures, which can be related to the narrowing of the conductance peaks and the corresponding much better visibility of the molecular features (e.g. plateaus) in the conduction histograms.

In the case of the salen architecture, more exploration is needed to draw conclusions. Preliminarily, the salophen structure gives rise to a lower conductance but a better defined plateau behavior, in the case of meta-substitution. This may indicate that the aliphatic chain together with the meta-substitution 'deactivate' the pathway through the organic framework, promoting in this way conduction through the metal ion.

## REFERENCES

- [1] T. P. Yoon and E. N. Jacobsen, *Privileged chiral catalysts*, *Science* **299**, 1691 (2003).
- [2] N. S. Venkataramanan, G. Kuppuraj, and S. Rajagopal, *Metal–salen complexes as efficient catalysts for the oxygenation of heteroatom containing organic compounds—synthetic and mechanistic aspects*, *Coordination Chemistry Reviews* **249**, 1249 (2005).
- [3] M. Orio, O. Jarjayes, H. Kanso, C. Philouze, F. Neese, and F. Thomas, *X-Ray structures of copper(II) and nickel(II) radical salen complexes: The preference of galactose oxidase for copper(II)*, *Angewandte Chemie - International Edition* **49**, 4989 (2010).
- [4] O. B. Dor, S. Yochelis, A. Radko, K. Vankayala, E. Capua, A. Capua, S.-H. Yang, L. T. Baczewski, S. S. P. Parkin, R. Naaman, *et al.*, *Magnetization switching in ferromagnets by adsorbed chiral molecules without current or external magnetic field*, *Nature Communications* **8** (2017).
- [5] L. Chiang, K. Herasymchuk, F. Thomas, and T. Storr, *Influence of Electron-Withdrawing Substituents on the Electronic Structure of Oxidized Ni and Cu Salen Complexes*, *Inorganic Chemistry*, 150527115639006 (2015).
- [6] T. Kurahashi and H. Fujii, *One-electron oxidation of electronically diverse manganese(III) and nickel(II) salen complexes: Transition from localized to delocalized mixed-valence ligand radicals*, *Journal of the American Chemical Society* **133**, 8307 (2011).
- [7] Y. Yuanyuan, H. Jingya, L. Bingxin, and X. Lan, *Enantioselective ito electrode modified with chiral salen co(ii) complex*, *Chemistry Letters* **39**, 690 (2010).
- [8] L. Chiang, K. Herasymchuk, F. Thomas, and T. Storr, *Influence of Electron-Withdrawing Substituents on the Electronic Structure of Oxidized Ni and Cu Salen Complexes*, *Inorganic Chemistry*, 150527115639006 (2015).
- [9] Y. S. Park, A. C. Whalley, M. Kamenetska, M. L. Steigerwald, M. S. Hybertsen, C. Nuckolls, and L. Venkataraman, *Contact chemistry and single-molecule conductance: a comparison of phosphines, methyl sulfides, and amines*, *Journal of the American Chemical Society* **129**, 15768 (2007).
- [10] R. Frisenda, S. Tarkuç, E. Galán, M. L. Perrin, R. Eelkema, F. C. Grozema, and H. S. J. van der Zant, *Electrical properties and mechanical stability of anchoring groups for single-molecule electronics*, *Beilstein Journal of Nanotechnology* **6**, 1558 (2015).
- [11] T. Markussen, R. Stadler, and K. S. Thygesen, *The relation between structure and quantum interference in single molecule junctions*, *Nano Letters* **10**, 4260 (2010).
- [12] C. M. Guédon, H. Valkenier, T. Markussen, K. S. Thygesen, J. C. Hummelen, and S. J. Van Der Molen, *Observation of quantum interference in molecular charge transport*, *Nature Nanotechnology* **7**, 305 (2012).

- [13] C. R. Arroyo, S. Tarkuc, R. Frisenda, J. S. Seldenthuis, C. H. M. Woerde, R. Eelkema, F. C. Grozema, and H. S. van der Zant, *Signatures of quantum interference effects on charge transport through a single benzene ring*, *Angewandte Chemie International Edition* **52**, 3152 (2013).
- [14] G. C. Solomon, D. Q. Andrews, T. Hansen, R. H. Goldsmith, M. R. Wasielewski, R. P. V. Duyne, and M. A. Ratner, *Understanding quantum interference in coherent molecular conduction*, *The Journal of Chemical Physics* **129**, 054701 (2008).
- [15] C. R. Arroyo, R. Frisenda, K. Moth-Poulsen, J. S. Seldenthuis, T. Bjørnholm, and H. S. van der Zant, *Quantum interference effects at room temperature in opv-based single-molecule junctions*, *Nanoscale Research Letters* **8**, 234 (2013).
- [16] J. Ponce, C. R. Arroyo, S. Tatay, R. Frisenda, P. Gaviña, D. Aravena, E. Ruiz, H. S. J. van der Zant, and E. Coronado, *Effect of metal complexation on the conductance of single-molecular wires measured at room temperature*, *Journal of the American Chemical Society* **136**, 8314 (2014).
- [17] Z. F. Liu, S. Wei, H. Yoon, O. Adak, I. Ponce, Y. Jiang, W. D. Jang, L. M. Campos, L. Venkataraman, and J. B. Neaton, *Control of single-molecule junction conductance of porphyrins via a transition-metal center*, *Nano Letters* **14**, 5365 (2014).
- [18] M. L. Perrin, C. J. Verzijl, C. A. Martin, A. J. Shaikh, R. Eelkema, J. H. Van Esch, J. M. Van Ruitenbeek, J. M. Thijssen, H. S. Van Der Zant, and D. Dulić, *Large tunable image-charge effects in single-molecule junctions*, *Nature Nanotechnology* **8**, 282 (2013).
- [19] S. Fujii, S. Marqués-González, J.-Y. Shin, H. Shinokubo, T. Masuda, T. Nishino, N. P. Arasu, H. Vázquez, and M. Kiguchi, *Highly-conducting molecular circuits based on antiaromaticity*, *Nature Communications* **8**, 15984 (2017).
- [20] F. Schwarz, G. Kastlunger, F. Lissel, C. Egler-Lucas, S. N. Semenov, K. Venkatesan, H. Berke, R. Stadler, and E. Lörtscher, *Field-induced conductance switching by charge-state alternation in organometallic single-molecule junctions*, *Nature Nanotechnology* **11**, 170 (2016).
- [21] M. Ruben, A. Landa, E. Lörtscher, H. Riel, M. Mayor, H. Görls, H. B. Weber, A. Arnold, and F. Evers, *Charge transport through a cardan-joint molecule*, *Small* **4**, 2229 (2008).
- [22] S. Marques-Gonzalez, D. S. Yufit, J. A. K. Howard, S. Martin, H. M. Osorio, V. M. Garcia-Suarez, R. J. Nichols, S. J. Higgins, P. Cea, and P. J. Low, *Simplifying the conductance profiles of molecular junctions: the use of the trimethylsilylethynyl moiety as a molecule-gold contact*, *Dalton Trans.* **42**, 338 (2013).
- [23] S. J. Higgins and R. J. Nichols, *Metal/molecule/metal junction studies of organometallic and coordination complexes; what can transition metals do for molecular electronics?* *Polyhedron* **140**, 25 (2018), molecules for devices: the inorganic chemistry behind modern technologies.

- [24] D. Z. Manrique, C. Huang, M. Baghernejad, X. Zhao, O. a. Al-owaedi, H. Sadeghi, V. Kaliginedi, W. Hong, M. Gulcur, T. Wandlowski, M. R. Bryce, and C. J. Lambert, *A quantum circuit rule for interference effects in single-molecule electrical junctions*, [Nature Communications](#) **6**, 1 (2015).



# 8

## THE CONDUCTANCE OF MISCELLANEOUS MOLECULAR SYSTEMS

*Valía más renunciar, porque la renuncia a la acción era la protesta misma y no su máscara.  
It was worthier quitting, because quitting is the very action of protest and not its mask.*

Rayuela, Julio Cortazar

*In this chapter we discuss other interesting molecular systems that have been studied in lesser detail but that shine some light on the kind of problems and new possibilities that the field of molecular electronics offers. Finally, we reflect on the directions that single-molecule electronics is going and which ones in our opinion are the most promising ones.*



## 8.1. OTHER INTERESTING SYSTEMS

In this chapter we discuss other interesting molecular systems that have been studied in lesser detail but that shine some light on the kind of problems and new possibilities that the field of molecular electronics offers. Finally, we reflect on the directions that single-molecule electronics is going and which ones in our opinion are the most promising ones.

## 8.2. REDOX CENTERS: TTF-INDENOFLUORENES

An interesting molecular system comprises the indenofluorene (IF) backbone, functionalized with tetrathiofulvene moieties (TTF)<sup>1</sup>. Our conductance measurements are framed in the context of the study of the TTF groups embedded in different backbones [1–3]. Since the early days of molecular electronics TTF compounds attracted a lot of attention because polymers containing them showed a measurable conductance, an unexpected property in those days. With the development of single-molecule electronics TTF became an attractive candidate to be used as active parts of single-molecule wires. Because unpaired spins (radicals) can be generated upon oxidation, these systems have a big potential for applications in spintronics as well as in electronics when used as an electrochemical molecular switch [4, 5].

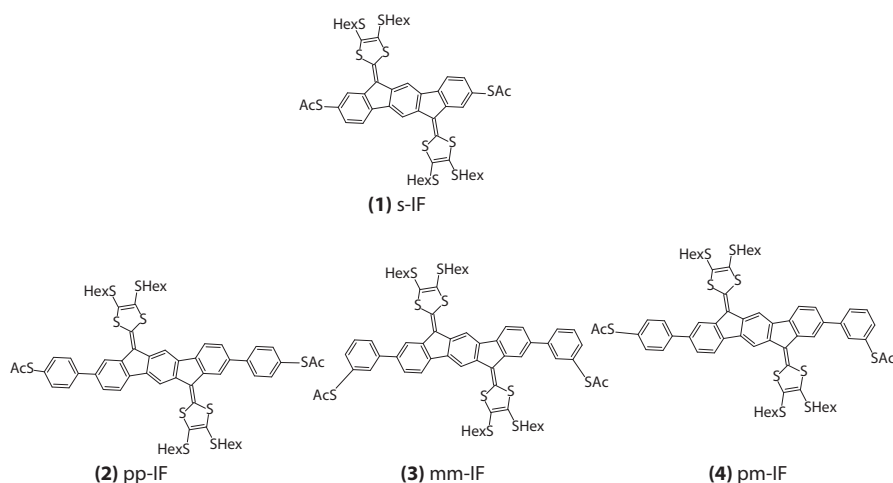


Figure 8.1: Schematic of the molecular systems addressed in this section: 1) the un-extended IF (s-IF) 2) para-para phenyl-extended IF (pp-IF), 3) meta-meta phenyl-extended IF (mm-IF) and para-meta phenyl-extended IF (pm-IF).

The molecules considered here are displayed in Fig. 8.1. The chemical design, in contrast to previous attempts [2, 3], uses a planar indenofluorene (IF) backbone to couple two

<sup>1</sup>We thank Prof. Mogens Brøndsted Nielsen from the University of Copenhagen for synthesis and basic characterization of the TTF-Indenofluorenes. Part of this section has been published in [1]

TTF units perpendicular to the charge carrier pathway [5]. The coupling with the electrode is achieved by thiol groups at the ends of the molecules and it is completed after the cleavage of the acetyl protecting group by the usage of tetrabutylammonium hydroxide. In compound (1) (s-IF) the thiol group is attached directly to the indenofluorene structure. In the three remaining compounds phenyl spacers are located between the thiol groups and the central part; the difference among them is the way the first and second phenyl rings are connected: (2) (pp-IF) para-para, (3) meta-meta (mm-IF) and (4) para-meta (pm-IF) respectively.

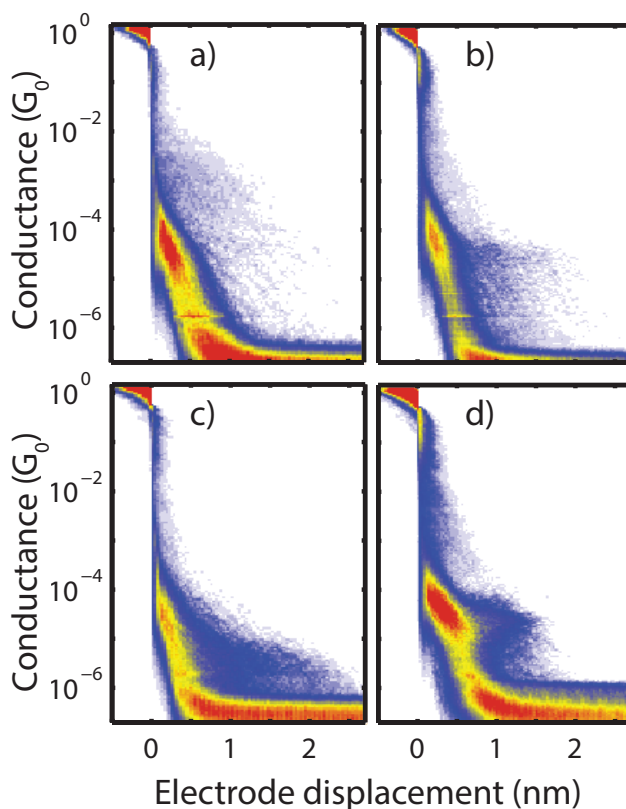


Figure 8.2: Two-dimensional conductance vs. electrode displacement histograms constructed from 5000 individual traces of compounds a) s-IF (1), b) pp-IF (2), c) mm-IF (3) and d) pm-IF (4). The molecules were drop casted from a 0.5  $\mu\text{M}$  solution in  $\text{CH}_2\text{Cl}_2$ ; a concentrated solution of tetrabutylammonium hydroxide ( $\text{Bu}_4\text{NOH}$ ) in  $\text{CH}_2\text{Cl}_2$  was used to cleave the acetyl group to form the thiolate end group. The bias voltage was 0.1 V and the electrode speed was 6 nm/s.

As mentioned in the introduction of this dissertation the incorporation of a meta-connected phenyl ring in the electron pathway can drastically reduce the conductance of a molecule due to destructive quantum interference. Therefore one would expect

that the conductance of these molecules should follow the sequence: s-IF (1) > pp-IF (2) > pm-IF (3) > mm-IF (4).

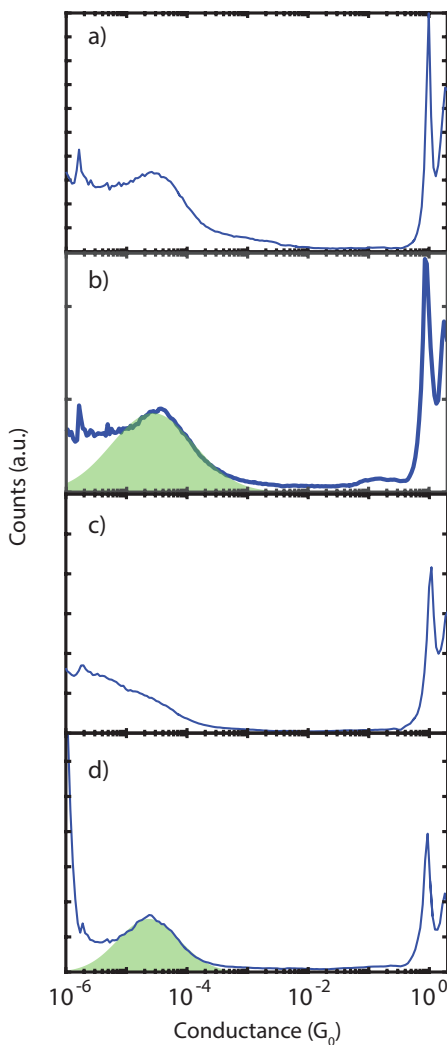


Figure 8.3: One-dimensional conductance histogram of the full data corresponding to the same measurements of Fig. 8.2. Histograms correspond to (1)s-IF a), (2)pp-IF b) (3)pm-IF c) and (4)mm-IF a). Green areas correspond to log-normal distributions fitted to the data. For compounds (1) and (3) such fits did not describe the features observed in the 2D-conductance vs. displacement histograms.

Figure 8.2 displays the two-dimensional conductance vs. electrode displacement histograms of the compounds. The histograms predominantly show an accumulation of counts in the region from 0 to 0.5 nm of displacement dropping from around  $1 \times$

$10^{-4} G_0$  to the noise level of about  $2 \times 10^{-7}$ . This behavior corresponds to the one expected for single-barrier tunneling, in which no molecule bridges the electrodes after the gold contacts snap apart. On top of this signal, regions can be identified in which the conductance vs. displacement traces show step-like features at characteristic conductance values; these traces are attributed to molecular junctions. The yield for these traces is approximately 5–20% depending on the specific molecule; this is a typical value for these types of MCBJ experiments.

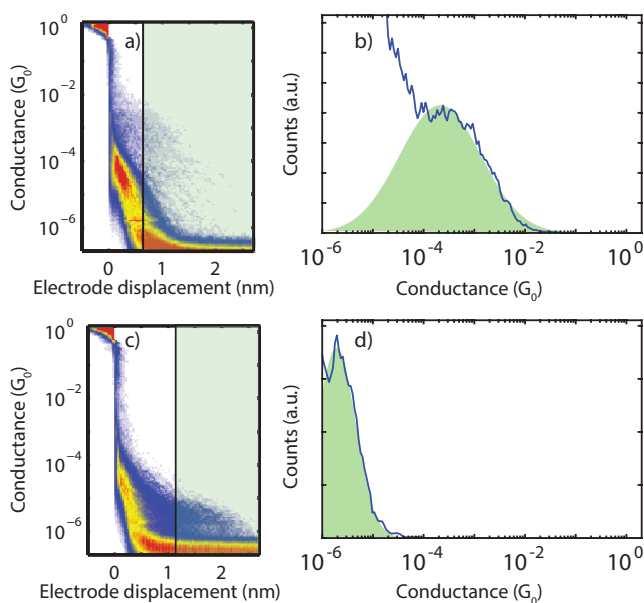


Figure 8.4: a) Two-dimensional conductance vs. electrode displacement of s-IF (**1**). Shaded area corresponds to the displacement section considered to build its partial one-dimensional conductance histogram displayed in b). c) Two-dimensional conductance vs. electrode displacement of pm-IF (**3**), shaded area correspond to the displacement section consider to build its partial conductance histogram displayed in d). The green shaded areas in b) and d) depict log-normal distributions fitted to the data.

To obtain the most probable conductance values of the compounds, one-dimensional histograms have been constructed. A log-normal distribution was fitted in the regions of conductance where plateau-like features are observed. For s-IF there is a low yield of junction formation and the peak seen in the conductance histogram does not correspond to the feature seen in the two-dimensional conductance vs. electrode displacement histogram. Similarly, in the case of pm-IF the features of molecular conductance appear near the noise level, thus there is no clear peak in the conductance histogram. To obtain the single-molecule conductance value in both of these cases a partial conductance histogram has been constructed by integration of the two-dimensional histogram for a limited displacement range as indicated by the shaded areas in Fig. 8.4a) and c). The resulting one-dimensional conductance histograms are displayed in Fig. 8.4 b) and

d). The most probable conductance value for the molecular is obtained by fitting a log-normal distribution to these data sets.

The most probable conductance values obtained from the fits are listed in table 8.1, for at least 2 different samples for each molecule. Surprisingly, contrary to the intuition, the progression of conductance values follows the rule s-IF>pp-IF>mm-IF> pm-IF. Examples of the quantum interference rule in phenyl rings being turned up side down are not common. For example in reference [6] two meta connected phenyl rings give rise to a higher charge transfer rate than its para connected counterpart when used as a bridge between a donor and an acceptor unit. Nevertheless those result are not directly transferable to charge transport measurements. Indeed the same two phenyl ring system gives rise to a high conductance in the para configuration and a low conductance in the meta configuration.

We must, however, look at these result with a bit of skepticism. Although the results unambiguously show a higher conductance value for mm-IF than for pm-IF, we must be cautious on concluding that in this case the replacement of a para-connected phenyl ring by a meta-connected ring increases the sulfur to sulfur molecular conductance. In this respect, a few observations can be made: first the length of the mm-IF's traces is shorter than the ones of pm-IF and almost as long as the ones of s-IF. Furthermore, the conductance value obtained from mm-IF lies near the conductance peak observed in s-IF in Figure 8.3. This may indicate the presence of other type of configuration in which, for example, the electron injection (or collection), does not happen through the thiol groups but through the  $\pi$ -cloud of one of the phenyl rings. If that is the case then the observed conductance peak of mm-IF could be the result of a different configuration and the conductance of the sulfur to sulfur configuration may be below the detection limit as intuition would predict.

molecule	Conductance ( $G_0$ )		
	sample 1	sample 2	sample 3
1) s-IF	$2.1 \times 10^{-4}$	$1.4 \times 10^{-4}$	
2) pp-IF	$3.4 \times 10^{-5}$	$2.8 \times 10^{-5}$	$2.8 \times 10^{-5}$
3) mm-IF	$1.4 \times 10^{-5}$	$1.5 \times 10^{-5}$	$2.1 \times 10^{-5}$
4) pm-IF	$2.1 \times 10^{-6}$	$1.4 \times 10^{-6}$	

Table 8.1: Most probable conductance values for the compounds extracted from a log-normal fitting of the conductance histograms. For compounds (1) and (3) the values are obtained from partial conductance histograms as described in Figure 8.4.

To exploit the potential magnetic properties of these molecules cryogenic temperatures are needed. In reference [1] this topic has been addressed with electromigrated break junction measurements.

### 8.3. POLYOXOMETALATES (POM)

Another interesting branch of molecular electronics is the coupling of inorganic clusters to electrodes through organic ligands, in other words, molecular systems that can sustain localized clusters of inorganic material. A remarkable example of this is a family

of transition metal oxygen anion clusters (polyoxometalates or POMs for convenience) which are compounds that consist of three or more transition metal oxyanions linked together by shared oxygen atoms to form closed 3-dimensional frameworks [7, 8]. The POM architecture offers a way to accommodate a specific number of atoms caged in a robust oxometallic frame.

The capability to encase a well-defined 3-dimensional arrangement of inorganic atoms grants these compounds the potential to study and perhaps control of the properties of, for example, the spin degree of freedom of single atoms within the structure. It is particularly interesting to electronically address these degrees of freedom and test if single-molecule electronics techniques allow for control of these systems. Compared to other magnetic systems like spin crossover molecules [9], or molecules with a multitude of magnetic atoms. These molecules poses the particularity that the central atom(s) can be framed in a rigid three-dimensional inorganic cage and that the flexibility of organic chemistry can be used for connections to metallic electrodes. In the context of molecular electronics there has been interest in measuring inorganic clusters connected to metallic electrodes through organic frameworks [10, 11], because it provides a tool to exploit the magnetic degree of freedom of heavy elements and in the future use them for spintronic applications. In this work we have characterized the conductance features of the two compounds displayed in Figure 8.5.

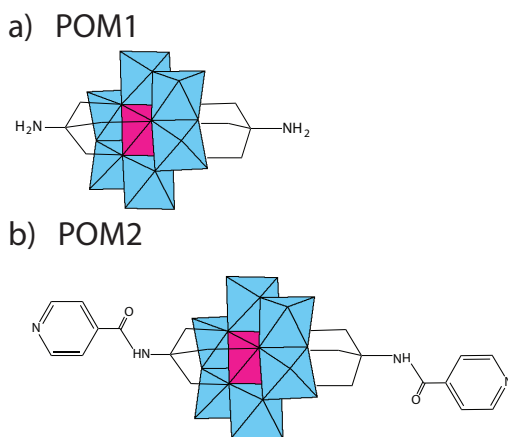


Figure 8.5: a) Structure of the molecules considered in this study based on the basic structure  $[\text{Mn}^{\text{III}}\text{Mo}_6\text{O}_{24}\text{L}_2]^{3-}$ . In a) the POM unit is directly connected to a amine group that is intended to be the anchoring position between the molecule and the metallic electrodes (POM1). In b) a spacer has been introduced between the molecule and the anchoring sites, and in this case the intended anchoring group are the pyridine end-groups (POM2).

The system considered here is depicted in Figure 8.5. It consists of an inorganic shell that surrounds a single manganese atom that provides the magnetic characteristic of the compounds. We have tested the possibility of measuring single-manganese POMs using the mechanical break junction technique. The experiments were performed by

Bias voltage (V)	Conductance ( $G_0$ )	FWHM (dec)
0.05	$2.2 \times 10^{-5}$	1.6
0.1	$1.9 \times 10^{-5}$	1.2
0.15	$1.4 \times 10^{-5}$	1.2
0.2	$1.2 \times 10^{-5}$	1.4
0.25	$8.3 \times 10^{-6}$	1.6

Table 8.2: Conductance value and full width half maximum of POM1.

drop-casting a solution with a low concentration of the target molecule ( $\approx 10 \mu\text{M}$ ) in acetonitrile. Then a set of 2000 conductance traces ( $G=I/V$ ) were measured at a electrode speed of 4 nm/s using bias voltages ranging from 0.05 to 0.3 V at intervals of 0.05 V.

The results of this experiment for the top molecule in Fig. 8.5 are summarized in Fig. 8.6. The two-dimensional conductance vs. electrode distance histogram (left panel) shows the absence of clear plateau-like features. Over all the trace length, however, is larger than the one of measurements on the device prior to drop-casting of the molecule. Next to the two-dimensional histograms the 1D-conductance traces of the measurement of the same junction at different bias voltage are displayed. The measurement at 0.1 V shows a clear peak at a few times  $1 \times 10^{-5} G_0$ . Remarkably, this feature moves to lower values as a function of bias voltage but at the same time its amplitude decreases. When a log-normal distribution is fitted to the histograms the obtained values of conductance, listed in Table 8.2, follow the same tendency.

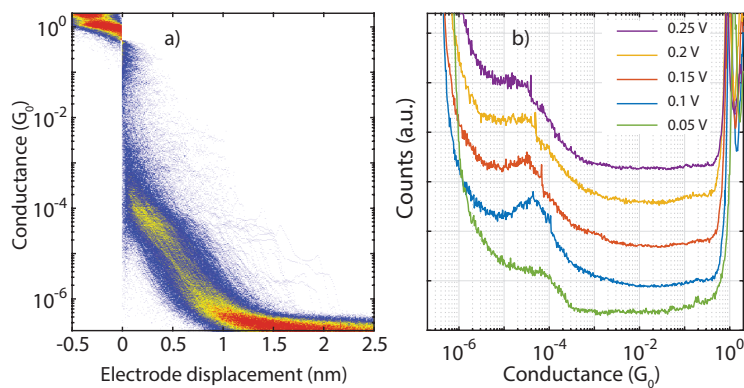


Figure 8.6: a) Example of a two-dimensional conductance vs. electrode displacement histogram constructed from 2000 consecutive traces of POM1. b) Series of one-dimensional conductance histograms at different bias voltages. They are offset in the vertical direction for clarity.

The lack of clear plateaus makes a further characterization difficult. In terms of chemical design it is desirable to have a longer molecule. In that way it would be easier to unambiguously recognize molecular traces from empty ones. With this in mind

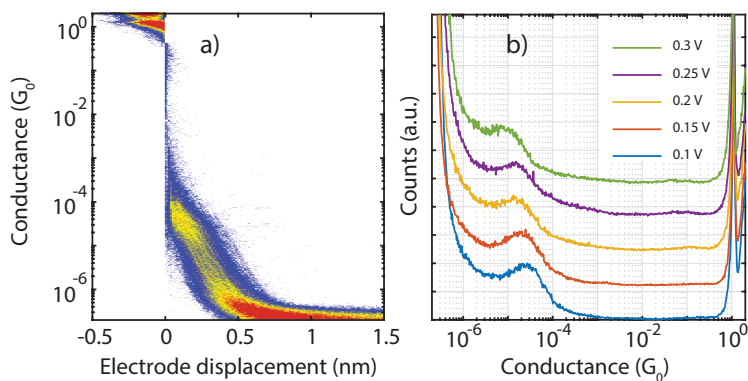


Figure 8.7: Example of a two-dimensional conductance vs. electrode displacement histogram constructed from 2000 consecutive traces of POM2. b) Series of one-dimensional conductance histograms at different bias voltages. They are offset for clarity.

we decided to measure the compound POM2 displayed on Fig. 8.5 b). This compound shares the same polyoxometalate center with the POM1 molecule and its main difference lies in its length; the amine end groups in POM1 are extended using a pyridine ring that is intended to be the new anchoring site.

In the case of the long POM2 the same experiment showed similar results. They are displayed in the same way as for POM1 in Fig. 8.7. In the whole range from 0.1 to 0.3 V of bias voltage the 1D-conductance histograms show a single peak in the same region as POM1. Intriguingly, the length of the traces in the latter case does not correspond to the difference in molecular length between POM1 and POM2; the traces even show the opposite trend. The conductance values obtained by fitting log-normal distributions to the data are displayed in Table 8.3. It is clear that the measured conductance values are approximately the same as for POM1 and they follow the same downwards trend as a function of voltage.

Bias voltage (V)	Conductance ( $G_0$ )	FWHM (dec)
0.1	$1.7 \times 10^{-5}$	1.4
0.15	$1.5 \times 10^{-5}$	1.4
0.2	$1.0 \times 10^{-5}$	1.5
0.25	$9.6 \times 10^{-6}$	1.7
0.3	$5.0 \times 10^{-6}$	1.7

Table 8.3: Conductance value and full width half maximum of POM2.

From the above mention experiments we conclude that the measured conductance of the POM2 molecule does not correspond to the fully extended molecule. The similarities between the measurements on the two compounds suggest that the measured fea-



tures on the POM2 molecule are a consequence of charge injection and collection at an intermediate site of the molecule, presumable, the nitrogen atom present in the spacer between the POM center and the pyridine groups which correspond to the position of the amine group of the POM1.

Few improvements in the chemical design can be suggested to make the POM molecules suitable for MCBJ studies. In the first place, the choice of anchoring moieties such as thiol or methylsulfide or even the one used for POM1, amine have shown a better coupling capability than pyridine [12]. The second design issue is the presence of the cross conjugation path between the POM center and the pyridine anchoring group given by the presence of the oxygen atom. Another ligand alternative that preserves a conjugated path from the anchoring moiety to the POM unit may increase the molecular conductance.

From another perspective the molecules analyzed in this section are interesting candidates for low-temperature, three-terminals measurements in a magnetic field. The single-spin nature of POM1 and POM2 makes them interesting for studying their single-molecule magnet properties that these molecules exhibit in bulk, on the level of a single molecule.

## 8.4. OUTLOOK

Throughout this dissertation we have discussed important aspect concerning single-molecule devices including molecular design, experiment design and statistical analysis. We have studied new strategies to bind molecules to metallic electrodes (chapter 3), in which we showed that the hybridization of carbon atoms involved in C-Au bonds provide a lower barrier when it is sp hybridized than when it is sp<sup>3</sup>. One of the puzzling features of the Alkynyl terminated oligo-phenylene (OPA) family is the non exponential dependence of the molecular conductance. We point out that there is no a clear explanation for such a behaviour. This is a good example of how single-molecule experiments resist simple explanations.

We have intensively worked on bio-inspired molecules; the curcuminoids and sa-  
lophens are good examples of compounds similar to molecules found in nature. The exiting part of this approach is that the chemical design can take advantage of the already set 'biological design' and apply it in a completely different context. Our work on curcuminoids has shown that simple architectures can give rise to various electronic features upon chemical modifications.

Finally, we have presented a couple of examples that extend this study to some other directions. The indenofluoreces are an example of combining the knowledge of the early days of molecular- and polymer-electronics, using the TTF units, with the molecular design for single-molecule measurements to achieve new functionalities. In contrast, the POMs' are a new architecture that combines the inorganic chemistry tool-set with the flexibility of organic ligands and exploit this combination to create systems with isolated high spins ground states.

The field of single-molecule electronics is growing in many ways. Up to now single-molecule experiments have contributed to the fundamental understanding of transport through organic molecules and their interaction with metals but, despite the efforts, there is not a foreseeable application in which single molecules could replace existing

electronic components. The main problem is still that there is no reliable way to arrange different molecules in a way that they would work as a designed circuit. Moreover, the reproducibility achievable in single conductance experiments relies on statistics, making the performance of a single device unpredictable.

From the technological perspective, single molecules are not yet a suitable replacement for silicon-based electronic components including transistors or diodes. The advantages of molecular design are masked by the lack of control over the binding configurations to the electrodes. At this point, it is hard to imagine that the existing architecture of electronics can be adapted to one that incorporates single-molecular components. Nevertheless, molecules do offer a new potential in a different scheme of devices. One could imagine devices (a sensor for example) with a high degree of redundancy that could rely on the switching or activation of a single-molecule. In other words, such a device would have various single molecule active sites, but its response only needs the activation of only one of them. Biological systems work somehow in this way; for example, the eye has receptors that can 'switch on' by the action of a single photon [13] and in some cases, this single switch is able to trigger brain activity. This kind of devices may need the combination of conventional electronics with ionic or electrochemical currents [14].

There is also another side of the coin that is at least as exiting. It is the one that touches upon the unknown fundamental questions that remain to be answered. To give a taste of the simplicity of a question that is still unanswered: it is still not clear how the molecular energy levels align with the electrode Fermi-energy. In summary, despite of the limited amount of atoms in a single molecule the abundance of degrees of freedoms makes it an intricate system to study. One the next experimental challenges is to couple single molecules to other kind of stimuli, light [15, 16] for example or to control molecular junctions in liquid environments, in which a chemical reaction takes place while a current is driven through a single molecule.

## REFERENCES

- [1] M. Mansø, M. Koole, M. Mulder, I. J. Olavarria-Contreras, C. L. Andersen, M. Jevric, S. L. Broman, A. Kadziola, O. Hammerich, H. S. J. van der Zant, and M. B. Nielsen, *Synthesis and single-molecule conductances of neutral and cationic indenofluorene-extended tetrathiafulvalenes: Kondo effect molecules*, *The Journal of Organic Chemistry* **81**, 8406 (2016).
- [2] Z. Wei, T. Li, K. Jennum, M. Santella, N. Bovet, W. Hu, M. B. Nielsen, T. Bjørnholm, G. C. Solomon, B. W. Laursen, and K. Nørgaard, *Molecular junctions based on sams of cruciform oligo(phenylene ethynylene)s*, *Langmuir* **28**, 4016 (2012).
- [3] C. R. Parker, Z. Wei, C. R. Arroyo, K. Jennum, T. Li, M. Santella, N. Bovet, G. Zhao, W. Hu, H. S. J. van der Zant, M. Vanin, G. C. Solomon, B. W. Laursen, K. Nørgaard, and M. B. Nielsen, *A new class of extended tetrathiafulvalene cruciform molecules for molecular electronics with dithiafulvene-4,5-dithiolate anchoring groups*, *Advanced Materials* **25**, 405 (2013).

- [4] S. J. van der Molen and P. Liljeroth, *Charge transport through molecular switches*, *Journal of Physics: Condensed Matter* **22**, 133001 (2010).
- [5] J. Fock, M. Leijnse, K. Jennum, A. S. Zyazin, J. Paaske, P. Hedegård, M. Brøndsted Nielsen, and H. S. J. van der Zant, *Manipulation of organic polyradicals in a single-molecule transistor*, *Phys. Rev. B* **86**, 235403 (2012).
- [6] N. Gorczak, N. Renaud, S. Tarkuc, A. J. Houtepen, R. Eelkema, L. D. A. Siebbeles, and F. C. Grozema, *Charge transfer versus molecular conductance: molecular orbital symmetry turns quantum interference rules upside down*, *Chem. Sci.* **6**, 4196 (2015).
- [7] M. Clemente-León, E. Coronado, C. J. Gómez-García, and E. Martínez-Ferrero, *Polyoxometalates as inorganic building blocks of multifunctional molecular materials*, *Journal of Cluster Science* **13**, 381 (2002).
- [8] G. Cao, J. Xiong, Q. Xue, S. Min, H. Hu, and G. Xue, *Organic–inorganic heteropoly blue based on dawson-type molybdosulfate and organic dye and its characterization and application in electrocatalysis*, *Electrochimica Acta* **106**, 465 (2013).
- [9] F. Prins, M. Monrabal-Capilla, E. A. Osorio, E. Coronado, and H. S. J. van der Zant, *Room-temperature electrical addressing of a bistable spin-crossover molecular system*, *Advanced Materials* **23**, 1545 (2011).
- [10] G. Lovat, B. Choi, D. W. Paley, M. L. Steigerwald, L. Venkataraman, and X. Roy, *Room-temperature current blockade in atomically defined single-cluster junctions*, *Nature Nanotechnology* **12**, 1050 (2017).
- [11] A. Lombana, C. Rinfray, F. Volatron, G. Izzet, N. Battaglini, S. Alves, P. Decorse, P. Lang, and A. Proust, *Surface organization of polyoxometalate hybrids steered by a 2d supramolecular ptdi/melamine network*, *The Journal of Physical Chemistry C* **120**, 2837 (2016).
- [12] R. Frisenda, S. Tarkuç, E. Galán, M. L. Perrin, R. Eelkema, F. C. Grozema, and H. S. J. van der Zant, *Electrical properties and mechanical stability of anchoring groups for single-molecule electronics*, *Beilstein Journal of Nanotechnology* **6**, 1558 (2015).
- [13] J. N. Tinsley, M. I. Molodtsov, R. Prevedel, D. Wartmann, J. Espigulé-Pons, M. Lauwers, and A. Vaziri, *Direct detection of a single photon by humans*, *Nature communications* **7**, 12172 (2016).
- [14] J. Zhang, A. M. Kuznetsov, I. G. Medvedev, Q. Chi, T. Albrecht, P. S. Jensen, and J. Ulstrup, *Single-molecule electron transfer in electrochemical environments*, *Chemical Reviews* **108**, 2737 (2008), PMID: 18620372.
- [15] R. Chikkaraddy, B. de Nijs, F. Benz, S. J. Barrow, O. A. Scherman, E. Rosta, A. Demetriadou, P. Fox, O. Hess, and J. J. Baumberg, *Single-molecule strong coupling at room temperature in plasmonic nanocavities*, *Nature* **535**, 127 (2016).

- [16] F. Benz, M. K. Schmidt, A. Dreismann, R. Chikkaraddy, Y. Zhang, A. Demetriadou, C. Carnegie, H. Ohadi, B. de Nijs, R. Esteban, J. Aizpurua, and J. J. Baumberg, *Single-molecule optomechanics in “picocavities”*, *Science* **354**, 726 (2016), <http://science.sciencemag.org/content/354/6313/726.full.pdf>.



## SUMMARY

This thesis describes an experimental investigation of the electronic properties of single molecules focusing on simple organic systems with the aim of shine light on their charge transport properties. Chapter 1 introduces the field of molecular electronics and focuses on the development of single-molecule electronics. The terminology and the main historical aspects of the field are presented and discussed. The relevant theoretical concepts are briefly described as well. The standard techniques to contact single molecules are presented, including electro-migrated junctions, scanning-probe based-break junctions and mechanically controlled break junctions (MCBJ). The latter is explained in more detail because it is the main tool in this dissertation.

chapter 2 describes the experimental methods used to obtain statistically relevant datasets. In the first part the distinction between empty and molecular traces is discussed and a method to filter the large datasets and split them in meaningful subsets is proposed. Then, the concept of junction formation yield is examined, and its impact on the information obtained from single-molecule conductance measurement is evaluated. The main conclusion is that when the yield of junction formation is high, the conductance values obtained from the one-dimensional conductance histogram may not represent the value of a single molecule in the junction. At the end of the chapter the problem of spurious contamination is systematically addressed and a protocol of cleaning is evaluated and standardized.

Chapter 3 presents the single-molecule conductance of a series of alkynyl terminated oligophenylenes (OPA) with 1 to 4 phenyl units. The result of the conductance measurement show that OPA 2, 3 and 4 produce stable metal-molecule-metal junction through a direct carbon gold bound thanks to the de-protonation of the alkynyl groups. Unexpectedly, the molecular conductance does not decay exponentially as the molecular length increases. The second part of the chapter shows that the same anchoring strategy allows for the formation of single-molecule junctions comprising functionalized compounds, in this case, a radical molecule. The experiments reveal that, at low temperature, Kondo-like behavior is present and, thus, we conclude that the spin degree of freedom is preserved after the formation of the single-molecule junction with direct Au-C anchoring.

Chapters 4, 5 and 6 describe the investigation of curcuminoid compounds. These molecules mimic the structure of curcumin, a molecule found in the Indian spice turmeric. The first of these chapters discusses the measurements of the single-molecule conductance of two isomers which only differ in the position of the sulfur atom in the thiophene rings that acts as anchoring moieties. There are two main conclusions out of this chapter. First, the position of the sulfur atom in the thiophene end group drastically changes the conductance value and the number of configurations in which the molecule can attach to the electrodes. Sulfur atoms positioned in the outer part of the molecule show a high-conductance state related to a covalent binding to the electrodes and a low-conductance state related to a non-covalent binding. When the sulfur atom is positioned in the inner

part of the thiophene ring only a low-conductance state was observed. This latter observation is consistent with a non-covalent binding configuration. The second important conclusion refers to the potential of curcuminoids as test bed for single-molecule experiments since the molecules showed comparable conductance values to well known systems such as oligophenyl-ethylenes.

In chapter 5 the electronic properties of a family of curcuminoids are studied. Different anchoring groups and functionalizations to the central backbone of the curcumin structure are tested. The most remarkable conclusion refers to the existence of two distinguishable conductance states of a curcuminoid compound when the beta-diketone group is replaced by a boron-difluorine ( $\text{BF}_2$ ) group and, at the same time, the anchoring groups are methyl-sulfide moieties. In contrast, the free ligand and the copper containing functionalization do not show the same behavior; neither do molecules with the same  $\text{BF}_2$  group but with different anchoring groups. Further measurements show that a similar, but shorter molecular architecture gives rise to the same qualitative behavior under the same combination of functionalization and anchoring strategy.

Chapter 6 explores another kind of modification to the curcumin backbone, in this case, the inclusion of nitrogen-containing groups, namely, pyrazole and isoxazole groups. The data show that these compounds have two distinctive conductance states related to different electrode displacements. This suggests that the nitrogen inclusions act as alternative anchoring groups providing another pathway for charge carriers to cross the molecule. Experiments showing that the high conductance state (related to shorter displacements) can be connected and disconnected by modulating the inter-electrode distance, further supporting this interpretation. Although the experiments were performed at room temperature both molecular configurations were stable on the time scale of seconds. As a control, another compound with a nitrogenated modification is tested, the molecule contains a phenyl ring with the intention to block the accessibility of the nitrogen atoms as anchoring groups. Despite that the high-conductance molecular states were still visible, the yield of that configuration was lower. Moreover, when the inter-electrode distance was modulated the high conductance state was not recovered. Thus, pyrazole and isoxazole groups do provide another anchoring site that also acts as a charge injection (or collection) point. The inclusion of bulky groups near the nitrogen atoms partially, but not totally, reduces the availability of these sites for binding to the electrodes.

In chapter 7 the research on two families of molecules, salens and salophenes is presented. These compounds have an asymmetric organic ligand frame that allows for a variety of metalizations. The conductance measurements show the pathway for charge carriers is important. Specifically, the configuration (meta or para) on which the anchoring moieties are connected to the organic backbone of the molecule plays a crucial role in the conductance value of the molecule. The metalization of the compounds, on the other hand, has a small effect on the conductance. These observations involve quantum interference effects and the data suggest that the most important pathway for charge carriers is through the organic backbone and not the metallic atom.

Finally, in chapter 8 various measurements on different sets of molecules are discussed. They are presented in the context of the directions toward the field of single-molecule electronics could follow. Measurements on tetrathiofulvane-functionalized

indenofluorenes are presented; these molecules show a counterintuitive trend. Three isomers are measured each one connected to the central part of the molecule either via two para-connected, two meta-connected or one meta- and one para-connected phenyl rings. The conductance values of the molecules follows the sequence para-para > meta-meta > meta-para. This contradicts the intuition of quantum interference in single-molecules. The other example presented involves polyoxometalates (POM) which are well controlled inorganic frameworks that can be combined with organic ligands. This kind of compounds may be a good test bed of well-isolated spin systems that can be electronically addressed with single-molecule electronics techniques. Finally, we discuss aspects of the future of single-molecule electronics based on the systems discussed during the body of this dissertation.





# SAMENVATTING

Dit proefschrift beschrijft een experimenteel onderzoek naar de elektronische eigenschappen van afzonderlijke moleculen, het onderzoek behelst eenvoudige organische systemen met als doel licht op hun ladingstransporteigenschappen te laten schijnen. Hoofdstuk 1 introduceert het vakgebied van de moleculaire elektronica en richt zich op de ontwikkeling van ‘single-molecule’ elektronica. De terminologie en de belangrijkste historische aspecten van het veld worden gepresenteerd en besproken. De relevante theoretische concepten worden ook kort beschreven. De standaardtechnieken om contact te maken met afzonderlijke moleculen worden gepresenteerd, inclusief elektrisch gemigreerde verbindingen, op aftasting gebaseerde breekverbindingen en mechanisch gestuurde breekverbindingen (MCBJ). De laatste techniek wordt in meer detail uitgelegd omdat het de belangrijkste is in dit proefschrift.

Hoofdstuk 2 beschrijft de experimentele methoden die worden gebruikt om statistisch relevante datasets te verkrijgen. In het eerste deel wordt het onderscheid tussen lege en moleculaire verbindingen besproken en wordt een methode voorgesteld om de grote datasets te filteren en te splitsen in subsets. Vervolgens wordt het concept van het rendement van de bindingsformatie onderzocht en wordt de impact op de informatie verkregen uit de meting van de geleiding van een enkel molecuul geëvalueerd. De hoofdconclusie is dat wanneer het rendement van de bindingsformatie hoog is, de geleidingswaarden verkregen uit het eendimensionale geleidingshistogram mogelijk niet de waarde van een enkel molecuul vertegenwoordigt. Aan het einde van het hoofdstuk wordt het probleem van mogelijke vervuiling besmetting systematisch aangepakt en wordt een reinigingsprotocol geëvalueerd en gestandaardiseerd.

Hoofdstuk 3 presenteert de geleiding van een enkel molecuul van een reeks van alkynyl-getermineerde olygofenylenen (OPA) met 1 tot 4 fenyleenheden. Het resultaat van de geleidingsmeting is dat OPA 2, 3 en 4 een stabiele metaal-molecuul-metaal verbinding produceren via een directe koolstof-goud binding door de de-protonering van de alkynylgroepen. Onverwacht daalt de moleculaire geleiding niet exponentieel als de moleculaire lengte toeneemt. Het tweede deel van het hoofdstuk laat zien dat dezelfde verankeringsstrategie de vorming mogelijk maakt van verbindingen met een enkel molecuul die een functie verbindingen bevatten, in dit geval een radicaalmolecuul. De experimenten onthullen dat bij lage temperatuur Kondo-achtig gedrag aanwezig is. Dit betekent daarom concluderen we dat de spinvrijheidsgraad behouden blijft na de vorming van de single-molecule verbinding met directe Au-C verankering.

Hoofdstukken 4, 5 en 6 beschrijven het onderzoek naar curcuminoïde verbindingen. Deze moleculen bootsen de structuur van curcumine na, een molecuul dat te vinden is in de Indiase specerij turmeric. De eerste van deze hoofdstukken bespreekt de metingen van de geleiding van een enkel molecuul van twee isomeren die alleen verschillen in de positie van het zwavel atoom in de thiofeenringen die als de ankers met het goud vormen. Er zijn twee hoofdconclusies uit dit hoofdstuk. Ten eerste verandert de posi-

tie van het zwavel atoom in de thiofeen eindgroep drastisch de geleidingswaarde en het aantal configuraties waarin het molecuul zich kan hechten aan de elektroden. Zwavelatomen gepositioneerd in het buitenste deel van het molecuul vertonen een hoge geleidingstoestand die gerelateerd is aan een covalente binding aan de elektroden en een lage geleidingstoestand die gerelateerd is aan een niet-covalente binding. Wanneer het zwavel atoom aan de binnenkant van de thiofeenring is geplaatst, wordt alleen een toestand met een lage geleiding waargenomen. Deze laatste waarneming is consistent met een niet-covalente bindingsconfiguratie. De tweede belangrijke conclusie verwijst naar het potentieel van curcuminoiden als model systeem voor experimenten met een enkel molecuul, omdat de moleculen vergelijkbare geleidingswaarden vertonen met algemeen bekende systemen zoals oligofenyl-ethylenen.

In hoofdstuk 5 worden de elektronische eigenschappen van een familie van curcuminen bestudeerd. Verschillende verankeringsgroepen en functies van de centrale ruggengraat van de curcumine structuur worden getest. De meest opmerkelijke conclusie verwijst naar het bestaan van twee onderscheidbare toestanden in de geleiding van een curcuminoid-verbinding wanneer de beta-diketon-groep wordt vervangen door een boor-difluorine ( $\text{BF}_2$ ) groep; deze bistabiliteit wordt alleen gezien met methylsulfide als verankerings-groepen. De verankeringsgroepen methyl- sulfidedelen. Daarentegen vertonen de vrije ligand en de koperbevattende functionalisatie niet hetzelfde gedrag; evenmin moleculen met dezelfde  $\text{BF}_2$  groep maar met een andere verankeringsgroepen. Vervolg metingen tonen aan dat een vergelijkbare, maar kortere moleculaire architectuur hetzelfde kwalitatieve gedrag oplevert onder dezelfde combinatie van functionalisatie en verankeringsstrategie.

Hoofdstuk 6 onderzoekt een andere vorm van modificatie van het curcumin skelet, in dit geval de toevoeging van stikstofhoudende groepen, namelijk pyrazol- en isoxazol-groepen. De gegevens tonen aan dat deze verbindingen twee onderscheidbare geleidbaarheidstoestanden hebben die verband houden met verschillende elektrode-verplaatsingen. Dit suggereert dat de stikstofhoudende groepen fungeren als alternatieve verankeringsgroepen die een andere route verschaffen voor ladingsdragers om het molecuul te passeren. Experimenten die aantonen dat de hoge geleidingsstatus (gerelateerd aan kortere verplaatsingen) kan worden gemaakt en ontkoppeld door de interelektrodeafstand te moduleren, ondersteunen deze interpretatie. Hoewel de experimenten bij kamertemperatuur werden uitgevoerd, waren beide molecuul configuraties stabiel op de tijdschaal van seconden. Als controle werd een andere verbinding met een stikstofbevattende modificatie getest, het molecuul bevat een fenytring met de bedoeling de toegankelijkheid van de stikstofatomen als ankergruppen te blokkeren. Ondanks dat de moleculaire toestanden met hoog geleidingsvermogen nog steeds zichtbaar waren, was het rendement van die configuratie lager. Bovendien werd, wanneer de afstand tussen de elektroden werd gemoduleerd, de toestand van hoge geleidbaarheid niet teruggewonnen. Aldus verschaffen pyrazool- en isoxazoolgroepen een derde verankeringsplaats die ook als een ladingsinjectie- of verzamelpunt fungeert. Het opnemen van volumineuze groepen nabij de stikstofatomen vermindert de beschikbaarheid van deze plaatsen voor binding aan de elektroden gedeeltelijk, maar niet volledig.

In hoofdstuk 7 wordt het onderzoek naar twee families van moleculen, salens en salophenen gepresenteerd. Deze verbindingen hebben een asymmetrisch, organisch li-

gandframe dat verschillende metalliseringen mogelijk maakt. De geleidingsmetingen laten zien dat de route voor ladingdragers belangrijk is. In het bijzonder speelt de configuratie (meta of para) waarop de verankeringsdelen zijn verbonden met de organische ruggengraat van het molecuul een cruciale rol in de geleidingswaarde van het molecuul. De metallisatie van de verbindingen, aan de andere kant, heeft een klein effect op de geleiding. Deze waarnemingen brengen kwantuminterferentie-effecten met zich mee en de gegevens suggereren dat de belangrijkste route voor ladingsdragers via de organische hoofdketen is en niet via het metaalatoom.

Tenslotte worden in hoofdstuk 8 diverse metingen aan verschillende sets van moleculen besproken. Ze worden gepresenteerd in de context van de richtingen die het vakgebied van elektronica met één molecuul kan volgen. Metingen op tetrathiofulvaan-gefunctionaliseerde indenofluorenen worden gepresenteerd; deze moleculen vertonen een contra-intuïtieve trend. Drie isomeren werden gemeten, elk verbonden met het centrale deel van het molecuul, hetzij via twee para-gehoppelde, twee meta-gehoppelde of één meta- en één para-gehoppelde fenylingen. De geleidingswaarden van de moleculen volgen de sequentie para-para > meta-meta > meta-para. Dit is in tegenspraak met de intuïtie van kwantuminterferentie in enkele moleculen. Het andere gepresenteerde voorbeeld betreft polyoxometalaten (POM), die goed gecontroleerde anorganische kaders zijn die kunnen worden gecombineerd met organische liganden. Dit soort verbindingen kan een nieuw model systeem zijn van goed geïsoleerde spin-systemen die elektronisch kunnen worden uitgelezen met de elektronica-technieken met één molecuul. Ten slotte bespreken we aspecten van de toekomst van moleculaire elektronica op basis van de moleculaire verbindingen die besproken zijn in dit proefschrift.



# ACKNOWLEDGEMENTS

*Yo no sufro de locura,  
la distruto a cada minuto  
I do not suffer from madness,  
I enjoy every minute of it.*

Les Luthiers

Dear reader, finally I have the freedom to address you. If you are reading this, it means that, for one reason or another, you care about who I am as a person beside the science that precedes this section. I honestly thank you for taking the time to read these lines. Let me tell you that this dissertation is just a small part of all the experiences that this PhD has signified. Please forgive me if I miss you in the following text that expresses my gratitude towards the important persons that played a role in my (PhD) life.

Herre, I cannot start this acknowledgment without thanking you for the amazing opportunity and for the mentor you have been. This feels the right occasion to tell you that what struck me the most about you was that you value your father's poems among the better of Dutch literature. There is a little tribute of this fact somewhere in the thesis. I really admire the way you combine an extremely efficient way of working with a nice and fulfilling personal life. It is something that I would like to take with me.

Diana, I think that the way Mickael described you is illustrative enough, you are the most colorful person in the lab. Thank you for the long conversations, your advice and support, and the optimism in the long days in the lab. Good luck in all the future projects.

Nuria, we have worked hard to put the curcuminoids in the world of single-molecule electronics. I really thank you, and by extension all chemists involved, for providing us with one of the most exciting systems to work with. I was also happy to realize that both of us share the appreciation for GATTACA (Not everything is written in your DNA). I wish you the best. Jos, thanks for being part of my committee, I have always admired the way that you explain complicated subjects in simple terms. Peter, thank you in the first place for reading my thesis but more especially for being always calm and curious with an honest interest for others' research. Ismael, thanks for your kind answers to my e-mails and for your feedback. Jan, you are one of my references as a scientist. I always enjoyed your interventions in the meetings and the discussions you enabled.

There are several groups or teams of people to whom I owe a lot. The first of them is the one composed by Dorine, Maria, Heleen, Etty, Marije and Erika. Thank you all for keeping everything working in order. I have a great deal of admiration for you because I am sure that I would not be able to do the same. Dorine, thank you especially for coming to see me performing in the circus. Masha, Tino, Ronald, you have been the people that keep the labs running. Thank you for making our PhDs' possible and the social environment more alive. The Kavli nanolab staff, thanks for keeping the clean-room running smoothly for the most part of the year. Our work would be so much difficult

without you. Thank you all Marc, Marco, Anja, Charles, Eugene, Ewan, Hozanna, and everybody else.

My fellow Chileans in Delft and The Netherlands, you have been such an important connection to my roots. Paola and Bas, thank you for the support, and the invaluable help you have given Rocio and me. I truly owe you a big one. Carlos, Paula, Daniel, Susan, Lisset and Cristobal, we have missed you all, thank for all those fun moments and games nights. Pablo, vecino, you have been a discovery on our lives, the conversations, drinks and food that we shared meant a lot. I believe that this will be a long-lasting friendship and our conversation will be again long and intricate. Pelo, I had the privilege of training you for a short period of time. You are one of the kindest people I know and I'm sure that our paths will cross again at some point. Until then, good luck and success. Accel, Dory, Ale and Luzma we are the old ones now, you know how little the community was back then. I wish you happiness and strength for the future. To the other Chileans in the lab: Jacqui, you were the most cheerful being in the lab and Cristian, we will be a bit more careful with the beers next time. I hope that none of the rest slip my mind, thank you all, Javier and Nicol, Camila, Oscar and Maca, Seba, Pato and Ari. I guess you will have to find someone else to take care of barbecue. To the people in Amsterdam: Diego, I would not have entered this country if it were not for you; Naty, it was a pleasure to become your friend; Camilo you are the last representative of Blanco Encalada 2008 you have to welcome the ones to come.

Dear colleagues, all of you that stand at the frontier of knowledge, I truly thank you for making research something more than just a job. Those of you that knew the MED and the ones that came afterwards, thank for the parties, the outings and more importantly all the little moments that made us deliciously imperfect (yes imperfect). Girodano, the man for whom I was kicked out of a party. I hope to listen to you playing the piano again. Dejan, the man on the cellphone, our conversations during lunches and breaks were enlightening specially when Joao, Dirk and Mafalda participated. Santiago, the wrecking ball, your presence was unmistakable, and now, missed. Thank you for sharing some of your secrets with me. Floriano, the man of the ring, I really appreciate your commitment to improve the working environment in the department I wish you the best in the next steps. Nikos, the only true DJ inside the group, you were the nicest company for those long evening in the lab. You are an amazing guy. Richard, you were a great officemate. Your enthusiasm is contagious. I would like to listen to you playing the violin once. Emre, if you ever read this, you will always be the sultan of the office. Ranko, the always tidy singer, we shared funny moments, including that crazy week of moving from one apartment to the next. It was not fun then, but it makes me smile now. Thank you for being such a nice officemate. Joao you are one of the nicer persons I know to have a discussion with, there was always something to reconsider after talking with you. There are a lot more people that deserve to be mentioned the postdocs and colleagues, the smiley Marck, Holgar, Nicola, Daniel, the other Marck, the Españoles Mari, David and Miguel, Martijn, Ines, Thierry, Luigi, Lorenzo and the old ones Albert (the trumpet first and then the congas), Ronald, Michele, Anna, Shun and Sal, Christian. The colleagues outside Delft were also a nice part of the PhD. Either in conferences or meetings it was always nice to see you and have a conversation. Sasha and Sander, I don't think we will ever see you closer together, thanks for all the little moments. Cansel and Darma on the

side of the chemists keep pushing.

The People in the lab deserve their own paragraph, those who have suffered the indifference of their molecules and the broke down of a piece that takes a week to replace, thank you all for making the environment so nice. Riccardo, thanks for being my mentor. In a more personal aspect, I admire your dedication to photography and your cooking skills, but your musical choices were, how to say it? Discomforting. Mickael, you were always the man to go when things got complicated. Thank you for all the answers and will to help and for the fascinating stories of how you risk your life climbing, in crazy races or skiing. Max, the sailor, you were the representation of the Dutch culture for me, you have the best of my wishes for your parenting life. Anastasia keep fencing and researching. Vera, I enjoy talking with you about politics and culture, you have a very mature opinion in most subjects and the will to do what you think is right. Alexandra, I admire your determination and pride. Enrique, you are the kindest postdoc I ever met; it was a pleasure to work with you. Rocco, the most epistemic of the scientist I met in the Netherlands, I wish you the most gratifying trip through knowledge and I am curious of when I will be reading your books. Sabina, you have an amazing artistic sense and an impressive capability for science, thanks for all your feedback on my work and your supportive attitude. Pascal, the enthusiastic brewer, your presence in the lab has been refreshing. Thank you for revitalizing the social environment of the lab. Joeri, you are such a talented scientist, I admire the versatility for theory and experiments. I wish you success with that fridge. Julien, you sick man, a great wisdom and a bit of madness, or was the other way around? Mucha felicidad para ti, Mary y Lila. Matthijs thanks for passing by each time you are in town. Chun Wei, you will be in charge of the lab at some point, please take care of it. Maria, yes you are in the lab paragraph, you are incredibly friendly girl and a meticulous scientist. From these lines I give you the welcome to the lab and my congratulations for your graduation. The man that never touched a single set-up, José, only theoretician working with molecules (PhD) and only other latin-american, you are a charismatic person. I loved your talks during the meetings and conferences. Senja, my one and only bachelor student, thanks for your work and commitment. And the rest of them Damien, Jorik, Luuk (thank for the help with Dutch), Jochem and Esmee good luck to all of you. Benjamin, I almost forget you... the warrior of the lab... I think it was because you went away before my defense, success in NASA.

There have been people that have helped me on bearing this northern Europe culture of telegraphic proxemics. Dancers are these people that 'speak' another language which involves abandoning the fear of interpersonal proximity and use the music and the body to express themselves. Daniel, Jeroen, Regina, Chunwei, Lidia, Chara, Jessica, Sofia, Victor, Diego, Leon, Camila, Victoria, Mousa and all the SoSalsa members, the performers of the shows that I have the privilege to lead, I own you (and the dances we had together), my sanity (the little that I have). See you on the dance floor. From these group a remarkable guy stands out, my canijo. Victor, I once taught you a few dance moves, since then you became one of my best friends, always there in the parties and always supportive. I am honored to have you as my paranyph. Keep working hard, but do not overdo it, the PhD is not everything.

There is also an aspect of my life that drift apart from sanity; circus artist are the icons of madness and I pride myself for training with them. Johanes you have opened



the doors of your gym and home to me and there is so much that I want to thank you for, but overall for your friendship and teachings; you are a really selfless person. Stephany, Marieke, Ramona you have been my training partners in the air thanks for all the time we have shared. Roosje you are a kind of hybrid in my life, an aerialist and a dancer, probably you are the person with whom I have the most in common, even with your dislike for beer. I treasure our friendship as one of the most important relations I have build in the Netherlands. To all the acrobats and friends Anja, Stef, Sequoia, Dana, Evert, Melissa, Anne, Paco, Farid, Djeena, Thami, Kaj, all the Mariekes and the ones that now slip my mind thank you for the trainings, the shows and the nice moments.

There are a few people that I have deliberately skipped until now. Davide, you are probably the most significant friend inside the University, thanks for your kindness and this twisted kind of humor that we share. There is a long list of activities we shared, some bouldering, conferences, games, dinners and endless office days. You became a great friend of mine. I had no doubt that I wanted you as my paranyph. If at any time I could help you please do not hesitate in contacting me. For the time being, keep pushing and don't overstress.

Nandini, you were like a little sister to me. I am very happy that you are achieving the things you wanted and I am terribly sorry for not being there for your wedding. We have shared the good and the bad moments. Your support was crucial in the hard times. Thanks for believing in me. I wish you happiness and an intense life, just as you are. Of course, have a terrific honeymoon. Send my regards to Ash.

Por último a mi familia, papá, mamá y hermanos no puedo más que agradecerles todo, sus visitas, el ánimo que enviaban, su preocupación. Ya saben que para mi esto de las graduaciones no es importante, pero quiero aprovechar estas líneas para decirles que los quiero y nunca dejé de sentir su apoyo. Que estoy feliz que la Naty esté viviendo independientemente, que la Ale esté estudiando algo que la apasiona y que Francisco esté tan lleno de proyectos. Estoy orgulloso de pertenecer a esta familia, los admiro a todos por sus inmensas capacidades y logros. Un abrazo apretado a todos y cada uno. A la tía Ani, gracias por su visita, y sus cariñosos mails de saludos. Gracias también a todos los primos y tíos que han preguntado por mi. Tío Nancho, gracias por las conversaciones, las comidas y las historias que compartiste conmigo. Saludos a la Tía Elisa y a la Dominga.

Chio, has sido el pilar fundamental que me ha mantenido de pie, me has ayudado más de lo que yo hubiese creído posible. Pero 'gracias' no refleja lo que siento por ti. Te amo, haces de mi vida algo exitante. Me encanta compartir la vida e imaginar el futuro contigo.

# CURRICULUM VITÆ

## Ignacio José OLAVARRIA CONTRERAS

09-12-1986      Born in Santiago, Chile.

### EDUCATION

2005–2009      Bachelor in Science with Mention in Physics  
Universidad de Chile, Santiago, Chile

2010–2014      Master in Science with Mention in Physics  
Universidad de Chile  
Santiago, Chile  
*Thesis:*      Copper nucleation on TiO<sub>2</sub> (001) by electrodeposition  
*Promotor:*    Dr. Victor Fuenzalida

2014-2018      PhD. in Applied Physics  
Delft University of Technology  
Delft, The Netherlands  
*Thesis:*      Single-molecule conductance measurements:  
Correlations between chemical design and electronic properties  
*Promotor:*    Prof. dr. H.S.J. van der Zant



# LIST OF PUBLICATIONS

5. Sabina Caneva, Pascal Gehring, Víctor M. García-Suárez, Amador García-Fuente, Davide Stefani, **Ignacio J. Olavarria-Contreras**, *et al.*, *Mechanically Controlled Quantum Interference in Graphene Break Junctions*. [arXiv:1803.05642 \[cond-mat.mes-hall\]](#)
4. Francesc Bejarano, **Ignacio Jose Olavarria-Contreras**, Andrea Droghetti, *et al.* *Robust Organic Radical Molecular Junctions Using Acetylene Terminated Groups for C–Au Bond Formation*, *Journal of the American Chemical Society* **140**, 5 (2018).
3. **Ignacio J. Olavarría-Contreras**, M. L. Perrin, Z. Chen, *et al.* *C–Au covalently bonded molecular junctions using nonprotected alkynyl anchoring groups*, *Journal of the American Chemical Society* **138**, 27 (2016).
2. Etcheverry-Berríos, **I. Olavarría**, M. L. Perrin *et al.*, *Multiscale Approach to the Study of the Electronic Properties of Two Thiophene Curcuminoid Molecules*, *Chemistry - A European Journal* **22**, 36 (2016).
1. V.M. Fuenzalida, D.G. Galvez-Arancibia, **I.J. Olavarría-Contreras**, *et al.*, *Tungsten oxide nanoparticles grown by condensation in gas using domestic appliances*, *Materials Letters* **65** (2011) 3061–3063.